OXYGEN CHEMISORPTION ON CARBON ADSORBENTS[1]

BY WILLIAM V. LOEBENSTEIN AND VICTOR R. DEITZ

Contribution from the National Bureau of Standards, Washington, D. C.

A detailed study was made of the chemisorption of oxygen at 200° by a new bone char, two service bone chars, a coconut-shell charcoal and a carbon black. After a preliminary heating for 24 hours in a stream of nitrogen at the maximum temperature of the experiment (400°), the sample was exposed to oxygen. The combustion products formed were allowed to remain in the system. A quantitative recovery of the oxygen was obtained in product gases by a second 24-hour nitrogen sweeping at 400°. The oxygen participating in chemisorption was distinguished from that resulting in combustion and both were expressed in terms of the residual (or unreacted) oxygen. Characteristic curves were obtained for each of the materials investigated. Hydrogen treatment at 200° and at 400° was found to influence the subsequent oxygen chemisorption by bone char at 200°. Three additional factors were discussed in detail: the percentage of total oxygen consumed which appeared as combustion products and as desorption products, the distribution of desorbed oxygen between carbon dioxide and carbon monoxide, and the ratio of the carbon to the hydrogen, both of which participated in the reactions with oxygen.

I. Introduction

The reaction of oxygen with carbon has long been known to involve a fixation of oxygen[2] by the surface carbon atoms to form a chemical bond. This more-or-less stable "oxide" layer has been variously termed "oxygen complex" or "chemisorbed oxygen." This investigation is an effort to study the properties of the surface oxide layer which forms at comparatively low temperatures (up to 200°) and which decomposes at or below 400°. This constitutes an important fraction of the total chemisorbed oxygen present on the carbon surface.

Oxygen was contacted with the sample in a closed system and the product gases, whose formation accompanies that of the oxygen complex, were not removed until the reaction virtually ceased. These gases consisted entirely of H_2O, CO_2 and CO and are referred to in this work as "combustion products" to distinguish them from the same gases which were subsequently formed during the controlled decomposition of the chemisorbed oxygen. Oxygen remaining as O_2 at the end of an experiment is termed "Residual Oxygen." The appreciable amounts of H_2O among both the combustion products and the decomposition products of the oxygen complex were derived from the hydrogen contained in the carbonaceous matter of the sample.

II. Apparatus and Procedure

The carbon adsorbents investigated included a new bone char, two service bone chars which had been employed in the refining of cane sugar and a coconut shell charcoal. Also, a channel black used in the compounding of rubber was included. The surface areas (B.E.T.) and the carbon contents of these materials may be found in Table VII.

Attainment of a reproducible state with respect to the amount of oxygen chemisorbed was a necessity both at the beginning and at the end of each experiment. This was accomplished by heating the sample for 24 hours in a stream of purified nitrogen at 400°. This length of time was sufficient for the purpose of these experiments. The increase in the amount of these gaseous products formed as the result of more than doubling this 24-hour period was only about 6%.

Apparatus.—The apparatus[3] is sketched in Fig. 1. The sample was contained in the adsorption tube T. This tube was connected to each of two 200-ml. calibrated gas burets P and S. By means of the mercury leveling bulbs M and L a gas contained in one buret could be forced through the sample and into the second buret and the process reversed. The leveling bulb M served also as a manometer. Nitrogen entering the system could be caused to by-pass buret P and pass directly through the sample. Two tared U-tubes, containing absorbents for the retention of H_2O and CO_2, could be connected to either buret. The exit gas from these U-tubes was passed over CuO (350°) to oxidize the CO, and the resulting CO_2 was absorbed in a third tared U-tube.

Procedure.—A typical chemisorption experiment was conducted in six steps. (1) The conditioned sample was evacuated, purified O_2 introduced into buret P, only, and the pressure measured. The quantity of O_2 was determined from the equation of state of the gas. (2) The oxygen was then contacted with the sample by means of the cycling technique already mentioned. The sample at room tempera-

(1) This investigation was sponsored as a joint research project undertaken by the Bone Char Research Project, Inc., and the National Bureau of Standards, Washington 25, D. C.

(2) T. F. E. Rhead and R. V. Wheeler, *J. Chem. Soc.*, **103**, 461, 1210 (1913).

(3) W. V. Loebenstein and V. R. Deitz, *J. Research Natl. Bur. Standards*, **46**, 51 (1951), RP 2174.
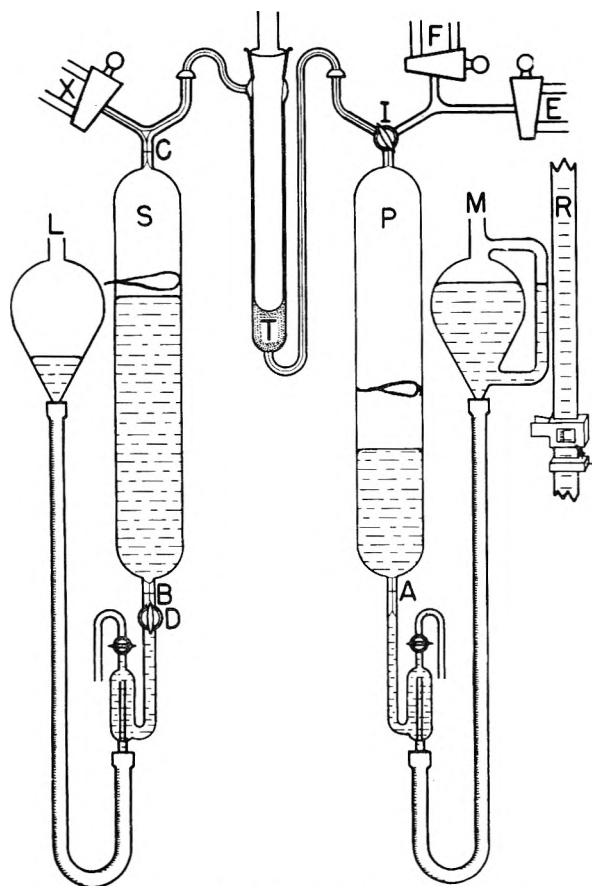
Fig. 1.—Apparatus.

ture was slowly brought to the desired temperature (100, 150 or 200°) where it was held for 24 hours. (3) The pressure of the gas mixture remaining in the system was determined and the portion of the mixture contained in buret P was trapped off. (4) The gas mixture remaining in the sample tube T (a small fraction of the total), together with the gas desorbed at the temperature of the experiment, was analyzed without raising the temperature of the sample by sweeping this part of the system for 24 hours with purified nitrogen and passing the gases through the U-tube analysis train connected at point X in Fig. 1. (5) Additional gaseous products were desorbed by raising the temperature of the sample tube to 400° and sweeping the system for another 24 hours through the analysis train. (6) Finally, the combustion products which had been trapped in buret P were passed through the analysis train connected at point F and this was followed by repeated rinsings of the buret with nitrogen. This final determination made it possible to distinguish between the combustion products trapped off in step (3) and the gases desorbed at the temperature of the experiment. The dead space of the sample tube was determined with helium each time a new sample was introduced.

In the last series of experiments, samples of the new bone char were preheated in a constant stream of hydrogen either at 200° or at 400° for 24 hours. In each case this was followed immediately by the 400° conditioning in nitrogen. The rest of the experiment was the same as that already described. Oxygen chemisorption experiments were carried out with all hydrogen-treated samples.

III. Results

The disposition of oxygen after the chemisorption experiments at 200° is given in Table I. The resulting quantities of oxygen contained in the CO_2, CO and H_2O are given for each of the three gas mixtures: (1) combustion products, (2) those desorbed at 200°, (3) the additional gas desorbed on

heating from 200 to 400°. The oxygen is expressed, whether free or combined, as milliatoms.[4] The first four experiments with new bone char listed in Table I were undertaken with a different sample for each. The remaining determinations with this same material were performed successively upon the same sample and are referred to as "sequence experiments." The residual carbon in the sample at the beginning of each experiment was corrected for that consumed during the previous experiment. The amount of oxygen introduced, as shown in column 3, Table I, was varied randomly over wide limits.

In another series of experiments, the temperature of chemisorption was maintained either at 100 or at 150°. Detailed breakdowns into the various products are given in Table II. These samples were also conditioned at 400° in the manner already described, each sample then cooled to room temperature, the oxygen introduced and the sample then brought to the desired temperature.

Hydrogen was found to react with the new bone char at 400° with the formation of H_2O. Table III shows a typical treatment with H_2 at constant flow in which the H_2O was produced at a constant rate, whereas the simultaneous formation of CO_2 fell off markedly during the same 24 hours similar to heating in nitrogen. The water produced by reaction with different original samples of new bone char at 400° is shown in Table IV. About 200 volumes of H_2 were required on the average to produce one volume of H_2O under the conditions of the experiment. Hydrogen treatments were also made at 200° on samples of new bone char which had been conditioned at 400° in nitrogen. No appreciable H_2O was evolved during the latter treatment.

The detailed results of the oxygen chemisorption by hydrogen-treated bone char are given in Table V. An independent experiment, in which a measured volume of H_2 was admitted to the sample at 200° and cycled for 24 hours, showed that adsorption of H_2 could not be detected volumetrically. The analysis of the remaining gas by means of a mass spectrometer disclosed no detectable contamination of H_2 by carbon-containing gases.

IV. Discussion

One important and significant result of this investigation is the quantitative recovery of the added oxygen, once the sample had been conditioned at 400°. The total of the oxygen recovered for each group of experiments in Tables I, II and V is substantially equal to the sum of the oxygen introduced. The particular oxygen complex, which was thermally unstable at that temperature, was therefore stripped quantitatively from the char. Upon re-exposure to oxygen, the conditioned carbon behaved as though each part of the surface formed a particular oxygen complex that was capable of being removed from that part of the surface by reheating to 400°. It was not necessary, for example, to heat to higher temperatures for the removal of any part of this oxygen, a technique recently employed by Anderson and Emmett[5] for carbon blacks.

(4) A "milliatom" is defined as the atomic weight in milligrams.

(5) R. B. Anderson and P. H. Emmett, THIS JOURNAL, **56**, 753 (1952).

TABLE I

DISPOSITION OF OXYGEN IN CHEMISORPTION EXPERIMENTS AT 200°

Milliatoms of oxygen

1	2	3	4	5	6	7	8	9	10	11	12	13	14
	Wt. of carbon in sample, g.		As H_2O from →			As CO_2 from →			As CO from →				Recovery of oxygen, %
Expt. no.		Introduced	Combustion	Desorption at 200°	Additional desorption up to 400°	Combustion	Desorption at 200°	Additional desorption up to 400°	Combustion	Desorption at 200°	Additional desorption up to 400°	Residual	
(a) New bone char (Char 2) using differential original samples													
101	1.1562	14.67	0.02	0.00	0.68	1.99	2.14	7.53	0.11	0.01	0.25	0.04	87
131	0.9386	7.95	.05	.00	1.31	0.66	1.96	5.25	.05	.03	.16	0.05	120
133	.8800	27.33	.04	.07	0.64	3.73	2.68	6.37	.11	.05	.19	13.21	99
135	.9213	15.16	.01	.00	0.57	1.96	1.99	5.87	.07	.03	.18	4.42	100
(b) Char 2 using the same sample for successive expt.													
4	0.6831	15.22	0.15	0.01	0.18	2.34	1.97	4.52	0.04	0.01	0.19	4.21	90
5	.6273	8.41	.16	.00	.19	0.73	1.61	3.73	.01	.02	.15	1.59	97
6	.5887	8.55	.02	.02	.42	.99	1.95	4.02	.02	.02	.18	1.69	109
7	.5444	5.84	.03	.00	.02	.22	1.15	2.39	.02	.09	.17	0.54	79
8	.5098	6.00	.05	.02	.05	.32	1.22	2.53	.01	.07	.15	1.48	98
9	.4827	3.43	.03	.01	.08	.08	0.82	2.09	.01	.08	.16	0.41	109
10	.4619	3.66	.19	.02	.10	.03	0.76	2.02	.01	.10	.14	0.23	98
11	.4420	11.37	.05	.01	.12	.65	1.15	1.95	.01	.07	.17	6.68	95
12	.4166	20.94	.14	.03	.23	1.68	1.79	3.02	.02	.07	.20	14.37	103
(c) Service bone chars (Char 32) using the same sample for successive expt.													
13	1.1505	15.13	0.07	0.56	0.64	3.91	1.08	2.27	0.24	0.17	0.59	5.11	97
14	1.0951	11.37	.03	.08	.28	2.54	0.86	2.48	.02	.01	.18	4.71	99
15	1.0573	7.29	.25	.05	.35	2.02	1.03	2.51	.01	.11	.18	0.98	103
16	1.0203	3.44	.02	.00	.22	0.66	0.68	1.76	.02	.10	.12	0.02	105
17	0.9987	19.05	.19	.17	.32	3.30	1.61	2.63	.01	.16	.18	10.60	101
(d) Service bone char (Char P 1) using the same sample for successive expt.													
123	1.9297	14.60	0.02	0.09	0.42	3.92	2.06	3.96	0.03	0.02	0.06	0.66	77
125	1.6011	30.01	0.07	0.90	0.67	7.88	1.65	4.11	0.09	0.01	0.19	13.52	97
(e) A coconut shell charcoal (Char 1) using the same sample for successive experiments													
18	0.8168	15.62	0.14	0.05	0.01	4.28	0.27	0.35	0.14	0.12	0.09	10.20	100
19	.7833	7.21	.10	.03	.00	1.98	.18	.24	.08	.45	.13	4.38	105
20	.7610	0.51	.02	.04	.01	0.31	.06	.14	.02	.10	.09	0.00	158
21	.7554	17.34	.16	.03	.02	2.82	.19	.24	.10	.20	.21	13.63	101
22	.7417	1.53	.14	.03	.03	0.54	.10	.12	.04	.23	.13	0.41	116
23	.7323	11.72	.19	.04	.00	1.82	.14	.18	.07	.47	.22	9.03	104
(f) A channel black using the same sample for successive expt.													
111	8.644	15.29	0.23	0.32	0.06	3.51	0.33	1.33	0.66	0.04	0.64	4.65	77
112	8.597	7.27	0.13	0.50	0.26	1.15	0.28	0.74	0.25	0.09	0.42	3.31	98
113	8.575	14.85	0.28	0.31	0.22	2.24	0.30	1.00	0.43	0.07	0.50	8.42	93

Although carbon and hydrogen contained in the sample was consumed as a result of the sequence chemisorption experiments, there was no selective removal of either constituent. Analysis showed that the ratio of carbon to hydrogen in the total gaseous products remained substantially constant. The average for the values of C/H in the experiments on new bone char (determined from Table I) was 5 which corresponds to a weight ratio of 60 to 1.

The results in Tables I, II and V are grouped according to whether the products resulted (1) from combustion at $t°$, the temperature of chemisorption, (2) from the decomposition of the complex in a stream of N_2 at $t°$ and (3) from the additional decomposition of the complex upon heating the sample above $t°$ up to 400°. The quantity of reacted oxygen (sum of the oxygen contained in the CO_2, CO and H_2O) in each of these categories was totaled for each series of the experiments with each adsorbent given in Table I and expressed as percentages of the oxygen reacted. These are reported in Table VI.

One important observation obtained from Table VI is the appreciable magnitude of the oxygen desorbed at 200° relative to that contained in the combustion products at the same temperature. As explained in the Procedure, the combustion products were allowed to accumulate and were in constant contact with the adsorbent during the chemisorption process. Before the desorption at 200° in a stream of nitrogen, the major part (~95%) of the gas phase (which included the combustion products and the residual O_2) was trapped off and had no further contact with the carbon adsorbent. Since the vast majority of the residual O_2 was removed, the additional oxygen contained in the CO_2, CO and H_2O realized at 200° had to come from the original chemisorbed complex. It is difficult, therefore, to avoid the conclusion that the combustion products had a retarding

TABLE II

DISPOSITION OF OXYGEN IN CHEMISORPTION EXPERIMENTS FOR A NEW BONE CHAR (CHAR 2) USING DIFFERENT ORIGINAL SAMPLES

1	2	3	4	5	6	7	8	9	10	11	12	13	14
						Milliatoms of oxygen							
			—As H_2O from—			—As CO_2 from—			—As CO from—				
Expt. no.	Wt. of carbon in sample, g.	Introduced	Combustion	Desorption at expt. temp.	Additional desorption up to 400°	Combustion	Desorption at expt. temp.	Additional desorption up to 400°	Combustion	Desorption at expt. temp.	Additional desorption up to 400°	Residual	Recovery of oxygen, %
(a) Chemisorption at 100°													
24	0.9191	15.02	0.16	0.04	0.62	0.00	0.05	3.04	0.02	0.44	0.42	11.42	108
119	1.0507	23.95	.01	.01	.25	.02	.03	3.52	.02	.03	.19	19.05	97
120	1.0265	18.10	.07	.00	.25	.04	.01	3.46	.05	.02	.17	14.77	104
126	1.0282	4.77	.02	.00	.47	.00	.01	3.44	.01	.03	.15	0.87	105
127	1.0464	2.71	.00	.00	.88	.00	.00	2.75	.02	.00	.13	0.03	141
129	1.3437	2.93	.00	.02	1.01	.01	.00	1.71	.01	.01	.05	0.31	107
(b) Chemisorption at 150°													
136	0.9048	22.32	0.03	0.00	0.14	0.53	1.61	5.62	0.08	0.05	0.20	12.14	91
137	.8544	14.70	.03	.00	.22	.27	0.91	4.33	.07	.04	.16	8.32	98
138	.9068	8.00	.01	.00	.28	.11	0.90	4.68	.05	.06	.18	1.01	91
139	.9041	19.61	.03	.03	.35	.49	1.18	5.91	.07	.07	.22	10.47	96
140	.9062	8.38	.03	.04	.22	.10	0.68	4.33	.08	.07	.16	1.68	88
141	.9045	13.77	.00	.01	.32	.32	1.00	5.29	.07	.09	.19	5.58	93

TABLE III

RATES OF FORMATION OF H_2O AND CO_2 DURING THE SWEEPING OF NEW BONE CHAR AT 400° WITH HYDROGEN

Time, hr.	H_2O	CO_2
	mmoles/g. of carbon/hr.	
2.0	0.49	0.265
4.0	.45	.055
6.0	.46	.043
24.7	.53	.019

TABLE IV

WATER PRODUCED BY PASSAGE OF HYDROGEN THROUGH CONDITIONED ORIGINAL SAMPLES OF A NEW BONE CHAR (CHAR 2) AT 400°

Expt.	Flow of H_2, ml./min.	Total H_2, mmoles	H_2O produced/g. carbon, mmoles
115	178.8	8,140	27.1
114	136.1	5,650	25.0
106	27.7	1,780	14.0
107	202.3	13,000	76.5

influence on the decomposition of the chemisorption complex at 200°.

The quantity of oxygen desorbed in the products at 200° was always an appreciable amount regardless of the magnitude of the residual O_2. Reference to Table I will show that the residual O_2 varied considerably and depended, of course, on the quantity of O_2 originally introduced. It is important to note that residual O_2 was present in the final mixture even when only a fraction of the limiting chemisorption was realized. This fact also points to the retarding influence of the combustion products on the decomposition of the chemisorbed complex.

The increase in temperature from 200 to 400° released an additional quantity of chemisorbed oxygen which was one- to three-fold greater in magnitude than that released at 200°, the extent depending on the particular carbon adsorbent used.

The total chemisorbed oxygen determined from the sum of the decomposition products at $t°$ and at 400° and expressed in milliatoms per gram of car-

bon in the sample, is plotted as a function of the residual O_2 in Fig. 2. There is a definite leveling-off of these curves with increase in residual O_2. This has been interpreted as a trend toward saturation of the surface with oxygen. In the case of new bone char, shown in Fig. 2II, the limiting values for chemisorption at 100° (curve G), 150° (curve F) and 200° (curve E) were estimated to be 4.0, 8.3 and 12.5 milliatoms per gram, respectively. These values seem to be linearly dependent on temperature.

The oxygen chemisorbed on the four materials at 200° as a function of the residual oxygen is given in Fig. 2I. The limiting values for chemisorption are given in Table VII. From the B.E.T. surface area and the carbon content, the limiting chemisorption per square meter of surface was calculated for each material. It was assumed that the carbonaceous residue covered all of the surface area. The limiting chemisorption corresponded to surface coverages of 1 to 6% that of a monolayer of covalent oxygen atoms (0.66 Å. radius) in close-packed formation. The monolayer corresponded to 0.11 milliatom oxygen per square meter, an obviously high figure because all of the B.E.T. area of the adsorbent could not chemically react with the oxygen. The value given for the limiting oxygen chemisorption, stable in the interval between $t°$ and 400°, was only a fraction of the absolute magnitude of oxygen on the surface. Because of these two opposite tendencies, the percentages of oxygen coverage given in Table VII were much smaller than the actual coverages.

Hydrogen Treatment.—One result of the hydrogen treatment at 400°. see Table V, was to increase the oxygen chemisorbed from the limiting value of 12.5 to 14.2 milliatoms oxygen per gram of carbon in the sample (see Fig. 2III). The increase of about 14% falls short of that which might be expected on the basis of the H_2O formed in the prior hydrogen treatment. Presumably covalent C–H bonds were formed as a result of the treatment.

There was no detectable change in the surface

Table V

DISPOSITION OF OXYGEN IN CHEMISORPTION EXPERIMENTS AT 200° FOR A NEW BONE CHAR (CHAR 2) AFTER PRELIMINARY TREATMENT WITH HYDROGEN AT EITHER 400 OR 200°

1	2	3	4	5	6	7	8	9	10	11	12	13	14
								Milliatoms of oxygen					
			As H_2O from			As CO_2 from			As CO from				
Expt. no.	Wt. of carbon in sample, g.	Introduced	Combustion	Desorption at 200°	Additional desorption up to 400°	Combustion	Desorption at 200°	Additional desorption up to 400°	Combustion	Desorption at 200°	Additional desorption up to 400°	Residual	Recovery of oxygen %
					(a)	Hydrogen	treatment at 400°						
104	1.1330	13.94	0.03	1.33	2.00	1.75	2.93	6.35	0.04	0.03	0.31	0.02	106
106	1.0431	14.57	.03	1.36	1.89	1.60	2.69	5.37	.05	.14	.29	0.01	96
107	1.0498	14.13	.03	1.30	1.33	2.39	2.99	5.38	.04	.05	.25	0.05	98
114	1.0419	19.42	.06	1.19	1.97	3.74	2.89	7.05	.17	.07	.30	1.26	96
115	1.0584	28.70	.05	1.39	1.84	6.04	3.97	7.54	.18	.02	.33	6.71	98
					(b)	Hydrogen	treatment at 200°						
108	1.0486	14.96	0.04	1.37	1.37	4.51	3.74	7.23	0.09	0.06	0.23	2.95	144
109	1.0394	14.77	.01	0.83	1.24	4.09	3.51	7.28	.10	.10	.27	2.73	137
110	1.0000	14.65	.01	.42	1.19	3.69	2.86	6.94	.08	.05	.24	4.12	134
130	0.9841	7.46	.02	.03	0.80	0.49	1.50	5.10	.05	.02	.18	0.00	110
132	0.9924	28.85	.05	.14	1.35	6.47	3.21	8.10	.24	.03	.21	8.90	99
134	1.0001	22.27	.03	.16	0.89	4.31	0.68	7.39	.14	.03	.21	5.86	89

Table VI

OXYGEN WHICH REACTED IN EACH SERIES OF EXPERIMENTS (200° CHEMISORPTION) REGROUPED ACCORDING TO COMBUSTION PRODUCTS AND DECOMPOSITION PRODUCTS

Carbon adsorbent	No. of expt.	Combustion products at 200°, %	Decomposition products, % at 200°	Decomposition products, % 200° < $t°$ ≤ 400°
New bone char (a) Char 2 (different initial samples)	4	19	19	62
New bone char (b) Char 2 (sequence expt.)	9	16	26	58
Service bone char (c) Char 32	5	36	20	44
Service bone char (d) Char P-1	2	46	18	36
Coconut shell charcoal (e) Char 1	6	73	15	12
Channel black	3	54	14	32

area of the new bone char as a consequence of the hydrogen treatments. The B.E.T. areas after experiments 106, 114 and 110 (see Table V) were 121, 122 and 124 m.²/g., respectively; these values agree with those of the original samples. Also, no significant change in B.E.T. area was observed as a result of the oxygen chemisorption experiments at 200°.

The value of C/H in the total gaseous products was lowered as a consequence of the prior hydrogen treatment of the sample. The average value of 5 (atomic ratio) without the hydrogen treatment was reduced to 1.1 when the prior H_2 treatment was at 400°, and to 2.3 when that treatment was at 200°. Furthermore, oxygen which combined to form water in appreciable quantities during the chemisorption experiments with hydrogen-treated samples did not appear in the combustion products (see columns 4, 5 and 6 in Table V). Heating up to 400° was necessary to decompose that part of the complex containing the largest amount of hydrogen which had been introduced during the prior hydrogen treatment. These results definitely indicate that hydrogen had been incorporated in the carbonaceous residue. Although a significant change in C/H occurred in the hydrogenation at both 200 and 400°, only the treatment at 400° seemed to have an influence on the subsequent oxygen chemisorption as shown in Fig. 2 (curve H is significantly different from curve A (or E) although curve I probably is not).

Ratio of Oxygen Content in CO_2 to that in CO in the Descrption Products.—One significant difference was observed between chemisorption in the sequence experiments and those in which an original

Table VII

FRACTIONAL SURFACE COVERAGE BY OXYGEN CHEMISORPTION

Char	Surface area, m.²/g.	C, %	Limiting chemisorption (milliatoms oxygen) Per g. carbon	Per g. adsorbent	Per sq. meter surface	Coverage %
New bone char (Char 2)	121	6.1	12.5	0.76	0.0063	6
Service bone char (Char 32)	63	6.8	5	.34	.0054	5
(Char P-1)	50	6.0	5	.30	.0060	6
Coconut shell charcoal (Char 1)	1700	94	1	.94	.00055	0.6
Channel black	147	96	0.3	.29	.0020	2
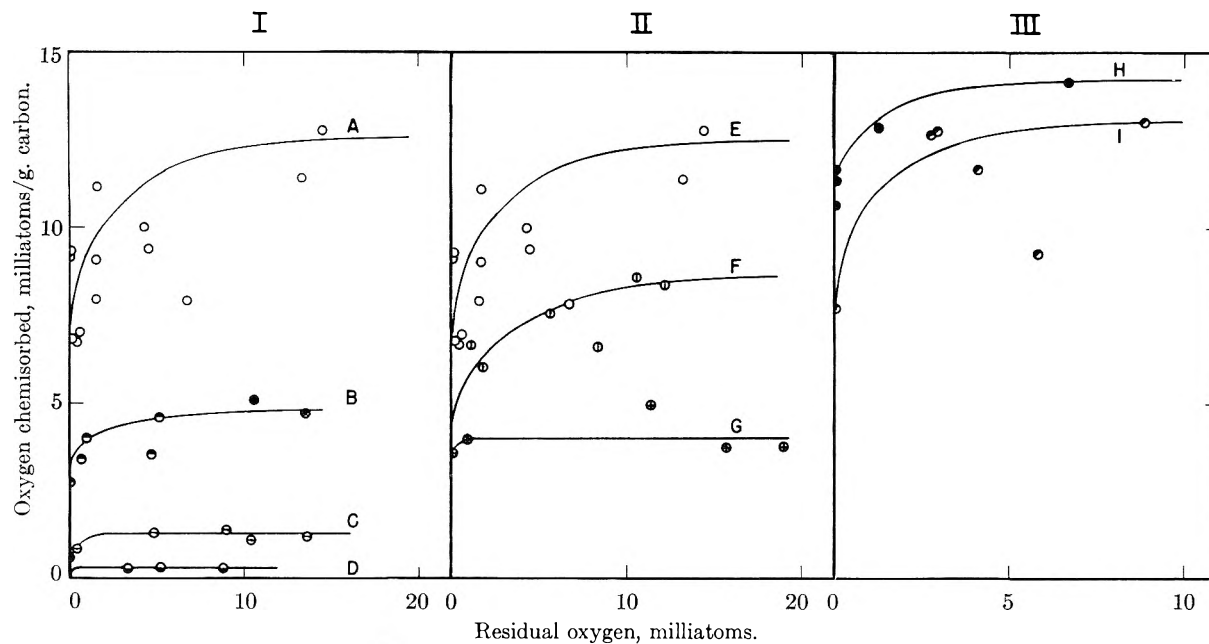
Fig. 2.—Chemisorption of oxygen by carbons under various conditions: I, comparison of different carbons when exposed to oxygen at 200°: (A) new bone char (Char 2), (B) service bone chars (Char 32 and Char P-1), (C) coconut shell charcoal (Char 1), (D) channel black; II, effect of temperature of exposure upon the amount of oxygen chemisorbed by a new bone char (Char 2): (E) 200° (same as curve A), (F) 150°, (G) 100°; III, effect of prior hydrogen treatment upon the amount of oxygen chemisorbed by a new bone char at 200°: (H) 400° hydrogen treatment, (I) 200° hydrogen treatment.

sample was used. The ratio of oxygen in CO_2 to that in CO contained in the desorption products de-

creased (rapidly at first) from one experiment to the next in the sequence experiments. The oxygen

TABLE VIII

RATIOS (R) OF OXYGEN AS CO_2 TO THAT AS CO IN THE TOTAL DESORPTION GASES (ORIGINAL DATA IN TABLES I, II, III)

Expt. no.	O in CO	R	Expt. no.	O in CO	R	Expt. no.	O in CO	R
			New bone char (Char 2) using original samples					
	at 200°			at 500°			at 100°	
101	0.26	37	136	0.25	29	24	0.86	4
131	.19	38	137	.20	26	119	.22	16
133	.24	38	138	.24	23	120	.19	18
135	.21	37	139	.29	24	126	.18	19
			140	.23	22	127	.13	21
			141	.28	22	129	.06	28
Av.	.23	38	Av.	.25	24	Av.	.21	18
			New bone char (Char 2)					
				150°				
				H_2 treatment at 400°			H_2 treatment at 200°	
	In sequence at 200°			O_2 chemisorbed at 200°			O_2 chemisorbed at 200°	
4	0.20	32	104	0.34	27	108	0.29	38
5	.17	31	106	.43	20	109	.37	29
6	.20	30	107	.30	28	110	.29	34
7	.26	14	114	.37	27	130	.20	33
8	.22	17	115	.35	33	132	.24	47
9	.24	12				134	.24	36
10	.24	12						
11	.24	13						
12	.27	17						
Av.	.23		Av.	.36	27	Av.	.27	36
	Channel black in sequence			Char 1 in sequence			Char 32 in sequence	
	at 200°			at 200°			at 200°	
111	0.68	2.4	18	0.21	3.0	13	0.76	4
112	.51	2.0	19	.58	0.7	14	.19	17
113	.57	2.3	20	.19	1.1	15	.29	12
			21	.41	1.0	16	.22	11
			22	.36	0.6	17	.34	12
			23	.69	0.5			
Av.	.59		Av.	.40		Av.	.26	

desorbed as CO (Table VIII) remained remarkably constant and the decrease in this ratio was, therefore, the result of change in the oxygen desorbed as CO_2. When original samples of new bone char (Char 2) were employed, a constant ratio of 38 was obtained. Table VIII shows a definite initial decrease in this ratio for a given sample of Char 2 as the oxygen was successively chemisorbed and the decomposition products removed. (It should be noted that several exposures to oxygen had preceded expt. 4 which accounts for the initial value of 32 instead of about 38.) The ratio seemed to approach a limiting value of 12 for both new and service bone chars.

The ratios of oxygen appearing as CO_2 to that as CO in the desorption products for new bone char were smaller the lower the temperature at which the oxygen complex had formed. The average values of this ratio for original samples at 200, 150 and 100° were 38, 24 and 18, respectively. Again, the oxygen desorbed as CO remained substantially constant over this temperature interval. It did vary, however, with the type of carbonaceous material: bone chars, 0.23; coconut shell charcoal, 0.40 and channel black, 0.59.

V. Concluding Remarks

In view of the apparent aging effects indicated by the changing ratio of oxygen in CO_2 to that in CO in the desorption products, there is the possibility that the final state of the surface attained after the treatment at 400° for 24 hours was not an exact replica of the initial state. The quantitative recovery of oxygen in each experiment indicates a reproducible effect insofar as the mass transfer of oxygen is concerned. This is consistent with the findings of McKie.[6]

It has been shown that oxygen stripped from the char by hydrogenation was not quantitatively replenished by subsequent oxygen chemisorption. This can be explained by the fact that some of the hydrogen actually entered into combination with the carbonaceous residue during the hydrogen treatment. In this way the access of additional oxygen was denied by a chemical modification of the surface.

The two processes of chemisorption and combustion do not occur independently of one another. The curves shown in Fig. 3 show the reacted oxygen as a function of residual O_2 divided according to that in the adsorbed complex and that in gaseous products. The curves for new bone char are shown

(6) D. McKie, *J. Chem. Soc.*, 2870 (see page 2882) (1928).
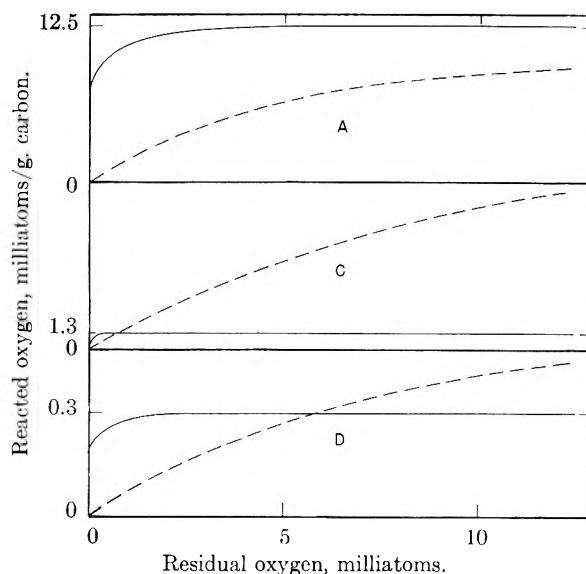
Fig. 3.—Division of reacted oxygen into chemisorption complex (unbroken curves) and combustion gases (broken curves) for different carbonaceous materials: (A) bone chars; (C) coconut shell charcoal; (D) channel black.

in Fig. 3A. The relative positioning of the two curves (chemisorption and combustion) was also found to be the same for service bone chars (Chars 32 and P-1). The magnitude of the ordinate for the service bone chars, however, was lowered in the same proportion shown by curves A and B in Fig. 2I.

The general shapes of all the chemisorption curves (Figures 2 and 3) were similar. Differences between the various adsorbents were shown, however, by differences in the relative magnitudes of chemisorption and combustion associated with each material. The chemisorption curve was above the combustion curve for bone chars (curve A of Fig. 3) and the reverse was true for the coconut shell charcoal (curve C of Fig. 3), while the channel black (curve D of Fig. 3) showed a crossing of the two curves.

The above results indicate that the chemisorption complexes formed in the presence of excess oxygen may be made to decompose in two ways: (1) by an increase in temperature to an extent determined by the relative stabilities of the complexes; (2) by a removal of the decomposition products, either by flow of an inert gas or by evacuation. The presence of the combustion products in contact with the complex appears to exhibit an inhibiting influence on its decomposition.

STUDIES ON THE SOL–GEL TRANSFORMATION OF THE FERRO- AND FERRICYANIDES OF SOME METALS. PART I. GEL FORMATION OF PRUSSIAN AND TURNBULL BLUES

By Khwaja Nasiruddin, Wahid U. Malik and Abani K. Bhattacharya

Physical Chemistry Section, Chemical Laboratories, Muslim University, Aligarh, India

Received November 9, 1953

Prussian and Turnbull blue gels were prepared by von Weimarn's method at the optimum concentration of the reactants. It has been observed that the sol–gel transformation becomes possible at a particular range of molecular concentrations of the reactants. The time of setting of the gel was determined by observing the intensity of the transmitted light through the gelation mixture, the intensity of transmission being measured by using a thermopile with galvanometer in the circuit. It was found that the time of setting of the gel depended on the range of proportions in which the reactants were mixed in equivalents. The range of proportions of mixing the reactants, $FeCy_6^{----}/Fe^{+++}$, for Prussian blue was found to lie between 1.404 and 1.5. In the case of Turnbull blue, the range of proportion of mixing the reactants, $FeCy_6^{---}/Fe^{++}$, was between 1.01 to 1.5.

It is difficult to define a gel because the properties of different types of inorganic and organic gels are so variegated that no rigid definition of the gel state has so far been possible. Neither has it been possible to give any general explanation of different types of jellies. But the fact remains that inorganic gels are usually rigid and non-elastic as distinguished from the organic jellies. The inorganic gel formation, according to von Weimarn,[1] takes place due to supersaturation in such a manner that particles of suitable dimensions, obtained by varying the concentration of the reactants, may condense to assume the gel structure.

Previous authors[2-17] have studied the sol–gel transformation from several aspects of many inorganic colloids such as silicic acid, metallic hydroxides, arsenates, molybdates, phosphates, borates, etc.

Fig. 1.—Apparatus for time of setting of jellies: G, galvanometer; T, thermopile; J, gelation mixture; P, aperture; N, convex lens; W, water cell; L, bulb; R, variable resistance; A, ammeter.

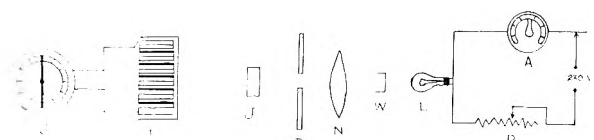Little work, however, has been done on the gel forming behavior of metallic ferro- and ferricyanides. Recently Bhattacharya and co-worker[13] have studied the sol–gel transformation of zinc ferrocyanide at different temperatures and concentrations and have also observed the changes in conductivity during gel formation.

We have studied the sol–gel transformation of Prussian and Turnbull blues from two aspects, *viz.*, (i) the limiting ranges of concentration and proportion of the respective reactants which favor gel formation and (ii) the variation in the time of setting of the gels with respect to the ratio of mixing of the reactants ($FeCy_6^{----}/Fe^{+++}$ and $FeCy_6^{---}/Fe^{++}$).

In this paper, we communicate the results of our investigations on the conditions which favor the gel formation of Prussian and Turnbull blues by von Weimarn's method, and our findings on the time of setting of these gels, determined by observing the variation in the intensity of the transmitted light using a thermopile galvanometer arrangement.

Experimental

The solutions were all prepared by dissolving A. R. or recrystallized samples in distilled water. Their strengths were as follows: 1, $K_4Fe(CN)_6$ solution—0.712 M (estimated volumetrically against $KMnO_4$ solution); 2, $FeCl_3$ solution—2.87 M (estimated as Fe_2O_3); 3, $K_3Fe(CN)_6$ solution—1.35 M (estimated iodometrically); 4, $FeSO_4$ (recrystallized) solution—2.14 M (estimated volumetrically against $K_2Cr_2O_7$ solution).

The concentrations of the different solutions were adjusted according to requirements.

The conditions of gel formation were determined by mixing the reactants at different concentrations and ratios. It was observed in the case of Prussian blue that gels were formed by mixing K_4FeCy_6 of concentrations ranging between 0.5 and 0.7 M with $FeCl_3$ between 1.9 and 2.7 M, in the ratio $FeCy_6^{----}/Fe^{+++}$ between 1.404 and 1.50. In the case of Turnbull blue the gels could be formed by mixing K_3FeCy_6 between 0.5 and 1.25 M with $FeSO_4$ between 0.4 and 1.9 M, in the ratio $FeCy_6^{---}/Fe^{++}$ between 1.01 to 1.50. Gentle shaking of the mixture after mixing the reactants was very necessary for the formation of the gels in all cases. The temperature was maintained throughout at $33 \pm 0.1°$.

Determination of the Time of Setting of Prussian and Turnbull Blue Gels.—The method based on the variation of scattered light was used by Mardles[19] and also by Mata Prashad and co-worker (ref. 12) to determine the time of setting. Our arrangement is shown diagrammatically in Fig. 1. The source of radiation was a bulb of 300 watts running at 230 volts and 1.3 amperes and the light was focussed for a parallel beam of long focal length. The beam

(1) P. P. von Weimarn, "Zur Lehre von den Zustanden der Materie," Leipzig, 1914.
(2) W. Flemming, *Z. physik. Chem.*, **41**, 427 (1902).
(3) H. N. Holmes and R. E. Rindfusz, *J. Am. Chem. Soc.*, **38**, 1970 (1916).
(4) H. N. Holmes and R. Arnold, *ibid.*, **40**, 1014 (1918).
(5) H. N. Holmes and P. H. Fall, *ibid.*, **41**, 763 (1918).
(6) M. E. Laing and J. W. McBain, *J. Chem. Soc.*, **117**, 1506 (1920).
(7) E. O. Kraemer, Colloid Symp. Monograph, Wisconsin, Vol. I, 1923, p. 66.
(8) A. Szvergi and F. E. Schalek, *Kolloid Z.*, **32**, 318 (1923).
(9) A. Kuhn, *ibid.*, **40**, 299 (1928).
(10) Wo. Ostwald, *ibid.*, **45**, 248 (1928).
(11) S. Prakash and N. R. Dhar, *J. Ind. Chem. Soc.*, **6**, 391 (1929).
(12) Mata Prasad and R. R. Hattiangadi, *ibid.*, **6**, 653 (1929).
(13) C. I. Vardawan, *Proc. Ind. Acad. Sci.*, **7A**, 327 (1938).
(14) V. C. Vora, P. M. Barve and B. N. Desai, *ibid.*, **13A**, 100 (1941).
(15) A. N. Pang Tai and Min-chi Hsu, *J. Chinese Chem. Soc.*, **13**, 17 (1946).
(16) W. K. Kpaczenski, *Bull. soc. chim. France*, 149 (1950).
(17) G. K. Sukhla and S. Ghosh, *J. Ind. Chem. Soc.*, **27**, 323 (1950).
(18) A. K. Bhattacharya and S. A. Joffrey, *ibid.*, **29**, 626 (1952).
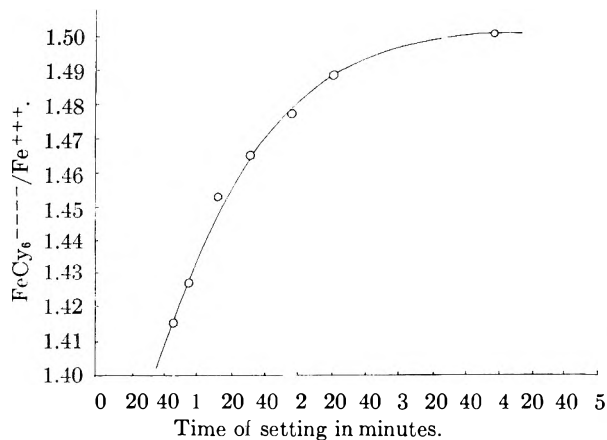(19) E. W. J. Mardles, *Trans. Faraday Soc.*, **18**, 318 (1923).

Fig. 2.—Times of setting of Prussian blue gels obtained by mixing 0.6 M $K_4Fe(CN)_6$ with $FeCl_3$ of concn. range 2.0 to 2.7 M.

was then allowed to pass through a rectangular cell containing water to remove most of the heat rays. It was then allowed to fall on a rectangular cell containing the gel forming mixture. The intensity of light was measured by a thermopile attached to a galvanometer with a lamp and scale arrangement. The distance between the light source and the cell was kept constant throughout.

The amount of $K_4Fe(CN)_6$ required for the particular gel was introduced in the rectangular cell and the corresponding amount of ferric chloride was added slowly from the buret. The mixture was now gently stirred and left to form the gel; the stopwatch was immediately started after stirring. The deflection of galvanometer was noted at regular intervals of time; it decreased rapidly at first and then slowly till it reached a constant value and remained so for about 10 minutes. Two sets of readings were recorded for every gelation mixture. In the first set deflections were noted at intervals of half a minute, while in the second set, readings were recorded every five seconds in order to measure the time of gelation correct within this short range.

In this connection it was necessary to determine the sensitivity of the apparatus by measuring the movements of the mirror galvanometer on the scale, brought about by changing the intensity of light. This was done as follows:

The change in the intensity of the same source of light placed at different distances from the thermopile was read in the galvanometer. The relative decrease in the intensity of the transmitted light was calculated from the relationship $I \propto 1/r^2$ where I is the intensity of the light and r, the distance of the light source from the thermopile. It was calculated from the observed values that 0.42% fall in intensity corresponded to 1 mm. deflection on the scale. The sensitivity of the instrument was thus up to 0.42% fall of intensity of the light used.

The maximum difference in the deflection recorded during the gel formation of Prussian blue was 9.3 cm. on the scale, corresponding to 41.04% fall in the intensity of the original source. The maximum differences of deflection observed in the case of Turnbull blue for gels obtained with different concentrations of the reactants were 9.8, 13.8 and 16.5 cm. corresponding to 41.6, 73.3 and 80.0% fall in intensity, respectively. The opacity of the gel may, therefore, be assumed to correspond to the fall in intensities calculated from the changes in deflections of the galvanometer during the setting of different gels.

The experimental results showing the relationship between the ratio of the reactants ($FeCy_6^{----}/Fe^{+++}$; $FeCy_6^{---}/Fe^{++}$) and the times of setting have been represented graphically in Figs. 2 and 3. Prussian blue gels containing varying proportion of the reactants ($FeCy_6^{----}/Fe^{+++}$) were obtained by mixing calculated volumes of 0.6 M $K_4Fe(CN)_6$ and $FeCl_3$ of concentrations ranging between 2.0 and 2.7 M. For Turnbull blue, however, a wider concentration range (0.625 to 1.25 M) could be used to obtain the gels. The concentration ranges for different gels used were $FeSO_4^{---}$ 0.6 to 1.5 M, 0.8 to 1.9 M and 0.9 to 1.9 M for $K_3Fe(CN)_6$ solution of concentrations 0.6, 1.0 and 1.25 M, respectively (represented by curves 1, 2 and 3 in Fig. 2).
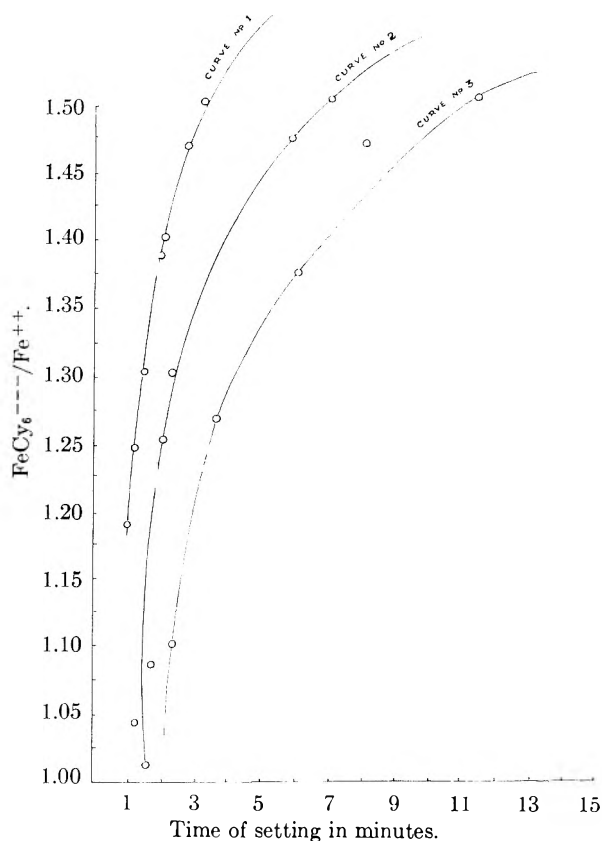
Fig. 3.—Times of setting of Turnbull blue gels obtained by mixing: 1, 0.6 M $K_3Fe(CN)_6$ with $FeSO_4$ of concn. range 0.6 to 1.5 M; 2, 1.0 M $K_3Fe(CN)_6$ with $FeSO_4$ of concn. range 0.8 to 1.9 M; 3, 1.25 M $K_3Fe(CN)_6$ with $FeSO_4$ of concn. range 0.9 to 1.9 M.

Discussion

Our experimental results on the study of gelation of Prussian and Turnbull blues in relation to the concentration and proportion of mixing the reactants present the following interesting points:

(1) Prussian and Turnbull blues tend to form a gel within specific concentration and proportion range of the reactants (vide Experimental).

(2) The time of setting of the Prussian blue gel is considerably influenced by the ratios of $FeCy_6^{----}/Fe^{+++}$. The gelation time at first increases with the ratio of $K_4Fe(CN)_6$: $FeCl_3$ up to the value 1.452:1.0 after which the time of gelation increases more rapidly as $FeCy_6^{----}/Fe^{+++}$ increases from 1.452 to 1.50 (vide Fig. 2). In the gelation of Turnbull blue the variations of the time of gelation with the ratio $FeCy_6^{---}/Fe^{++}$ are similar, though not identical (vide Fig. 3). It may be noted that Turnbull blue was prepared by adding $FeSO_4$ while Prussian blue was prepared by adding $FeCl_3$. The difference in the role of Cl^- and SO_4^{--} ions during gel formation may be an important factor and hence the question of identical results does not arise.

The time of setting for Turnbull blue is longer for the higher concentration (1.25 M) than for the lower concentration (0.625 M) of potassium ferrocyanide. But in the case of Prussian blue the concentration range of potassium ferrocyanide is as narrow as 0.5 to 0.7 mole per liter.

According to von Weimarn the gelation is controlled by the dispersion coefficient δ of the precipitate as given by the equation $\delta = c/s\,\eta$ where c/s is the degree of supersaturation and η is the viscosity. At suitable higher concentrations of the reactants, they eventually set into a viscous jelly. But our observations suggest that both concentration and proportion of mixing the reactants are the controlling factors in the formation of Prussian and Turnbull blue gels. The optimum dispersion coefficient of the precipitate governed by the concentrations of the reactants, however, does not furnish an explanation to the different times of setting observed by changing the ratio of $FeCy_6^{----}/Fe^{+++}$ or $FeCy_6^{---}/Fe^{++}$. Since the tendency of gelation is also governed by the hydration of the colloidal micelle, it follows that the time required in the setting of the gel would depend on the hydration of the particles. Dhar[20] and co-workers established that the hydration depends upon the charge on the particles. Bhattacharya and Dhar[21] showed that the adsorption of ferrocyanide ions by Prussian blue is 100 times greater than the adsorption of $FeCy_6^{---}$ by Turnbull blue sol prepared by mixing the reactants

under identical conditions in the molecular proportion 1:1.5. From the foregoing evidence it follows that the hydration of Prussian blue micelle will fall more considerably by the concentration of $FeCy_6^{----}$ than that of Turnbull blue by increasing the concentration of $FeCy_6^{---}$. Hence the range of ferrocyanide ions concentration for the setting of Prussian blue gel would be lower than that of Turnbull blue gel, and this has actually been observed.

Our observations further suggest that the ratios of $FeCy_6^{----}/Fe^{+++}$ or $FeCy_6^{---}/Fe^{++}$ influencing the time of gelation are specific for the optimum range of the concentrations of the reactants. The ratio of $FeCy_6^{----}/Fe^{+++}$ or of $FeCy_6^{---}/Fe^{++}$ and the corresponding time of gelation (vide Figs. 1 and 2) are only for those concentrations of the reactants as has been obtained by trials in our experiments. Hence at concentrations other than those employed by us, the gelation may not take place at all, because it appears that the formation of inorganic jellies is not only controlled by dispersion coefficient but also by the optimum hydration of the dispersed particles.

Further work on the gelation of precipitates is in progress in these laboratories.

Thanks of the authors are due to Prof. M. O. Farooq, Head of the Department of Chemistry, for his keen interest in this work.

(20) K. C. Sen, P. B. Ganguly and N. R. Dhar, THIS JOURNAL, **28**, 313, 457 (1924); N. R. Dhar and V. Gore, J. Ind. Chem. Soc., **6**, 641 (1929); N. R. Dhar and K. C. Sen, Kolloid Z., **34**, 362 (1924).

(21) A. K. Bhattacharya and N. R. Dhar, Z. anorg. Chem., **213**, 240 (1933).

STUDIES ON THE SOL–GEL TRANSFORMATION OF METALLIC FERRO- AND FERRICYANIDES. PART II. STUDIES ON THE CONDUCTIVITY CHANGES OF THE DIALYZED PRUSSIAN AND TURNBULL BLUES DURING THEIR GEL FORMATION

BY WAHID U. MALIK AND ABANI K. BHATTACHARYA

Physical Chemistry Section, Chemical Laboratories, Muslim University, Aligarh, India

Received November 9, 1953

Prussian and Turnbull blues were precipitated by mixing different concentrations of $FeCl_3$ with $K_4Fe(CN)_6$ (Prussian blue) and of $FeSO_4$ with $K_3Fe(CN)_6$ (Turnbull blue) in the ratio $FeCl_3:K_4Fe(CN)_6$ as 1:1.5 equivalents, and also $FeSO_4:K_3Fe(CN)_6$ in the same ratio. The turbid precipitate so obtained was dialyzed, and changes in conductivity were measured at different intervals. On pipetting out the dialyzed samples in test-tubes, it was curiously observed that at particular stages of dialysis, the dispersed precipitate was transformed into gel. The conductivity changes, during the period of dialysis when gelation took place, were either very small or practically constant, depending upon the specific concentration of the reactants mixed. It was further observed that the gelation of Prussian blue was not much influenced by varying the concentration of $FeCl_3$ over a wide range (0.5 to 1.5 M) while the gelation of Turnbull's blue was very much distributed by changing the concentration of $FeSO_4$ within as narrow a range as 0.4 to 0.35 M.

In continuation of our observations on the sol-gel transformation of Prussian and Turnbull blues in Part I, we have studied the conductivity changes brought about in the turbid precipitate during its transformation into gel by dialysis.

Changes in conductivity during gelation have been studied for silicic acid, cerium hydroxide and thorium hydroxide and other gels by a number of workers.[1-5] These authors observed that in some

cases there was no conductivity change during gelation while in others marked changes could be observed and that no general relationship could be arrived at for inorganic gel-forming systems. In this paper we communicate our results on the conductivity changes on dialysis of the precipitates of Prussian and Turnbull blues obtained by mixing the reactants at different concentrations.

Experimental

Solutions were prepared by dissolving A. R. or recrystallized samples of the reactants in conductivity water and their strengths determined. The strengths were as follows: $K_4Fe(CN)_6$ solution—0.5 M (estimated volumetrically against $KMnO_4$ solution); $FeCl_3$ solution—2.05 M (estimated as Fe_2O_3); $K_3Fe(CN)_6$ solution—1.04 M (estimated iodometrically); $FeSO_4$ (recrystallized) solution—1.16 M (estimated volumetrically against potassium dichromate).

(1) M. E. Laing and J. W. McBain, J. Chem. Soc., **117**, 1506 (1920).

(2) N. R. Dhar and D. N. Chakravarty, Z. anorg. allgem. Chem., **168**, 209 (1927); N. R. Dhar and S. Prakash, J. Ind. Chem. Soc., Prafulla No. 104 (1933).

(3) D. S. Datar and M. Qureshi, J. Osmania Univ. Z., 5 (1939).

(4) B. N. Desai, P. M. Barve and Y. S. Paranjpe, Proc. Roy. Soc. Edinburgh, **59**, 22 (1939).

(5) V. C. Vora and B. N. Desai, Proc. Ind. Acad. Sci., **13A**, 100 (1941).

Prussian and Turnbull blues obtained by mixing concentrated solutions of the reactants in the ratio $1:1.5$ equivalents resulted in the formation of a turbid precipitate, which, on dialysis, dispersed in such a manner as to form a gel depending on the period of dialysis. On prolonged dialysis it was observed that the dispersion lost its gel-forming character, ultimately changing into a sol. No gel formation was, however, observed when $FeSO_4$ solution of concentration less than $0.4\ M$ was used for the precipitation of Turnbull blue.

Conductivity measurements were carried out by a Kohlrausch bridge (Griffin and Tatlock) at $25 \pm 0.1°$ and observations were recorded at intervals of half an hour or more. The cell used was of Hittorf's type with platinized electrodes. The dialyzed sample at each interval was pipetted out from the dialyzing bag into the cell for measuring conductivity, as well as in a test-tube (left undisturbed) to note whether gelation takes place or not. This was indicated when the liquid ceased to flow on inverting the test-tube. The interval required to attain this condition from the time of pipetting the sample in the tube was taken as the setting time of the gel.

In the case of Prussian blue, the following concentrations of the reactants in the ratio $1.5:1$ equivalents $(FeCy_6^{----}/Fe^{+++})$ were used: (1) 300.0 cc. of $0.5\ M$ $K_4Fe(CN)_6$ was mixed with 89.0 cc. of $1.5\ M$ $FeCl_3$; (2) 225.0 cc. of $0.5\ M$ $K_4Fe(CN)_6$ was mixed with 135.0 cc. of $0.7\ M$ $FeCl_3$; (3) 225.0 cc. of $0.5\ M$ $K_4Fe(CN)_6$ was mixed with 200.0 cc. of $0.5\ M$ $FeCl_3$.

The changes in conductivity at different hours of dialysis for the precipitates no. 1, 2 and 3 are graphically represented by curves no. 1, 2 and 3, respectively, in Fig. 1. Gel formation was observed in all the three cases. Gelation did not take place in the dialyzed precipitates of Turnbull blue prepared by keeping the concentration of $K_3Fe(CN)_6$ constant and varying the concentration of $FeSO_4$ as was done in the case of Prussian blue. Hence Turnbull's blue precipitates were studied by varying the concentration of $K_3Fe(CN)_6$ also. The following concentration of the reactants in the ratio $1.5:1$ equivalents $(FeCy_6^{---}/Fe^{++})$ were used: (1) 138.9 cc. of $0.3\ M$ $K_3Fe(CN)_6$ was mixed with 104.2 cc. of $0.4\ M$ $FeSO_4$; (2) 208.4 cc. of $0.2\ M$ $K_3Fe(CN)_6$ was mixed with 104.2 cc. of $0.4\ M$ $FeSO_4$; (3) 104.2 cc. of $0.4\ M$ $K_3Fe(CN)_6$ was mixed with 139.0 cc. of $0.3\ M$ $FeSO_4$; (4) 104.2 cc. of $0.4\ M$ $K_3Fe(CN)_6$ was mixed with 208.4 cc.

of $0.2\ M$ $FeSO_4$; (5) 118.8 cc. of $0.35\ M$ $K_3Fe(CN)_6$ was mixed with 118.8 cc. of $0.35\ M$ $FeSO_4$.

The changes in conductivity at different stages of dialysis for precipitates no. 1, 2, 3, 4 and 5 are graphically represented by curves no. 4, 5, 6, 7 and 8. Gel formation was only observed for precipitates no. 1 and 2 while in the other three precipitates no gelation was observed.

Discussion

In discussing the observations on the behavior of the dialyzed precipitates of Prussian and Turnbull blues in relation to changes in conductivity, the following points are striking:

(1) The conductivity changes are more pronounced in the earlier stage but the rate of fall of conductivity of the dialyzed sample becomes very small after a certain interval. This slow rate of change continues for some time giving practically constant values during which the sol is characterized by its gel-forming properties observed in the test-tubes, (vide curves 1–5, Figs. 1 and 2).
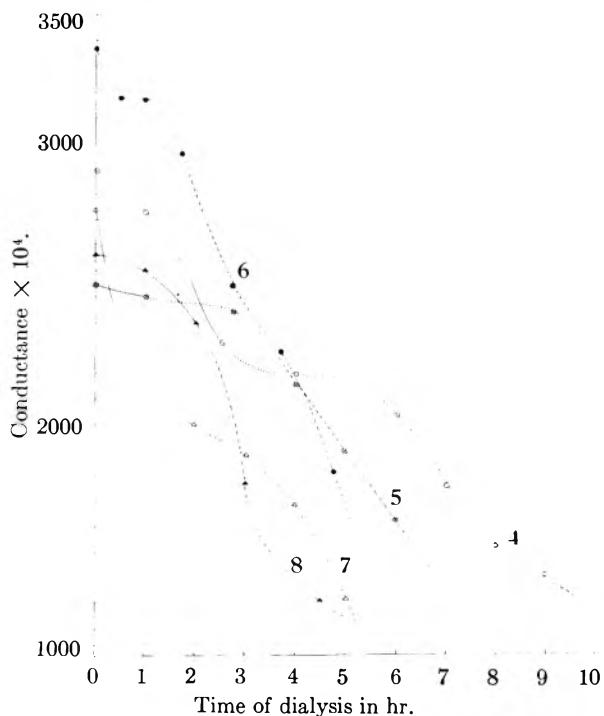
Fig. 2.—Change in conductivity on dialysis of the reaction mixture (Turnbull blue). Reactants mixed in the ratio $FeCy_6^{---}:Fe^{++}$ as $1.5:1$ equiv.: 4, mixture containing 138.9 cc. of $0.3\ M$ $K_3Fe(CN)_6$ and 104.2 cc. of $0.4\ M$ $FeSO_4$; 5, mixture containing 208.4 cc. of $0.2\ M$ $K_3Fe(CN)_6$ and 104.2 cc. of $0.4\ M$ $FeSO_4$; 6, mixture containing 104.2 cc. of $0.4\ M$ $K_3Fe(CN)_6$ and 139.0 cc. of $0.3\ M$ $FeSO_4$; 7, mixture containing 104.2 cc. of $0.4\ M$ $K_3Fe(CN)_6$ and 208.4 cc. of $0.2\ M$ $FeSO_4$; 8, mixture containing 118.8 cc. of $0.35\ M$ $K_3Fe(CN)_6$ and 118.8 cc. of $0.35\ M$ $FeSO_4$... ...⊙...⊙..., region of gelation; --○--○---, region of sol formation.

(2) At a later stage of dialysis, the dispersed particles lose their gel-forming character, changing into a stable sol.

(3) Both in the case of Prussian and Turnbull blues the concentration of the reactants played a very important role in gel formation. The range of concentration of $FeCl_3$ favoring gelation of Prussian blue was 0.5 to $1.5\ M$, while the gelation of Turnbull blue was not possible by changing the concentration of $FeSO_4$ within as narrow a range
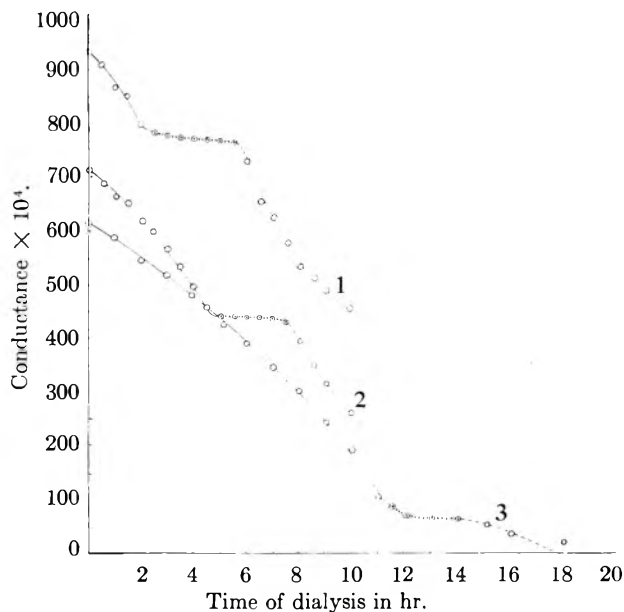
Fig. 1.—Change in conductivity on dialysis of the reaction mixture (Prussian blue). Reactants mixed in the ratio $FeCy_6^{----}:Fe^{+++}$ as $1.5:1$ equiv.: 1, mixture containing 300.00 cc. of $0.5\ M$ $K_4Fe(CN)_6$ and 89.0 cc. of $1.5\ M$ of $FeCl_3$; 2, mixture containing 225.0 cc. of $0.5\ M$ $K_4Fe(CN)_6$ and 135.0 cc. of $0.7\ M$ $FeCl_3$; 3, mixture containing 225.0 cc. of $0.5\ M$ $K_4Fe(CN)_6$ and 200.0 cc. of $0.5\ M$ $FeCl_3$. ...⊙...⊙..., region of gelation; ---○---○---, region of sol formation.

as 0.4 to 0.35 M. This specificity of concentration range of $FeCl_3$ and $FeSO_4$, respectively, appears to be a very essential characteristic of this type of gel-forming system (vide curves no. 6, 7, and 8).

(4) The time of setting of the dialyzed samples to a gel as observed in test-tubes was found to depend on the period of dialysis. (This period was marked by the constancy of conductance (vide curves 1–5). A longer time of setting was observed for a longer period of dialysis within the optimum range of constant conductance.

While it is difficult to experimentally determine all such factors as are responsible for the specific nature of changes described above, it may be observed that the formation of Prussian and Turnbull blue gels studied by dialysis appears to depend on the combined influence of the following factors: (1) hydration of the colloidal micelles which depends upon the net charge on the colloidal particle,

(2) coagulating action of K^+ ions present in the system, (3) the stability factor of the micelles, depending on the nature of entrainment of stabilizing ions and the coagulating effect of the oppositely charged ions.

In course of dialysis, the dispersed particles should have the optimum conditions regulating the above factors to ensure the formation of a gel, sooner or later, depending upon the extent of dialysis.

Further work is in progress in these laboratories on the formation of metallic ferro- and ferricyanide gels by dialysis.

THE BEHAVIOR OF CHROMIUM ON CATHODIC AND ANODIC POLARIZATION

By I. M. Issa, I. A. Ammar and H. Khalifa

Chemistry Department, Cairo University, Giza, Cairo, Egypt

(1) The behavior of chromium on cathodic and anodic polarization was studied at pH 2.02–11.80 using current densities ranging from 7.5×10^{-5} to 7.5×10^{-4} in case of cathodic and 7.5×10^{-5} to 1.5×10^{-3} amp./cm.^{2} in case of anodic polarization. (2) Tafel lines constructed from these results possessed slopes (b) which amounted to 0.15–0.17 and from 0.127–0.17 for hydrogen and oxygen overvoltage except at pH 2.02 at which (b) is 0.088 and 0.080, respectively. (3) Tafel lines for hydrogen overvoltage directly measured in presence of phosphate, borate and phthalate possessed also higher slopes than those at pH 2 and pH 13 (0.15 N NaOH) in absence of the above anions. (4) Calculation of the electron number λ yielded a value of 1 which denotes a slow discharge mechanism for both hydrogen and oxygen evolution.

Various theories have been suggested to explain the mechanism of the electrolytic evolution of hydrogen[1] and oxygen.[2] In a recent publication, Bockris and Potter[3] have discussed the importance of a parameter, λ, called the electron number in elucidating the mechanism of hydrogen overvoltage. The electron number is the number of electrons involved in each act of the rate-determining step. However, little work[4] has been done on hydrogen and oxygen overpotential of chromium. The aim of the present work is to study the behavior of chromium in the course of cathodic and anodic polarization.

Experimental

Two series of measurements were performed; in the first series the potential was measured as a function of time during polarization while in the second series Tafel lines representing the overvoltage for the cathodic evolution of hydrogen were constructed.

(1) J. O'M. Bockris, *Chem. Revs.*, **43**, 525 (1948); J. Horiuti and M. Polanyi, *Acta Physicochim.*, *U.R.S.S.*, **2**, 505 (1935); H. Eyring, S. Glasstone and K. Laidler, *J. Chem. Phys.*, **7**, 1053 (1939); T. Erdey-Gruz and H. Wick, *Z. physik. Chem.*, **A162**, 63 (1932).

(2) V. A. Roiter and R. B. Yampolskaya, *Acta Physicochim*, *U.R.S.S.*, **7**, 247 (1937); J. O'M. Bockris, *Faraday Soc. Disc.*, **1**, 229 (1947); R. W. Gurney, *Proc. Roy. Soc. (London)*, **A134**, 137 (1931).

(3) J. O'M. Bockris and E. C. Potter, *J. Electrochem. Soc.*, **99**, 169 (1952); *J. Chem. Phys.*, **20**, 614 (1952).

(4) J. O'M. Bockris, *Trans. Faraday Soc.*, **43**, 417 (1947).

Series I.—The electrolytic cell shown in Fig. 1a was used. It consisted of a glass vessel A, provided with a tightly fitted rubber stopper B, having the necessary holes. The rubber stopper was cleaned with dilute hydrochloric acid, followed by distilled water and it was finally wrapped with a clean tin foil. Under no condition, the solution in A was allowed to touch the tin foil. The anode C was in the form of a platinum sheet, sealed to a glass tubing. To minimize the diffusion of the anodic gaseous products toward the cathode, the anode was surrounded by a glass jacket ending in a sintered glass disc D. The cathode E (Fig. 1b) was in the form of a chromium rod, about 5 mm. in diameter prepared by mechanical shaping of Kahlbaum metal lumps and fitted to a bent glass tube F by means of paraffin wax, so that only the upper surface, with an apparent area of 0.33 cm.^{2}, was exposed to the solution. Resting upon the electrode surface was a Luggin capillary G, connecting the electrode with a saturated calomel reference electrode. Electrical contact with the cathode was made through a copper wire H soldered to the inner end of the chromium rod. The electrolytic solution used was boiled and cooled in an atmosphere of purified nitrogen, which was bubbled through the solution via the inlet I and was only stopped directly before the polarization was started.

Measurements of the time-potential curves were taken in unstirred solutions. The cathodic polarization was started at a constant current density (between 7.5×10^{-5} to 7.5×10^{-4} a./cm.^{2}) after the electrode had attained steady-state potential, and was continued for a period of 60 minutes during which the potential assumed a new steady-state value. The current was then interrupted and the potential was allowed to decay during a period of 60 minutes, after which the anodic polarization was started and continued for a period of 120 minutes.
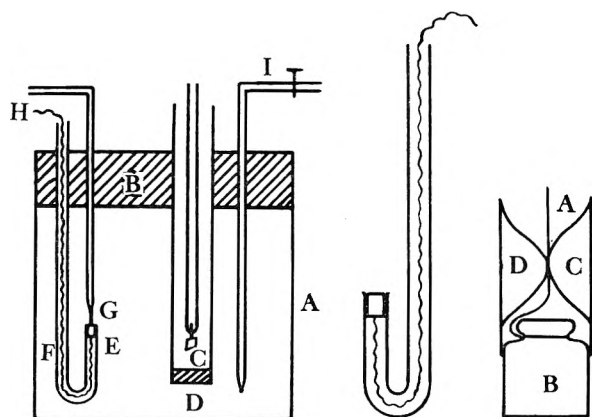
Fig. 1.

The electrolytes used were the Clark and Lubs buffers[5] having the pH values of 2.02, 3.99, 6.24, 8.0 and 10.3 and the Ringer buffer[6] with a pH value of 11.8.

Series II.—For the measurements of hydrogen overvoltage, the electrolytic cell used was similar to that of Bockris and Potter.[3] The cathode was in the form of a chromium Kahlbaum rod (apparent area = 0.73 cm.²), sealed to a glass tubing in the manner shown in Fig. 1c. A thin tungsten wire A was wrapped around one end of the chromium rod B which was squeezed inside a glass tubing and the glass was melted over the tungsten wire at C.

The electrolytes used were pre-electrolyzed[7] for a period of 5 hours on a separate platinum cathode, before the measurements were started. The Tafel lines were traced from high current densities (ca. 6.8 × 10⁻³ a./cm.²) to low current densities (ca. 3.4 × 10⁻⁵ a./cm.²). The electrodes were cathodically polarized at 7 × 10⁻³ a./cm.² for a period of 1 hour in the pre-electrolyzed solution before the measurements were started.

Measurements were taken in solutions of pH 1.9 (HCl and KCl) and pH 13.0 (ca. 0.15 N NaOH), with and without the addition of surface active anions such as phosphate, borate and phthalate.

The potential–time relation for a chromium electrode cathodically polarized at 6.8 × 10⁻⁴ a./cm.², in a solution of pH 13.0 (ca. 15 N NaOH) was also traced using the electrolytic cell of Bockris and Potter.[3]

In both series of experiments, the polarizing current was drawn from a constant device making use of a saturated pentode and a voltage regulator. The direct method of measurements was used and the potential was measured with a Cambridge potentiometer. Measurements were carried out at a constant temperature of 25°.

Results

Representative time–potential polarization curves, at a current density of 7.5 × 10⁻⁵ a./cm.² (for both cathodic and anodic polarizations) are shown in Fig. 2A, for solutions of pH 2.02 (I), 3.99 (II), 6.24 (III), 8.0 (IV), 10.3 (V) and 11.8 (VI), respectively. The cathodic part of the time–potential curve, in a solution of pH 13.0 (ca. 0.15 N NaOH), at a current density of 6.8 × 10⁻⁴ a./cm.², is given in Fig. 2B. The potentials (E_h) referred to the reversible hydrogen electrode are given in millivolts and the time t, is in hours.

The cathodic part, ab, of the polarization curves is characterized by an initial jump in potential, followed in most cases by a region of nearly constant potential. In solutions of pH 2.02 (curve I, Fig. 2A) and pH 13.0 (Fig. 2B), the cathodic part of the curve exhibits a hump before the constant

(5) W. M. Clark and H. A. Lubs, J. Biol. Chem., 25, 479 (1916).

(6) Cited in H. T. S. Britton, "Hydrogen Ions," Vol. I, Chapman and Hall, London, 1942, p. 311.

(7) A. Azzam, J. O'M. Bockris, B. Conway and H. Rosenberg, Trans. Faraday Soc., 46, 918 (1950).
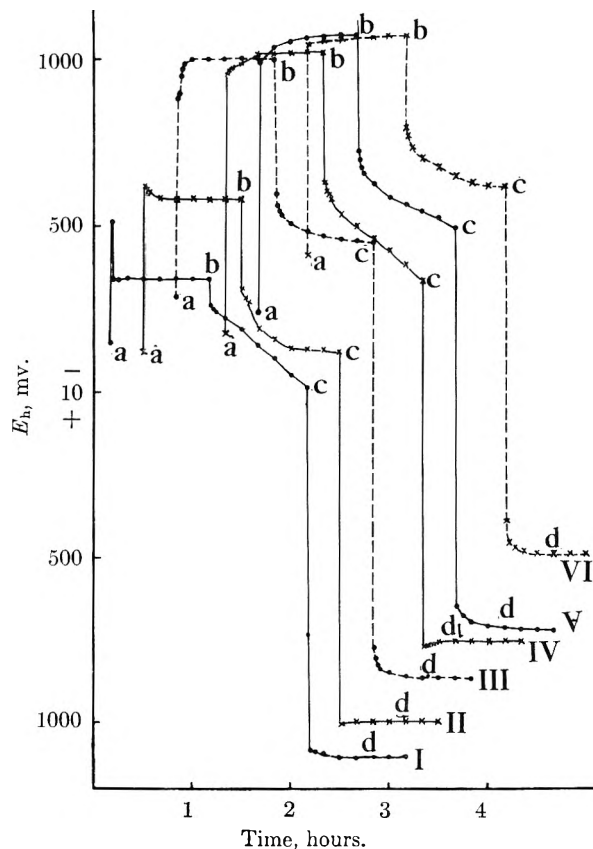
Fig. 2A.—Time vs. E_h in mv.; cathodic and anodic current density = 7.5 × 10⁻⁵ amp./cm.².

potential is attained. This hump also appears, although with a smaller magnitude in a solution of pH 3.99 (curve II, Fig. 2A). The cathodic decay part, bc, of the above curves, is characterized by an initial drop followed by a less steep change lying in
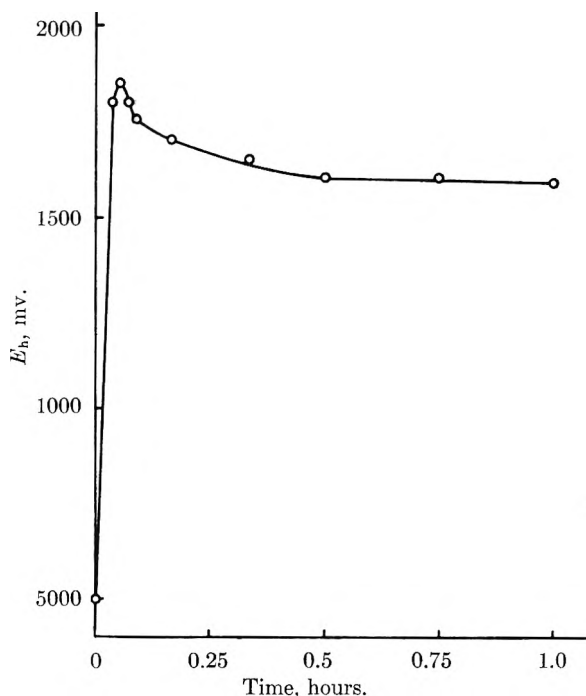

Fig. 2B.—Time vs. E_h in mv.

pH	η at 7.5×10^{-5} (v.)	η at 3×10^{-4} (v.)	η at 7.5×10^{-4} (v.)	i_0 (a./cm.²)	b	λ
2.02	−0.228	−0.275	−0.282	2.0×10^{-7}	0.088	1.34
3.99	− .340	− .450	− .560	6.3×10^{-7}	.170	0.70
6.24	− .640	− .720	− .816	2.5×10^{-8}	.180	.66
8.00	− .530	− .648	− .704	3.0×10^{-7}	.160	.74
10.31	− .440	− .510	− .585	1.0×10^{-8}	.150	.79
11.80	− .365	− .455	− .510	2.5×10^{-7}	.150	.79

Table II
Tafel Line Parameters for O_2 Evolution

pH	η at 7.5×10^{-5} (v.)	η at 7.5×10^{-4} (v.)	η at 1.5×10^{-3} (v.)	i_0, (a./cm.²)	b	λ
2.02	−0.008	...	0.095	5.0×10^{-6}	0.080	1.48
3.99	.014	0.142	.182	9.0×10^{-6}	.127	0.93
6.24	.025	.160	.248	1.3×10^{-5}	.160	.74
8.00	.016	.160	.248	1.2×10^{-5}	.150	.79
10.31	.120	...	.495	3.0×10^{-6}	.170	.70
11.80	− .021	.140	.196	2.5×10^{-5}	.185	.64

the region of the hydrogen electrode potential. With anodic polarization (part cd), the potential rapidly rises toward more positive values. This is followed by a region of constant potential at d.

Tafel lines for the cathodic hydrogen evolution in solutions of pH 2.02, 3.99, 6.24, 8.0, 10.3 and 11.8 are obtained from the time–potential curves by plotting the constant potentials (identified with hydrogen overvoltage η) at the end of the cathodic polarization period against the logarithm of the current density. Values of η at three different current densities together with the parameters (exchange currents, i_0 and slope b) of the Tafel line are recorded in Table I. Tafel lines for the anodic evolution of oxygen are similarly obtained by plotting the constant potentials (identified with oxygen overvoltage η) at the end of the anodic polarization period against the logarithm of the current density. The parameters of the Tafel lines for oxygen evolution are given in Table II.

Values of the electron number, λ, for both hydrogen and oxygen evolution are calculated from the expression[3] for the Tafel line slope, $b = (2.303RT/\lambda\beta F)$, assuming that the energy barriers for the rate-determining steps in both reactions are symmetrical, i.e., taking $\beta = 0.5$. The calculated values of λ are recorded in Table I and II.

Tafel lines for hydrogen evolution, directly measured using the electrolytic cell of Bockris and Potter[3] (series II), in solutions of pH 1.9 (HCl + KCl),[5] pH 3.8 (solution of pH 1.9 made ca. 0.05 N with respect to potassium hydrogen phthalate), pH 9 (solution of pH 1.9 made ca. 0.05 N with respect to borax), pH 13.0 (ca. 0.15 N NaOH), pH 10.2 (ca. 0.15 N NaOH, solution made ca. 0.05 N with respect to borax) and pH 12.9 (0.15 N NaOH solution made ca. 0.1 N with respect to disodium hydrogen phosphate) are shown in Figs. 3 and 4. In Table III the slopes of the Tafel lines shown in Figs. 3 and 4 are recorded, together with the corresponding values of λ and i_0.

Discussion

(i) Time–Potential Variation. (a) Cathodic Region.
—The initial jump of potential manifested in the

cathodic part of the time-potential curves (cf. Fig. 2) in all solutions studied is attributed to the build up of the double layer. Once the double layer is completely built, the potential assumes a steady-state value (corresponding to the region of constant potential) and hydrogen will be evolved with a certain rate depending on the magnitude of the polarizing current. At this steady state, the rate of hydrogen deposition on the electrode surface is equal to the rate of hydrogen desorption. However, in an acid solution of pH 2.02 (curve I, Fig. 2A), in a solution of ca. 0.15 N NaOH with a pH value of 13.0 (Fig. 2B) and to a less extent in a solution of 3.99 (curve II, Fig. 2A), the build up of the double layer is followed by an exceptional rise in potential above that corresponding to the steady-state values. This phenomenon can be explained by the fact that chromium is always covered with an oxide film to which is attributed the passivity of this metal.[8]

Table III
Anion Effect on Tafel Line Slope

pH	b	λ	i_0 (a./cm.²)
1.9	0.105	1.12	1.2×10^{-6}
9.0	.185	0.64	9.5×10^{-7}
3.8	.150	0.79	2.8×10^{-7}
13.0	.115	1.03	2.1×10^{-7}
12.9	.175	0.67	6.7×10^{-7}
10.2	.175	0.67	8.7×10^{-7}

This oxide film causes a resistance overpotential which adds to the magnitude of hydrogen overvoltage. Once this oxide layer is removed, the resistance overpotential vanishes and the potential drops to that corresponding to the steady state. The fact that the time–potential curve in a solution of pH 3.99 exhibits a less defined hump and the curves in solutions of pH 6.24, 8.0, 10.3 and 11.8 do not exhibit this hump might be due to the presence of sorbable anions and perhaps to the incomplete removal of the oxide film. It is possible that phos-

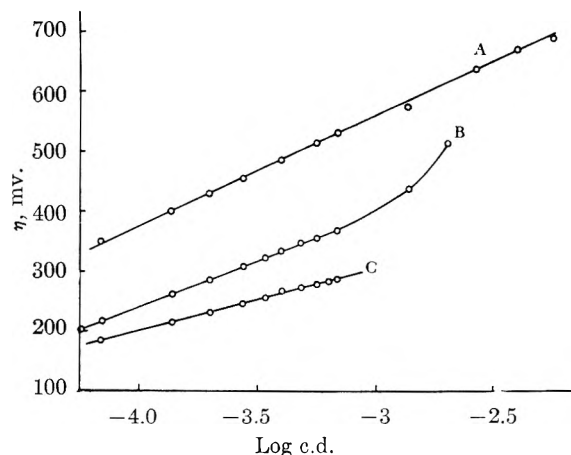(8) C. W. Bennett and W. S. Burnham, This Journal, 21, 107 (1917); U. R. Evans, J. Chem. Soc., 1020 (1927).

Fig. 3.—Log c.d. vs. η in mv.: A, pH 9.0, b = 0.185; B, pH 3.8, b = 0.150; C, pH 1.9, b = 0.105.
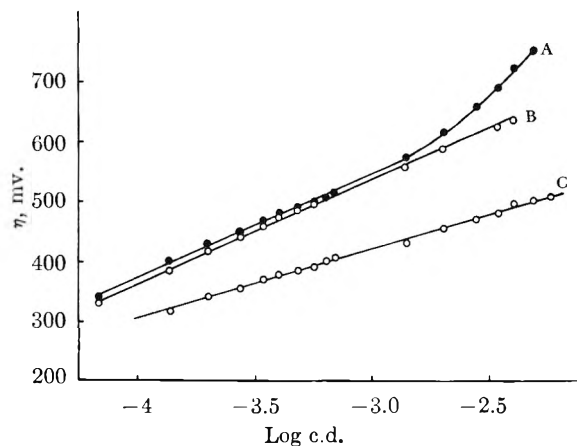

Fig. 4.—Log c.d. vs. η in mv.: A, pH 12.9, b = 0.175; B, pH 10.2, b = 0.175; C, pH 13.0, b = 0.115.

phate, phthalate and borate ions are adsorbed on the electrode surface, thus hindering access of cathodically evolved hydrogen to the oxide film.

(b) **Cathodic Decay.**—The rapid decay of the hydrogen overvoltage is due to the application of high polarizing currents such that the different phenomena often encountered during decay processes such as ionization of hydrogen, its depolarization and the collapse of the double layer do not distinctly appear in the decay curves of chromium.

(c) **Anodic Region.**—The anodic part of the time–potential polarization curves shows a steep change in potential corresponding to the formation of the anodic double layer. The consequent passivation of the electrode is accompanied by an arrest occurring near the region of oxygen evolution. The potentials corresponding to the above mentioned arrests vary with the logarithm of the anodic current density indicating that such potentials are associated with oxygen overvoltage.
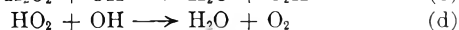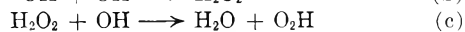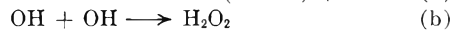
(ii) **Hydrogen Overvoltage.**—It has been shown by Bockris and Potter,[3] that the slope of the Tafel line b is given by $b = 2.303RT/\lambda\beta F$, where β is a criterion for the symmetry of the energy barrier of the rate-determining step and λ is the number of electrons necessary for each act of the rate-determining process. In most of the electrochemical reactions the energy barrier is symmetrical and the value of β is therefore = 0.5.

In the case of the cathodic hydrogen evolution, the steps constituting the over-all reaction are: (I) the diffusion of hydrogen ions from the bulk of solution toward the cathode, (II) the discharge of hydrogen ions either by the transfer of the ions to the electrode surface or by the transfer of electrons to the hydrogen ions in the Helmholtz double layer, (III) the catalytic combination of adsorbed hydrogen atoms to form molecular hydrogen and the neutralization of hydrogen ions on adsorbed atoms giving hydrogen molecules. Under the condition when the solution is not too dilute the diffusion process (I) occurs rapidly, and it is not therefore rate determining. Mechanism II, usually called the slow discharge mechanism, is characterized by a slope of 0.116 at 20° and a value of $\lambda = 1$. The electrochemical mechanism IV has two slopes of 0.116 and 0.039 at high and low current densities,

respectively, and a value of $\lambda = 2$. The catalytic mechanism III has two slopes of 0.029 and ∞ at low and high current densities and a value of $\lambda = 2$.

However, as may be seen from Tables I and III, the values of λ for chromium electrodes vary between 0.66 and 1.34 (assuming a symmetrical energy barrier) and since λ is always an integral number, the number of electrons involved in the rate-determining step for hydrogen evolution on chromium is "one." This value of λ, together with values of the Tafel line slopes which vary between 0.088 and 0.185, exclude the possibility of having a catalytic combination or an electrochemical process as rate determining. The slope = 0.088 occurring in a solution of pH 2.02 is the nearest to the directly measured slope of 0.105 in a solution of pH 1.9 (cf Fig. 3) and of 0.115 in a solution of 0.15 N NaOH (cf. Table III and Fig. 4). Higher slopes are, however, attributed to the occurrence of films of scrbable anions (namely, phthalate in buffer solutions of pH 3.99 and 6.24, borate in pH 10.3 and phosphate in pH 8.0 and 11.8) on the electrode surface as is clear from Fig. 3, Fig. 4 and Table III.

(iii) **Oxygen Overvoltage.**—From Table II it is clear that in the discharge of oxygen on chromium most of the values of λ lie between 0.65 and 0.94 with an exceptionally high value of 1.5 in a solution of pH 2.02. It is therefore possible to conclude that one electron is involved in the rate-determining step in the anodic oxygen evolution on chromium in solutions of pH values higher than 2.02. The processes representing the discharge of oxygen can be summarized in the following[9]

$$OH' \longrightarrow OH \text{ (radical)} + e \qquad (a)$$
$$OH + OH \longrightarrow H_2O_2 \qquad (b)$$
$$H_2O_2 + OH \longrightarrow H_2O + O_2H \qquad (c)$$
$$HO_2 + OH \longrightarrow H_2O + O_2 \qquad (d)$$
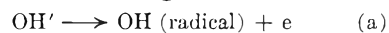
Steps a, b, c and d involve 1, 2, 3 and 4 electrons respectively. By comparison with the values of λ in Table II, it may be concluded that the discharge of OH' ions is the slowest step, in the anodic evolution of oxygen on chromium.

The authors wish to express their thanks to Professor A. Riad Tourky for his interest in this work.

(9) M. C. R. Symons, J. Chem. Soc., 3956 (1953); Kortum-Bockris, "Text Book of Electrochemistry," Elsevier Publishing Co., New York, N. Y., 1951, p. 455.

THE ADSORPTION OF HYDROCARBONS FROM METHANOL AND ETHANOL SOLUTIONS BY NON-POROUS CARBONS[1,2]

By ROBERT S. HANSEN AND ROBERT D. HANSEN[2]

*Contribution No. 371 from the Institute for Atomic Research and Department of Chemistry,
Iowa State College, Ames, Iowa*

Isotherms for the adsorption of octane, decane and dodecane from methanol solution by Graphon, Spheron-6 and DAG-1 have been determined at 25° over the range of hydrocarbon solubilities. Multimolecular adsorption of all of these hydrocarbons is demonstrable on Graphon and Spheron-6, and strongly indicated on DAG-1. Isotherms for the adsorption of decane and dodecane from ethanol by these same adsorbents have been determined over the entire concentration range. Primary dependence of adsorption on solute activity referred to pure liquid solute as standard state is again demonstrated. Surface excesses of hydrocarbon on Graphon markedly exceed those on Spheron-6 and DAG-1 at given hydrocarbon activities, and the latter two adsorbents show adsorption inversion in the completely soluble systems.

Introduction

In a recent study of the adsorption of aliphatic alcohols and acids from aqueous solution, Hansen and Craig[3] found that adsorption tended to be independent of position in a homologous series if compared at the same solute activity, and pointed out that this led to a rational basis for Traube's rule. The present work represents an extension of this study to non-aqueous systems.

Experimental

Preparation of adsorbents has been described previously.[3] Surface areas as determined by nitrogen adsorption were 114.0, 78.7 and 102.4 meters^2/g. for Spheron-6, Graphon and DAG-1, respectively.

All alcohols and hydrocarbons used in the experiments were central fractions from distillation through a 30-plate vacuum jacketed Oldershaw column at reflux ratio of 10:1. Prior to distillation the ethanol was purified by the method of Lund and Bjerrum[4] and the hydrocarbons were purified by extraction with concentrated sulfuric acid until the acid layer was colorless, washing with water and sodium carbonate solution, drying over sodium hydroxide pellets, and distillation from sodium. Starting materials and final boiling ranges corrected to 760 mm. were

Methanol (General Chemical Co. Reagent grade)	64.76– 64.86°
Ethanol (Commercial grade abs.)	78.62– 78.70°
Octane (Phillips Petroleum pure grade)	125.88–126.00°
Decane (Eastman Kodak Co. white label)	174.10–174.34°
Dodecane (Eastman Kodak Co. practical grade)	216.52–216.77°

Adsorption isotherms were determined according to the techniques described by Hansen, Fu and Bartell[5] with modifications described by Hansen, Hansen and Craig[6] and with the further modification that in most determinations adsorption equilibration was carried out in Pyrex test-tubes which had been drawn prior to addition of solution and sealed off subsequent to this addition. Solubilities were determined by interferometric comparison of saturated solutions prepared by equilibration for approximately 24 hour periods in a shaker at 25.0° with concentrated solutions of known composition.

Treatment of Data

Experimental results in the form of quantities $V\Delta C/m$ (V is the number of ml. of solution added

to m grams of adsorbent, ΔC is the solute concentration decrease due to adsorption in moles/liter) were converted to surface excesses $\Gamma_2^{(V)}$ of the Guggenheim and Adam convention by division by specific surface area of adsorbent.[7]

Activities of the hydrocarbons in methanol solution were estimated from the Margules equation using constants calculated from solubilities, thus

$$a/a_0 \approx \frac{c}{c_0} \left(10^{2\beta x_0 (1 - c/c_0)} \right) \qquad (1)$$

where

$$\beta = \frac{1}{1 - 2x_0} \log \frac{1 - x_0}{x_0} \qquad (2)$$

In these expressions a is the hydrocarbon activity based on pure liquid hydrocarbon as standard state, c is hydrocarbon concentration in moles per liter, and x is hydrocarbon mole fraction. a_0, c_0 and x_0 are the values of these quantities for a saturated solution of hydrocarbon in methanol. This treatment amounts to assuming the hydrocarbon–methanol system to be a regular solution, and should be an improvement over an assumption that Henry's law is obeyed from zero to saturation concentration. Neither assumption is exact.

Activity data for the systems ethanol–decane and ethanol–dodecane appear to be unavailable, nor does there appear to be a reasonable approximate method for estimating them.

Results

Results for the adsorption of hydrocarbons from methane solution are presented graphically in Figs. 1–3, in which surface excess of hydrocarbon, $\Gamma_2^{(V)}$, are presented as functions of reduced hydrocarbon activity a/a_0. Results for the adsorption of hydrocarbons from ethanol are presented graphically in Figs. 4 and 5, in which surface excesses of hydrocarbon, $\Gamma_2(v)$, are presented as functions of hydrocarbon mole fraction, x_2. All results were obtained at 25.0 ± 0.1°. Tabular experimental data are available on request (RSH). Solubilities of the following hydrocarbons in methanol at 25° were determined in the course of this work.

Octane	19.25% by weight (1.282 moles/l.)
Decane	10.25% by weight (0.5613 mole/l.)
Dodecane	5.883% by weight (0.2696 mole/l.)

(1) Work was performed in the Ames Laboratory of the Atomic Energy Commission.

(2) Based in part on a dissertation submitted by Robert Douglas Hansen in partial fulfillment of the requirements for the degree of Doctor of Philosophy, Iowa State College, Ames, Iowa, July, 1953.

(3) R. S. Hansen and R. P. Craig, THIS JOURNAL, **58**, 211 (1954).

(4) H. Lund and J. Bjerrum, *Ber.*, **64B**, 210 (1931).

(5) R. S. Hansen, Y. Fu and F. E. Bartell, THIS JOURNAL, **53**, 769 (1949).

(6) R. S. Hansen, R. D. Hansen and R. P. Craig, *ibid.*, **57**, 215 (1953).

(7) (a) E. A. Guggenheim and N. K. Adam, *Proc. Roy. Soc. (London)*, **A139**, 218 (1933); (b) R. S. Hansen, THIS JOURNAL, **55**, 1195 (1951).
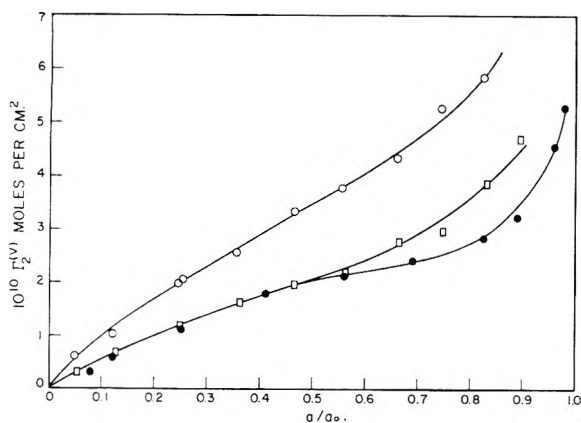
Fig. 1.—Adsorption of n-octane from methanol solution by non-porous carbons: ○, Graphon; □, Spheron-6; ●, DAG-1.
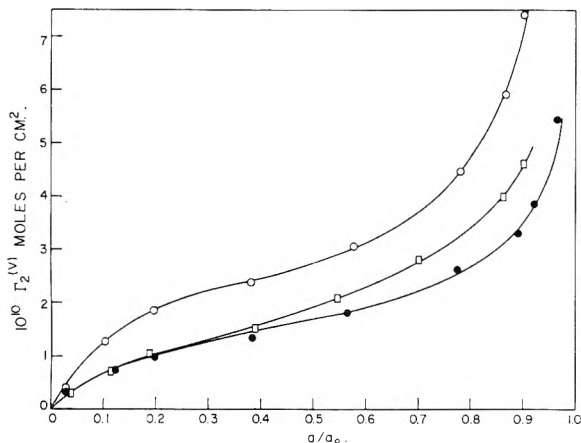
Fig. 2.—Adsorption of n-decane from methanol solution by non-porous carbons: ○, Graphon; □, Spheron-6; ●, DAG-1.
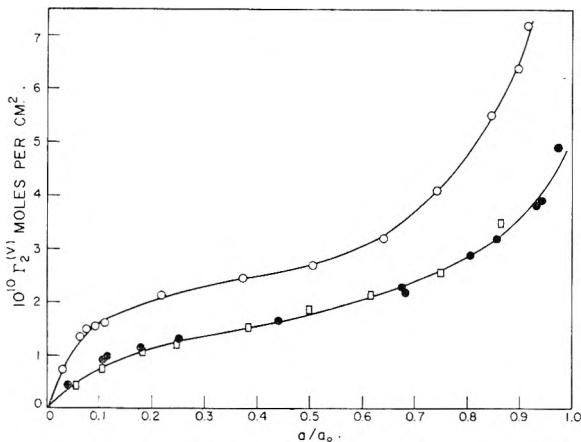
Fig. 3.—Adsorption of n-dodecane from methanol solution by non-porous carbons: ○, Graphon; □, Spheron-6; ●, DAG-1.

Fig. 4.—Adsorption of n-decane from ethanol solution by non-porous carbons: ○, Graphon; □, Spheron-6; ●, DAG-1.
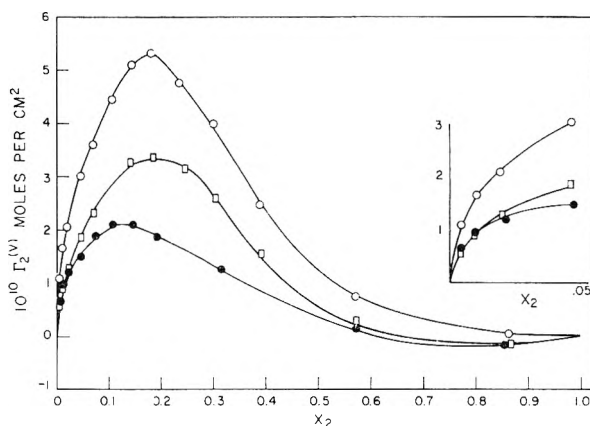
Fig. 5.—Adsorption of n-dodecane from ethanol solutions by non-porous carbons: ○, Graphon; ●, Spheron-6; □, DAG-1.

Discussion

Isotherms for the adsorption of octane, decane and dodecane from methanol are all of a definite sigmoid character, and are thus similar to isotherms in limited-solubility aqueous-fatty acid and aqueous-alcohol systems previously studied.[3,5] Surface excesses greater than 8.3×10^{-10} moles/cm.[2], corresponding to areas per hydrocarbon molecule less than 20 Å.[2], were obtained at high reduced activities in all three solvent pairs with the adsorbents

Graphon and Spheron-6; such surface excesses are greater than can be accommodated in a unimolecular layer even in the most compact arrangement, and the multimolecular character of adsorption in these systems is therefore proved (points not show on graphs due to space limitation). In view of the similarity of isotherms obtained with DAG-1 to those obtained with the other two adsorbents, multimolecular character of adsorption by DAG-1 is to be presumed.

Isotherms for the adsorption of the different hydrocarbons from methanol by a given carbon are remarkably similar functions of reduced activity; this result is again to be expected from the study of aqueous systems.[3,5] Adsorption of octane from methanol by Graphon at reduced activities above 0.3 appears higher than would be expected from this rule; adsorption of octane by the other carbon adsorbents appears to be slightly higher than adsorption of the other hydrocarbons in the intermediate reduced activity range. At reduced activities less than 0.25 there is a definite progression of adsorption values at a given reduced activity of the sort: dodecane > decane > octane, suggesting that at least at low coverage the hydrocarbons may be adsorbed in a "lying down" configuration with resulting progression in adsorption energy. Areas per molecule in such a configuration are estimated to be 67, 81 and 94 Å.[2] for octane, decane and dode-

cane, respectively; corresponding amounts of hydrocarbon required for complete unimolecular coverage are 2.48, 2.06 and 1.77 $\times$ 10^{-10} mole/cm.^{2}, which values are rather close to the values at the "shoulders" of the Graphon isotherms.

Surface excesses in the slightly soluble hydrocarbon–methanol systems are fairly well represented for the adsorbents Graphon and Spheron-6 by functions of the sort $b \log^{-1/2} a_0/a$ in the range $0.3 < a/a_0 < 0.9$, and nearly as well by functions of the sort $c \log^{-1/3} a_0/a$. This suggests that adsorption potentials in these systems are inversely proportional to the square or cube of the distance from the surface; such functions do not, however, represent adsorption of aliphatic acids and alcohols from aqueous solution by the same adsorbents.

In the completely miscible hydrocarbon–ethanol systems, surface excesses for a given carbon at a given mole fraction are markedly higher for dodecane than for decane at low hydrocarbon mole fractions, and slightly lower at high mole fractions. Hydrocarbon adsorption from ethanol at low mole fractions is probably a function of hydrocarbon activity very similar to that for adsorption of hydrocarbons from methanol by the same adsorbent. According to Ferguson, Freed and Morris[8] the activity of heptane in ethanol, based on pure liquid heptane as standard state, is 0.897 at mole fraction heptane of 0.337, and 0.609 at mole fraction 0.092. The same activities should be reached by the higher hydrocarbons at lower mole fractions. The slightly greater adsorption of decane at high activities could well be attributed to its smaller size.

Comparing the different adsorbents, it is evident that surface excesses on Graphon are markedly greater than those on the other two adsorbents at all concentrations. In the slightly soluble systems surface excesses on DAG-1 and Spheron-6 are nearly the same at low reduced activities, while surface excesses on Spheron-6 generally exceed those on DAG-1 at high reduced activities. In the completely miscible systems surface excesses on Graphon are positive over the entire concentration range, while isotherms on DAG-1 and Spheron-6 show definite inversions. These results suggest existence of surface oxygen complexes on Spheron-6 and DAG-1; evidence for such complexes in the case of Spheron-6 has been presented by Anderson and Emmett.[9] Qualitatively, such complexes would have the effect of reducing the area fraction in which hydrocarbon adsorption was preferential in the first layer, and decreasing the preference for hydrocarbon over alcohol in higher adsorbed layers; these effects are in accord with observation. Data on both slightly soluble and completely soluble systems suggest that the decrease in adsorption potential with distance is more rapid with DAG-1 than with Spheron-6, but that the adsorption potentials in the neighborhood of the first adsorption layer are nearly the same with these two adsorbents.

(8) J. B. Ferguson, M. Freed and A. C. Morris, THIS JOURNAL, **37**, 87 (1933).

(9) R. B. Anderson and P. H. Emmett, *ibid.*, **56**, 753, 756 (1952).

A SURFACE STUDY OF MYOSIN MONOLAYERS AND CERTAIN BIOLOGICALLY IMPORTANT SUBSTRATES. I. ADENOSINE TRIPHOSPHATE

BY K. KASHIWAGI[1] AND B. RABINOVITCH

Contribution from the Chemistry Department, Illinois Institute of Technology, Chicago, Ill.

An actin-free myosin takes a finite and measurable time to spread on an aqueous KCl solution at pH 5.4 and is dependent upon the area at which it is allowed to spread. An expression derived to follow the kinetics of spreading leads to the suggestion that the forces retarding spreading might be due to ion–dipole interaction. The presence of adenosine triphosphate (ATP) in the substrate materially alters the rate of spreading and the equilibrium pressure obtained. The mechanism of spreading appears to be different under these circumstances, while the state of the equilibrium film obtained is easily explained on the basis of a physical binding of the ATP molecules to the protein in the surface. By reference to the titration curve of myosin in the presence of K$^+$ ions, the extent of binding of ATP is readily explained.

Few studies have been made on the physical or chemical interaction between a protein film spread at an air–water interface and biologically important substrates. Rideal[2] has summarized and discussed some of these, while more recently Geiduschek and Doty[3] have worked in this way with antigen–antibody reactions and Munch-Petersen[4] has worked on the myosin–adenosine triphosphate (ATP) reaction. The reason for this limited application of a potentially useful tool in protein chemistry probably arises from the difficulty of obtaining a stable and reproducible protein film.[5–7]

That adenosene triphosphate (ATP) plays an important part in the mechanism of muscle contraction is well recognized. The function of ATP in muscle tissue appears to be twofold, firstly to keep the muscle in a physically supple state and secondly to supply the substrate from which myosin, the main muscle protein, can extract the energy necessary for muscle contraction.[8] The former of these functions probably arises from a physical interaction between the protein and its

(1) This publication is based upon a thesis submitted by K. Kashiwagi in partial fulfillment of the requirements for the degree of Master of Science at Illinois Institute of Technology, February, 1954.

(2) E. K. Rideal, *J. Chem. Soc.*, 423 (1945).

(3) P. Geiduschek and P. M. Doty, *J. Am. Chem. Soc.*, **74**, 3110 (1952).

(4) A. Munch-Petersen, *Nature*, **162**, 537 (1948).

(5) J. S. Mitchell, *Trans. Faraday Soc.*, **33**, 1129 (1937).

(6) E. G. Cockbain and J. H. Schulman, *ibid.*, **35**, 1266 (1939).

(7) J. H. P. Jonxis, *Biochem. J.*, **33**, 1743 (1939).

(8) A. Szent-Gyorgyi, "Chemistry of Muscular Contraction," Academic Press, Inc., New York, N. Y., 1951, Chapter VI.

substrate,[8] the latter certainly from a chemical interaction.[9]

It is the purpose of this paper to examine the interaction of myosin, spread at an air–water interface with an ATP substrate. In order to do this, some study of the mechanism of spreading of myosin at an air–water interface has been undertaken, both in the presence and absence of ATP in the substrate.

Experimental

Apparatus.—The surface balance used was obtained from the Central Scientific Company and is adequately described in their catalog of equipment. The complete balance was placed in a wooden air-thermostat, kept at a temperature of 30.0 ± 0.2° by means of a 250-watt heating mat, a slow moving circulating fan driven from outside of the box, a mercury to mercury regulator and a Fisher Servall relay. The temperature variation from extreme corner to corner within the box was never greater than ±0.5°. All manipulations could be made from outside the box and observed through windows in the box.

All normal precautions were taken in using the surface balance to ensure a confined film, such precautions being described by Adam.[10] The sensitivity of the surface balance was determined by the usual calibration method[10] and found to be 5.67 ± 0.02°/dynes per cm.

Preparation of Materials. (a).—Myosin was extracted from the dorsal and leg muscles of a freshly decapitated rabbit by means of the method described in great detail by Szent-Gyorgyi.[8] The actomyosin was removed from the myosin by dilution to a KCl concentration of 0.3 M when the actomyosin was precipitated and separated by high speed centrifugation in a Sorvall High Speed Angle Centrifuge. In all steps of the extraction, glass distilled water was used and the procedure described by Szent-Gyorgyi closely adhered to. The description of the method is so explicit and detailed, and the successful conclusion of the extraction by the present authors so evident that it was deemed unnecessary to characterize the myosin obtained by viscosity measurements. The possible presence of a small concentration of actomyosin in the myosin solution was considered to be of small importance in this study. The myosin was kept as a stock solution in a medium of one part 0.6 M KCl and one part glycerol. Its acidity was maintained at a reading of 7.0 on a Beckman pH meter. This stock solution of myosin was kept at −25° by means of a bath of solid CO_2. These conditions are very similar to those described by Szent-Gyorgyi as being optimal for the maintenance of ATPase activity.

(b).—ATP was obtained from Schwarz Laboratories, Inc., and was a product of a fermentation process. Nitrogen and phosphorus determinations showed the product to be about 80% pure, as follows: nitrogen—observed 11.70%, theoretical 13.78%; phosphorus—observed 14.85%, theoretical 18.28%. The following procedure was used as a means of purification:

The ATP was precipitated as its barium salt by addition of an excess of a barium acetate solution to a 5% solution of the ATP in water. This precipitate was filtered off, washed with distilled water and redissolved in 0.2 N nitric acid. The precipitation step was repeated with barium acetate and the precipitate washed several times with distilled water. The barium–ATP salt was dissolved in 100 ml. of 0.2 N nitric acid and sufficient 0.4 N sulfuric acid added to precipitate all the barium as barium sulfate, leaving a slight excess of sulfuric acid in the remaining solution. The barium sulfate was separated by filtration and the ATP precipitated from solution by the addition of a large excess of 95% ethanol. The ATP was filtered off, washed several times with 100% ethanol and finally with dry ether. Phosphorus analysis of the purified product showed it to contain 18.01% phosphorus, which agreed closely with the theoretical value of 18.28%.

Methods.—The concentration of the myosin stock solution was determined by the precipitation of the myosin in

50-ml. quantities by the addition of a large excess of distilled water. The gelatinized precipitate was separated in a medium sintered glass filter, washed with a small quantity of distilled water and dried at a temperature of 98° to constant weight. The results gave a concentration of myosin in the stock solution of 39 ± 1 mg./100 ml.

The myosin solution was added to the surface in accurately known quantities by means of a micrometer syringe as described by Alexander.[11] This syringe was calibrated in terms of ml. of distilled water expressed per unit distance travelled by the syringe piston, and found to be 0.0376 ml. per inch, constant over the available length of the barrel to within ±0.0002 ml.

The aqueous substrate used in all the surface measurements described here contained 0.16 M KCl at a pH of 5.4 unless otherwise stated. This represents a compromise between those conditions considered best for the spreading of myosin (0.6 M KCl, pH 5.4) and those which give the maximum ATPase activity in myosin (0.16 M KCl, pH 7.0).[8]

In applying the myosin solution to the surface of the substrate, the air thermostat inevitably was exposed to the temperature of the room for approximately three minutes. The resultant drop in temperature within the thermostat (2–3°) was rapidly made up and, by ensuring that the temperature of the substrate, at the time of spreading, was not higher than 32°, it was found that thermal equilibrium between the substrate and the thermostat was established within ten minutes from the time of spreading. Unless otherwise stated, the myosin was spread at infinite area, i.e., with the movable barrier removed to its limiting position. The same quantity, 0.075 ml., of myosin stock solution was added to the surface in all experiments.

Results

Figure 1 shows force–area (F–A) curves of myosin spread under a variety of substrate conditions. Curve A shows conclusively that myosin spreads very incompletely on distilled water. Curve B indicates that the highly charged myosin film, on a substrate of a strong acid at a pH of 2.4 (isoelectric point 5.4), spreads very well and is a highly expanded film. This can be readily understood from the nature of the coulombic repulsions between the myosin molecules in the film at this pH.
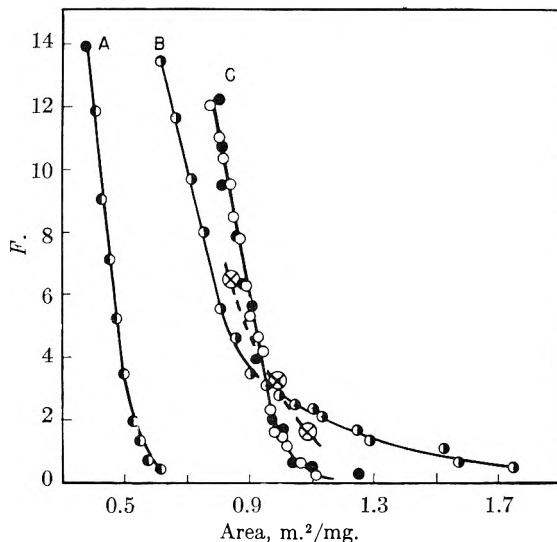
Fig. 1.—Force–area curves of myosin spread on various substrates: A, on distilled water; B, on strong acid at pH 2.4; C, on substrate of pH 5.4 (I.P.); O, [KCl] 0.16; ●, [KCl] 0.6; ⊗, equilibrium values obtained after expansion at limited areas.

Curve C in Fig. 1 shows the results of measurements on a myosin film spread close to the isoelec-

(9) V. A. Engelhardt and M. N. Lyubimoba, *Nature*, **144**, 668 (1939).

(10) N. K. Adam, "The Physics and Chemistry of Surfaces," Oxford University Press New York, N. Y., 1944, pp. 27–31.

(11) A. E. Alexander, "Surface Chemistry," Longmans, Green and Co., New York, N. Y., 1951, p. 30.

tric point on two widely different substrate salt concentrations. Both sets of points may be satisfied by the same curve and demonstrate that our standard set of substrate conditions, 0.16 M KCl and pH 5.4, fulfills the requirements for a fully spread film. Rough extrapolation to zero surface pressure shows the "close-packed" film to occupy about 1 m.² per mg., a figure commonly found for proteins.

These films were all spread at infinite area, in which condition they were allowed to remain for 20 minutes before F and A measurements were made. However, that spreading is not an essentially instantaneous process but time dependent is shown by Fig. 2. Here the myosin was again spread from solution at infinite area, but allowed to remain so for 3.5 ± 0.5 minutes after which time the film was rapidly compressed to a predetermined area and force measurements made with time. It can be seen that an equilibrium pressure is obtained only after 100, 120 and 155 minutes for expansion at limited areas of 1.09, 0.99 and 0.865 m.² per mg., respectively. From these curves it may be estimated that by expansion at infinite area (an area of approximately 2 m.² per mg.) an equilibrium pressure will be established well within 20 minutes.
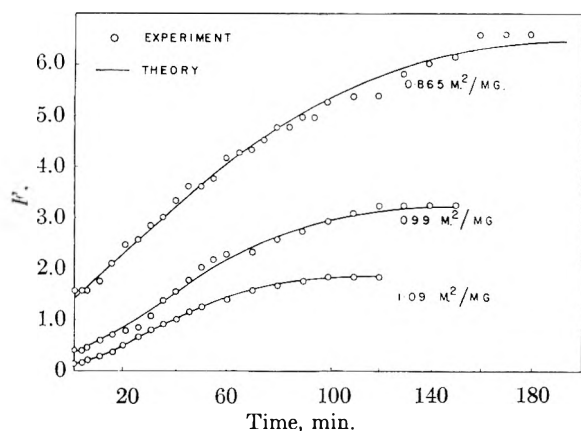
Fig. 2.—Rate of expansion, as measured by the increase of the surface pressure (F) with time, of myosin films on a 0.16 M KCl, pH 5.4 substrate.

When the myosin film is spread on a substrate 0.16 M in KCl and 10^{-6} M in ATP, under conditions identical with those in Fig. 2, a similar time dependence of the surface pressure is noted (see Fig. 3). However, a quantitative difference between the two sets of curves is apparent inasmuch as at the largest area the rise in surface pressure is much more rapid on the ATP substrate while the reverse is true for the smallest area.

It would appear from this that there is a definite interaction between the ATP in the substrate and the myosin in the film. This can be most clearly shown by an examination of F–A curves of myosin on ATP substrates. Figure 4 shows a set of such curves. Curve D is a reproduction of the one shown in Fig. 1. Curve A was obtained by spreading the myosin on a 0.16 M KCl, 10^{-6} M ATP substrate at infinite area but allowing the film to remain thus expanded only five minutes. There appears to be a rather abrupt change in slope at a surface pressure of about 7.5 dynes per cm. This is
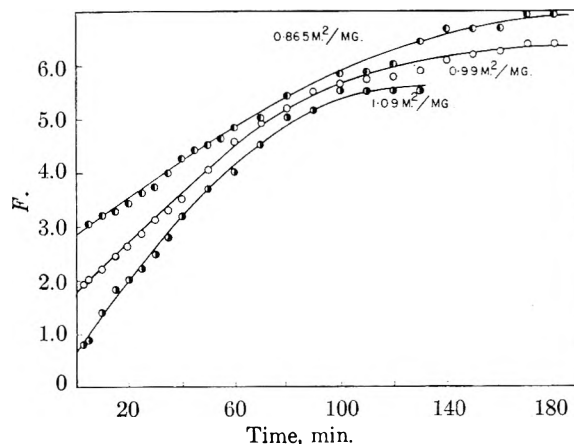
Fig. 3.—Rate of expansion, as measured by the increase of the surface pressure (F) with time, of myosin films on a 0.16 M KCl, pH 5.4 substrate containing 10^{-6} M ATP.

also observed in curve (B) where the substrate was 0.6 M in KCl and 1.2×10^{-4} M in ATP and the spreading conditions identical with those of curve A.
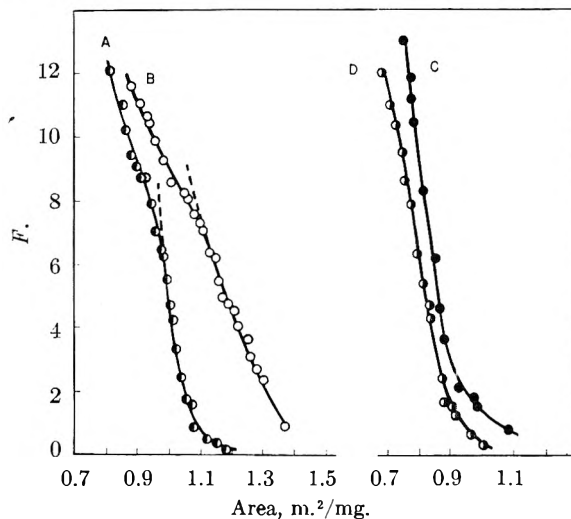
Fig. 4.—Force–area curves of myosin spread on ATP substrates, 0.16 M KCl, pH 5.4: A, 10^{-6} M ATP, spread at infinite area for 5 minutes; B, 1.2×10^{-4} M ATP, spread at infinite area for 5 minutes; C, 10^{-6} M ATP, spread at limited area of 0.865 m.² per mg. for 3 hours; D, no ATP.

A direct comparison between Fig. 4 curves A and B on the one hand and (D) on the other is certainly not permissible inasmuch as the former curves were obtained under non-equilibrium conditions. However, even under such non-equilibrium conditions, an abrupt change of slope in an F–A curve cannot be expected and it may well be that we are observing a second-order transition resulting from reorientation of the molecules in the surface.

In order that a more direct comparison may be made between F–A curves of myosin spread in the presence and absence of ATP in the substrate, an experiment was performed in which the myosin was spread on a 0.16 M KCl, 10^{-6} M ATP substrate at a limited area of 0.865 m.² per mg. and left in this condition for three hours. The film was rapidly expanded and then slowly compressed with simultaneous F and A measurements. The results of this

experiment are shown in Fig. 4, curve C. It will be noted that there is no evidence of an abrupt change in slope in this curve. Moreover, comparison of the compressibility curves (Fig. 5) would tend to justify a close similarity between curves C and D in Fig. 4.

Discussion of Experimental Results

If the mechanism given by Jonxis[7] is accepted as being operative during the rise in surface pressure with time, then a quantitative relationship may be derived to describe this rate process.

Let us consider that a surface film of a protein spread at an air–water interface at infinite area and then compressed rapidly to an area A will give an increase in the surface pressure with time due to the slow unfolding of the molecules in the surface. This time dependence may be attributed to the opposition of two forces, the one arising from the intermolecular or intramolecular attractions of the protein molecules, which may be of a van der Waals or of a coulombic nature, preventing the protein from spreading, and the other arising from forces of attraction between the hydrophilic groups of the protein and the substrate, compelling the protein to spread.

If the state of the film at any time during the spreading process may be said to be liquid expanded, we may say that

$$(F + F^0)(A - A_0) = RT/10^{23}M = C \qquad (1)$$

where

F = measured surface pressure at time t in dynes/cm.

F^0 = constant contribution that *would* be made to the total surface pressure *if* there were no cohesion between the protein molecules in the surface

A = total area occupied by the film in m.^{2} per mg.

A_0 = area occupied by the unfolding molecules at time t, in m.^{2} per mg., *i.e.*, the co-area

M = molecular weight of the protein

As the protein molecules unfold in the surface, so A_0 increases and an increase in F is observed. It would appear not unreasonable to assume that the rate of increase of A_0 is proportional to the pressure under which the film finds itself at time t. The simplest way of expressing this is

$$dA_0/dt = k(F_e - F) \qquad (2)$$

where F_e = the final equilibrium pressure.

From equation 1, we have

$$A_0 = A - C/(F + F^0)$$

and

$$dA_0 = CdF/(F + F^0)^2$$

whence, from equation 2

$$dF/dt = k(F + F^0)^2(F_e - F)/C \qquad (3)$$

Integration of equation 3 gives

$$\frac{1}{(F_e + F^0)^2} \ln \frac{(F_e - F_0)(F + F^0)}{(F_e - F)(F_0 + F^0)} +$$
$$\frac{1}{(F_e + F^0)} \left\{ \frac{1}{(F_0 + F^0)} - \frac{1}{(F + F^0)} \right\} = kt/C \qquad (4)$$

where F_0 = the surface pressure at zero time. In equation 4 only one parameter F^0 need be adjusted to give a best fit to the experimental data. In Fig. 2, the full lines represent the curves calculated from this equation using the best values of F^0; it can be seen that a remarkably close fit can be obtained.
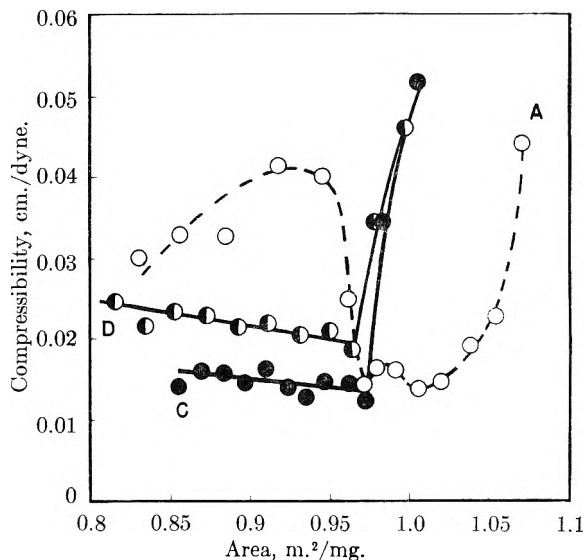
Fig. 5.—Compressibilities of myosin films under different conditions: A, on a 10^{-6} M ATP, 0.16 M KCl substrate, spread at infinite area for 5 minutes; C, on a 10^{-6} M ATP, 0.16 M KCl substrate, spread at a limited area (see Fig. 4C); D, on a 0.16 M KCl substrate.

The values of F^0 obtained in this way are 5.0 ± 0.5; 2.0 ± 0.2 and 1.0 ± 0.1 dynes per cm. for the limiting areas 0.865, 0.99 and 1.09 m.^{2} per mg., respectively.

If the assumptions involved in the derivation of equation 4 are valid, then F^0 should be simply related to the distance apart of the protein molecules in the surface film. This may be expressed as proportional to $(A - A_0)$, on the basis of the simple model of elongated molecules in the surface, the lateral forces between which are confined to the direction perpendicular to the chain and not in the direction of the chain. Consideration of equation 1 shows that the fractional free surface area $(A - A_0)/A$ is a very small quantity at all values of F, indicating that the surface film is almost completely spread from the outset. Consider the film at equilibrium; then

$$(F_e + F^0)(A - A_{0e}) = C \qquad (5)$$

and

$$\frac{1}{(A - A_{0e})} \propto (F_e + F_0)$$

Whence

$$F^0 \propto \frac{1}{(A - A_{0e})^n} \propto (F_e + F^0)^n \qquad (6)$$

A plot of log F^0 against log $(F_e + F^0)$ shows n to have a value of 3, which might correspond to ion–dipole interaction.

When the values of F_e are compared with those in Fig. 1C at corresponding areas, a marked difference is noted, there being agreement by interpolation at an area of about 0.96 m.^{2} per mg. It would appear therefore that the state of the film finally established after spreading at a limited area is different from that established after spreading at infinite area. The same observation can be made by comparing the F_e values obtained from Fig. 3 with Fig. 4A, there being coincidence once again at an area of about 0.96 m.^{2} per mg.

The significance of this area of 0.96 m.² per mg. becomes apparent on consideration of the compressibilities of these films. The compressibility of a surface film is defined as $-dA/(A \cdot dF)$, and Fig. 5 shows the variation of compressibility with area derived from the smooth curves of Fig. 4A, C and D. In all cases a minimum occurs at 0.96–0.97 m.² per mg. indicating that this area represents a close packed film. We suggest that the difference between the state of the film spread at infinite area and that spread at a limited area is simply one of orderliness. When a film is allowed to spread at infinite area and then compressed slowly to a limited area, we would expect the molecules in the surface to have assumed a more ordered state than those of the film which is spread at the same limited area. It would follow that if this limited area is greater than that corresponding to close-packing, the latter film would give a higher surface pressure than the former. On the other hand, if the limited area is smaller than that corresponding to close-packing, then the film spread at the limited area would be in a greater state of collapse than that spread at infinite area and subsequently compressed to this limited area.

Comparison of curves C and D in Fig. 5 indicates that here the surface films are in corresponding physical states and quite different from that of the film represented by curve A in this figure. It would be reasonable to say therefore that the area occupied by a myosin molecule in the close-packed film on an ATP substrate is not affected by the presence of ATP. The fact that the close-packed area of the myosin film is the same, whether in the presence or absence of an ATP substrate, may be interpreted as meaning that in this close-packed condition no ATP finds itself in the surface; yet the observed higher pressure of the close-packed film on an ATP substrate indicates once again an interaction between the myosin and ATP molecules.

Comparison of curves C and D in Fig. 4 indicates that the introduction of ATP in the substrate causes a close-packed myosin film to expand to the extent of 0.035 m.² per mg. *if* the pressure is kept at 3 dynes per cm. Since there is no free surface available to the ATP, this increase in area must be due to the presence of strongly adsorbed ATP in the surface. That the adsorbed ATP must be in the surface follows from the fact the close-packed myosin film on ATP occupies an area of 0.96 m.² per mg. and exerts a pressure of about *4.5* dynes per cm.

In the light of these considerations, a simple calculation may be made. At the low pressure of 3 dynes per cm., ATP molecules in the surface will be lying flat and from an examination of Fisher–Hirschfelder models of the molecule it may be estimated that it would occupy an area of approximately 100–120 Å.² Thus, 0.035 m.² per mg. would represent 50–60 ATP molecules per myosin molecule, assuming the molecular weight of the myosin to be 10^6. Examination of the titration curve for myosin in the presence of 0.16 M KCl,[12] we see that at a pH of 5.4 there are about 100 bound protons per myosin molecule. The presence of KCl shifts the isoelectric point of myosin firstly toward the alkaline side, and above a [KCl] of 0.025 back toward and beyond pH 5.4. However, in the presence of ATP, the iso-electric point is always reestablished at pH 5.4 indicating the replacement of chloride ions by ATP ions to an extent equivalent to the total bound H⁺ and K⁺ ions. The ATP molecule is a tetrabasic acid which may readily be likened to pyrophosphoric acid, and the pyrophosphate ion may be readily shown to be divalent at a pH of 5.4. Thus the figure of 50–60 ATP molecules (or ions) adsorbed per myosin molecule fits in well with the figure of 100 bound protons per myosin molecule, if it is assumed that few or no K⁺ ions are bound under these conditions to the myosin. In fact, Banga[13] has shown that the binding of K⁺ ions is a subtle property of myosin, readily lost on storage.

It is instructive to note that equation 4 in no way describes the rate of expansion of myosin on an ATP substrate, but that if the assumption expressed in equation 2 is replaced by

$$dA_0/dt = k(A_{0e} - A_0) \qquad (7)$$

we will arrive, by way of a similar derivation to that already described, at the expression

$$\ln \frac{(F_e - F_0)(F + F^0)}{(F_e - F)(F_0 + F^0)} = kt \qquad (8)$$

This expression is an excellent representation of the curves in Fig. 3.

It remains only to be said that a different mechanism is probably operative in the two processes corresponding to equations 2 and 7 but that, at present, these equations tell us nothing about the processes.

(12) M. Dubuisson, *Arch. intern. physiol.*, **51**, 199, 154 (1941).
(13) A. Szent-Gyorgyi, "Chemistry of Muscular Contraction," Academic Press Inc., New York, N. Y., 1951, Chapter VI, p. 49.

TEMPERATURE VARIATION STUDIES IN THE CHEMISORPTION OF HYDROGEN ON COBALT CATALYSTS

By M. V. C. Sastri[1] and V. Srinivasan

General Chemistry Section, Indian Institute of Science, Bangalore 3, India

The isobaric chemisorption of hydrogen was investigated on three cobalt Fischer–Tropsch catalysts using the temperature variation method of Taylor and Liang. Desorption–readsorption phenomena typical of an energetically heterogeneous surface were observed during temperature variation, in the case of the freshly reduced catalysts as well as those taken through different stages of sintering. Sintering was found to redistribute the energy of activation of the various adsorptive centers in addition to causing an over-all decrease in the adsorptive capacity. Evidence is presented to show that in this case the desorption–readsorption phenomena arise predominantly from surface effects and reflect the heterogeneity of the catalyst surface and are not to be explained by postulating the solution of gas into the catalyst interior as was done by Beeck or as due to the presence of traces of residual oxygen on the surface as suggested by Schuit and de Boer.

Introduction

Sadek and Taylor[2] investigated the isobaric chemisorption of hydrogen at different temperatures on some reduced nickel catalysts by the technique of changing rapidly from one temperature to another without the usual intermediate evacuation of the catalysts. Their results revealed desorption–readsorption phenomena similar to those observed with oxide surfaces by Taylor and Liang[3] and were interpreted likewise on the basis of the heterogeneity of the active centers. This view was supported by the mathematical analyses of Halsey[4a] and of Sastri and Ramanathan.[4b] The same phenomenon has been observed with evaporated nickel films by Beeck, Ritchie and Wheeler[5] and with evaporated tungsten films by Rideal and Trapnell.[6] These authors, while agreeing that the desorption immediately following a temperature increase is a genuine surface effect, attribute the slow up-take observed after it, to absorption rather than adsorption. In this connection, Beeck[7] observes that if it can be shown that absorption or solution is not involved, "the method of Taylor and Shou Chu Liang could indeed become a powerful technique in the investigation of the degree of heterogeneity of surfaces." On the basis of the results obtained by them with sintered and carefully reoxidized nickel catalysts, Schuit and de Boer[8] suggest that the slow stage of the adsorption of hydrogen on metal surfaces is due to chemisorption of hydrogen "on top" of chemisorbed oxygen atoms presumably present on the surface and not due to activated adsorption on metallic sites. They therefore considered that the desorption–readsorption phenomenon cannot be taken as evidence for the heterogeneity of a pure metal surface.

In the present paper are reported results of the study of the isobaric adsorption of hydrogen on a series of cobalt catalysts at various stages of ther-

mal sintering using the method of temperature variation without intermediate evacuation. The results obtained here clearly indicate that the desorption–readsorption phenomena observed originate in the surface, as it is difficult to interpret them on the alternative bases of absorption or presence of surface oxides.

Experimental

Preparation and Pretreatment of the Catalysts.—The catalysts investigated were prepared by precipitation from hot solutions of the nitrates with potassium carbonate in presence of acid washed, calcined kieselguhr (B.D.H. product, surface area = 1.44 sq. m./g.) following the procedure of Anderson, *et al.*[9] All the chemicals used were guaranteed analytical reagents.

The catalysts were reduced thoroughly passing a rapid stream of pure electrolytic hydrogen, at 300° in the case of catalyst A and 350° for catalysts B and C, until no more water vapor was detected in the exit gas with a weighed phosphorus pentoxide tube. This took about 12 hours, but the hydrogen was passed at the same temperature for a further 48 hours. Before proceeding with regular adsorption experiments, the catalysts were alternately evacuated for eight hours at the reduction temperature and exposed to hydrogen at atmospheric pressure at the same temperature for 12 hours to check reproducibility of adsorption values. These precautions ensured in every case that catalysts suffered no further reduction during the adsorption experiments.

Each adsorption run was preceded by evacuation for eight hours at the temperature of reduction.

Sintering of the catalysts was carried out by heating the catalysts *in vacuo* for 12 hours. Catalyst A was thus sintered at 360 and 400°, catalyst B at 375 and 425° and catalyst C at 400 and 425°.

Gases.—Electrolytic hydrogen, carbon monoxide prepared by dehydration of formic acid,[10] cylinder nitrogen and cylinder helium were all freed from traces of oxygen by passing through hot copper, potassium hydroxide-pellets and granular magnesium perchlorate.

Adsorption Measurements.—The apparatus and experimental technique employed were almost the same as described in an earlier communication from this Laboratory.[11]

For the 5 to 7 g. of each catalyst, the adsorption values were reproducible to within 0.05 ml. The adsorption values given here in ml. N.T.P. per gram of reduced catalyst were therefore correct to 0.01 ml.

The temperatures of adsorption were attained by using liquid air (−191°), melting toluene (−95°), solid CO₂–acetone (−78°), melting ice (0°), boiling acetone (53°), boiling xylene (134°) and boiling nitrobenzene (204°). For higher temperatures a small electric furnace controlled with a Sunvic Energy Regulator to ±1° was used.

The surface areas of the catalysts at various stages of sintering were determined.

(1) Applied Chemistry Department, Indian Institute of Technology, Kharagpur, India.

(2) H. Sadek and H. S. Taylor, *J. Am. Chem. Soc.*, **72**, 1168 (1950).

(3) H. S. Taylor and S. C. Liang, *ibid.*, **69**, 1306 (1947).

(4) (a) G. D. Halsey, Jr., This Journal, **55**, 21 (1951); (b) M. V. C. Sastri and K. B. Ramanathan, *ibid.*, **56**, 220 (1952).

(5) O. Beeck, A. W. Ritchie and A. Wheeler, *J. Coll. Sci.*, **3**, 505 (1948).

(6) E. K. Rideal and B. M. W. Trapnell, *Discs. Faraday Soc.*, **8**, 114 (1950).

(7) O. Beeck, "Advances in Catalysis," Vol. II, Academic Press Inc., New York, N. Y., p. 151.

(8) G. C. A. Schuit and N. H. de Boer, *Rec. trav. chim. Pays-Bas*, **70**, 1067 (1951).

(9) R. B. Anderson, A. Krieg, B. Seligman and W. E. O'Neill, *Ind. Eng. Chem.*, **39**, 1548 (1947).

(10) J. G. Thompson, *ibid.*, **21**, 389 (1929).

(11) J. C. Ghosh, M. V. C. Sastri and G. S. Kamath, *J. chim. phys.*, **49**, 500 (1952).

SURFACE AREAS, CO CHEMISORPTIONS AND MAXIMUM HYDROGEN CHEMISORPTIONS

$V_{m(N)}$ = vol. of nitrogen in saturated, physically adsorbed monolayer at $-191°$. V_{CO} = vol. of CO chemisorbed at $-191°$ = total vol. CO adsorbed $-$ vol. N_2 adsorbed at equal relative pressures. $V_{H(max)}$ = maximum vol. of hydrogen chemisorbed at -78 or $-95°$ at atmospheric pressure with temperature decreasing. $V_{m(H)}$ = computed monolayer value for chemisorption of hydrogen = 2.5 × CO chemisorption

Catalyst	Pretreatment	$V_{m(N)}$, ml./g.	Surface area, sq. m./g.	V_{CO}, ml./g.	$V_{CO}/V_{m(N)}$	V_H max., ml./g.	$(V_H/V_{m(H)})$ ×100
A. Co–KG, 100:200	Reduced at 300°	4.66	20.3	2.04	0.436	2.95	57.8
	Sintered at 360°	3.81	16.6	1.77	.465	2.50	56.7
	Sintered at 400°	3.17	13.8	1.21	.382	2.30	76.2
B. Co–ThO₂–KG, 100:18:200	Reduced at 350°	21.30	92.7	4.25	.200	3.25	32.6
	Sintered at 375°	20.08	87.4	3.52	.176	3.45	39.2
	Sintered at 425°	18.95	82.5	3.52	.185	3.55	40.4
C. Co–ThO₂–MgO–KG, 100:6:12:200	Reduced at 350°	17.93	78.1	5.51	.308	5.6	40.6
	Sintered at 400°	15.79	68.7	2.82	.179	3.6	51.1
	Sintered at 425°	15.04	65.5	2.82	.188	3.4	48.2

Results and Discussion

Surface Areas and CO Chemisorption.—The
values of the nitrogen monolayer adsorption, the corresponding surface areas and the chemisorption of carbon monoxide are given in Table I for the freshly reduced as well as the sintered catalysts. The difference between the nitrogen and carbon monoxide adsorption isotherms at liquid air temperature was taken as equal to the CO chemisorption, following Anderson, Hall and Hofer,[12] though the assumptions involved in using this method of computation are not quite valid, as shown elsewhere.[13] The ratio of CO chemisorption to the nitrogen monolayer volume (V_{CO}/V_m) gives an approximate figure for the extent of "free" cobalt atoms on the surface of the catalyst.

variation are shown in Figs. 1 to 6. Temperature variations above 53° show desorption–readsorption phenomena, which are regarded as reflecting the heterogeneous character of the surface. A blank experiment, performed with helium in place of hydrogen, showed that in each case temperature equilibrium was established in less than three minutes.

The amounts of desorption following the various temperature increases and the sharp ascents in adsorption (readsorption) following the corresponding decreases of temperature are grouped for ready reference in Table II. These values show that the two processes of desorption and readsorption are in the main interrelated since in most of the cases the amounts of hydrogen desorbed on increase

TABLE II

AMOUNTS OF HYDROGEN DESORBED ON RAISING THE TEMPERATURE AND READSORBED ON LOWERING THE TEMPERATURE

Temp., °C.		CATALYST A						CATALYST B						CATALYST C				
		Fresh		Sint. 360°		Sint. 400°		Fresh		Sint. 375°		Sint. 425°		Fresh		Sint. 400°		Sint. 425°
T_1	T_2	Des.	Reads.	Des.	Reads.	Des.	Reads.	Des.	Reads.	Des.	Reads.	Des.	Reads.	Des.	Reads.	Des.	Reads.	Des.	Reads.
0	53	0.03	Nil	Nil	Nil	Nil	Nil	Nil	0.11	Nil	0.18	Nil	0.14	Nil	0.15	Nil	0.16	Nil	0.12
53	97	.08	0.03	0.14	0.08	0.09	0.06	0.16	.11	0.10	.07	0.07	.09	0.18	.15	0.08	.12	0.07	.15
97	134	.32	.17	.23	.09	.12	.08	.14	.17	.18	.14	.09	.14	.20	.22	.13	.15	.13	.15
134	204	.12	.12	.30	.17	.18	.14	.09	.09	.12	.05	.09	.21	.68	.41	.33	.18	.29	.24

The surface area increases with the addition of the promoters, thoria being more effective than magnesia in this respect. Likewise, the values of CO chemisorption per gram of the reduced catalysts increase with the incorporation of the promoters, though the proportion of cobalt by weight is reduced thereby. On the other hand, the fraction of free cobalt on the surface, V_{CO}/V_m, is about twice as much in the unpromoted catalyst as in the promoted ones. Heat treatment up to 400 or 425° decreases the surface areas of all the catalysts, this effect being most pronounced on the unpromoted catalyst. The chemisorption of carbon monoxide also decreases with sintering, presumably due to the formation of larger crystallites of metallic cobalt. These observations are in general agreement with those of Anderson, et al.,[12] on the function of promoters in cobalt catalysts.

Desorption–Readsorption Phenomena.—The ki-
netics of hydrogen adsorption on the catalysts at constant atmospheric pressure with temperature

(12) R. B. Anderson, W. K. Hall and L. J. E. Hofer, J. Am. Chem. Soc., 70, 2465 (1948).

(13) M. V. C. Sastri and V. Srinivasan, Curr. Sci., 23, 154 (1954).

of temperature from T_1 to T_2 are, respectively, nearly equal to the amounts readsorbed on reversing this temperature change.

The adsorption isobars, shown in Figs. 7 to 9, have been obtained by plotting the final values of adsorption at each temperature, both with the temperature ascending and with the temperature descending. The isobars have the same general shape for the freshly reduced and for the sintered catalysts, with the difference that the absolute values for the latter are lower. An interesting exception to this generalization is provided by the (temperature) descending isobars of catalyst B (Co–ThO₂–KG).

Adsorption values determined 10 minutes after each temperature ascent are also plotted on the same graphs. It is seen that the "10 minute isobars" (broken lines) follow closely the pattern of the main isobars drawn from the final values.

At the temperatures of minimum adsorption all the catalysts show very poor adsorption. Especially catalyst A after sintering at 400° manifests negligible adsorption of hydrogen at $-95°$. This

Fig. 1.—Adsorption of hydrogen at 68 cm. pressure on catalyst A on raising temperature: O-O, before sintering, ⊗-⊗, after sintering at 360°, △-△ after sintering at 400°. A, change from −191 to −95°; C, from −95 to −78°; D, from −78 to 0°; E, from 0 to 53°; F, from 53 to 97°; H, from 97 to 134°; J, from 134 to 204°; L, final value at 204°.

establishes the total absence of van der Waals adsorption at this temperature and above.

In all the cases, the 10 minutes and the final adsorption values increase steeply as the temperature is raised from −78 to 53°, but remain almost stationary with further increase in temperature. As the maximum of activated adsorption is reached at about 53° for the promoted as well as unpromoted catalysts, it may be concluded that this increase in adsorption from −78 to 53° is associated not with the promoter molecules, but with the portion of the surface containing cobalt.

In the (temp.) descending isobars for catalyst A, the adsorption levels off below 53° down to −78° at which temperature van der Waals adsorption is still negligible. That is, in the range −78 to 53°, there is neither desorption nor readsorption to follow the respective changes of temperature. With catalysts B and C, however, though no desorption is noticed as the temperature is increased from −78 to 0° and thence to 53°, a sharp rise in adsorption ensues after each drop in temperature in the reverse order. As a result, the descending isobars for these catalysts show a steady rise in activated adsorption down to −78°. This behavior of hydrogen adsorption on catalysts B and C is comparable with that observed with Manganous oxide–chromic oxide by Taylor and Liang,[14] who have shown that it could occur where the rate

(14) H. S. Taylor and S. C. Liang, *J. Am. Chem. Soc.*, **69**, 2989 (1947).
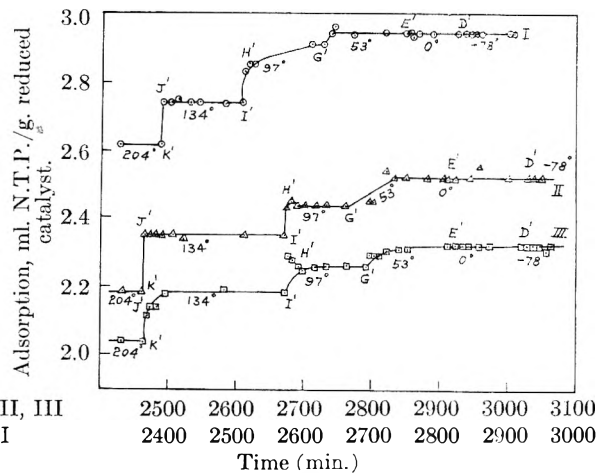
Fig. 2.—Adsorption of hydrogen at 68 cm. pressure on catalyst A on lowering temperature: O-O, before sintering; △-△, after sintering at 360°; □-□, after sintering at 400°: K′, change from 204 to 134°; I′, from 134 to 97°; G′, from 97 to 53°; E′, from 53 to 0°; D′, from 0 to −78°.

of desorption following the temperature rise is slower than that of the simultaneous adsorption on other parts of the surface.

A comparison of the effect of sintering on the adsorption of hydrogen by these catalysts is presented in Table III, which gives the 10 minutes and final adsorption values at 53 and 204° for the freshly reduced and the fully sintered catalysts. It is seen that in all cases the adsorption at 53°

Fig. 3.—Adsorption of hydrogen at 68 cm. pressure on catalyst B on raising temperature: O–O, before sintering; △–△, after sintering at 375°; □–□, after sintering at 425°. A, change from −191 to −95°; C, from −95 to −78°, D, from −78 to 0°; E, from 0 to 53°; F, from 53 to 97°, H, from 97 to 134°; J, from 134 to 204°; L, final value at 204°.

decreases more than that at 204° as a result of sintering. This is an indication that the thermal sintering affects the sites active at low temperatures more than those operative at high temperatures.

uptake of hydrogen at low pressures and different temperatures on thin films of nickel and iron prepared by evaporation in high vacuum. They observed that with increase of temperature the total uptake of hydrogen increased, reached a maximum

TABLE III

EFFECT OF SINTERING ON HYDROGEN ADSORPTION (ML./G.) AT 53 AND 204°

Temp., °C.	Time, min.	Catalyst A			Catalyst B			Catalyst C		
		Fresh	Sint. 400°	Diff.	Fresh	Sint. 425°	Diff.	Fresh	Sint. 425°	Diff.
53	10	2.61	1.49	−1.12	1.99	1.56	−0.43	4.67	1.60	−3.07
	Final	2.77	1.79	−0.98	2.34	1.95	−0.39	4.80	1.87	−2.93
204	10	2.53	1.77	−0.76	2.30	2.10	−0.20	4.13	1.96	−2.17
	Final	2.62	2.04	−0.58	2.45	2.66	+0.21	4.55	2.64	−1.91

These results on cobalt catalysts are in many respects similar to those obtained by Sadek and Taylor[2] on nickel catalysts and have been interpreted likewise on the basis that the uptake of hydrogen is almost wholly a surface event and that the desorption–readsorption phenomena reflect the energetic heterogeneity of the catalyst surface. In this connection, the "solution" hypothesis of Beeck and the "adsorption on surface oxide" hypothesis of Schuit and de Boer have both been examined and found inapplicable to the results presented here.

In their recent publication Beeck and his co-workers[5] determined the isobaric changes in the

usually at about 0° and then decreased, and, further, that the isobaric sorption value measured with decreasing temperature were clearly above the ascending temperature isobars. Progressive sintering of the metal films greatly reduced their specific surface areas and the absolute values of hydrogen uptake. The difference between the values on the ascending and descending isobars at any temperature remained fairly constant with respect to temperature and was therefore ascribed to a process of absorption of hydrogen into the lattice structure of the metal and not to activated adsorption. More recently, however, Dr. Beeck is stated to have admitted in a private communica-

I	2400	2500	2600	2700	2800	2900
II	2600	2700	2800	2900	3000	3100
III	2500	2600	2700	2800	2900	3000

Time (min.).

Fig. 4.—Adsorption of hydrogen at 68 cm. pressure on catalyst B on lowering temperature: O–O, before sintering; △–△, sintered at 375°; □–□, sintered at 425°. K′, change from 204 to 134°; I′, from 134 to 97°; G′, from 97 to 53°; E′, from 53 to 0°; D′ from 0 to −78°.

tion to Dr. Emmett[15] that the solubility effect found on nickel films was not exhibited by ordinary nickel catalysts formed by the reduction of nickel oxide. The following considerations show that no appreciable solubility effect occurs in the cobalt catalysts used in the present investigation.

(1) The amounts of hydrogen taken up by catalysts (2 to 4.5 ml. per gram of the catalyst or 6 to 13.5 ml. per gram of cobalt) between the ascending and descending isobars are many times the known solubilities of the gas in the metal. They are also not constant with respect to sintering with any of our catalysts, as can be seen from the figures given for −78 and 0° in Table IV. This is similar to the observations of Sadek and Taylor with nickel–kieselguhr. In the case of catalyst C the differential adsorption decreases almost in parallel with the decrease in the "free cobalt" surface, but this is not true of the other two catalysts, where the differences increase with the degree of sintering. This behavior of catalysts A and B is not surprising since activated adsorption is a specific property and would be influenced by many

(15) H. H. Podgurski and P. H. Emmett, THIS JOURNAL, **57**, 159 (1953).
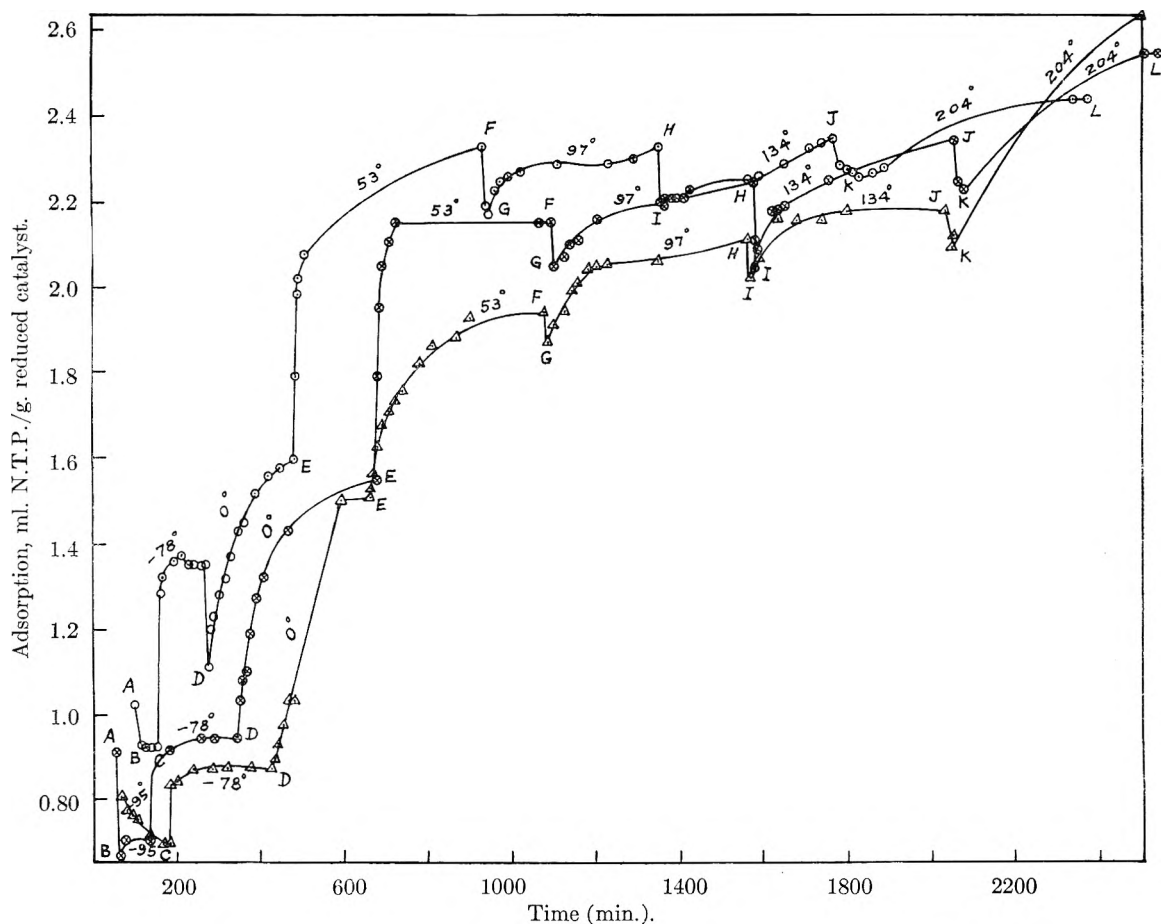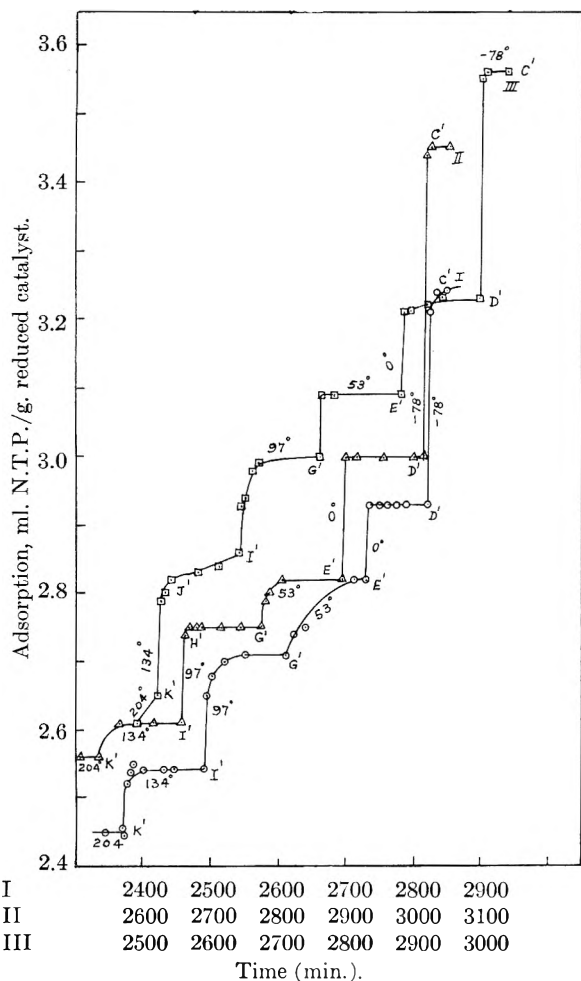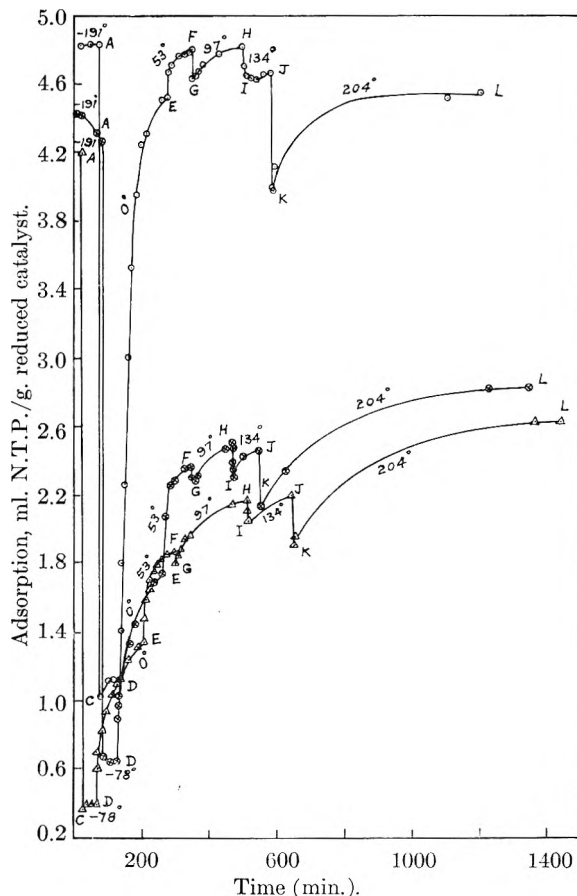

Fig. 5.—Adsorption of hydrogen at 68 cm. pressure on catalyst C on raising temperature: O–O, before sintering; ⊗–⊗, after sintering at 400°; △–△, after sintering at 425°. A, change from −191 to −78°; D, from −78 to 0°; E, from 0 to 53°; F, change from 53 to 97°; H, from 97 to 134°; J, from 134 to 204°; L, final value at 204°.

factors such as a change of structure in the metal lattice, redistribution of the energetics of the sites due to heat treatment, etc.

TABLE IV

DIFFERENTIAL ADSORPTION AT −78° AND 0°

Catalyst	Difference between ascending and descending isobars (ml./g.)	
	−78°	0°
A, reduced at 300°	2.42	0.34
A, sintered at 360°	2.01	0.64
A, sintered at 400°	2.26	1.11
B, reduced at 350°	2.21	1.33
B, sintered at 375°	2.51	1.45
B, sintered at 425°	2.69	1.72
C, reduced at 350°	4.52	0.93
C, sintered at 400°	2.90	1.69
C, sintered at 425°	3.06	1.96

(2) At the temperatures of minimum adsorption all the catalysts show very poor adsorption. This is especially marked in the case of catalyst A, which when sintered at 400° manifests negligible adsorption at −95° (see Fig. 7), indicating thereby the virtual absence of van der Waals adsorption at this temperature and above. With further increase of temperature the uptake of gas increases to about 1.8 ml. at 97°, which on Taylor's theory is due to the setting in of activated adsorption with appreciable
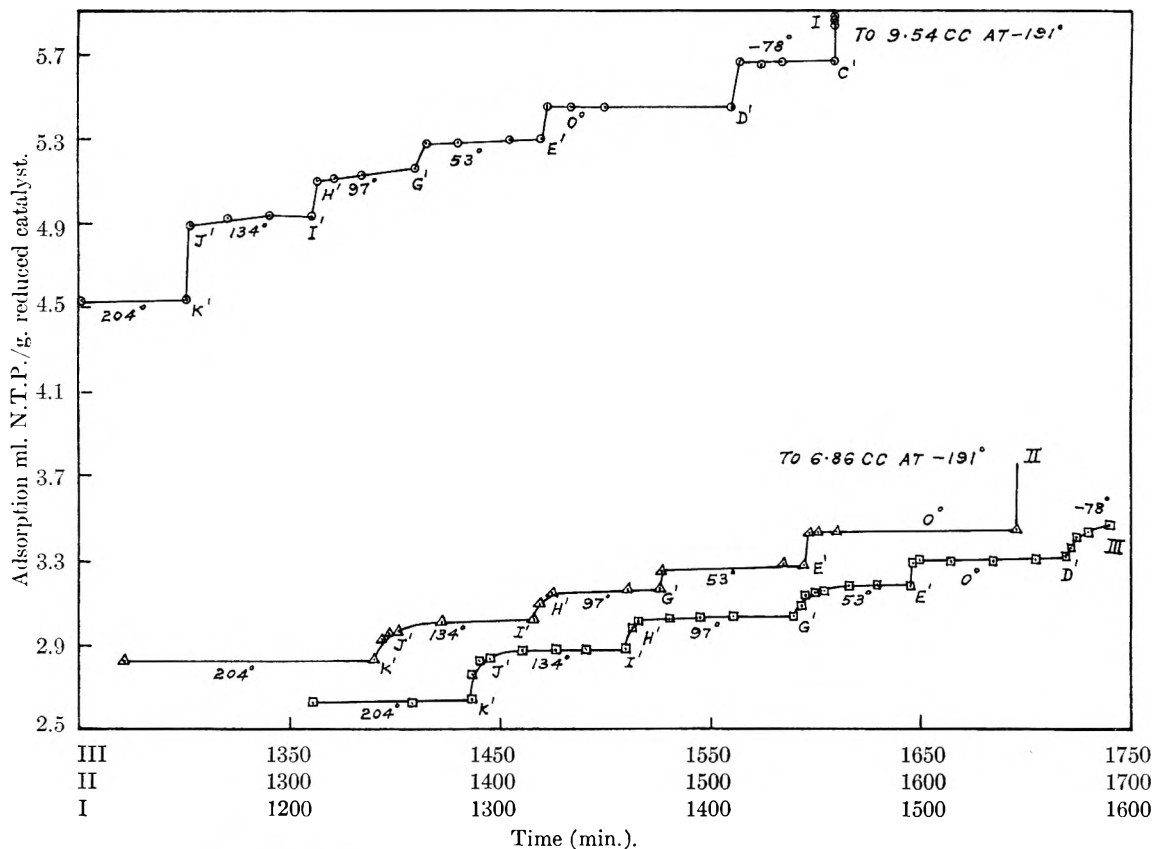
Fig. 6.—Adsorption of hydrogen at 68 cm. pressure on catalyst C on lowering temperature: O–O, before sintering; △–△ after sintering at 400°; □–□, after sintering at 425°. K', change from 204 to 134°; I' from 134 to 97°; G', from 97 to 53°; E', from 53 to 0°; D', from 0 to −78°; C', from −78 to −191°.

Fig. 7.—Adsorption isobars of hydrogen on catalyst A at 68 cm. pressure: O,Q, freshly reduced catalyst; △,△, sintered at 360°; □,□, sintered at 400°; ----, 10 min. after temperature change.
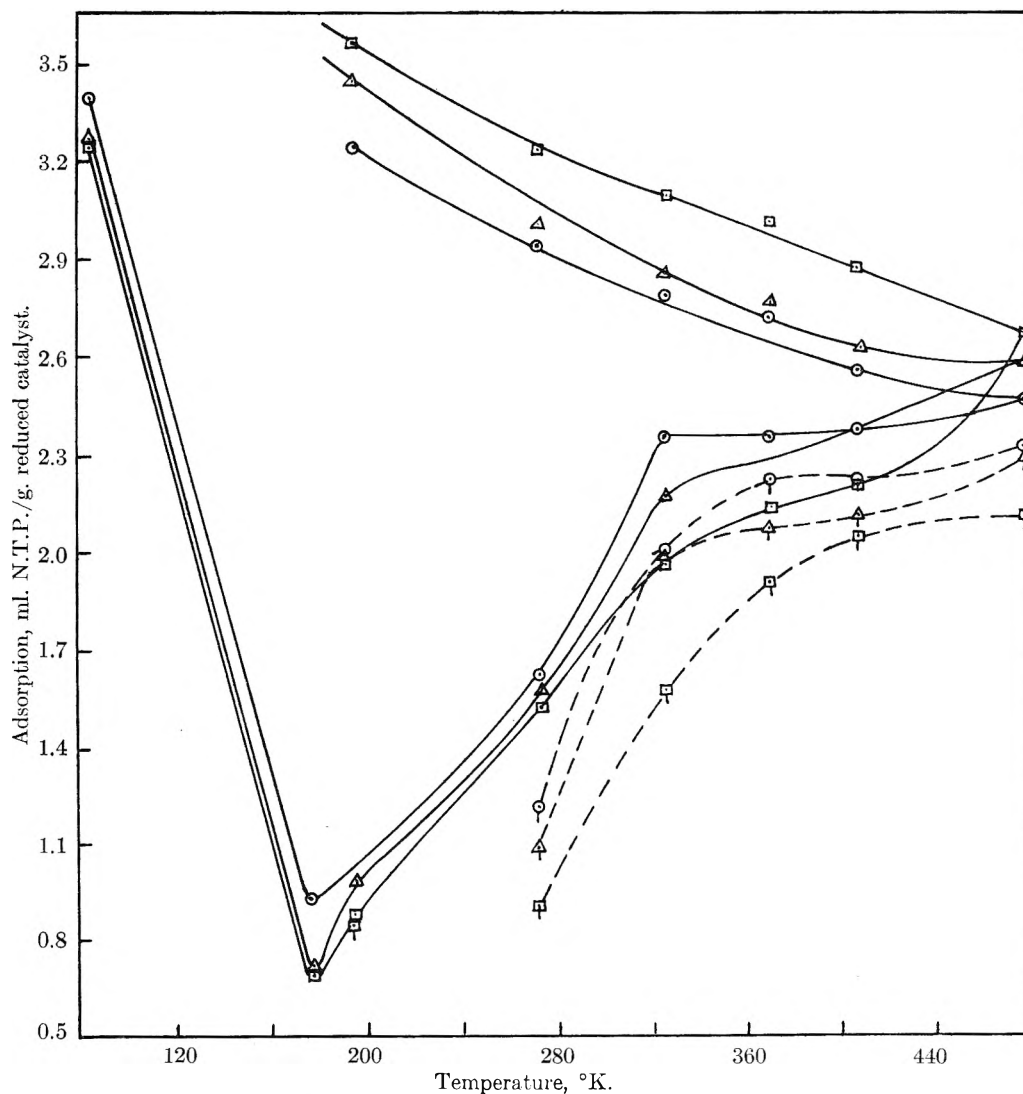
Fig. 8.—Adsorption isobars of hydrogen on catalyst B at 68 cm. pressure: O,O, freshly reduced catalyst; △,△, sintered at 375°; □,□, sintered at 425; ----, 10 min. after temperature change.

velocity. Beeck and co-workers, on the contrary, attribute the rise in uptake with temperature to the solution or absorption of the gas in the metallic structure. The desorption effects observed after each increase in temperature in the range 0 to 134° are, however, difficult to explain on the latter hypothesis. It was observed that in the course of this stepwise increase in temperature on aggregate amount of 0.40 ml. (i.e., nearly 22% of the total increase in gas uptake) is desorbed from the surface. Remembering that the surface was virtually bare at −95°, it is obvious that this amount of hydrogen desorbed must have formed part (only a part of the gas taken on the surface, i.e., adsorbed increasingly with increase in temperature.

Further, Beeck's concept of the uptake of gas as due to solution in the metallic structure would imply in the present case that the hydrogen sinks into the interior of the metal while the surface is substantially bare: this is highly unlikely.

(3) From the configuration of the cobalt atoms in the possible crystal faces of metallic cobalt, Anderson, Hall and Hofer,[12] have shown that as a result of steric limitations imposed by the size of the

CO molecule, on an average, one CO molecule is chemisorbed for every five atoms of cobalt on the surface. Since each metal atom chemisorbs a hydrogen atom, the average ratio of CO chemisorption to monolayer hydrogen chemisorption is 2:5. On our catalysts, the maximum values of hydrogen adsorption (read from the descending isobars at −95 or −78°) lie between 32 and 77% the monolayer saturation values for the part of the surface consisting of free cobalt, (shown to be underestimated from the computed CO chemisorption at −78°[13]). This shows that a considerable proportion of the metal atoms on the surface is left bare in each case, making it highly improbable for the hydrogen atoms to penetrate into the mass of the metal.

(4) Although the weight proportion of cobalt is greater in the unpromoted catalyst A, than in the promoted ones, B and C, the latter chemisorb hydrogen more than the former, as may be seen from a comparison of the values on the descending isobars at −78° for instance. At least for the freshly reduced catalysts the hydrogen adsorption maxima run nearly parallel to the extent of free cobalt on the surface, thus showing that the observed sorption
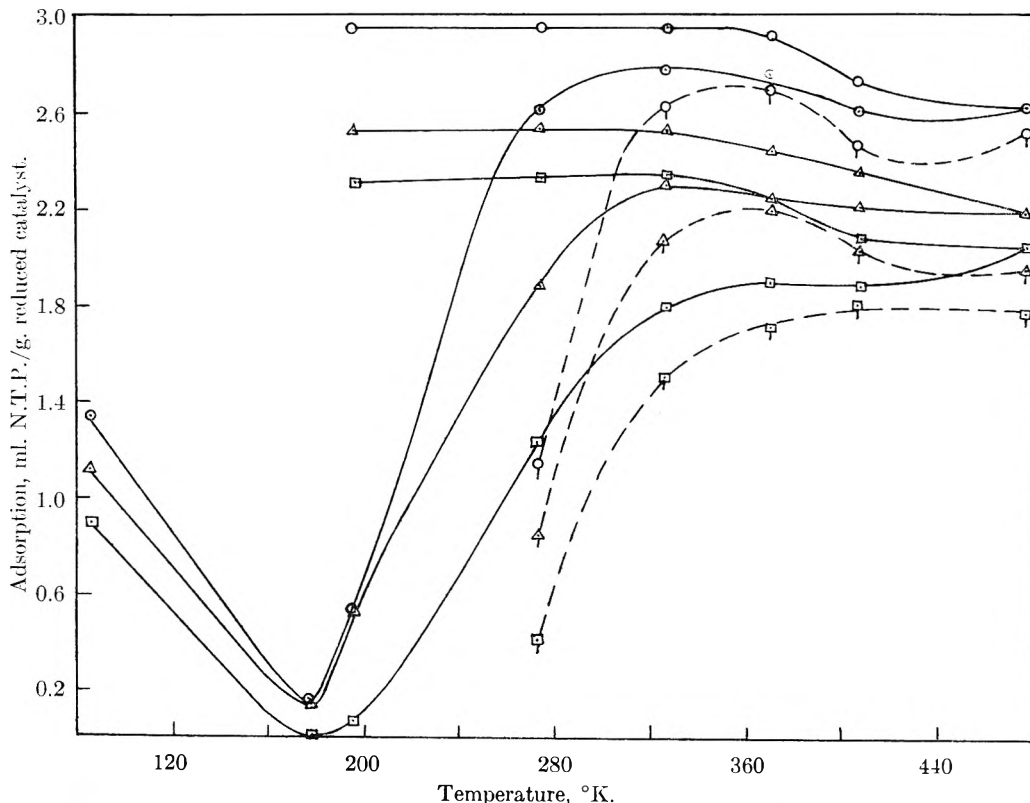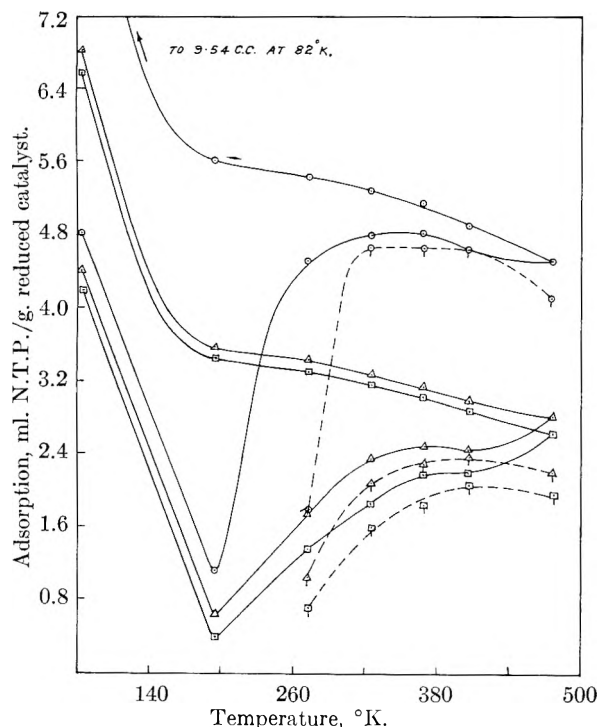
Fig. 9.—Adsorption isobars of hydrogen on catalyst C at 68 cm. pressure: ○,◎, freshly reduced catalyst; △,▲, sintered at 400°; □,◻, sintered at 425°; ----, 10 min. after temperature change.

of the gas is predominantly a surface phenomenon rather than a mass effect as postulated by Beeck.

Schuit and de Boer[8] postulated that the slow stage of adsorption at intermediate temperatures was due to chemisorption of hydrogen on top of oxygen atoms brought to the surface from within the catalyst when the latter was subjected to high temperature *in vacuo* or in an inert atmosphere. It may be pointed out that the nickel–silica catalysts used by Schuit and de Boer were prepared by coprecipitation while the cobalt catalysts used in the present study were precipitated on the surface of the support. It is known that the coprecipitated catalyst being very intimately intermixed with the support, would be much more difficult to reduce than catalysts deposited on the surface of the carrier. Hence there is considerably less likelihood of the existence of an oxygen concentration gradient between the bulk and the surface, in our catalysts.

To test whether any appreciable amount of oxygen appeared on the surface during the evacuation process, the following experiment was conducted. A fully reduced sample of catalyst B was evacuated for 12 hours at 350° to 375° and treated with a fairly rapid stream of pure, dry, hydrogen. The exit gas was conducted through a condensing train consisting of a stopcock, a trap cooled in liquid air, a small mercury manometer and a second stopcock in tandem. After an hour, the catalyst was evacuated through the condensing train at the same temperature, at first slowly and then in the usual way for 2 hours. This cycle of streaming hydrogen and evacuating was repeated carefully thrice, after which the two stopcocks at either end of the condensing unit were closed. When the liquid air-bath

was withdrawn and the trap allowed to warm up to room temperature, the manometer attached to the trap continued to read dead vacuum, without even as much as a deflection in the curvature of the mercury meniscus. A repeat run at 400° gave the same result.

The capacity of the condensing trap being 25 ml. even 0.003 ml of. water vapor would have sufficed to register a pressure of more than 0.1 mm. which could easily have been detected. Thus it is clear that little or no oxygen is brought up to the surface during evacuation of these cobalt catalysts and hence the slow adsorption of hydrogen cannot be regarded as occurring on top of chemisorbed oxygen on the surface.

This experiment also shows that the observed desorption following temperature changes is intepretable only as the desorption of hydrogen present on the surface and not as that of water vapor formed by the action of hydrogen on any residual oxygen that might have been conceivably present on the surface since the temperatures involved in the adsorption runs are much lower and the other experimental factors much less favorable to reduction than in the test experiment described above.

The difference between the 10 minute and the final values constitutes, at each temperature, the slow stage of the sorption process, which Schuit and de Boer designate as Type B and interpret as chemisorption of hydrogen "on top" of chemisorbed oxygen atoms (surface oxide) on the surface of the metal. Reference to Table V shows that in many cases the amount of this slow uptake of hydrogen forms a considerable proportion of the corresponding CO chemisorption. For instance on catalyst A, the slow uptake at 0° ranges from 59 to 72% of the CO chemisorption values for the different degrees of sintering. On the Schuit–de Boer hypothesis this would imply that a considerable part of the cobalt surface is unreduced, which is highly improbable under the conditions of reduction reported here.

Moreover, in almost every case the slow uptake decreases with temperature in the range 0 to 134°, whereas chemisorption on reducible oxides should actually increase with temperature.

While at lower temperatures the amount of slow adsorption does not vary in a uniform manner with degree of sintering, at the highest temperature (204°) the extent of this creep and the over-all rate of this slow uptake both increase uniformly with degree of sintering in each catalyst, as can be seen from Table V. In the case of the Co–thoria–kieselguhr catalyst, B, this effect, coupled with the rather close final values at 134°, leads to a reversal of the normal order of adsorption with the degree of sintering.[16]

This unusual feature of the slow uptake by hydrogen at 204° cannot be attributed to reduction of (or even chemisorption of hydrogen on) surface cobalt oxide for reasons already stated. It might, however, be due to the onset of another type of activated adsorption setting in at this temperature or even below. Such an occurrence of more than one type of activated adsorption of the same gas on the

(16) The same effect was noticed with another sample of reduced catalyst B prepared anew from the original ingredients.

TABLE V

SLOW ADSORPTION OF HYDROGEN

| Catalyst | Difference in ml./g. between 10-min. and final adsorption values in the temp. variation expt. | | | | | Difference in adsorption between 10-min. and 210 min. after change to 204° |
	0°	53°	97°	134°	204°	
A, reduced at 300°	1.47	0.16	0.09	0.14	0.09	0.09
A, sintered at 360°	1.05	.24	.06	.18	.23	.18
A, sintered at 400°	0.81	.30	.19	.08	.27	.17
B, reduced at 350°	0.40	0.35	0.14	0.16	0.14	0.03
B, sintered at 375°	.47	.20	.20	.27	.30	.14
B, sintered at 425°	.62	.39	.23	.16	.55	.39
C, reduced at 350°	2.72	0.12	0.17	0.00	0.42	0.22
C, sintered at 400°	0.71	.28	.21	.08	.63	.32
C, sintered at 425°	0.65	.27	.33	.11	.69	.45

solid is not without precedent. Emmett and co-workers[17,18] found three types of chemisorption of hydrogen on iron occurring at −195, −78 and 100°, respectively. These were ascribed by them to the uptake of hydrogen by different crystal-

(17) S. Brunauer and P. H. Emmett, *J. Am. Chem. Soc.*, **62**, 1732 (1940).

(18) J. T. Kummer and P. H. Emmett, This Journal, **56**, 258 (1952).

lographic planes of the reduced iron. The isobars of hydrogen (Figs. 7–9) show another minimum below 204° which is clearly discernible in the sintered catalysts. Since the slower uptake of hydrogen at 204° occurs to a greater extent on the sintered catalysts it may be identified with adsorption on the more closely packed faces of cobalt which may be expected to be produced as a result of sintering.

VISCOSITY AND DENSITY OF THE NITRIC ACID–NITROGEN DIOXIDE–WATER SYSTEM[1,2]

By David M. Mason, Ira Petker and Stephen P. Vango

Jet Propulsion Laboratory, California Institute of Technology, Pasadena, Cal.

The viscosity and density of the HNO_3–NO_2–H_2O system were measured at 0, 25 and 40° for compositions in the range from 75 to 100 wt. % HNO_3, 0 to 20 wt. % NO_2 and 0 to 5 wt. % H_2O. In this range of composition and temperature the absolute viscosity varies between approximately 0.6 and 2.9 centipoises, and the density varies between approximately 1.46 and 1.62 g./cc. The viscosity of HNO_3 solutions increases with an increase in NO_2 or H_2O, and the density increases with an increase in NO_2 and decreases with an increase in H_2O. The viscosity and density of the HNO_3–NO_2 system were measured at 0° over the range of compositions from 0 to 52 and from 99.6 to 100 wt. % NO_2. Two liquid phases are present at 0° in this binary system in the intervening range of compositions. At 0° both the viscosity and the density of the system exhibit a maximum near 45 wt. % NO_2. The viscosity and density of the HNO_3–H_2O system were measured at 0° for compositions of 0 to 10 wt. % H_2O. Experimental values of viscosity and density are presented in tabular form. The uncertainty in the experimental viscosity measurements is ±0.5% and in the density measurements is ±0.03%.

I. Introduction

Viscosity and density data for the HNO_3–NO_2–H_2O system are necessary in certain applications in which the system is used as an oxidant. Also these physicochemical properties provide further information on the ionic equilibria associated with this system.[3,4] Few data, however, for these properties of the ternary system appear to be available in the literature although some data are available for the binary systems of HNO_3–NO_2 and HNO_3–

H_2O. Schofield,[5] Bingham and Stone,[6] and Chanukvadze[7] have reported values of the viscosity of the HNO_3–H_2O system, but no viscosity data for the HNO_3–NO_2 system appear to be available. Klemenc and Rupp[8] have reported values of the density of the HNO_3–NO_2 system. Chanukvadze,[7] Veley and Manley,[9] Schulze,[10] and Ostwald[11] have reported values of the density of the HNO_3–H_2O system. It was the purpose of the present investigation to obtain values of these properties for both practical and theoretical use.

II. Description of Equipment and Methods

The design of instruments for the measurement of the viscosity and density of the HNO_3–NO_2–H_2O system was

(3) (a) I. C. S. Goulden and D. J. Millen, *J. Chem. Soc.*, 2620 (1950); (b) J. Chédin and S. Fénéant, *Compt. rend.*, **228**, 242 (1949).

(4) E. D. Hughes, C. K. Ingold and R. I. Reed, *J. Chem. Soc.*, 2400 (1950).

(5) D. Schofield, *Bull. Chem. Soc. (Peru)*, **6**, 7 (1935).

(6) E. C. Bingham and S. B. Stone, This Journal, **27**, 701 (1923).

(7) O. P. Chanukvadze, *J. General Chem. (USSR)*, **17**, 411 (1947).

(8) A. von Klemenc and J. Rupp, *Z. anorg. allgem. Chem.*, **194**, 51 (1930).

(9) V. H. Veley and J. H. Manley, *London, Edinburgh Dublin Phil. Mag. and J. Sci.*, **3**, 118 (1902).

(10) A. Schulze, *Z. anal. Chem.*, **21**, 167 (1882).

(11) W. Ostwald, *J. prakt. Chem.*, **18**, 328 (1878).
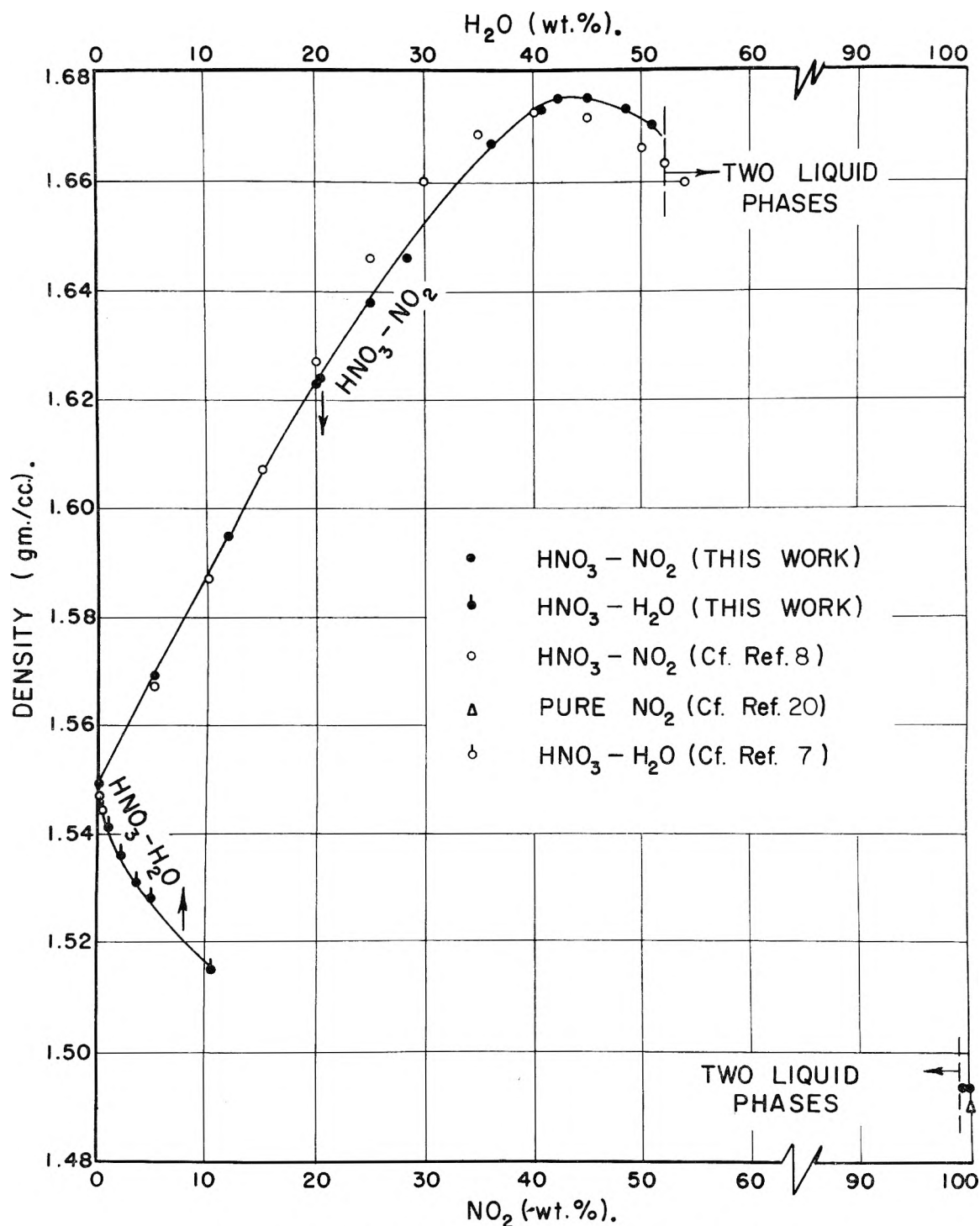
Fig. 1.—Density of the HNO_3–NO_2 and HNO_3–H_2O systems at 0°.

dictated by the relatively high vapor pressure and hygroscopicity of this system. In order to eliminate loss of components from the system or pickup of H_2O from the atmosphere closed instruments were employed.

A. Viscosity Measurements.—Viscosity was measured with an Ostwald-type capillary viscometer modified for closed systems by Zhukov.[12] Three viscometers of similar dimensions were constructed to permit measurements on samples of three different compositions to be made at a given

temperature. The viscometer was closed to the atmosphere by means of a ground-glass stopper.

Acid of known composition was weighed intc the viscometer which was submerged in a constant-temperature waterbath. Composition of a sample in the viscometer was varied by adding directly to the sample a known weight of one of the components, NO_2 or H_2O. The viscometer was suspended in the bath by means of a clamp manufactured by the Harshaw Company, which ensured reproducibly near-vertical alignment. Temperature regulation in the bath was maintained within ±0.03° for the measurements at 25 and 40° by means of a mercury thermoregulator. The bath was filled with a mixture of ice and water for measurements at 0°.

(12) A. Weissberger, "Physical Methods of Organic Chemistry," Vol. I, Part I, Interscience Publishers, Inc., New York, N. Y., 1949, p. 332.
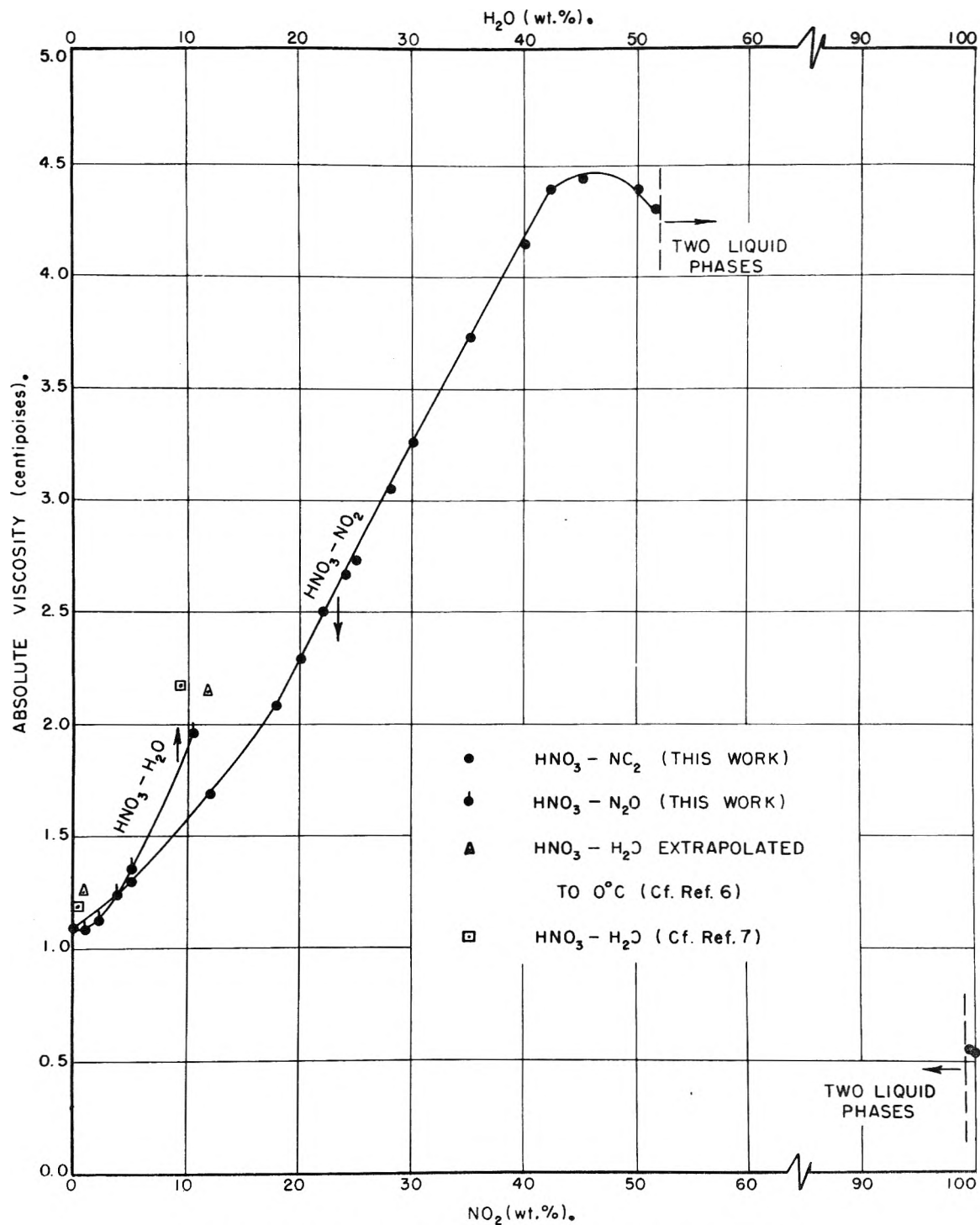
Fig. 2.—Absolute viscosity of the HNO₃–NO₂ and HNO₃–H₂O systems at 0°.

The temperatures of the bath were measured with a total immersion mercury-in-glass thermometer calibrated by the Bureau of Standards. The interval of time for the meniscus of the liquid to move between marks on the capillary tube was recorded by means of a mechanical stopwatch. For a series of five measurements on a given sample, average flow times were reproducible to within 5 parts in 1000 for flow times of about 100 seconds and were reproducible to within 2 parts in 1000 for flow times greater than 4 minutes. Measurements of viscosity on each sample of acid were made at 0, 25 and 40° and again at 0° in the order given. The duplicate measurements at 0° were made to detect possible changes in viscosity caused by changes in composition that

may have occurred from thermal decomposition[13] at the higher temperatures. It was found that the final values of viscosity at 0° did not differ measurably from the initial values at 0°.

One of the major uncertainties in obtaining accurate viscometric data lies in the calibration of the viscometer. As seen from the theoretical relationship for laminar flow in a round tube[12]

$$\eta = c\rho\theta - (c'\rho/\theta) \qquad (1)$$

(13) G. D. Robertson, "The Kinetics of the Thermal Decomposition of Nitric Acid in the Liquid Phase, Part I (thesis)," California Institute of Technology, Pasadena, Calif., 1953.

TABLE I

EXPERIMENTAL VALUES OF KINEMATIC VISCOSITY, DENSITY AND ABSOLUTE VISCOSITY OF THE HNO₃–NO₂–H₂O SYSTEM

Compositions are expressed in weight per cent. NO₂ and H₂O with the remainder HNO₃ to make 100 wt. %.

Composition (wt. %)		Kinematic viscosity (centistokes)	0.0° Density (g./cc.)	Absolute viscosity (centipoises)	Kinematic viscosity (centistokes)	25.0° Density (g./cc.)	Absolute viscosity (centipoises)	Kinematic viscosity (centistokes)	40.0° Density (g./cc.)	Absolute viscosity (centipoises)
NO₂	H₂O									
0.00	0.00	0.705	1.549	1.032	0.496	1.504	0.746	0.418	1.477	0.617
.00	1.01	.704	1.541	1.085						
.00	2.10	.731	1.536	1.123	.513	1.493	.766	.435	1.468	.639
.00	3.63	.804	1.531	1.231						
.00	5.09	.878	1.528	1.342	.591	1.486	.878	.492	1.461	.719
.00	10.37	1.300	1.515	1.969						
4.80	5.18	1.086	1.549	1.682	.705	1.506	1.062	.571	1.479	.845
4.97	1.73	0.874	1.559	1.363	.603	1.517	0.915	.499	1.488	.743
5.06	0.00	0.834	1.569	1.309	.572	1.525	0.873	.480	1.498	.720
11.21	5.63	1.413	1.570	2.22	.860	1.527	1.313	.676	1.500	.980
11.63	2.11	1.148	1.584	1.818	.755	1.542	1.163	.608	1.515	.921
11.88	0.00	1.053	1.595	1.680	.700	1.553	1.087	.572	1.525	.873
17.75	0.00	1.290	...	2.08						
19.02	5.14	1.766	1.593	2.81	1.022	1.550	1.584	.779	1.521	1.185
19.70	1.74	1.548	1.614	2.50	0.941	1.572	1.479	.731	1.543	1.128
20.05	0.00	1.425	1.623	2.3_	.893	1.581	1.412	.707	1.553	1.099
20.34	.00	...	1.624							
22.02	.00	1.540	...	2.51						
24.03	.00	1.634	...	2.67						
24.96	.00	...	1.638							
25.04	.00	1.695	...	2.7_						
28.05	.00	1.858	...	3.06						
28.33	.00	...	1.646							
30.03	.00	1.977	...	3.26						
35.05	.00	2.24	...	3.7_						
36.19	.00	...	1.665							
40.02	.00	2.49	...	4.1_						
40.68	.00	...	1.673							
42.35	.00	2.62	1.675	4.39						
45.09	.00	...	1.675							
45.16	.00	2.65	...	4.44						
48.40	.00	...	1.673							
50.00	.00	2.63	...	4.39						
50.86	.00	...	1.670							
51.91	.00	2.58	...	4.30						
99.58	.00	0.365	1.494	0.545						
100.0	.00	0.359	1.494	0.536						

the absolute viscosity η, as determined by the total time θ for a given volume of liquid to flow through the tube, depends upon two-dimensional constants c and c' of the instrument. The second term, $c'\rho/\theta$, where ρ is the density of the fluid, in the present experiments was approximately 1% of the first term. In order to obtain data of greater accuracy than 1%, this second term must be accurately evaluated. In actuality c' is a function of η and ρ; thus equation 1 is strictly not valid over wide ranges of viscosity.

In the present investigation equation 1 was assumed to be valid over the range of viscosities studied, and to ensure reasonable applicability of this equation, constants c and c' were calculated by measuring flow times on substances of known viscosity in this range. From the resulting data a set of simultaneous equations of the form of equation 1 was solved for c', but this method gave a wide spread of values for c'. The value of c' was also determined by relating it theoretically to the volume of the viscometer bulb and length of the capillary of the viscometer,[12] but this method does not give good correlation with experimental data.

Finally a graphical method was employed in the calibration procedure. Since the kinematic viscosity ν is defined as

$$\nu = \eta/\rho \qquad (2)$$

substituting ν in equation 1 and rearranging gives

$$\nu\theta = c\theta^2 - c' \qquad (3)$$

H₂O[14,15] and carbon tetrachloride[16–18] at 0, 25 and 40°, whose kinematic viscosities are known, were both used to calibrate each viscometer. A plot of the form of equation 3 was made from these data, the values of $\nu\theta$ for H₂O and carbon tetrachloride being plotted vs. θ^2. A straight line was drawn through the experimental points, and the average deviation of these points from the line was 0.5% for each of the three viscometers used. Values of kinematic viscosity of samples of nitric acid mixtures were obtained from experimental flow times by use of these calibration curves.

B. Density Measurements.—A glass pycnometer consisting of a bulb and stem was used for the density measurements. The stem consisted of the calibrated portion of a precision nitrometer manufactured by the Kimble Glass Company with a scale that could be read to 0.001 cc. The pycnometer was calibrated by adding known amounts of distilled water to the system. The total volume of the bulb and stem is approximately 5 cc. An error of less than about 1 part in 5000 occurred in the measurement of the volume of a sample. Since gravimetric measurements were more accurate than volumetric measurements, volumetric measurements limited the accuracy of the values of density. Density measurements on samples of nitric acid mixtures were reproducible to ±0.0005 g./cc.

In brief, the procedure followed was to weigh a quantity of acid of known composition into the pycnometer and then to place the pycnometer in the constant-temperature bath so that the liquid level of the acid was below the water level of the bath. After enough time for thermal equilibrium to be approached between the pycnometer and its contents and the bath, the scale reading of the pycnometer at the meniscus of the acid was recorded, and the total volume of the sample was determined from this reading, together with the calibration data. With one sample in the closed pycnometer the density was measured at 0, 25 and 40°.

III. Materials

HNO₃ was prepared by vacuum distillation at about 40° of a mixture of reagent-grade, 95 wt. %[19] H₂SO₄ and Baker and Adamson reagent-grade KNO₃ and collected in a flask

(14) E. C. Bingham and G. F. White, *Z. physik. Chem.*, **80**, 670 (1912).

(15) J. R. Coe, Jr., and T. B. Godfrey, *J. App. Phys.*, **15**, 625 (1944).

(16) E. Van Aubel, *Bull. classe sci. Acad. roy. Belg.*, **18**, 1026 (1932).

(17) G. P. Luchinskii, *J. Phys. Chem. (USSR)*, **6**, 607 (1935).

(18) R. Furth, *Proc. Cambridge Phil. Soc.*, **37**, 281 (1941).

(19) Throughout this report compositions are referred to on the basis of formal weight per cent. for each compound, i.e., in terms of the formula of the compound disregarding the molecular species that may result from its solution.

immersed in a bath of acetone and Dry Ice. The acid was stored in a deep-freeze box, and acid was transferred within the box so that absorption of H_2O or loss of NO_2 was minimized. All samples were prepared gravimetrically by the addition of NO_2 and H_2O to pure HNO_3. NO_2 of 99.8 wt. % purity was obtained from the Allied Chemical and Dye Corporation. This material was purified by fractional crystallization. Laboratory prepared distilled H_2O was used.

IV. Results

In Table I are shown experimental values of kinematic viscosity and density for the HNO_3–NO_2–H_2O system at 0, 25 and 40° in the approximate composition range 0 to 100 wt. % HNO_3, 0 to 52, and 99.6 to 100 wt. % NO_2 and 0 to 10 wt. % H_2O. The values of absolute viscosity shown in Table I were obtained from the experimental values of kinematic viscosity and the corresponding experimental values of density when available. Smoothed values of density were employed for those compositions in which experimental density data were not obtained. Since for compositions between about 52 and 99.6% NO_2 a two-phase liquid system exists at 0°, no measurements were made in this range of total composition.

In Fig. 1 experimental values of density at 0° for the HNO_3–NO_2 and HNO_3–H_2O system are plotted. For comparison, density data from the literature for the HNO_2–NO_2 system[8,20] and the HNO_3–H_2O system[7] are included. In Fig. 2 are shown values of absolute viscosity at 0° for the HNO_3–NO_2 and HNO_3–H_2O systems. For comparison, a few viscosity data from the literature for the HNO_2–H_2O system[6,7] are included. It is seen from Figs. 1 and 2 that between 0 and 45% NO_2 the addition of NO_2 to HNO_3 results in an increase in density and viscosity. At approximately 45% NO_2 maximum density and viscosity are attained. Beyond 45% NO_2 until the two-phase liquid region is reached at approximately 52% NO_2, addition of NO_2 to HNO_3 results in a decrease in both density and viscosity.

Smoothed values of the kinematic viscosity, density and absolute viscosity of the HNO_3–NO_2–H_2O system between −5 and 45° for a range of composition of 0 to 20% NO_2 and 0 to 5% H_2O are available elsewhere.[2] Linear extrapolation may be used with these data.

V. Analysis and Conclusions

Approximate values of viscosity and density at temperatures outside the temperature range measured may be obtained by extrapolating at constant compositions plots of $\log \eta$ vs. $1/T$ to obtain viscosity and ρ vs. T to obtain density (T is the absolute temperature). Both of these relationships were found to be approximately linear between 0 and 40° as predicted by simplified theories.[21]

The intersecting kinematic viscosity and density curves depicted in Fig. 3 suggest a possible application in the chemical analysis of fuming nitric acid. In a ternary system the measurement of at least a pair of separate physical properties is necessary to

(20) Pascal and Garnier, *Mémoires présentés a la société chimique*, **25-26**, 309 (1919).

(21) S. Glasstone, "The Elements of Physical Chemistry," D. Van Nostrand Co., New York, N. Y., 1946.

determine the composition of the system. If the kinematic viscosity and density are directly measured, the composition of the system in terms of HNO_3, NO_2 and H_2O is determined. The fact
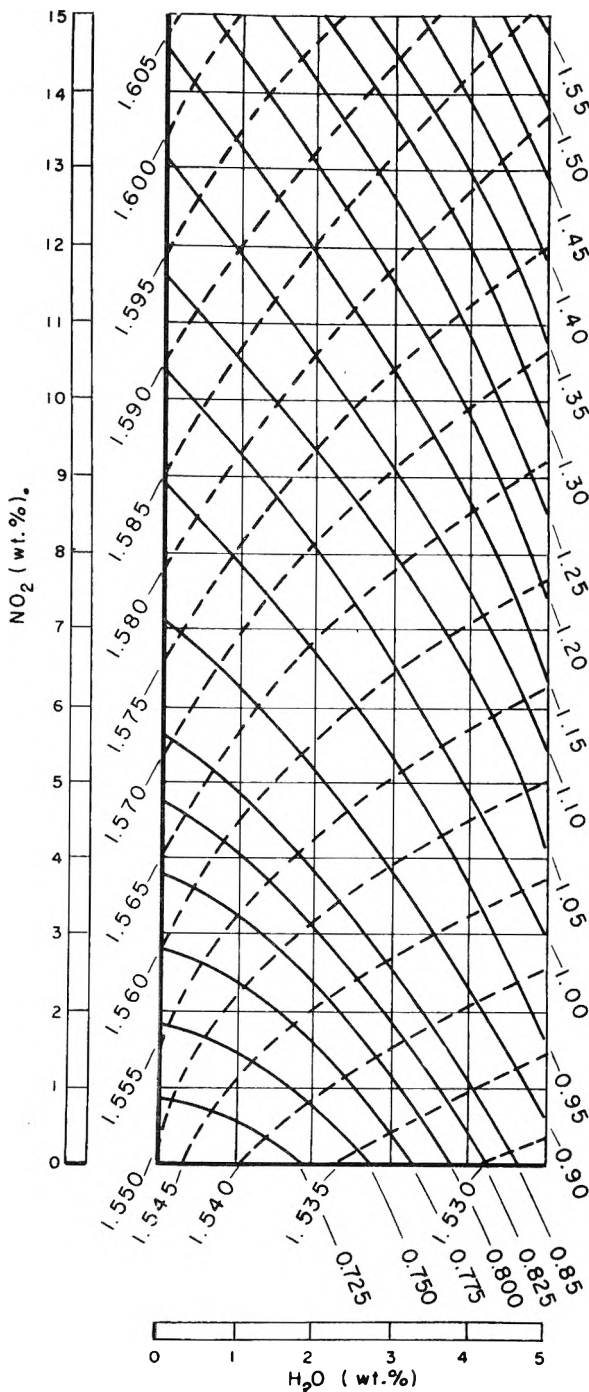
Fig. 3.—Curves of constant kinematic viscosity and density for the HNO_3–H_2O system at 0°: ———, kinematic viscosity (centistokes); ------, density (g./cc.).

that lines of constant kinetic viscosity intersect lines of constant density at nearly right angles makes this pair of measurements sensitive in determining the composition of the system. A single other physical property whose variation with composition is known, such as electrolytic conduct-

ance[22,23] or specific absorbance,[24] may, if appropriately combined with either kinematic viscosity or density, be used as a convenient method of analysis of HNO_3 solutions.

It is interesting to note that both the density and absolute viscosity (Figs. 1 and 2, respectively) of the HNO_3–NO_2 system at 0° increase with increasing NO_2 up to about 45 wt. % NO_2. This is not the behavior which would be expected on the basis of additive properties for each component since both the density (Fig. 1) and the absolute viscosity (Fig. 2) of pure NO_2 are less than the corresponding properties of HNO_3. This behavior may be due to the fact that NO_3^- which forms by ionization of NO_2 in HNO_3 solutions[3] according to the reaction

$$2NO_2 \rightleftharpoons NO^+ + NO_3^- \qquad (4)$$
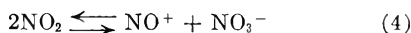
becomes associated with HNO_3 molecules according to

$$NO_3^- + 2HNO_3 \rightleftharpoons NO_3^-(HNO_3)_2 \qquad (5)$$

The equilibrium in equation 5 lies far to the right at 0° as measured by Raman spectral studies of KNO_3 in HNO_3.[3] A stable solid phase, $KNO_3 \cdot (HNO_3)_2$, can be isolated from solutions of KNO_3 in HNO_3.[23] It would be expected that the association represented by equation 5 would be accompanied by an increase of both viscosity and density of the solution.

(22) G. D. Robertson, Jr., D. M. Mason and B. H. Sage, *Ind. Eng. Chem.*, **44**, 2928 (1952).

(23) D. M. Mason, L. L. Taylor and S. P. Vango, "Conductometric Method for the Rapid Chemical Analysis of the Nitric Acid–Nitrogen Dioxide–Water System," Progress Report No. 20-205, Jet Propulsion Laboratory, Pasadena, Calif., 1954.

(24) S. Lynn, D. M. Mason and B. H. Sage, "Optical Absorbance of the Ternary System of Nitric Acid–Nitrogen Dioxide–Water," Progress Report No. 20-187, Jet Propulsion Laboratory, Pasadena, Calif., 1953.

It is of interest to note that the maxima in the curves of Figs. 1 and 2 lie slightly above about 42 wt. % NO_2, which represents the composition of the association compound $NO^+NO_3^-(HNO_3)_2$. Also the separation of the second liquid phase in the HNO_3–NO_2 system at 0° occurs slightly above this composition of NO_2.

The absolute viscosity (Fig. 2) decreases slightly with increasing water up to 1 wt. % H_2O. From 1 to 10 wt. % H_2O the viscosity increases with H_2O. On an additive basis the viscosity of the system might be expected to increase with H_2O since H_2O has a viscosity of about 1.79 at 0°.[14] The initial slight decrease in viscosity may be attributed partly to suppression of the self-ionization of HNO_3 by H_2O[4]

$$2HNO_3 \rightleftharpoons NO_2^+ + NO_3^- + H_2O \qquad (6)$$

The effect of this chemical reaction, which is predominant up to about 3 wt. % H_2O at 0°, may overshadow the expected additive relationship. Up to about 5 wt. % H_2O the following reaction is also prominent[25]

$$HNO_3 + H_2O \rightleftharpoons HNO_3 \cdot H_2O \qquad (7)$$

This association may cause the greater increase of absolute viscosity (Fig. 2) with H_2O in the range 1 to 10 wt. % H_2O than expected by the additive relationship.

With an increase in H_2O in the range 0 to 10 wt. % the density (Fig. 1) of the HNO_3–H_2O system at 0° decreases. This decrease is less than would be expected from an additive relationship for this property for each component, and the effects of association according to equation 7 may partly account for this behavior.

(25) R. Le Clerc and J. Chédin, *Mem. services chim. etat.*, **32**, 87 (1945).

HEATS OF SOLUTION OF NITROGEN DIOXIDE IN THE NITRIC ACID–NITROGEN DIOXIDE SYSTEM AT 0°[1]

By Keith Booman, Gerard W. Elverum, Jr., and David M. Mason

Jet Propulsion Laboratory, California Institute of Technology, Pasadena, California

The amount of heat evolved in dissolving liquid NO_2 in the HNO_3–NO_2 system was measured near 0° over a range of compositions from 0 to 50 wt. % NO_2 in a Dewar flask modified for use as a calorimeter. Isobaric heat capacities were measured incidentally in the course of obtaining heats of solution. The differential heat of solution of NO_2 in the HNO_3–NO_2 system is about 59 cal./g. of NO_2 at 0 wt. % NO_2 and 4 cal./g. of NO_2 at 50 wt. % NO_2. The integral heat of solution to give 50 wt. % NO_2 is about 16 cal./g. of solution. With increase in NO_2 from 0 to 50 wt. % the isobaric heat capacity of the resulting solution increases from about 0.41 to 0.43 cal./g.°. The thermal data are presented in graphical and tabular form, and the interpretation of these data in relation to ionic reactions occurring in the HNO_3–NO_2 system is discussed.

I. Introduction

The measurement of the amount of heat evolved when NO_2 is added to the HNO_3–NO_2 system[2] is of practical interest in estimating temperatures likely to be encountered in the preparation of the

(2) The formula NO_2 is used throughout this report to represent the equilibrium mixture NO_2–N_2O_4 in the liquid phase where actually the species N_2O_4 predominates.

common oxidant, fuming nitric acid. A knowledge of these heats of solution also permits precise determination of values of the heats of formation of the liquid HNO_3–NO_2 system which are necessary for calculations of performance in combustion processes. The contribution of the heat of solution to the over-all heat of formation of the HNO_3–NO_2 system is, however, very small.

Analysis of heats of solution data gives some insight into the ionic equilibria which exist in nitric acid solutions. Various physical properties of con-

centrated liquid nitric acid besides heats of solution indicate that ionic equilibria prevail in this system. Measurements of the Raman spectra[3] indicate that liquid HNO$_3$ undergoes self-ionization to give nitronium ions (NO$_2^+$) and NO$_3^-$ according to the equilibrium expression

$$2HNO_3 \rightleftharpoons NO_2^+ + NO_3^- + H_2O \qquad (1)$$
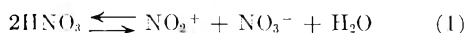
Measurements of freezing points[4] and of specific conductances[5,6] of nitric acid solutions support the existence of this ionization. NO$_2^+$ and NO$_3^-$ also are in equilibrium with respect to N$_2$O$_5$

$$N_2O_5 \rightleftharpoons NO_2^+ + NO_3^- \qquad (2)$$
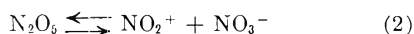
In solutions containing less than about 5 wt. % H$_2$O, association according to the following equation has been detected by Raman spectral measurements.[7]

$$HNO_3 + H_2O \rightleftharpoons HNO_3 \cdot H_2O \qquad (3)$$

In HNO$_3$ solutions containing over about 5 wt. % H$_2$O at 25°, ionization to hydronium ions (H$_3$O$^+$) and NO$_3^-$ according to the following equation becomes prominent[4-6]

$$HNO_3 + H_2O \rightleftharpoons H_3O^+ + NO_3^- \qquad (4)$$

In solutions of NO$_2$ in HNO$_3$, nitrosonium ions (NO$^+$) and NO$_3^-$ have been identified by Raman spectral studies,[8] and the existence of these species is supported by conductance measurements.[5,6] The resulting ionic equilibria may be written

$$2NO_2 \rightleftharpoons N_2O_4 \rightleftharpoons NO^+ + NO_3^- \qquad (5)$$
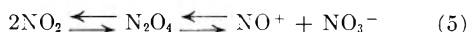
Raman spectral studies have also shown that the following equilibrium which involves association of HNO$_3$ molecules with NO$_3^-$ exists

$$2HNO_3 + NO_3^- \rightleftharpoons NO_3^- (HNO_3)_2 \qquad (6)$$

This association compound has been detected by these Raman spectral studies in solutions of KNO$_3$ in HNO$_3$.[9] Also a stable solid phase KNO$_3$(HNO$_3$)$_2$ exists,[10] giving further support to the existence of the equilibrium of equation 6. Since both NO$_2$ and H$_2$O affect the equilibria of equations 1 through 6, the effect should be reflected in the corresponding heats of solution of these species in HNO$_3$.

II. Description of Equipment and Methods

A. Apparatus.—The apparatus used in determining the heat of solution of NO$_2$ in the HNO$_3$–NO$_2$ system consists essentially of a Dewar flask, placed in an insulated ice-bath. Since the thermal measurements were made near 0°, the ice-bath reduced heat losses from the flask to the surroundings. The flask was closed by means of a neoprene stopper, the bottom of which was covered with a disk of Teflon[11] to

(3) E. D. Hughes. C. K. Ingold and R. I. Reed, *J. Chem. Soc.*, 2400 (1950).

(4) W. J. Dunning and C. W. Nutt, *Trans. Faraday Soc.*, **47**, 15 (1951).

(5) E. G. Taylor, E. M. Lyne and A. G. Fellows, *Can. J. Research*, **29**, 439 (1951).

(6) G. D. Robertson, Jr., D. M. Mason and B. H. Sage, *Ind. Eng. Chem.*, **44**, 2928 (1952).

(7) R. Leclerc and J. Chedin, *Mem. services chim. etat*, **32**, 87 (1945).

(8) J. C. S. Goulden and D. J. Millen, *J. Chem. Soc.*, 2620 (1950).

(9) J. Chedin and S. Feneant, *Compt. rend.*, **228**, 242 (1949).

(10) D. M. Mason, L. L. Taylor and S. P. Vango, "Conductometric Method for the Rapid Chemical Analysis of the Nitric Acid–Nitrogen Dioxide–Water System," Progress Report No. 20-205, Jet Propulsion Laboratory, Pasadena, Calif., 1954.

(11) Teflon is a solid polymerized fluorinated hydrocarbon manufactured by the E. I. du Pont de Nemours Co.

minimize attack of the stopper by fuming nitric acid. Liquid NO$_2$ maintained near 0° was added to a weighed quantity of HNO$_3$ in the Dewar flask by means of a 5-cc. buret. The weight of liquid NO$_2$ admitted to the system was determined from the volume measured with the buret, together with existing data on the density of liquid NO$_2$.[12]

The heat capacity of the calorimeter proper was determined in the conventional manner[13] by measuring the temperature rise in the system for a given measured input of electrical energy to H$_2$O whose isobaric heat capacity is known. The heat capacity of the calorimeter was about 23 cal./°. Temperature was measured with a Beckman-type thermometer, and a nichrome heating element enclosed in glass tubing filled with silicone oil was used as a source for the electrical energy. Agitation of the Dewar flask was maintained by means of a Teflon-covered magnetic rod driven by a magnetic agitator manufactured by the Arthur Thomas Company. The heat capacity of the system was calibrated with H$_2$O at different depths in the flask. Current was supplied to the heating element by four 6-volt storage batteries that were connected in parallel. Voltage and current were measured with a Leeds and Northrop (type K-2) potentiometer. The temperature of NO$_2$ entering the system was about 0.1°.

After an addition of NO$_2$ was made to the calorimeter and its contents near 0° and the corresponding temperature rise was measured, the temperature of the contents of the calorimeter was lowered to near 0° by inserting in the liquid a test-tube containing Dry Ice. The amount of electrical energy input necessary to raise the temperature of the acid through approximately the same range as occurred with the addition of NO$_2$ was then measured. The temperature attained by the addition of NO$_2$ to the system at 0°, together with a second measurement of the amount of electrical energy required to raise the system from 0° to the same final temperature, gives sufficient data to calculate the heats of solution.

B. Principles of Calorimetric Measurement of Heats of Solution.—In the present experiments, in order to avoid large temperature rises in the system with accompanying loss of volatile constituents and to avoid cumulative errors resulting from continuous additions from 0 to 50 wt. % NO$_2$, thermal measurements were made for relatively small incremental additions of NO$_2$ at several initial compositions in this range. The differential or partial specific heat of solution Q of NO$_2$ is defined as the total heat Q evolved per M_{NO_2} g. of NO$_2$ added to an infinite amount of solution at constant temperature T, pressure P, and mass of HNO$_3$ (M_{HNO_3}). Under these conditions

$$\bar{Q} = \left[\frac{\delta(Q)}{\delta M_{NO_2}} \right]_{T, P, M_{HNO_3}} \qquad (7)$$

However, since finite additions of NO$_2$ were made, a method of averaging was used in obtaining values of $\bar{Q}$. Values of Q were calculated from

$$\bar{Q} = Q/M_{NO_2} \qquad (8)$$

for the average composition encountered during an addition.

The total or integral heat of solution Q is here defined as the total heat evolved in the formation from pure HNO$_3$ of 1 g. of solution containing a given percentage of NO$_2$. Values of the integral heat of solution were obtained by graphically integrating the curve of $\bar{Q}$ (the differential heat of solution) vs. composition.

III. Materials

HNO$_3$ was prepared as described in the literature[14] by vacuum distillation of about 40° of a mixture of reagent-grade 95 wt. % H$_2$SO$_4$ and Baker and Adamson reagent-grade KNO$_3$ and collected in a flask immersed in a bath of acetone and Dry Ice. The acid was stored in a deep-freeze box and was transferred within the box so that absorption of H$_2$O or loss of NO$_2$ was minimized. NO$_2$ of 99.8 wt. % purity was obtained from the Allied Chemical and Dye

(12) Pascal and Garnier, *Mem. presentes soc. chim.*, **25–26**, 309 (1919).

(13) A. Weissberger, "Physical Methods of Organic Chemistry," Vol. I, part I, Interscience Publishers, Inc., New York, N. Y., 1949, p. 731.

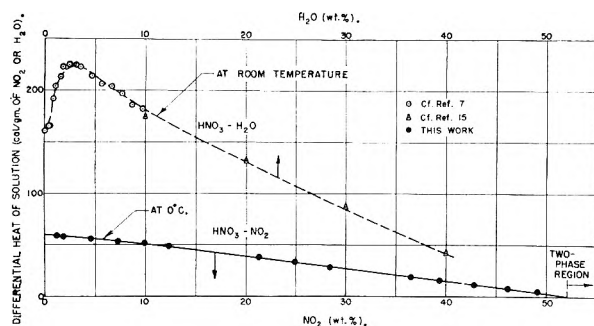(14) W. R. Forsythe and W. F. Giauque, *J. Am. Chem. Soc.*, **64**, 48 (1942).

Fig. 1.—Differential heat of solution at 0° of liquid NO₂ in the HNO₃–NO₂ system and H₂O in the HNO₃–H₂O system.

Corporation. This material was further purified by fractional crystallization.

IV. Results

Values for the isobaric heat capacity for the HNO₃–NO₂ system were obtained incidentally in the measurement of heats of solution of NO₂ in the system. In Table I are shown values of the average isobaric heat capacity of the HNO₃–NO₂ system as a function of composition from 0 to 50.5 wt. % NO₂. Data from the literature[14] for the isobaric heat capacity of pure HNO₃ as a function of temperature are available. Data for pure HNO₃ from the present investigation (Table I) are on the average approximately 2% lower than the data from the literature. It is evident from the literature data that the change of isobaric heat capacity of HNO₃ with temperature is very slight. This fact was utilized in assuming that values of the experimental isobaric heat capacity and heats of solution near 0° were the same as at 0°. Because of the large scatter, the exact values of the data are indeterminate; a straight line was drawn through the points, the average deviation from this line being about 1%. It is evident from these data that there is a trend for the heat capacity to increase with increasing NO₂ from 0 to about 50 wt. %.

TABLE I

EXPERIMENTAL VALUES OF ISOBARIC HEAT CAPACITY OF THE HNO₃–NO₂ SYSTEM

NO₂ (wt. %)	Av. isobaric heat capacity of system (cal./g. °C.)	Av. temp. (°C.)	NO₂ (wt. %)	Av. isobaric heat capacity of system (cal./g. °C.)	Av. temp. (°C.)
0	0.410	1.593	23.2	0.401	1.355
	.413	1.196	26.6	.403	0.464
	.407	1.984	30.2	.422	3.361
2.42	.414	3.747	37.6	.412	2.678
2.52	.414	1.163	41.2	.422	1.615
3.77	.408	1.982	44.6	.426	2.145
7.25	.407	1.438	47.7	.434	1.822
8.75	.426	2.714	50.5	.433	1.218
20.8	.422	1.493			
	.423	1.476			

In Table II are presented experimental values of the differential heats of solution of NO₂ in the HNO₃–NO₂ system near 0°. These data were obtained by applying equation 8 to the thermal measurements as described in Section II-B. In Table II the range of NO₂ added for each measurement and the corresponding rise in temperature are given.

In Fig. 1 these experimental values of the differential heats of solution of NO₂ in calories per gram of NO₂ are plotted vs. composition in weight percentage of NO₂. Included for comparison are data from the literature[7,15] for the differential heat of solution of H₂O in the HNO₃–H₂O system. It is evident from the data of Table II and Fig. 1 that the differential heats of solution of NO₂ vary from about 59 cal./g. of NO₂ for pure HNO₃ to about 4 cal./g. NO₂ for a solution containing 50 wt. % NO₂. Near 52 wt. % NO₂ at 0° a second phase appears which contains over 99 wt. % NO₂; thus it would be expected that the differential heat of solution at this composition would approach 0 cal./g. of NO₂. This behavior is evident from data in Table II and Fig. 1.

TABLE II

EXPERIMENTAL VALUES OF THE DIFFERENTIAL HEAT OF SOLUTION OF LIQUID NO₂ IN THE HNO₃–NO₂ SYSTEM

Range of NO₂ (wt. %)	Av. NO₂ (wt. %)	Temp. rise due to heat of soln. (°C.)	Av. temp. (°C.)	Differential heat of soln. of NO₂ (cal./g. NO₂)
0–2.52	1.26	2.877	3.636	58.6
0–3.77	1.88	4.374	1.947	58.4
3.04–5.89	4.47	3.108	2.043	56.0
5.89–8.59	7.24	2.715	1.524	54.1
8.59–11.1	9.9	2.747	1.510	51.6
11.1–13.54	12.3	2.535	1.703	48.9
19.5–23.2	21.3	3.247	2.331	38.1
23.2–26.6	24.9	2.653	1.921	33.6
26.6–30.2	28.4	2.499	1.503	27.3
35.0–37.6	36.5	1.392	1.249	18.4
37.7–41.2	39.4	1.613	0.044	14.9
41.2–44.6	42.8	1.177	0.860	10.3
44.6–47.7	46.1	0.650	0.806	7.2
47.5–50.5	49.1	0.467	0.255	4.53

Smoothed values of integral heats of solution (in cal./g. of solution), obtained by integrating graphically with a planimeter the smooth differential heat-of-solution curve such as shown in Fig. 1 from 0 to 50 wt. % NO₂, are shown, together with smoothed differential heat data, in Table III.

TABLE III

SMOOTHED VALUES OF THE DIFFERENTIAL AND INTEGRAL HEATS OF SOLUTION OF LIQUID NO₂ IN THE HNO₃–NO₂ SYSTEM AT 0°

NO₂ (wt. %)	Differential heat of soln. (cal./g. NO₂)	Integral heat of soln. (cal./g. of soln.)	NO₂ (wt. %)	Differential heat of soln. (cal./g. NO₂)	Integral heat of soln. (cal./g. of soln.)
0	59.1	0	30	25.8	13.35
5	56.0	2.89	35	19.2	14.45
10	51.4	5.58	40	13.3	15.28
15	45.9	8.0	45	8.3	15.79
20	39.4	10.15	50	4.2	16.11
25	32.5	11.92	52	0.5[a]	

[a] Extrapolated value.

V. Evaluation and Conclusions

From values of the integral heats of solution of Table III it is evident that, in mixing NO₂ with HNO₃ to make 1 g. of a solution 50 wt. % in NO₂, a

(15) G. L. Wilson and F. D. Miles, *Trans. Faraday Soc.*, **36**, 356 (1940).

total of about 16 cal. is liberated. Based on heat capacity data, this heat corresponds to a rise in temperature of about 37° for an adiabatic-mixing process. That this heat evolution for solution of NO_2 is relatively small compared with that for H_2O is evident from a comparison of the area under the dashed curve for HNO_3–H_2O in Fig. 1 with the smaller area under the solid curve for HNO_3–NO_2. The heat of solution of NO_2 to make a 50 wt. % NO_2 mixture represents about 4% of the additive heats of formation of HNO_3 and NO_2 for this mixture.

In Fig. 1 it is evident from the curve for the differential heat of solution of NO_2 in the HNO_3–NO_2 system that a net exothermic effect between NO_2 and HNO_3 predominates. The data are in keeping with the exothermal association according to equation 6 of HNO_3 molecules with NO_3^- formed by the ionization of NO_2 according to equation 5. Measurements of the integral heat of solution of KNO_3 in HNO_3[7] give 6 cal./g. of solution for a 10 wt. % solution of KNO_3. In terms of equivalents of NO_3^- in the additive, 10 wt. % KNO_3 corresponds to about 9.2 wt. % NO_2. About 5.1 cal./g. of solution is liberated in dissolving NO_2 in HNO_3 to give a solution 9.2 wt. % in NO_2. Thus it appears that NO_2 and KNO_3 dissolved in HNO_3 behave thermally in a similar manner, and both are probably engaged in the association equilibrium of equation 6. As would be expected, the heat evolved per gram of NO_2 added diminishes as equilibrium according to equation 6 is shifted farther to the right. This behavior is reflected in the curve for the HNO_3–NO_2 system in Fig. 1.

The maximum in the curve for the HNO_3–H_2O system[7,15] in Fig. 1 is of interest. Although the predominant exothermic reaction throughout the composition range shown in Fig. 1 is probably the hydration of HNO_3 according to equation 3, some initial endothermic reaction which is increasingly suppressed as H_2O is added from 0 to 3 wt. % probably accounts for the initial rise in the curve. Below about 5 wt. % H_2O the self-ionization of HNO_3 of equation 1 is prominent. When a little H_2O is added to pure HNO_3, the equilibrium of equation 3 is shifted to the right by the addition of H_2O, causing an evolution of heat; and the equilibrium of equation 6 is shifted to the left (because of removal of NO_3^- by reaction of equation 1), causing absorption of heat. The thermal effect due to the shift of equilibrium of equation 1 to the left is uncertain. The decreasing endothermic effect of the reverse of the equilibrium reaction of equation 6 with increasing H_2O probably accounts for the rise of the dashed curve in Fig. 1 to a maximum. To the right of this maximum the exothermic hydration reaction of equation 3 and the ionization in accordance with equation 4 predominate. The absence of a maximum in the differential-heat curve for NO_2 (Fig. 1) suggests that no appreciable endothermic reactions result from the addition of small amounts of NO_2 to pure HNO_3. It appears that the expected shift in the equilibrium of equations 1 and 3, due to NO_3^- formed from NO_2 in accordance with equation 5, does not cause a significant thermal effect. Thus a maximum does not appear in the differential-heat curve for NO_2 shown in Fig. 1.

THE ENTROPY AND STRUCTURE OF THE PERVANADYL ION[1]

By M. J. LaSalle[2,3] and James W. Cobble[3]

Radiation Laboratory and Department of Chemistry and Chemical Engineering, University of California, Berkeley, Cal.

The entropy of the pervanadyl ion has been determined as -5.4 ± 0.5 e. u. Comparison of this value with previously proposed structures supports the structure VO_2^+. Thermodynamic functions are also given for VO^{++} and $V_2O_5 \cdot H_2O$.

I. Introduction

Vanadium is one of the few elements which forms rather well defined aqueous oxycations. The only others listed by Latimer,[4] with the exception of the actinide elements, are AsO^+, SbO^+, BiO^+, MoO_2^+, TiO^{++}, ZrO^{++} and Be_2O^{++}; in addition there is some evidence for MoO_2^{++}.[5] Unfortunately, most of these have not been well characterized.

The vanadyl and pervanadyl ions, VO^{++} and VO_2^+, appear to form single species over a wide range of acid concentrations and are well suited to a thermodynamic study. Düllberg[6] first noted that vanadium(V) migrates to the cathode in acid solution. Coryell and Yost[7] studied the VO^{++}–VO_2^+ cell couple in HCl solutions and their data were consistent with the oxidation–reduction reaction

$$VO^{++} + H_2O = VO_2^+ + 2H^+ + e^- \qquad (1)$$
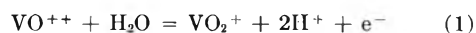
Carpenter[8] repeated these measurements in perchloric acid to avoid possible complex ion formation and essentially confirmed the Coryell and Yost findings. The latter had suggested $VO_2^+ \cdot 2H_2O$ or $V(OH)_4^+$ as the form of the oxygenated species, but

(1) This research was performed under the auspices of the Atomic Energy Commission.

(2) Based on the thesis of M. J. LaSalle submitted in partial fulfillment of the requirements for the M.S. degree in the University of California at Berkeley, February, 1955.

(3) Department of Chemistry, Purdue University, Lafayette, Indiana.

(4) W. M. Latimer, "Oxidation-Potentials," Second Edition, Prentice–Hall, Inc., New York, N. Y., 1952.

(5) F. H. Nicholls, H. Saenger and W. Wardlaw, *J. Chem. Soc.*, 1443 (1931); see, however, M. M. Jones, *J. Am. Chem. Soc.*, **76**, 4233 (1954).

(6) P. Düllberg, *Z. physik. Chem.*, **45**, 129 (1903).

(7) C. D. Coryell and D. M. Yost, *J. Am. Chem. Soc.*, **55**, 1909 (1933).

(8) J. E. Carpenter, *ibid.*, **56**, 1847 (1934).

Carpenter favored VO_2^+, as did Hart and Partington[9] who measured the same cell potentials in HCl and H_2SO_4.

Thermodynamically, there is no way in which these two alternatives, VO_2^+ and $V(OH)_4^+$, can be distinguished. One reason used to support the choice of the $V(OH)_4^+$ is simply because it indicates a higher coördination for vanadium. The recent studies[10] on the actinide element ions such as NpO_2^+, NpO_2^{++}, PuO_2^{++} and AmO_2^+, however, clearly indicate that a lesser degree of coördination is very possible. With the success of various methods[11,12] in correlating the entropy and structure of aqueous ions, it seemed desirable to determine the entropy of the pervanadyl ion and compare this value with that for another ion of similar known structure, NpO_2^+, whose entropy can be obtained from the data of Cohen and Hindman.[13] Such a comparison has been made and favors the structure VO_2^+.

II. Determination of the Solubility of V_2O_5

It appeared that the best method of obtaining the entropy of VO_2^+ was to determine the ΔS° value for the reaction

$$V_2O_5(c) + 2H^+ = 2VO_2^+ + H_2O \qquad K_2 = \frac{VO_2^+}{H^+} \quad (2)$$
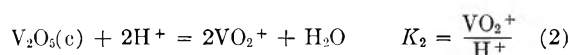
The reasons for this choice were primarily (1) a low but finite solubility in perchloric acid and (2) the entropy of $V_2O_5(c)$ has been experimentally determined. Thus a determination of the value of K_2, extrapolated to infinite dilution along with a calorimetric heat of solution, similarly extrapolated, would fix the entropy of VO_2^+.

The solubility of the pentoxide in various strong acids has been reported previously by Coryell and Yost[7] in HCl, Britton and Welford[14] in HCl, H_2SO_4 and $HClO_4$; Meyer and Aulich[15] in H_2SO_4, and most recently by Ducret[16] in HCl, H_2SO_4 and $HClO_4$. Unfortunately, none of these authors agree on the equilibrium solubility under similar conditions of temperature and concentration of acid. Indeed, some of the data are not internally consistent as shown by (1) a solubility in excess of available hydrogen ion as given by equation 2; (2) different solubilities on undersaturation and supersaturation approaches to equilibrium. It appeared that most of the difficulty arose from allowance of insufficient times[17] to approach a true equilibrium with the solid phase and also possible impurities of lower vanadium oxides, which are much more soluble than V_2O_5 itself.

Preliminary studies in $HClO_4$ solutions indicate that equilibrium in the V_2O_5–$HClO_4$ system is ap-

(9) A. B. Hart and J. R. Partington, *J. Chem. Soc.*, 1532 (1940).

(10) L. H. Jones and R. A. Penneman, *J. Chem. Phys.*, **21**, 542 (1953).

(11) J. W. Cobble, *ibid.*, **21**, 1443 (1953).

(12) R. E. Connick and R. E. Powell, *ibid.*, 2206 (1953).

(13) D. Cohen and J. C. Hindman, *J. Am. Chem. Soc.*, **74**, 4682 (1952).

(14) H. T. S. Britton and G. Welford, *J. Chem. Soc.*, 895 (1940).

(15) J. Meyer and M. Aulich, *Z. anorg. Chem.*, **194**, 278 (1930).

(16) L. P. Ducret, *Ann. chim. (Paris)*, [12] **6**, 705 (1951).

(17) It should be noted that for solubility-time curves which are changing slowly, a constant equilibrium constant (in this case, VO_2^+/H^+ ratios) as a function of added reagent (in this case H$^+$) is not necessarily a sufficient criteria for equilibrium unless such a constant or ratio is *independent with time*.

proached at some acid concentrations so slowly that it is doubtful if even approximate values of the solubility can ever be obtained at 25° by approaching equilibrium from only one direction (under saturation approach). Thus preliminary shaking experiments gave rise to a smooth curve of solubility *vs.* $HClO_4$ concentration going through a maximum at concentrations of about 1–2 M $HClO_4$, and falling off on both sides, clearly an impossible *equilibrium* situation if the solid phase remained $V_2O_5(c)$. It was believed that this observation was simply the result of non-equilibrium behavior in that the rate of approach to equilibrium was slower at the high acid concentrations. Such a conclusion was later demonstrated to be correct.

Because of this confusion in the solubility data, it was apparent that only if equilibrium concentrations were approached from both supersaturated and undersaturated solutions could a significant value for the free energy of solution of V_2O_5 be obtained.

Experimental

Apparatus.—The solubility experiments were carried out in a series of stirred double-necked round-bottom flasks mounted in a thermostat bath. Through one neck of the flask a stopper fitted with a filtering stick (F grade) was inserted and through the other a glass stirrer was centered and surrounded with a plug of glass wool to minimize evaporation loss of water from the solution.

The flasks, each containing 200 ml. of solution which covered the end of the filter stick, were assembled in pairs, each pair at a given ionic strength ($HClO_4$ + NH_4ClO_4) but at different hydrogen ion concentrations. Sampling was carried out at periodic intervals by withdrawing some of the solution up into the filter stick. Duplicate 0.500-ml. aliquots were then withdrawn with calibrated 500λ pipets (which had previously been coated with Dri-film) and evaporated to dryness under an infrared lamp in small, previously weighed, platinum cups pressed in the shape of a hat. The excess solution in the filter stick was forced back into the flask and stoppered to prevent trapping small quantities of solution in it.

The evaporated solutions were ignited and weighed as V_2O_5. Previous tests showed the platinum suffered no loss in weight by possible oxidation through this procedure. The balance used in these weighings had a sensitivity of ±0.02 mg.; duplicate samples showed a total weighing and volumetric error of the order of ±0.05 mg. or less.

Chemicals.—Vanadium pentoxide was obtained from the A. D. Mackay Co. and leached for several hours with approximately 1 M $HClO_4$, washed and slurried repeatedly with distilled water, dried in a vacuum desiccator over P_2O_5, analyzed and kept in small sealed vials. Just prior to addition of this material to the solubility flasks, a portion was tested for the presence of lower oxides with a few drops of 0.1 M $KMnO_4$ in a perchloric acid slurry. Spectrographic analyses indicated that the contaminates present in greatest abundance were barium and zinc (<0.1 and 0.05 p.p.m., respectively).

Stock solutions of Baker and Adamson $HClO_4$ were prepared by dilution of 72% doubly-distilled acid with distilled water and standardized against 1.000 N NaOH with phenolphthalein indicator. The ammonium perchlorate stock solutions were prepared from C.P. grade dried NH_4ClO_4 and distilled water. Volatile ammonium perchlorate was used to adjust the ionic strengths since it simplified the analytical procedure. It was demonstrated that ignition of the V_2O_5 samples containing NH_4ClO_4 did not result in explosive loss of detectable quantities of the V_2O_5, nor did the NH_4ClO_4 itself leave any detectable residue.

Solubility Results.—A typical run was carried out as follows: when the various pairs of solutions were at temperature equilibrium a previously estimated amount of V_2O_5 (in excess of the equilibrium value) from a sealed vial was added. At intervals sampling was carried out and the results plotted on a typical concentration–time curve (Fig. 1).
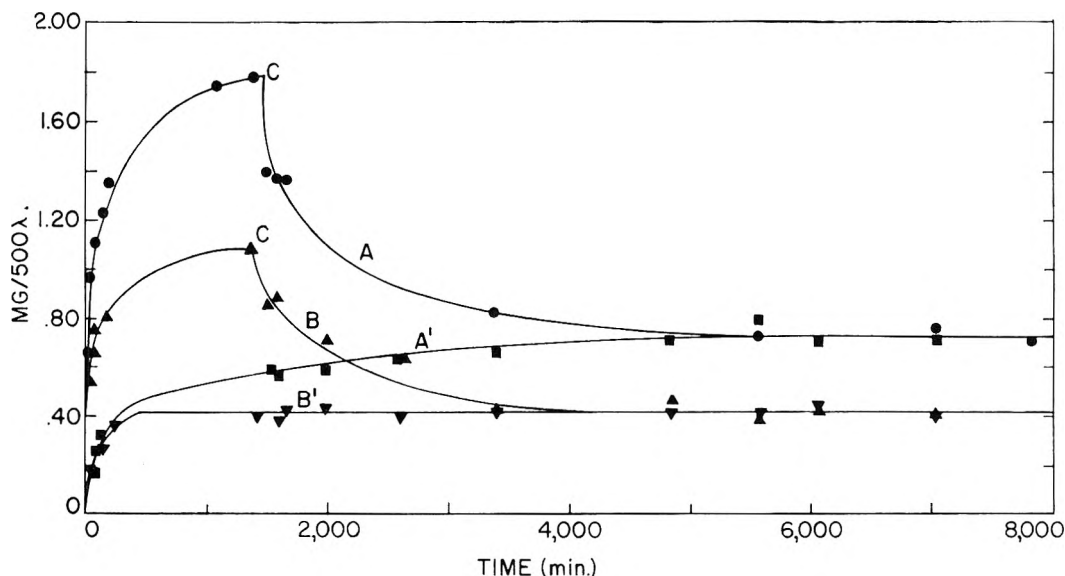
Fig. 1.—Typical solubility curves of V_2O_5 in $HClO_4$–NH_4ClO_4 solutions. A' and B' represent approach to equilibrium from undersaturation; solutions represented by A and B are supersaturated after point C.

In Fig. 1 two typical sets of solubility curves are illustrated. Concentrations of the two sets of solutions (A, A' and B, B') are given in mg. of $V_2O_5/500\lambda$. At point C, NH_4OH had been added to solutions A and B; such curves clearly define the approach to equilibrium from two directions, and add considerable confidence to the values for the solubility at a given ionic strength calculated from the intersection of these curves.

During the first run, it was noted that the solid phase in *some* of the flasks slowly changed color (usually from the typical yellow of the anhydrous material to some shade of orange, red, rust or brown). No matter what color the residue assumed, however, the filtered solutions always displayed the characteristic clear pale-gold color. Portions of the residues in some of the flasks were washed with absolute alcohol, air dried and analyzed. Calculations indicated the formula of all but the yellow residues was $V_2O_5{\cdot}H_2O$, or HVO_3. No color change was observed in the samples while the material was being alcohol-washed, but all passed through the typical yellow color of the anhydrous V_2O_5 prior to melting, or returned to it if desiccated over P_2O_5. The addition of the NH_4OH in small amounts over the period of an hour was found somewhat effective in preventing or retarding this color change of the solid phase. Other portions of the residues were also washed with absolute alcohol and their X-ray diffraction powder patterns were determined.[18] These results indicated that the samples either had a pattern of the anhydrous oxide or a new pattern which was assigned to the hydrated species on the basis of the chemical analysis. This diffraction pattern for $V_2O_5{\cdot}H_2O$ or HVO_3 is given in the Appendix.

Some preliminary Raman work on the solutions (considering such photographs as a very sensitive Tyndall test) gave no indication of any colloid formation, nor did the absorption spectra determinations (section IV).

It was most fortunate that some of the solutions reached equilibrium with the solid phase in the anhydrous state, since the entropy of the hydrated species has not yet been determined. Inspection of the data (Table I) indicates that within the limits of the experimental errors there is no difference in the solubility of V_2O_5 or its monohydrate. This implies a $\Delta F°$ of essentially zero for the conversion of one species to the other.

From an analysis of the solubility curves it was apparent that the time to reach an equilibrium value in the saturated solution was proportional to some power of the acid concentration greater than unity. Approximate extrapolation to 1 M $HClO_4$ clearly indicated that about six months would be needed to reach equilibrium from an undersaturation

approach using these experimental techniques, and explains in part the previous disagreements in the reported solubilities. The solubility data and analyses of the solid phases are given in Table I along with values of the $VO_2{}^+/H^+$ ratio, (K_2). Experiments were not performed at (II$^+$) <0.1 N to avoid complications from the formation of complex vanadic acids at these low acid concentrations.

III. Calorimetry

The other thermodynamic function needed to calculate $\Delta S°$ for eq. 2 is $\Delta H°$, the heat of solution; it was determined by measuring the heat of solution of V_2O_5 in various perchloric acid solutions calorimetrically.

Experimental

Apparatus.—The experiments were carried out in a solution-type calorimeter which has been described elsewhere[19–21] with the V_2O_5 samples suspended on the central axis of the calorimeter stirrer in thin-walled glass bulbs. At the proper time, the V_2O_5 bulb was broken in the calorimeter perchloric acid solution. In some experiments the nature of the stirring, rate of solution and amount of V_2O_5 placed in the bulb were such that not all of the oxide dissolved, even though the temperature–time measurements indicated that the reactions were complete. Since these values agreed well with those in which the sample did completely dissolve, no difficulty was encountered in the interpretation of these former runs. The preparation of the chemicals was as previously described.

Calorimetric Results.—The results of seven calorimetric determinations are given in Table II; the extrapolated value of the heat of solution to infinite dilution is −5,780 ± 90 cal./mole V_2O_5. Since the solubility of V_2O_5 is low, this exothermic reaction heat requires that the solubility have a negative temperature coefficient, and is qualitatively in agreement with previously reported solubility–temperature studies (Section I).

IV. Absorption Spectra

Although there had previously been no reason for doubt, it seemed desirable to investigate spec-

(19) B. J. Fontana, "The Chemistry and Metallurgy of Miscellaneous Materials: Thermodynamics," edited by L. L. Quill, McGraw-Hill Book Co., Inc., New York, N. Y., 1950, National Nuclear Energy Series, Plutonium Project Record, Vol. 19B, p. 321.

(20) H. W. Zimmerman and W. M. Latimer, *J. Am. Chem. Soc.*, **61**, 1550 (1939).

(21) Our thanks are due to Professor Latimer for kindly offering the use of his calorimetric equipment.

(18) We are indebted to Mrs. C. H. Dauben, Chemistry Department of the University of California, Berkeley, California, for determining these patterns.

Table I

Results of the Solubility Studies

Solid phase[a]	Initial (H+)	Final (H+)	μ	Equilibrium solubility in mole/l. VO2+				(VO2+)/(H+)
				Supersat. approach	Undersat. approach	Av.	Final av.	
bHyxc	0.0970		0.122	0.0092		0.0090	0.0090	0.236 ± 0.029
oHyx	.0472	0.0382	.122		0.0088			
ruHyxc	.0970	.0798	.219		.0172	.0172		
oHyx	.194		219	.0158		.0158	.0165	0.205 ± .014
oHyx	.0970	.0812	.219		.0158			
yAnhx	.194	.160	.343		.0340	.0340		
reHyxc	.194	.159	.343		.0350	.0350	.0334	0.207 ± .007
ruHyc	.292		.343	.00318		.0312		
ruHyc	.194	.163	.343		.0306			
yAnhx	.292	.233	.443		.0594	.0594	.0590	0.253 ± .005
reHyxc	.292	.234	.443		.0584	.0584		
yAnhx	.394	.318	.543		.0756	.0756		
reHyx	.394	.315	.543		.0794	.0794	.0790	0.251 ± .03
ruHyc	.394	.312	.543		.0818	.0818		

[a] Symbols as follows: Hy, hydrated form $V_2O_5 \cdot H_2O$; Anh, anhydrous form V_2O_5; x, X-ray evidence; c, chemical evidence; b, brown; o, orange; ru, rust; y, yellow; re, red.

Table II

Results of the Calorimetric Determinations

Run	Heat evolved (cal.)	V_2O_5 dissolved (g.)	Final (VO2+) (moles/l.)	Final (H+) (moles/l.)	μ	$-\Delta H$ (kcal./mole V_2O_5)	$-\Delta H$ (av.) (kcal./mole V_2O_5)
V-10	65.12	1.635	0.0171	0.627	0.644	7.24	7.24
V-1	106.642	2.792	.0320	.405	.437	6.95	7.00 ± 0.04
V-2	61.815	1.597	.0174	.419	.437	7.04	
V-11	43.11	1.118	.0120	.314	.327	7.01	6.74 ± 0.28
V-12	41.916	1.181	.0124	.314	.327	6.46	
V-3	70.724	2.092	.0232	.158	.181	6.17	6.23 ± 0.05
V-4	74.03	2.144	.0242	.157	.181	6.28	
0 (Extrapolated)							5.78 ± 0.09

trophotometrically that the ionic species in final equilibrium with the solid V_2O_5 or V_2O_5 (hydrate)—what might be termed an "aged" pervanadyl solution—was identical with the ionic species formed immediately when V_2O_5 is dissolved in acid solution (as in the calorimetric experiments). Therefore the absorption spectra of all the solutions obtained from the various solubility determinations and a solution simulating that resulting from the calorimetric experiments were determined. For reference, the spectra of V_2O_4 dissolved in approximately 0.1 N HClO₄ (vanadyl perchlorate) also was determined.

Experimental

Apparatus.—A Beckman quartz spectrophotometer, model DU, was used for the spectral determinations.

Chemicals.—The pervanadyl solutions already have been described. The vanadium tetroxide was obtained for these experiments by adding concentrated NH₄OH to a solution of vanadyl sulfate. The dark blue-grey precipitate was digested for several hours, filtered, washed repeatedly with distilled water, dried in a vacuum desiccator over P_2O_5, analyzed and stored in a nitrogen-filled dry-box. A portion was then dissolved in 0.09440 N HClO₄, and the resulting blue solution analyzed by evaporating 500λ aliquots on platinum plates and igniting to V_2O_5 as before.

Procedure.—Portions of the pervanadyl solutions from the solubility experiments were centrifuged and aliquots were removed with calibrated micropipets. The proper dilution was made with solutions of the same hydrogen ion concentration and ionic strength. The reference cell contained solutions identical in hydrogen ion concentration and ionic strength with those to be determined except for vanadium content.

Spectra Results.—The absorption spectra of the pervanadyl and vanadyl solutions are given for reference in Fig. 2, curves A and B, respectively. These curves essentially confirm those results reported previously, but less completely, by Garner, et al.,[22,23] for these ions. The solutions obeyed Beer's law and gave no evidence of any but normal ionic behavior. The calculated molar extinction coefficient for the pervanadyl ion at the peak $\lambda = 2250$ Å. was 2,240 ± 40. The corresponding value for the vanadyl ion was 15.9 at $\lambda = 7500$ Å., which value may be compared to 17.0 reported by Furman and Garner[22] at this wave length.

All of the solutions from the solubility determinations, regardless of the color or form of the equilibrium solid phase, gave identical absorption spectra and extinction coefficients, as did the solution simulating experimental conditions in the calorimeter. These comparisons are further good evidence that the solubility studies and calorimetry experiments involved the same ionic species independent of hydrogen ion concentration, ionic strength and "age" of the solution.

V. Thermodynamic Calculations and Discussion

Pervanadyl Ion.—From the solubility studies of Section II (Table I) a value for the VO2+/H+ ratio extrapolated to infinite dilution of 0.207 ± 0.011 was obtained; thus ΔF^0 for reaction 2 is 1870 ± 60 cal. When combined with the similarly extrapolated ΔH^0 value of $-5,780 \pm 90$ cal., a ΔS^0_2 value of -25.7 ± 0.4 e.u. is obtained. Using $S^0_{H+} \equiv 0$ e.u., $S^0_{H_2O} = 16.72$ e.u. and $S^0_{V_2O_5} = 31.3 \pm 0.5$ e.u.,[24] the entropy of VO2+ becomes -5.5 ± 0.5 e.u.

(22) S. C. Furman and C. S. Garner, *J. Am. Chem. Soc.*, **72**, 2422 (1950).

(23) H. A. Tewes, J. B. Ramsey and C. S. Garner, *ibid.*, **72**, 1785 (1950).

(24) Supplementary values from U. S. Bureau of Standards, "Selected Values of Chemical Thermodynamic Properties," 1949,

This value of the entropy of the pervanadyl ion may be compared to the entropy of the neptunyl ion, NpO_2^+. A value for the entropy of this latter ion can be estimated satisfactorily from the data of Hindman and Cohen[13] who determined entropy differences between the Np^{+3}–Np^{+4}, Np^{+4}–NpO_2^+ and NpO_2^+–NpO_2^{++} ions in 1 M $HClO_4$. The equation given by Latimer and Powell[25] allows one to estimate an entropy for the Np^{+3} ion at zero ionic strength from which a value for the entropy of NpO_2^+ of -1 ± 2 e.u. is obtained. An alternate method is to assume that the entropies of closely similar NpO_2^{++} and UO_2^{++} are the same, namely, -17 ± 5 e.u. as experimentally determined for uranyl ion at zero ionic strength.[24] This value when combined with the NpO_2^+–NpO_2^{++} difference leads to a value of -8 ± 5 e.u. for NpO_2^+. Thus the two alternate methods lead to an average value of -5 ± 4 e.u. for NpO_2^+ which is within the experimental uncertainty of both estimates, especially with the obvious errors in mixing infinite dilution and 1 M values. However, these latter errors are probably not serious when only the entropy values themselves are being considered.

Although the latest evidence[10] indicates that the NpO_2^+ ion probably has a linear structure and VO_2^+ is believed to be bent (see below), this should have only a minor effect in comparison of the two structures. Such a comparison of entropy and formula indicates that the structure VO_2^+ is consistent with its entropy: NpO_2^+, -5 ± 4 e.u.; VO_2^+, -5.5 ± 0.5 e.u.

Examination of the structure–entropy comparison of the other proposed form is also enlightening. If the structure of the pervanadyl ion was in reality $V(OH)_4^+$, the experimentally determined entropy would then be $-5.5 + 2S^0_{H_2O} = 27.9 \pm 0.5$ e.u. While there is no experimentally determined entropy available for a similar ion, the method given by Cobble[26] would indicate a value of approximately 65 ± 10 e.u. for such a structure.[27] Thus this comparison also favors the structure VO_2^+.

In a discussion of the crystal structure of $KVO_3 \cdot H_2O$, Christ, et al.,[28] reported there are two markedly short vanadium–oxygen bonds with an angle of $105°$ between them and bond lengths of $V–O_I = 1.68$ Å. and $V–O_{II} = 1.66$ Å.; the other two oxygens are at 1.91 and 2.01 Å. This situation is very similar to that found in some actinide element compounds and is good evidence for the existence of a VO_2^+ ion in the solid state as well.

Vanadyl Ion.—For the reaction

$$VO^{++} + H_2O = VO_2^+ + H^+ + {}^1\!/_2 H_2(g) \qquad (3)$$
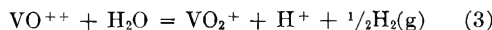
(25) R. E. Powell and W. M. Latimer, *J. Chem. Phys.*, **19**, 1139 (1951).

(26) J. W. Cobble, *ibid.*, **9**, 1451 (1953).

(27) Connick and Powell (ref. 12) previously had pointed out that for oxygenated anions, the entropy of $M(OH)_mO_n^{-x}$ was about equal to the entropy MO_n^{-x}, i.e., the OH grouping made practically no contribution to an oxygenated anion. They further suggested that similar results might be expected for oxygenated cations: $S^0_{Fe}^{++} = -27.1$; $S^0_{Fe(OH)}^{++} = -23.2$; such a general extrapolation to a "bare" ion certainly is questionable, and is believed to be accidental. For example, note that the entropy of the vanadyl ion (-26.0 e.u., see below) is also approximately equal to that for $Fe(OH)^{++}$ and, thus, this approximation does not appear to hold for oxygenated cations.

(28) C. L. Christ, J. R. Clark and H. T. Evans, Jr., *J. Chem. Phys.*, **21**, 1114 (1953).
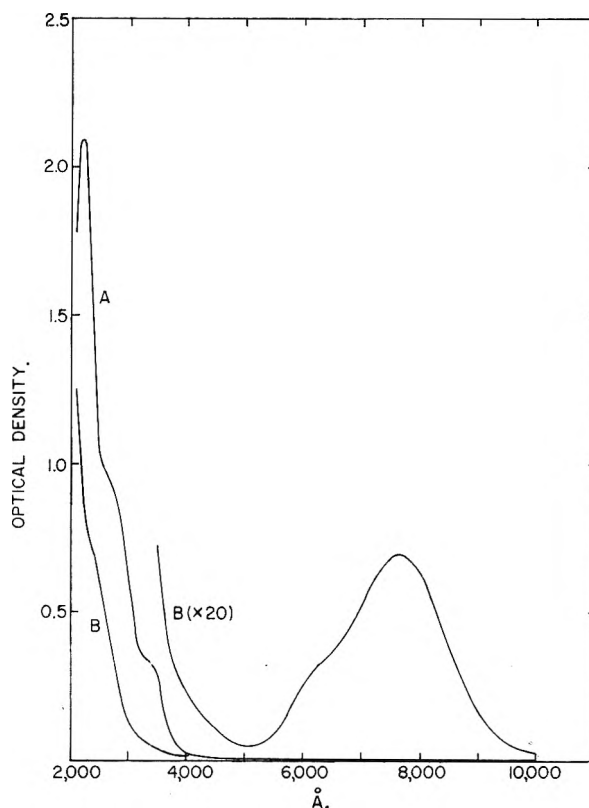
Fig. 2.—Typical absorption spectra of (A) pervanadyl ion and (B) vanadyl ion at $25°$ in $HClO_4$: $\epsilon_{VO_2^+}^{2250} = 2240$; $\epsilon_{VO^{++}}^{7500} = 15.9$. (Beckman model DU, 1-cm. quartz cells, slit width adjusted for maximum resolution).

in 1 N HCl, a $\Delta F^0 = 23,600$ cal. and $\Delta H^0 = 29,350$ cal. can be calculated from the data of Coryell and Yost[7] as corrected by Carpenter.[8] ΔS^0 then becomes 19.5 e.u. for this reaction. When the entropy value of -5.5 for VO_2^+ and other supplementary values from the Bureau of Standards compilation[24] are used, the entropy of VO^{++} becomes -26 ± 3 e.u.

This value for VO^{++} is admittedly approximate, since the calculation involves ΔS^0 values from 1 M HCl. However, if similar calculations are made at $\mu = 0.5$ from the same authors' data, the entropy of VO^{++} only changes 0.3 e.u., and it is therefore assumed that extrapolation to infinite dilution will not introduce serious errors in the vanadyl ionic entropy.

Vanadium Pentoxide (Hydrate).—From the observation that the solubility of $V_2O_5(c)$ and $V_2O_5 \cdot H_2O(c)$ are approximately the same, $\Delta F^0 \approx 0$ for the following reaction

$$V_2O_{5(c)} + H_2O = V_2O_5 \cdot H_2O \text{ (or } 2HVO_3) \qquad (4)$$
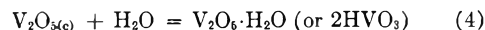
The entropy of the hydrate can be estimated from Latimer's rules[4] in two ways. If the structure were $V_2O_5 \cdot H_2O$ the estimated entropy would be $31.3 + 9 \approx 40$ e.u.; alternatively if 2 HVO_3 were the correct structure, the estimated entropy for $2HVO_3$ would be $2(0 + 20) \approx 40$ e.u. Thus ΔS^0 becomes -8 e.u. and $\Delta H^0 = -2,380$ cal. A summary of the experimental and estimated thermodynamic values, along with other supplementary values,[24] is given in Table III.

TABLE III

SUMMARY OF THERMODYNAMIC FUNCTIONS[a]

	ΔF^0	ΔH^0	S^0
$V_2O_5(c)$	−344	−373	31.3 ± 0.5
$V_2O_5H_2\cdot O(c)$	−401	−443	(40)
VO_2^+	−143	−155	−5.5 ± 0.5
VO^{++}	−110	−116	−26 ± 3

[a] Values for heats and free energies of formation in kilocal. mole^{-1}; entropies in cal. mole^{-1} deg.$^{-1}$.

It is interesting to note that the entropies of the VO_2^+ and NpO_2^+ ions appear to be uniformly lower than would be expected from any of the published correlations on the similar oxyanions. While a fuller discussion of the entropies of oxycations will be the subject of a future communication, it appears that this behavior may be due in part to different charge distributions on the oxycations, which are usually derived from metallic elements, as contrasted to the oxyanions derived from non-metallic elements.

Acknowledgments.—The authors wish to thank Professor G. T. Seaborg for his interest and encouragement in this research, and Professor R. E. Connick for his helpful suggestions and discussions of the problem.

Appendix

POWDER DIFFRACTION PATTERN FOR $V_2O_5\cdot H_2O$[a]

(CuKα radiation λ = 1.5418 Å.)

Sin$^2\theta$	Intensity[b]	Sin$^2\theta$	Intensity	Sin$^2\theta$	Intensity
0.01781	S	0.12173	S	0.26975	M
.02367	M	.12983	W	.27815	W
.02992	W$^-$	.13397	VW	.29265	M$^+$
.03240	W^{-c}	.14534	S	.30127	M
.04098	M^{-c}	.14621	W	.31157	M
.04685	M$^+$	.16388	M	.33277	VW^c
.05714	VS	.17343	W^c	.33854	VW^c
.06465	W	.18277	W$^+$	.35231	VW^c
.07106	S	.19011	W^c	.35749	VW^c
.07774	W	.19756	W	.37633	W
08441	W	.20385	M	.38498	W
.08943	W	.22011	W	.39519	W
.09621	M	.22432	W	.40442	VW
.09984	VW	.23179	M	.41542	W
.10386	W	.23890	M	.42523	W
.10967	W$^-$	.24985	M$^+$	.44288	W
.11485	W	.25318	W	.45156	VW
				.46704	W^{+c}

[a] Pattern determined by Mrs. C. H. Dauben, Chemistry Dept., University of California. [b] Symbols: S, strong; M, medium; W, weak; V, very. [c] These lines were found to be quite broad on the photographic film.

THERMAL CONDUCTIVITY OF MERCURY AND TWO SODIUM–POTASSIUM ALLOYS

By C. T. Ewing, R. E. Seebold, J. A. Grand and R. R. Miller

Contribution from the Naval Research Laboratory,[1] Washington, D. C.

A recently published work on the thermal conductivity of liquid sodium and potassium metals has been extended to include measurements on high purity mercury to 540° and on two sodium–potassium alloys (56.5 wt. % potassium to 520° and the eutectic composition, 77.7 wt. % potassium to 680°). The variation of thermal conductivity with temperature for each of these ideal liquids is shown to be accurately predicted by the electrical analog. Subsidiary conductivity measurements on two stainless steels, type 304 and 310, are also included.

Introduction

A thermal conductivity measuring system of the uni-axial type, which has been suitable for the precision study of high-conducting liquids at elevated temperatures, was designed and built at this Laboratory. The objective of the conductivity program has been to provide reliable coefficients for those liquid metals which are of interest as potential heat transfer media. As a rule, the coefficients for a particular liquid metal at higher temperatures, if existent, have been questionable due to wide disagreements in existing studies. The coefficients for high purity sodium and potassium metals have been published[1] recently. The program has now been extended to cover mercury and two alloys of sodium–potassium.

Experimental

Apparatus.—The uni-axial measuring unit and integral control systems employed for the measurement of mercury and the alloys were similar to those illustrated and described in the preceding article, and only a brief description will be included here to clarify the data presentation. The actual

conductivity measurements are made on a central bar (1.62″ dia.) which contains the liquid sample in a chamber at the middle of the bar. This conducting bar is compensated for radial heat exchange by the surrounding thick metal guard-ring (7″ o.d. and 5.5″ i.d.). Thermal gradients within the bar and compensating gradients in the guard-ring are established and controlled by direct current heaters at the top in combinations with uniform air-cooling points at the base. To permit radial equalization of temperatures in the region of the liquid specimen, auxiliary heating and cooling points are provided on the guard-ring. Thermal gradients are measured and controlled with thirty calibrated thermocouples suitably positioned at known levels on the bar and guard-ring. The entire guard-ring assembly is maintained at the temperature of measurement by a large electric furnace with eleven uniformly wound elements, which provide a secondary guarding action.

The measuring unit, bar and guard-ring of type 304 stainless steel, designated for the sodium–potassium alloy studies was essentially the same as that used for the pure metals except for minor changes, which were incorporated for increased accuracy. However, for the mercury experiments a completely new measuring unit, bar and guard-ring, were formed from type 310 stainless steel. The guard-ring used with the alkali metals was designed specifically to provide heat compensation for a tube containing a liquid of higher conductivity than the steel. The new guard-ring, on the other hand, was designed to compensate for liquids with conductivity higher or lower than the steel. Thus, another auxiliary heater was added to the guard-ring opposite the

(1) C. T. Ewing, J. A. Grand and R. R. Miller, *J. Am. Chem. Soc.*, **74**, 11 (1952).

top of the specimen chamber and a new cooling point was added opposite the base of the chamber. Only one significant modification was made in the control systems; the movable couple for the measurement of furnace temperatures was replaced by 12 individual couples installed on the thin metal shield between the furnace core and the guard-ring.

Procedure and Methods.—Extreme precautions were taken to assure the introduction of high purity mercury into a clean conductivity tube. To reduce contamination by the container tube, all welds were of the heli-arc type and were made with an inert gas inside the tube. The starting point for the mercury purification was a commercial triply-distilled material which had been passed through acid and water wash columns. The purification procedure which was designed to remove the last traces of water, organics, base and noble metal impurities, consisted of four distillation steps. The final high-vacuum distillation introduced the metal directly into the conductivity tube. A small filling tube at the top of the bar was welded closed under reduced pressure of nitrogen forming the usual closed system for measurement.

Spectrochemical analyses of the mercury before purification and after purification indicated, qualitatively, a rather complete removal of all trace materials. A chemical analysis was made on the mercury sample removed from the measuring apparatus. The surface of the mercury removed was slightly discolored, and the analysis of mercury, as presented below, represents that of the filterable residue based on the total mercury sample. In an additional analysis of the filtered sample of mercury, no container material was detected. These analyses indicate only a trace solubility of container materials in mercury at the higher measurement temperatures.

SPECTROCHEMICAL ANALYSIS OF COMMERCIAL MERCURY

Ag, Si	0.01 to 0.1%
Mg	0.001 to 0.01%
Cu, Al, Fe	less than 0.00001%

SPECTROCHEMICAL ANALYSIS OF PURIFIED MERCURY

| Mg | 0.0001 to 0.001% |
| Na, K, Si, B, Cu, Ag, Al, Pb, Sn, Cd, Zn, Fe, Ni | Nil |

CHEMICAL ANALYSIS OF MERCURY REMOVED FROM CONDUCTIVITY TUBE

Fe	0.0004 wt. %
Cr	.0002 wt. %
Ni	.0001 wt. %

The procedure for the filling of the sodium–potassium tubes was similar to that described for mercury. Each alloy was formed by the mixing of the high purity metals and was introduced to the tube through a sintered glass filter under high vacuum, purified nitrogen being used as covering gas. For these light metals, X-ray photographs of the specimen chamber were effective in the detection of voids as small as 0.1 ml. The same conductivity tube was used for both alloys.

A measurement of conductivity required the establishment of a steady heat flow state in which the temperatures at corresponding levels on the bar, guard-ring, and furnace were matched within predetermined limits. Temperature measurements on each assembly were made with platinum–platinum, 10% rhodium thermocouples with the usual 5 mil diameter couples on the bar and 15 mil couples on the guard-ring. A Rubicon, type C, double-microvolt potentiometer in an effectively shielded system permitted measurement of the couple voltages with the required high degree of accuracy. Precautions were observed in the couple measuring system to reduce the possibility of extraneous thermals, electrostatic charging, electromagnetic effects, current leakage to the system, parallel couples, etc. Room temperature and humidity were controlled for all measurements. The couples to be installed on each assembly were annealed for equal periods at 1150° and then intercalibrated against primary standard couples from the National Bureau of Standards. The couples were calibrated relative to each other by placing all junctions in a silver or platinum bar which was supported in the center of a long uniformly wound furnace. Intercalibrations were made at 100° intervals and

were accurate to at least 0.5 of a microvolt for the temperature range. The NBS couples were used to provide the absolute temperature base and to provide a check on the calibration work. A stability check for all couples was provided by maintaining the platinum bar at elevated temperatures for a long period of time with a subsequent recheck of lower temperature calibrations. As standard procedure, identical assembly in the measuring system for each couple was maintained for both the intercalibration and the conductivity experiments.

For higher precision, thermocouple readings during a measurement were made relative to one or more couples near the center of the bar. Two or more couples were also read relative to a cold junction for the absolute temperature base. The thermal gradient for each liquid was measured with the outer of three couples peened into the $1/_{32}$-inch wall of the specimen chamber. The middle couple was used only as evidence of the linearity of the liquid gradient as measured on the wall. An additional liquid gradient was obtained for each experiment by extrapolating temperatures in the stainless bar sections. Although this gradient was influenced by the small radial heat exchange and by any departure of the steel from a linear conductivity relationship with temperature, the average deviation from the directly measured value was only 0.5%. The agreement between gradients for the individual experiments is significant as an independent check on couple calibration and length measurements.

The equilibrium heat flow in the sample bar was obtained by an absolute measurement of power input to the sample heater by noting the voltage drop across the heater and that across the standard manganin resistor in series with the heater. Thermal conductivity coefficients were calculable from the equilibrium measurements of heat flow and thermal gradients using the standard conduction equation with due corrections for thermal expansion and heat exchanges.

Experimental Results

Mercury.—The measured coefficients for mercury and the two sodium–potassium alloys are presented in Table I. The coefficients for mercury, shown graphically in Fig. 1, extend 200° past the
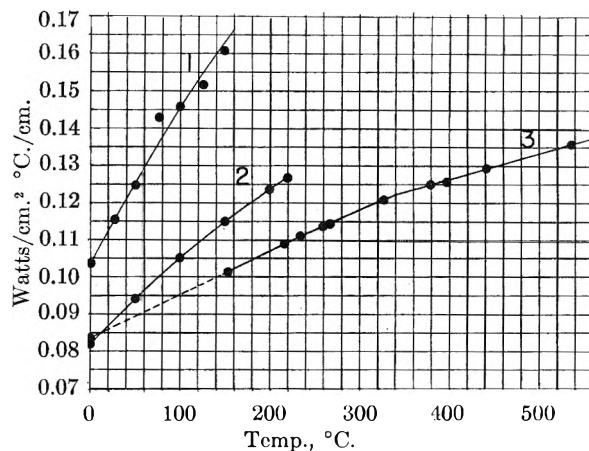
Fig. 1.—Thermal conductivity of mercury: 1, Gehlhoff and Neumeier; 2, Hall; 3, NRL.

normal b.p. and can be adequately expressed by two straight lines intersecting at a temperature near the normal b.p. The possibility of pressure influence on the results above 350° could not be overlooked where the absolute pressure over the mercury varied from about 1 to 25 atm. To investigate the effect of pressure, a series of experiments were made at an average mercury temperature of 388° in which the temperature of the reservoir was purposely elevated from the normal 480° to about 588°, increasing the usual pressure, for a run at this temperature, from 9 to 23 atm. For this run the
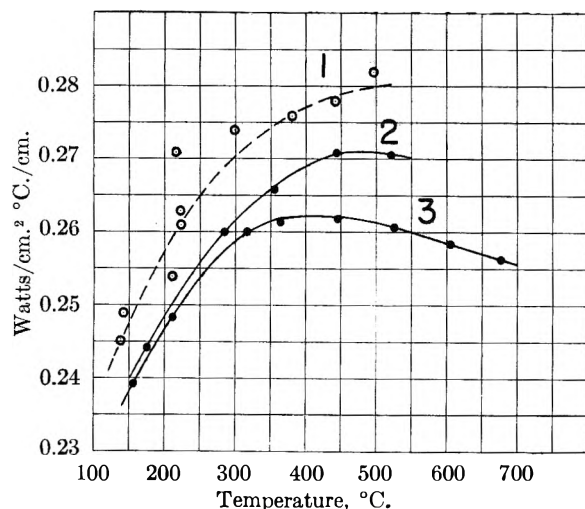
Fig. 2.—Thermal conductivity of sodium–potassium alloys: 1, Deem and Russell—48.3 wt. % K; 2, NRL—56.5 wt. % K; 3, NRL—77.7 wt. % K.

mercury conductivity was more accurately calculated from the known stainless steel bars due to the uncertainties in the large influx of heat at the top of the bar. This calculated coefficient was not influenced by the added pressure and was within 0.2% of the corresponding curve value.

TABLE I

THERMAL CONDUCTIVITY OF MERCURY AND SODIUM–POTASSIUM ALLOYS

(Units of K, abs. watt/cm.^{2} °C./cm.)

Temp.	Mercury K	77.7 wt. % K in Na Temp.	K	56.5 wt. % K in Na Temp.	K
153.2	0.1014	157.1	0.2393	175.8	0.2442
216.2	.1090	211.4	.2487	285.4	.2600
234.7	.1111[a]	316.2	.2600	354.5	.2658
259.7	.1139	364.0	.2614	443.1	.2709
267.7	.1144	445.2	.2618	521.0	.2706
327.1	.1209	525.5	.2607		
378.9	.1250	603.5	.2584		
396.8	.1256[a]	676.3	.2563		
441.8	.1293				
536.3	.1358				

[a] Second series of measurements for mercury.

The results for mercury at 234.7 and 396.8° represent a second series of measurements. These measurements were made with the same conductivity tube, but, in this case, the tube was assembled in a completely new guard-ring, furnace and measuring system. The new unit, also with a guard-ring of type 310 stainless steel, was one designed and built for higher temperature studies. The thermocouple measuring system was of identical construction but used a Rubicon, six-dial, thermofree potentiometer in place of the Rubicon, type C, in the other system. The agreement between comparable values measured in the two systems affords an excellent check on the absolute heat measurement, radial exchange of heat, and the measurement of couple voltages.

Previously published conductivities for mercury having any range of temperature are those of Hall[2]

(2) W. C. Hall, *Phys. Rev.*, **53**, 1004 (1938).

and Gehlhoff and Neumeier.[3] The data of these investigators are included on Fig. 1 for comparison with the NRL curve. In the work of Hall liquid sodium also was measured, and it is interesting that the agreement with sodium values of this Laboratory[1] is excellent (within 1%). In contrast, comparable mercury results are seen to deviate by as much as 15%. The extremely high values by Gehlhoff and Neumeier are less understandable. The value plotted at 0° represents the "Critical Tables" average of numerous limited measurements near this temperature. This average value is consistent with the slope trend of the NRL measurements as indicated by the dashed extension below 150°.

Sodium–Potassium Alloys.—The conductivity coefficients for the two alloys of sodium and potassium are presented graphically in Fig. 2. These coefficients are much lower than those for the pure metals, and indicate for the sodium–potassium system the U-shaped isotherms which are predicted by electrical conductivity measurements on the system.[4] The coefficients for the 48.3 wt. % potassium alloy were measured by Deem and Russell[5] and, being concentration-wise consistent with the data for the NRL alloys, have been included on the same figure. In the Deem and Russell report the alloy data were represented by a best linear curve. However, based on the data for the other alloys, the 48.3 wt. % potassium curve should appear roughly as drawn with a maximum above 500°. At the present time, any explanation of the unusual shape of the conductivity curves would be pure conjecture.

Stainless Steel Measurements.—Each conductivity tube has a solid stainless bar above and below the liquid chamber. Four thermocouples are positioned on each bar, permitting absolute measurements of the conductivity of the steel in each bar. Coefficients for type 310 stainless were measured during the mercury experiments (Fig. 3). The conductivity curves for the two bars are approximately
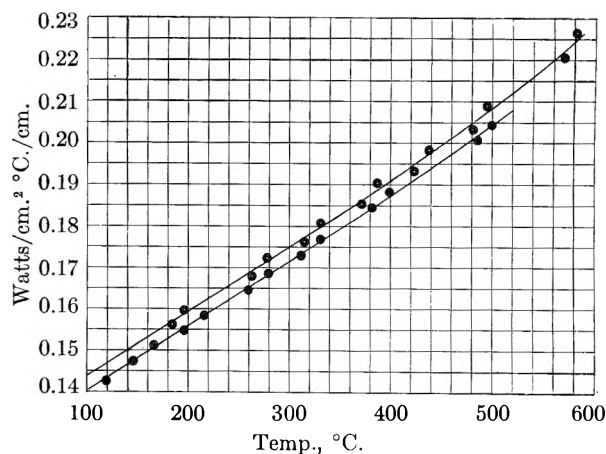
Fig. 3.—Thermal conductivity of type 310 stainless steel.

(3) Gehlhoff and Neumeier, *Verh. d. phys. Ges.*, **21**, 201 (1919); **15**, 876, 1069 (1913).

(4) Paul Müller, "Metallurgie," Vol. VII, Book 23, pp. 730–740, and Book 24, pp. 755–770, 1910.

(5) Herbert Deem and H. W. Russell, "Determination of the Thermal Conductivity of Sodium-Potassium Alloy at Elevated Temperatures," published in Argonne National Laboratory Report No. CT 3554.

linear with temperature but are displaced from each other by about 2%. This spread in coefficients is too great to be due to experimental uncertainty and, therefore, is considered to be a variation in the steel between the two bars.

Conductivity coefficients for type 304 stainless steel were similarly measured during the alkali metal experiments. Since at least one bar section on each of the three conductivity tubes, used for the previous measurements on the pure metals and for the present alloy work, were cut from adjacent material on a stock bar, an excellent means for cross-correlation of all the alkali metal measurements was afforded through the experimental coefficients for the steel. Figure 4 represents the conductivity results for this steel as measured during the sodium, potassium, and alloy experiments. The maximum deviation of any result from the best straight line for all measurements was about 1%.

Discussion of Results

Error.—Each result reported in Table I is based on an absolute heat measurement and represents a series of equilibrium experiments covering a period of 48 to 96 hours, during which time there was normally no calculable change in the coefficient. Space prohibits a complete resume of errors. However, for the calculation of error in the final conductivity result, probable uncertainties in the following were considered: radial exchange of heat, axial heat flow in the insulation, measurement of temperature differences, drift, measurement of dimensions, absolute heat measurement, conductivity of the stainless wall of the specimen chamber, heat conduction along couple leads and insulation, convection, and variation of conductivity with temperature. The calculated probable error from the sources outlined was 1.4% for the mercury result and 1.0% for the alloy result. The coefficients at a particular temperature were duplicable to better than 0.3%, which represents the precision of measurement.

Interface Resistance.—Initial experiments with the 56.5 wt. % potassium alloy (not included) were influenced by a thermal resistance at the upper interface, amounting to 0.51 deg./watt at 180°. Peculiarly, this resistance to heat flow decreased linearly as the temperature for the experiments was increased and disappeared entirely above 450°. Succeeding runs up and down the temperature scale were completely free of any interface resistance. It was impossible to analyze whether the resistance was caused by a void or by an interface-wetting condition. However, X-ray photographs of the specimen chamber, before the measurements, gave no indication of any void or foreign matter at the interface. No thermal resistance was evident in measurements with the other liquid metals; a resistance equivalent to a temperature difference of 0.2° would have been detectable.

Convection.—Conductivity measurement for a non-viscous liquid remain questionable unless supported by positive evidence that heat transfer by convection has not been included in the coefficients. For each conductivity tube, liquid movement induced by the non-symmetry of the conducting surface was precluded by maintaining close tolerances for all parts influencing symmetry at the
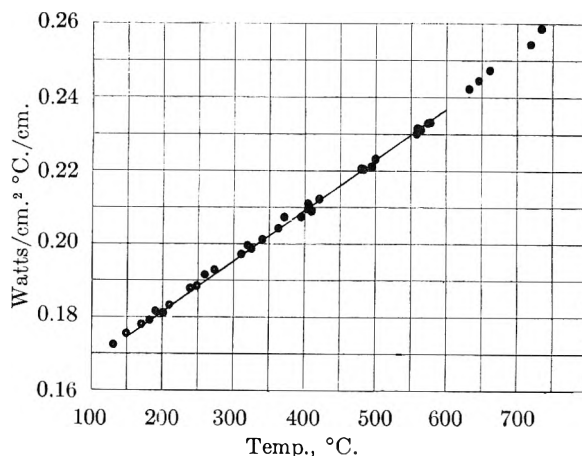
Fig. 4.—Thermal conductivity of type 304 stainless steel (experimental points from alloy work with best curve from pure metal work).

liquid sample. For mercury, it was shown, by a series of measurements at the same temperature, that an induced radial exchange between the bar and guard-ring from a normal 0.4 to 6.0% of bar heat produced no change in the calculated conductivity of the liquid, above that expected from the radial loss or gain of heat. It was further shown by measurement that a change from 7 to 20 watts in the bar heat flow produced no change in the expected conductivity. Assuming that the conditions contributing to convection were considerably magnified in the above experiments, one would expect no measurable convection to be present in the normal experiment. Data similar to that described for mercury, but with less drastic heat change limits, were taken during the sodium-potassium alloy experiments, and the same conclusions were reached.

Lorentz' Numbers.—Mercury and the sodium-potassium alloys are considered abnormal in that their conductivities increase with temperature; on the other hand, liquid sodium and potassium exhibit normal behavior. The relationship between the thermal and electrical analogs for these ideal liquids with their variety of conducting patterns should be of interest. Electrical resistivity figures over considerable temperature ranges are available for mercury,[6] 58 wt. % K alloy,[7] sodium,[7] and 80 wt. % K alloy.[8] The resistivity isotherms for the sodium–potassium system are relatively flat for intermediate compositions. Thus, the small differences in composition of these alloys from those on which the thermal measurements were made, can be neglected for the purposes of this study. Lorentz functions for each metal have been calculated over the temperature range of the available resistivity work and are presented in Table II. The function for each liquid is surprisingly constant. Mercury over the 200 degree temperature range shows a maximum variation of 1.9%; the 77.7 wt. % K alloy, 2.6% for 550 degrees; 56.5 wt. % K alloy, 2.5% for 300 degrees; and sodium, 2.2% for 300

(6) E. I. Williams, *Phil. Mag.* **50**, 589 (1925).

(7) Private Communication, Mine Safety Appliances Co., Pittsburgh, Pa.

(8) P. G. Drugas, I. R. Rohn and W. D. Wilkinson, "Resistivity of NaK," Argonne National Laboratory Report No. ANL-5115 (1953).

degrees. Thus, the trends of three distinct types of heat conductivity–temperature curves are accurately predicted by electrical resistivity data from three sources. This is further evidence for the direct relationship between the phenomena of electrical and thermal transfer in ideal liquid systems and one might conclude that the variation of thermal conductivity with temperature for other liquid metals can be accurately predicted from its electrical counterpart if the thermal conductivity for at least one temperature is known.

The value of the Lorentz number is predicted in the electronic theory of Rieche,[9] Drude[10] and

TABLE II

Temp., °C.	Thermal cond., watt/cm². °C./cm.	Elec. resistivity, microhm-cm.	Lorentz' number, $rk/T \times 10^8$
Mercury			
100	0.0952	103.35	2.64
184	.1051	112.65	2.59
256	.1133	121.82	2.61
288	.1168	126.19	2.63
297	.1178	127.51	2.64
Sodium-potassium alloy (77.7% wt. % potassium)			
150	0.238	41.6	2.34
200	.247	44.4	2.32
300	.259	51.3	2.32
400	.262	58.8	2.29
500	.262	67.3	2.28
600	.259	77.3	2.29
700	.255	89.2	2.34
Sodium-potassium alloy (56.5 wt. % potassium)			
200	0.249	47.23	2.49
300	.262	54.33	2.48
400	.269	62.21	2.49
500	.271	69.37	2.43
Sodium			
200	0.815	13.64	2.35
300	.757	17.47	2.31
400	.712	21.99	2.33
500	.668	27.27	2.36

(9) E. Rieche, *Ann. Physik und chemie*, **66**, 353, 545 (1898).
(10) P. Drude, *Ann. Physik*, **1**, 566 (1900).

others. Using the presently accepted values for the constants involved in the theoretical derivation, a value of 2.45×10^{-8} watt-ohm/(°C.)(Å.) is obtained. The calculated functions for the liquid metals have values approaching this theoretical value.

THE THERMODYNAMICS OF ABSORPTION BY FIBERS FROM MULTICOMPONENT BATHS SUCH AS DYE BATHS

By HOWARD J. WHITE, JR.

Textile Research Institute, Princeton, New Jersey

Absorption by fibers from multicomponent baths such as dye baths is discussed using a strictly thermodynamic approach. Equations are given which can be used to determine the equilibrium constant for any distribution equilibrium in the system in terms of measurable quantities and of conventions adopted in defining activity coefficients. Other equations are given for the free energy change, and hence the heat and entropy changes, for certain well defined processes which describe the absorption.

Methods of analyzing thermodynamic results for dyeing and allied processes have been studied for some time, since it has long been appreciated that an understanding of the energetics of such processes could provide insight into the molecular interactions involved. Two general approaches are possible. In the first a tentative model of the absorption process is postulated, relations holding for such a model are derived, and experimental tests of the relations are made. In the second a strictly thermodynamic analysis of the system is made, and relations between measurable quantities which will be true for all possible models are derived. The relations derived from the first method are obviously detailed but specific to the model, whereas those derived from the second method are general but unselective as to mechanism.

The first method has been used several times to provide insight into various dyeing problems; however, none of the models devised has been completely successful. The successes and failures of each of these attempts have been ably summarized by Vickerstaff[1] and need not be discussed further here.

(1) T. Vickerstaff, "The Physical Chemistry of Dyeing," 2nd Edition, Interscience Publishers Inc., New York, N. Y., 1954.

In this paper the second approach is taken and some thermodynamic relations are derived which are valid regardless of the exact molecular mechanism of absorption.

Description of System.—The system considered is composed of a fiber and a surrounding solution. The fiber is assumed to contain no obvious macroscopic pores or holes, and the boundary between the two parts of the system is assumed to envelop the visible external surface of the fiber.

The experimental separation of the parts of the system can be visualized as follows. If the fiber were a block of wood, it would be removed from the solution, wiped free from excess droplets of solution, and analyzed for diffusible components. With a fiber the process of "wiping" off excess droplets is somewhat more difficult, but methods have been devised which will be referred to later. Actually this method assumes a certain minimum size for the fiber. As the diameter of the fiber decreases, the material absorbed at the external surface between the fiber and the solution will become comparable in magnitude to the material within the fiber. At this point the "amount absorbed" as defined here will become so sensitive to the method of removing

droplets that it will be of doubtful value. The methods of this paper were developed primarily for application to textile fibers. These fibers are quite permeable and have diameters of at least 10 μ so that difficulties resulting from surface absorption should be negligible in most cases.

The position of the boundary between the parts of the system has been stressed because a considerable number of absorption experiments on fibers have been carried out using the change in concentration of the external solution as the definition of absorption. The two methods give the same results only when possible differences introduced by solvent absorption are negligible. When this is not true, the use of the concentration change itself as the definition of absorption involves an assumption as to the nature of the absorbed solvent which it is desirable to avoid for the sake of generality. If it should turn out that some of the material defined as absorbed can be described as a solution, identical with the external solution, in micropores within the fiber, no harm has been done. If not, any definition of the amount absorbed other than that used here is misleading.

Conditions of Equilibrium.—Since the two parts of the system can exchange heat, mechanical energy and diffusible components across the boundary, the conditions of equilibrium will be equality across the boundary of temperature, pressure and partial molal free energy of each diffusible component. A Gibbs–Duhem equation can be defined for each part of the system. It is evident that it is immaterial whether the fiber consists of one phase or more as far as these equilibrium conditions are concerned. For this reason the fiber will be referred to as the fiber phase, where convenient, from this point on without loss of generality.

Since dyes are often ionic it should be understood that the diffusible components referred to are chemically isolatable components and hence not individual ions. In cases where ion exchange occurs, an appropriate counter ion can be invoked so that the exchange process involves isolatable species. Only ionic absorbates are considered since the results can easily be converted to similar results for non-ionic absorbates.

Activities within the Fiber.—The fiber will be assumed to exchange two solutes, $R_{\nu_R}X_{\nu_X}$ and $H_{\nu_H}Y_{\nu_Y}$, the auxiliary species $R_{\nu'_R}Y_{\nu'_Y}$ and $H_{\nu'_H}X_{\nu'_X}$, and the Solvent, S, with the solution. The fiber phase will be denoted by the superscript, ϕ, the solution by the superscript σ. The conditions for chemical equilibrium across the fiber–solution boundary can be written in terms of appropriate partial molal free energies, as

$$\mu_i{}^\phi = \mu_i{}^\sigma \qquad (1)$$

where i is $R_{\nu_R}X_{\nu_X}$, $H_{\nu_H}Y_{\nu_Y}$, $R_{\nu'_R}Y_{\nu'_Y}$, $H_{\nu'_H}X_{\nu'_X}$, or S.

In the usual way equation 1 can be broken into concentration-independent terms and concentration-dependent terms composed of a concentration and an activity coefficient. For the ionic species represented in equation 1, terms for each ion will be included. The activity in the solution will be expressed in terms of the mole fraction, x, and the activity coefficient, γ. The activity in the fiber

will be expressed in terms of the number of moles absorbed per gram of pure fiber, Γ, and the activity coefficient, f. Thus equation 1 can be written

$$\nu_j\mu\phi_{oj} + \nu_k\mu\phi_{ok} + \nu_jRT \ln \Gamma_j f_j + \nu_k RT \ln \Gamma_k f_k =$$
$$\nu_j\mu^\sigma_{oj} + \nu_k\mu^\sigma_{ok} + \nu_j RT \ln x_j\gamma_j + \nu_k RT \ln x_k\gamma_k \quad (2)$$

where j is R or H, and k is X or Y for the ionic species, and

$$\mu_{os}\phi + RT \ln \Gamma_s f_s = \mu_{os}{}^\sigma + RT \ln x_s\gamma_s \qquad (3)$$

for the solvent. The subscript o has been used to denote terms not dependent on concentration. The Gibbs–Duhem equation for the fiber phase at constant temperature and pressure can be written

$$\Gamma_R d \ln \Gamma_R f_R + \Gamma_H d \ln \Gamma_H f_H + \Gamma_X d \ln \Gamma_X f_X + \Gamma_Y d \ln \Gamma_Y f_Y$$
$$+ \frac{1}{M_p} d \ln f_p + \Gamma_s d \ln \Gamma_s f_s = 0 \quad (4)$$

where f_p and M_p are the activity coefficient and the molecular weight of the pure fiber polymer. The molecular weight of the fiber enters because one gram of fiber has been chosen as the basic reference quantity for the fiber phase.

An additional equation can be written expressing the fact that, to a very good approximation chemically, the fiber is electrically neutral. The exact form of this equation depends on whether or not the fiber can act as an ion exchanger. If it cannot, the equation can be written

$$Z_R\Gamma_R + Z_H\Gamma_H + Z_X\Gamma_X + Z_Y\Gamma_Y = 0 \qquad (5)$$

if it can

$$Z_R\Gamma_R + Z_H\Gamma_H + Z_X\Gamma_X + Z_Y\Gamma_Y + N_p = 0 \qquad (6)$$

The symbol Z_i represents the valence of ion type i, and N_p represents the charge on one gram of fiber stripped of its counter ions. The absolute value of N_p is the ion-exchange capacity of one gram of fiber.

f_R, f_H, f_X, f_Y and $\gamma_R, \gamma_H, \gamma_X, \gamma_Y$ are single ion activity coefficients, as is f_p when the fiber is an ion exchanger. They always occur in combinations representing an activity coefficient for a neutral species. This is obvious from the origin of equation 2. To show it for equation (4), consider the fiber to be non-ionic and to be in equilibrium with such a solution that it contains $n\nu_R$ moles of R, $m\nu_H$ moles of H, $n\nu_X$ moles of X, and $m\nu_Y$ moles of Y. Then equation (4) can be written

$$n\, d\mu_{R_{\nu_R}X_{\nu_X}} + m\, d\mu_{H_{\nu_H}Y_{\nu_Y}} + \frac{1}{M_p}\, d\mu_p + \Gamma_s d\mu_s = 0 \quad (7)$$

It will always be possible to convert equation (4) into an equation similar to equation (7). If the fiber is a cation exchanger, for example, species such as PR^{N_p/Z_R} and PH^{N_p/Z_H} would occur.

Equations 2–4 can be used to solve for the free energy change on absorption of any neutral species in terms of directly measurable quantities and constants representing reference states. The reference states are a matter of choice. Since the activity coefficient of a solute becomes a constant as the concentration of the solute approaches zero, it is the custom to set the activity coefficients of solutes and the activity of the solvent equal to unity in a solution infinitely dilute in all solutes. In the case of a fiber which is not an ion exchanger, it seems logical to set analogous standard states, that is, to set the activity coefficients of the solutes and the

fiber and the activity of the solvent (of the external solution) equal to unity in a fiber saturated with solvent and infinitely dilute in solutes. In other words, the solvent-soaked fiber is used as the standard state. If the fiber is a cation exchanger, for example, the R and H forms must be differentiated. In this case it is logical to set the activity coefficient of the R form equal to unity when it is saturated with solvent and infinitely dilute with respect to RX or RY, with similar conditions for the H form. Gaines and Thomas[2] have used such conditions and a similar approach in determining equilibrium constants for ion-exchange equilibria. No complete analysis of dye absorption exists, although equations formally similar to equation 2 derived from a model of the absorption process, have been used to determine affinities for cellulose dyes.[1]

From a consideration of equation 2 it is evident that if the constant terms are combined on the left-hand side of the equation, they give the free energy change per mole of salt on transfer from the state of unit activity in solution to the state of unit activity within the fiber (the affinity[1]). This value is useful for comparing dyes, but it has one drawback. The exact composition of the states of unit activity is not always known (or even experimentally attainable) and can be expected to change with temperature. This makes interpretation of temperature changes in terms of heats and entropies of known processes complicated. The same remarks apply to the equilibrium constants for ion exchange mentioned above.

Free Energies, Heats and Entropies of Dyeing.— In order to derive expressions for free energy changes involving states of known composition, consider first the fiber which is not an ion exchanger in the vapor of the solvent at vapor pressure, p. The free energy change involved in transferring one mole of solvent from the liquid to a large amount of fiber at equilibrium at vapor pressure, p, can be written

$$\Delta\mu_1 = RT \ln p/p_0 \tag{8}$$

where p_0 is the saturation vapor pressure of the solvent. The total free energy change for the mixing of liquid solvent and dry fiber to give a fiber containing Γ_{SO} moles of water per gram of fiber (the amount absorbed from liquid solvent) is

$$\Delta F_1 = \int_0^{\Gamma_{SO}} (RT \ln p/p_0)d\Gamma_S \tag{9}$$

If this fiber which is in equilibrium with liquid solvent is transferred to increasingly concentrated solutions of a non-volatile solute until a concentration, x, is reached in the external solution, there is a further free energy change

$$\Delta F_2 = \int_0^X \left[\left(RT \ln \frac{a_1}{a_{1\,sat}} \right)\frac{\partial\Gamma_1}{\partial x} + (RT \ln a_S)\frac{\partial\Gamma_S}{\partial x} \right] dx \tag{10}$$

where a_1 is the activity of the solute, $a_{1\,sat}$, its activity in a saturated solution, and a_S, the activity of the solvent. The activity of the pure solvent has been taken to be unity. $\Delta F_1 + \Delta F_2$ gives the free energy change resulting from the mixing of liquid solvent, solid solute, and dry fiber to give the sol-

(2) G. L. Gaines, Jr., and H. C. Thomas, *J. Chem. Phys.*, **21**, 714 (1953).

vent-solute-fiber mixture which is in equilibrium with a solution of concentration x.

If the fiber is removed from the solution and dried, there is a further free energy change

$$\Delta F_5 = \int_{\Gamma'_S}^0 (RT \ln p/p_0)d\Gamma_S \tag{11}$$

where Γ'_S refers to the amount of solvent present in the fiber at equilibrium with a solution of concentration x.

The free energy change involved in mixing Γ_1 moles of solute and 1 g. of dry fiber is given by the sum $\Delta F_1 + \Delta F_2 + \Delta F_5$. This process is clearly defined, and values of the sum for more than one temperature can be broken into heats and entropies readily interpretable in terms of heats of interaction and entropies of mixing.

In most cases it should be possible to form the same composition of solvent, solute and fiber at different temperatures by varying the relative vapor pressure of the solvent. Thus the effect of varying amounts of solvent on the heats and entropies of absorption could be studied.

If two absorbable solutes are present in the solution, ΔF_2 can be written

$$\Delta F_2 = \int_0^{m_1} \left[(RT \ln a_S)\frac{\partial\Gamma_S}{\partial m_1} + \left(RT \ln \frac{a_1}{a_{1\,sat}} \right)\frac{\partial\Gamma_1}{\partial m_1} \right] dm_1 \tag{12}$$

and ΔF_3 can be defined by

$$\Delta F_3 = \int_0^{m_2} \left[(RT \ln a_S)\frac{\partial\Gamma_S}{\partial m_2} + \left(RT \ln \frac{a_1}{a_{1\,sat}} \right)\frac{\partial\Gamma_1}{\partial m_2} + \left(RT \ln \frac{a_2}{a_{2\,sat}} \right)\frac{\partial\Gamma_2}{\partial m_2} \right] dm_2 \tag{13}$$

In these equations the molality of the bath has been used in place of the mole fraction. It is assumed that m_1 stays constant during the process described by equation 13. The activities of component 2 are defined in the same way as those of component 1 and it also is assumed to be non-volatile. Obviously, other paths could be used in evaluating $\Delta F_2 + \Delta F_3$ if desirable. If the solutes are ionic of the form $R_{\nu_R}X_{\nu_X}$ and $H_{\nu_H}Y_{\nu_Y}$ it may be that some account of the subsidiary pair $R_{\nu'_R}Y_{\nu_Y}$ and $H_{\nu'_H}X_{\nu'_X}$ must be taken in describing the uptake by the fiber completely. This would introduce additional terms in the integral in equation 13, but otherwise would cause no difficulties.

The sum $\Delta F_1 + \Delta F_2 + \Delta F_3 + \Delta F_5$ represents the free energy change resulting from the mixing of Γ_1 moles of solid component 1, Γ_2 moles of solid component 2, and 1 gram of dry fiber. A fixed amount of water could be considered also as before.

Finally ion exchange must be considered. If the fiber exchanges dn_H moles of H^{Z_H} for dn_R moles R^{Z_R}, where $Z_H dn_H = Z_R dn_R = d\epsilon$ the number of equivalents exchanged, the fiber can be considered to absorb dn_R moles of $R_{\nu_R}X_{\nu_X}$ and desorb dn_H moles $H_{\nu_H}X_{\nu_X}$. The free energy change for this process can be written

$$dF = \left(\frac{RT}{Z_R} \ln \frac{a_{R_{\nu_R}X_{\nu_X}}}{a_{R_{\nu_R}X_{\nu_X}\,sat}} - \frac{RT}{Z_H} \ln \frac{a_{H_{\nu'_H}X_{\nu'_X}}}{a_{H_{\nu'_H}X_{\nu'_X}\,sat}} \right)d\epsilon \tag{14}$$

where solid $R_{\nu_R}X_{\nu_X}$ and $H_{\nu'_H}X_{\nu'_X}$ are reference states. If the fiber is considered to be in the H form in a solution of $H_{\nu'_H}X_{\nu'_X}$ and $R_{\nu_R}X_{\nu_X}$ is added keeping the molality of $H_{\nu'_H}X_{\nu'_X}$ constant, an ex-

change free energy term occurs which can be written

$$\Delta F_4 = RT \int_0^{mR_{\nu R}X_{\nu X}} \left[\frac{1}{Z_R} \ln \frac{a_{R\nu R}X_{\nu X}}{a_{R\nu R}X_{\nu X \, sat}} - \frac{1}{Z_H} \ln \frac{a_{H\nu'H}X_{\nu'X}}{a_{H\nu'H}X_{\nu'X \, sat}} \right] \frac{\partial \epsilon}{\partial m_{R\nu R}X_{\nu X}} dm_{R\nu X}X_{\nu X} \quad (15)$$

It should be noted that this term occurs in addition to ΔF_3 which describes changes in neutral solute and solvent composition within the fiber.

The use of the principles and equations described in this section should make possible the determination from experimental measurements of free energies, heats and entropies for well-defined processes for any multicomponent absorption system.

Application of Equations and Interpretation of Results.—Two types of experimental measurement are needed for the evaluation of the equations in the previous sections. First water absorption measurements are needed. These should extend from very low relative vapor pressures ($p/p_0 \cong$ 0.001) to very high. There are difficulties with capillary condensation in multifiber samples at high relative vapor pressures; however, this difficulty should be overcome with the use of single fiber samples and the vibroscope.[3] A number of ways have been devised to obtain results of the type needed on the uptake of various components of a solution including the solvent.[4-6] It has already been mentioned that caution is necessary if one wishes to use the change in concentration of the treating solution as a measure of the amount absorbed.

Some simplification should often be possible in practical cases. For example, if the treating solutions were all dilute aqueous solutions, the first term on the right-hand side of equation 12 or equation 13 would be small and probably negligible. Hence, measurements of the amount of solvent absorbed from solution would be unnecessary.

In some cases, phase changes may occur within the fiber during the process to which equation 11 refers; that is, dye might precipitate from the fiber during the drying process. (It might be noted that crystallization of vat dyes within cellulose fibers has been observed.) Such a precipitation would create no special problem as far as the analysis outlined in this paper is concerned, but would cause complications in the interpretation of the resulting thermodynamic quantities. It is also possible that metastable equilibria resulting from a large activation energy for diffusion through a dry fiber might occur. Again only complications in the interpretation of the results would be introduced. Evidence for a precipitation or metastable equilib-

rium would have to be obtained from some other type of experiment.

Experimental Results Available on Absorption by Fibers.—Although experimental results adequate for a complete thermodynamic analysis of an absorption process according to the equations developed here are not available, in many cases parts of the necessary measurements have been made. It may therefore be of some interest to note briefly the results available for various fibers. Particular emphasis will be placed on the technologically important process of dyeing.

Keratin.—The absorption of acids by keratin fibers has been studied extensively, and acid absorption results are available.[1] The absorption of water by acid-treated samples a'so has been studied,[7-9] and it may be interesting to note that appreciable changes in the water absorption isotherm do occur when keratin fibers are treated with acid. Unfortunately, results are available at only one temperature and do not cover as large a relative humidity range as is desirable. As a result only a free energy change of provisional accuracy could be obtained and no calculations are included here. Similarly, enough results are available for a rough calculation of the free energy of absorption of LiBr by human hair.[5] The acid dyeing of wool involves the presence of a mineral acid and usually an additional electrolyte as a levelling agent. Data for the complete analysis of such systems are not available.

Cellulose.—Direct dyeing of cellulose involves added electrolyte also. Usually two anions and one cation are present in the bath. There is rather extensive information on the dye uptake but little on electrolyte uptake and water absorption. Vat dyeing requires the presence of a reducing agent and alkali in the bath from which absorption takes place, and hence is more complicated and less susceptible to analysis than direct dyeing.

Other Fiber Types.—Polyamide fibers can be dyed with acid dyes, and some information on the absorption of acids and acid dyes by nylon is available. Water absorption results over a temperature range have not been reported, but scattered results are available for the dyeing of cellulose acetate, polyacrylonitrile and polyester fibers; these are less amenable to analysis at the present time. In many cases the dye baths themselves offer difficulties because of their colloidal nature.

(3) D. J. Montgomery and W. T. Milloway, *Text. Res. J.*, **22**, 729 (1952).

(4) W. S. Barnard and H. J. White, Jr., *ibid.*, **24**, 695 (1954).

(5) W. S. Barnard, A. Palm, P. B. Stam, D. L. Underwood and H. J. White, Jr., *ibid.*, **24**, 863 (1954).

(6) J. Farrar and S. M. Neale, *J. Colloid Sci.*, **7**, 186 (1952).

(7) P. Larose *J. Soc. Dyers Col.*, **70**, 77 (1954).

(8) C. H. Nicholls and J. B. Speakman, *J. Text. Inst.*, **45**, T267 (1954).

(9) A. F. Cacella and H. J. White, Jr., in press.

POLYMERIZATION AND PROPERTIES OF DILUTE AQUEOUS SILICIC ACID FROM CATION EXCHANGE

By M. F. Bechtold

Contribution No. 362 from the Chemical Department, Experimental Station,
E. I. du Pont de Nemours & Company, Wilmington, Delaware

Dilute aqueous silicic acid prepared by cation exchange of sodium silicate has been studied with regard to its polymerization kinetics, gelation and titration characteristics, copolymerization tendencies, and precipitation with organic compounds. When first formed, the silicic acid is of low molecular weight and in good solution in water. The kinetics of its polymerization as determined by light scattering and freezing point experiments can be accounted for by an ideal bimolecular condensation of a "monomer" with an apparent functionality of slightly over two (2.0004–2.05). Although some divergence from the ideal, such as cyclization or unequal functional group activity, is indicated and may in part account for this unexpectedly low value, the data indicate that the actual functionality cannot be as high as 3. The silicic acid solutions are also characterized by an optimum pH of about 5.05 for fastest gelation and by a sharp titration inflection point at a pH of about 4.65. Polymerization shifts these values to the vicinity of pH 5.85 and of pH 5.30, respectively, and this apparent decrease in hydrogen ion concentration during polymerization is independent of the titratable strong acid factor. The coöperative action of silicic acid in producing non-gelling or slowly gelling cation exchange effluents with certain other gelable metal acids and hydroxides is explained by copolymerization.

Introduction

The advent of cation exchange of alkaline silicate solutions as a convenient source of substantially salt-free silicic acid[1] and the development of light scattering[2] for the estimation of weight average molecular weights of dissolved organic polymers suggested an investigation of the nature of silica in water-soluble or aqueous dispersion form. In general, other investigators[3-7] have explained the chemical and physical properties of silica "sols" by considering them as composed of crystalloid and colloid phases and by separating the ordinary chemical reactions of the crystalloid phase from reactions tending to build up colloidal particles. It seemed desirable to test the concept that a study of the polymerization reaction could account for most of the physical and chemical properties of silica "sols."

Materials

The samples of commercial sodium silicate solutions used in this study were obtained from the Grasselli Chemicals Department of the du Pont Company, and designated as Grasselli 20-WW; the following analysis was typical: density at 25°, 1.388 g./cc.; SiO_2, 28.13%; Na_2O, 8.48%; Al_2O_3, 0.094%; TiO_2, 0.006%; Fe, 0.005%; and H_2O (by difference), 63.28%.

Sodium metasilicate nonahydrate ($Na_2SiO_3\cdot9H_2O$) J. T. Baker and Company C.P. grade was used. At 0.1 molal in water, the freezing point lowering (0.54°) was equivalent to about 2.9 moles of particles per formula weight.

"Nalcite" MX resin (National Aluminate Corp.), reported to be a condensation product of formaldehyde with o-, m- and p-phenolsulfonic acids, was used. On a dry basis, this resin contained 0.77% N and 65% was between 35 and 14 mesh.

The laboratory supply of distilled water, which contained 0.00065% SiO_2 and 0.00026% Na_2O was used. Concentrated sulfuric acid (C.P. Reagent, Grasselli) was diluted without purification for use as the regenerant for the cation exchange columns.

Method

A. Cation Exchange.—Vertical "Pyrex" brand glass tubes (22″ high × *ca.* 1″ dia.) were packed lightly with 140 g.

"Nalcite" MX, the bottom of the tube being fitted with a fine mesh screen over the outlet tube, which projected into a receiving flask. The top of the column was fitted with a separatory funnel to contain the influent solution, which was drawn through the column at the rate of 1–2 liters per hour by reducing the pressure in the receiving vessel, which was a vacuum filtering flask. The following procedure was adhered to throughout: (a) The column was back-washed with 2 liters of H_2O, (b) down-washed with 930 cc. of 2% (by weight) H_2SO_4, (c) down-washed with 2 liters of H_2O. The resin was then let stand covered with H_2O until used. (d) Diluted sodium silicate solution or other influent containing less base than the "break-through" quantity, equivalent to 6.7 g. Na_2O, was passed each time, displacing the water covering the resin into the receiving vessel.

Commonly used effluents were prepared from the following influent compositions: for standard silicic acid effluent—50.6 cc. Grasselli 20-WW silicate + 930 cc. H_2O, for standard metasilicic acid effluent—28.4 g. $Na_2SiO_3\cdot9H_2O$ + 983.8 g. H_2O.

B. pH **Determinations and Titrations.**—The Beckman Model G instrument was used with the standard glass electrode–calomel couple with temperature compensation and calibration with buffer solutions.

C. Analytical Methods.—In analyses for SiO_2, the sample was heated with concentrated HCl, filtered, ignited, weighed, then checked by volatilization as SiF_4. Sodium oxide was determined gravimetrically by precipitation with uranyl zinc acetate. In some instances, which are indicated, water was determined by titration with the Karl Fischer Reagent. Separations of alumina and silica were performed by digesting with HCl to dissolve alumina followed by filtration of silica, which was analyzed as usual.

D. Refractive Index.—A Zeiss–Pulfrich refractometer and a Bausch and Lomb dipping refractometer were used to determine the refractive indices (n) of various solutions containing silica at weight fraction (w). Stepwise dilution of an aqueous silica system (concentrated from standard silicic acid effluent by boiling off water) with successive refractive index measurements led to a value at 23° and 5460.7 ångströms of dn/dw as $w \rightarrow 0$ of 0.0722 ± 0.0015 with the Zeiss–Pulfrich and 0.070 ± 0.003 with the dipping refractometer. Since $dn/dw \rightarrow dn/dC$ in dilute aqueous solution, a value of 0.072 was used for dn/dC, where C is g. solute/cm.³ of solution in all calculations, except in one instance in which a direct measurement on a polymerizing system showed a value of 0.065. Although the choice of dn/dC within the range 0.065 to 0.072 influences the absolute values of molecular weight calculated later, there is little influence on the value of functionality calculated from the kinetic data.

E. Light Scattering and $\bar{M}_w$.—Right-angle light scattering measurements were made with a Zeiss–Pulfrich mechanical photometer equipped with a turbidity head, which was similar to the apparatus of ref. 8 with the following exceptions: (1) the collimating lens of the apparatus was close

(1) P. G. Bird, U. S. 2,244,325 (June 3, 1941).

(2) B. H. Zimm, R. S. Stein and P. Doty, *Polymer Bull.*, **1**, 90 (1945).

(3) W. D. Treadwell, *Trans. Faraday Soc.*, **31**, 297 (1935).

(4) R. W. Harman, This Journal, **30**, 359 (1926).

(5) C. B. Hurd and P. L. Merz, *J. Am. Chem. Soc.*, **68**, 61 (1946).

(6) R. C. Merrill, *J. Chem. Ed.*, **24**, 262 (1947).

(7) E. A. Hauser, This Journal, **52**, 1165 (1948).

(8) P. Doty, B. H. Zimm and H. Mark, *J. Chem. Phys.*, **12**, 44 (1944).

to the light source with only a window at the cell chamber entrance, (2) no diaphragm was used at the cell window entrance, instead (3) filters were used at this position instead of at L in the reference apparatus. Light scattering measurements were made on silicic acid solutions at SiO_2 concentrations of 2–0.05%. Each measurement was preceded by settling out or flotation (as judged by constant turbidity readings) of any large foreign particles acquired during cell filling or during dilution of the sample in the cell.

When turbidity (τ) changes with age of silicic acid solutions were followed, fresh samples were withdrawn from the stock solutions for each measurement, and, if weight average molecular weight ($\bar{M}_w$) measurements were desired, the samples were diluted appropriately in the turbidity cell.

The C/τ data were calculated from the measurements on the diluted solutions and the initial SiO_2 analysis. Then, the values of $\bar{M}_w$, B (the osmotic coefficient) and μ were calculated therefrom by the least squares method using the relations from ref. 8, $HC/\tau = 1/\bar{M}_w + 2BC/RT$ and $\mu = (0.5 - Bd^2_2M_1/RTd_1)$, where H is a function of dn/dC, M_1 = molecular weight of the solvent, d_1 = density of solvent and d_2 is the density of solute; a value of $d_2 = 2.3$ g./cm.^{3} was selected from measurements of the partial specific volume of SiO_2 in the silicic acid/H_2O systems. The symbol M_w* is used with the reported data to indicate the "apparent" $\bar{M}_w$. Many of the following uncertainties, which may result in only fair correlation of $\bar{M}_w*$ with the absolute value of $\bar{M}_w$, are later shown to be circumvented or of second order for the arguments presented: uncertainty in dn/dC for calculation of H, uncertainty in absolute measurement of turbidity, no correction for interference due to large particles[9] (dissymmetry of scattering), no correction for any possible depolarization, uncertainty of application of fluctuation theory to charged particles in a polar liquid,[10] presence of foreign light scattering particles, the polydispersity of SiO_2 phase, and changes during polymerization in nature of particles and size distributions due to stirring, catalysis, dilution, or concomitant effects, such as lowering of pH.

F. Freezing Point Lowering and $\bar{M}_n$.—The freezing points of the silicic acid solutions were determined as follows: to a one-pint Dewar flask packed in Filter-Cel and equipped with a Beckmann thermometer, inlet funnel, outlet pipet, and mechanically driven glass uplift screw stirrer through the cork was added 140 g. of shaved ice, then 200 cc. of ice-water. If the apparatus was previously near 0°, equilibrium was established within two minutes; if at room temperature, 5–10 minutes were required. After a reading of the control point, the water was removed by pipetting and was replaced with 200 cc. of the sample near 0°. The difference between the minimum temperature, which was attained within 1–10 minutes and which increased very slowly, and the minimum for water was recorded as $\Delta f.p.$ A sample, usually 50 cc., was then withdrawn for analysis to determine SiO_2 concentration. The control point in this apparatus was slightly dependent on room temperature, increasing by ca. 0.002° per 1°, increase in room temperature in the range of 20–30°.

The calculations of number average molecular weight ($\bar{M}_n$) were made from the formula

$$\bar{M}_n = 1000(1.86)W/W_0(\Delta f.p.)$$

where W/W_0 is the weight ratio of solute to solvent. The symbol $\bar{M}_n*$ is used with the data reported to indicate "apparent" $\bar{M}_n$. A value for the minimum possible $\bar{M}_n$ in a given solution was calculated by assuming all $\Delta f.p.$ due to SiO_2 in the sample. A maximum possible value of $\bar{M}_n$ was calculated in some cases by assuming all change in $\Delta f.p.$ with time as due to polymerization of silicic acid.

G. Gelation.—The incidence of non-pourability of a sample in a bottle about two square inches in cross-section was taken as the gel point.

Theoretical

Polarization Kinetics.—The following derived relationships are applied to "silicic acid," assuming it to polymerize by condensation. These have been

published separately,[11] and are repeated here for convenience (cf. ref. 12)

$$\bar{M}_w = M_0 \left[\frac{1 + 2fC_0Kt}{1 + (2f - f^2)C_0Kt} \right] \quad (1)$$

$$\bar{M}_n = M_0 \left[\frac{2 + 2fC_0Kt}{2 + (2f - f^2)C_0Kt} \right] \quad (2)$$

C_0 is the initial concentration of monomer of molecular weight M_0 with f functional groups condensing bimolecularly with rate constant K, and $\bar{M}_w$ and $\bar{M}_n$ are the weight average and number average molecular weights at polymerization time t. The calculations of f and K values giving curves fitting the experimental curves of $\bar{M}_w$ vs. t can be performed by the trial and error method[11] or, as was done in this work, by selection of two points on the experimental curve, say the mid-point and the highest point, then, using these two sets of coördinates in equation 1 to eliminate K and solve for f. After f is obtained, this value is reapplied to one of the points to find K. Other points on the curve are then calculated from this set of values for f and K. These equations are restricted to those cases in which the activity of the functional groups is not affected by the size of the molecule to which they are attached, functional groups on the same molecule do not react with each other (no cyclization), and the reverse reaction and the weight loss in condensation are negligible. The equations are valid only up to gelation, which occurs only when $f > 2$. Since at gelation time, t_{gel}, $\bar{M}_w = \infty$, the denominator of (1) must then be equal to 0, whence

$$t_{gel} = - \frac{1}{CK_0(2f - f^2)} \quad (3)$$

Plots of equations 1 and 2 relating $\bar{M}_w$ and $\bar{M}_n$ with t for various values of f, letting $C_0K = 0.1$, are shown in Fig. 1.[13,14] It is also obvious from equation 3 that violations of the restrictions on equations 1 and 2 that would perturb the value of $K(2f - f^2)$ upon dilution, such as cyclization, could be detected in gelling systems without knowledge of the actual values of f or K. In this case, a plot of t_{gel} vs. $1/C_0$ would not yield a straight line, unless there are compensations among the factors present.

Results

A. Silicic Acid from Sodium Silicates. 1. Characterization of Influents.—Preliminary light scattering measurements on the standard influent (without filtration) gave a turbidity of 1.5 $\times$ 10^{-4} cm.$^{-1}$ at an age of one day, and a plot of C/τ vs. C upon dilution leads to $\bar{M}_w*$ of 34,000[15,16] which is interpreted to be the maximum possible for the silica in this solution, since other light scattering particles were probably present.

2. Properties of Effluents. a. $\bar{M}_w*$, μ, B.—Preliminary light scattering results on standard effluents led to an $\bar{M}_w*$ of 44,500 at an age of one day and, in another instance, 21,400 at an age of two days. Thus, it appeared that ion exchange

(9) J. Waser, R. M. Badger and V. Schomaker. *J. Chem. Phys.*, **14**, 43 (1946).

(10) P. Doty and R. S. Steiner, *ibid.*, **17**, 743 (1949).

(11) M. F. Bechtold, *J. Polymer Sci.*, **4**, 219 (1949).

(12) G. Oster, *J. Colloid Sci.*, **2**, 291 (1947).

(13) G. S. Hattiagandi, *ibid.*, **3**, 207 (1948).

(14) M. Prasad and K. V. D. Doss, *ibid.*, **4**, 349 (1949).

(15) P. B. Ganguly, This Journal, **30**, 706 (1926).

(16) P. Debye and R. V. Nauman, *J. Chem. Phys.*, **17**, 664 (1949).
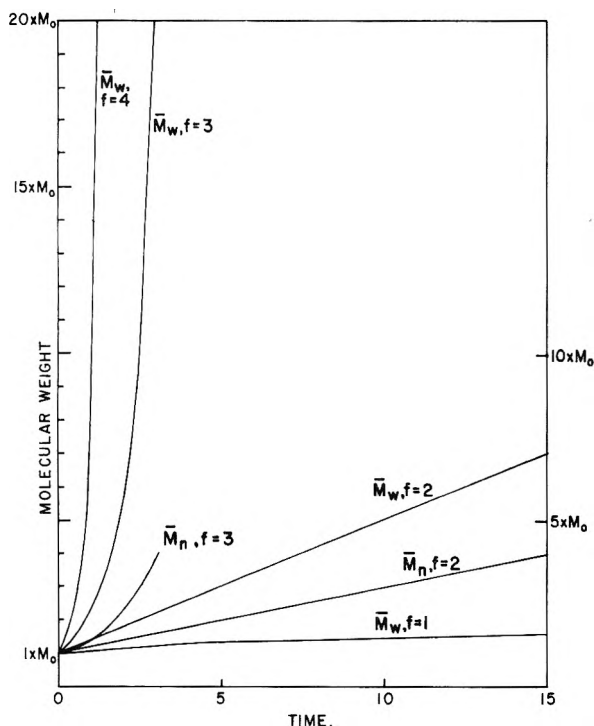
Fig. 1.—Molecular weight *vs.* time of polymerization (after equations 1 and 2, letting $C_0K = 0.1$).

was accomplished with little or no change affecting $\bar{M}_w$ in the region of 30,000. A determination of turbidity *vs.* time is shown in Fig. 2 for one effluent up to 30 days and for a low sodium effluent up to 21 days, at which time gelation was incipient. For the less turbid effluent, gelation was incipient at 14.5 days and, at complete gelation (24 days), an inflection point in the curve was found.
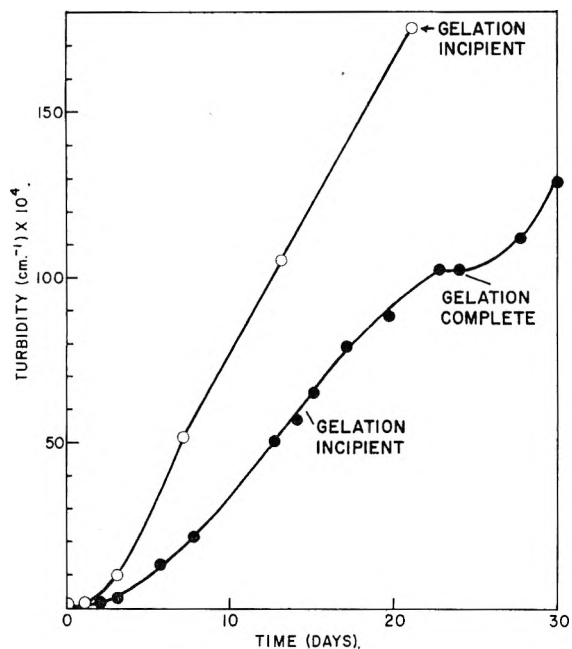
Fig. 2.—Turbidity in aqueous silicic acid *vs.* polymerization time at room temperature: ●, 1.83% SiO₂; ○, 1.78% SiO₂, SiO₂/Na₂O = 4450, pH *ca.* 4.5.

In order to determine the course of $\bar{M}_{w^*}$ with time at room temperature, samples removed from

the more turbid effluent in Fig. 2 were diluted with results shown in Figs. 3 and 4. The upward curvature of the line relating C/τ *vs.* C for high values of C in the two oldest solutions may be due to breakdown upon dilution with stirring of very large crosslinked molecules, which increases their scattering power due to decrease in interference. It might also be related to the polydispersity. Calculation from the data of the points of Figs. 3 and 4 led to
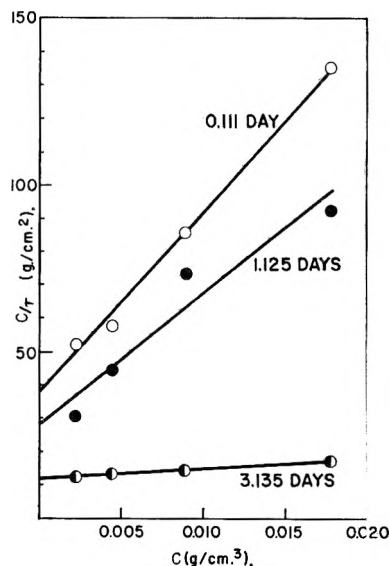
Fig. 3.—C/τ *vs.* C in progressive dilutions of samples of 1.78% silicic acid withdrawn at various polymerization times.
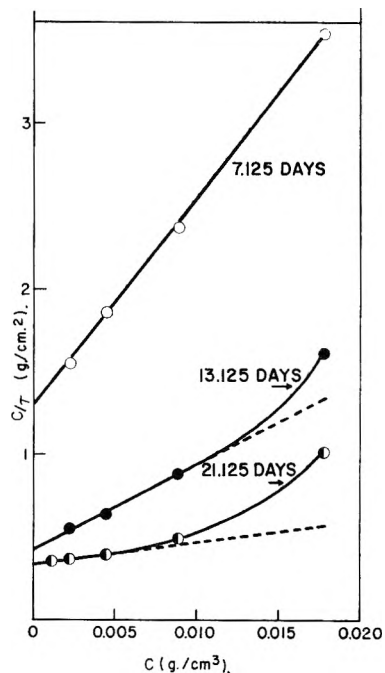
Fig. 4.—C/τ *vs.* C in progressive dilutions of samples of 1.78% silicic acid withdrawn at various polymerization times.

the $\bar{M}_{w^*}$ values plotted in Fig. 5. The decreasing slope (dotted line) past 10 days is probably due to interference, since $\bar{M}_w$ is actually equal to ∞ (gelation) at less than about 21 days. The dashed line

is drawn to show the more probable course of $\bar{M}_w$ vs. t. To determine it carefully an appropriate correction could be made for interference in light scattered from the large molecules present.
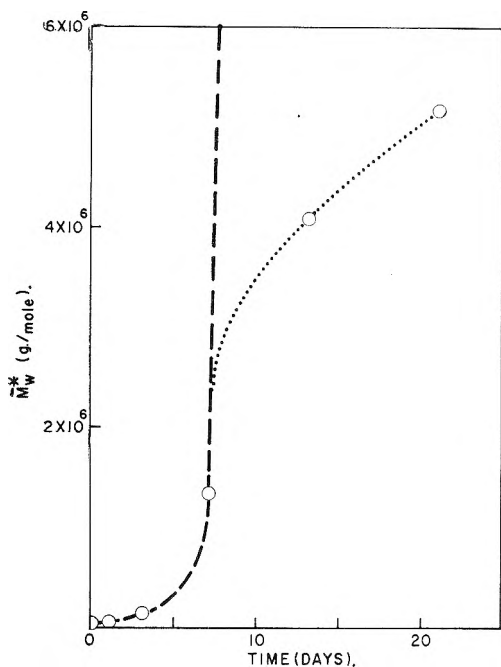
Fig. 5.—$\bar{M}_w{}^*$ vs. polymerization time calculated from data of Figs. 3 and 4: O, calculated values; - - - - -, probable course, if corrected for interference.

In addition to the simple assumption (i) obtained by extrapolation in Fig. 5 that M_0 of the SiO_2 species is about 47,100 two other general assumptions, both of which are later shown to be more rational, are possible: namely, (ii) all initial solute turbidity in excess of that for an aqueous solution of the siliceous species of degree of polymerization one is due to foreign particles, or, (iii), this excess turbidity is due to polymerization of the siliceous species prior to or during the ion exchange.

Attempts were made to analyze the data on the basis of these extreme assumptions in order to establish limits on the nature of the early stages of polymerization. Approximations within the scope of (ii) were made by subtracting the turbidity at zero time from later turbidity values. The calculated points are indicated with the best fitting curve calculated for equation 1, with appropriate values of f and K. In Fig. 6, a comparison is made with the early part of Fig. 5 in which interference does not play an important part in the results. The results show assumption (ii) to lead to much more linear reaction than assumption (i), and no interpretation of the results shows an apparent value of f of as much as 3. In Fig. 7 are shown the results of a further approximate correction of the data (for weight loss during polymerization) in which the $\bar{M}_w*$ was calculated on the basis that the average polymer unit is

$$-\!-\!-\mathrm{O}\!-\!\overset{\displaystyle \mathrm{OH}}{\underset{\displaystyle \mathrm{OH}}{\overset{|}{\underset{|}{\mathrm{Si}}}}}\!-\!-\quad(M_0 = 78)$$
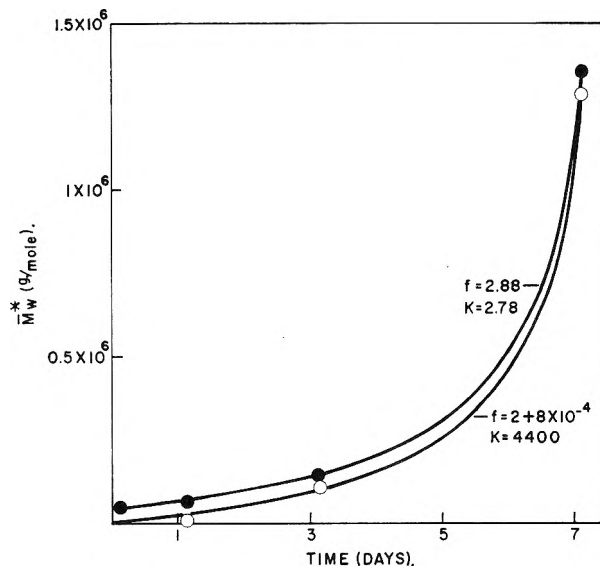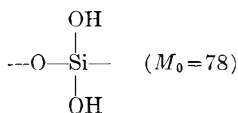
Fig. 6.—$\bar{M}_w{}^*$ vs. polymerization time calculated from assumptions (i): ●, M_0 = 47, 100, and (ii); O, M_0 = 60. Curves calculated from equation 1 using values of f and K indicated, zero weight loss and $dn/dC = 0.072$.

and a value of dn/dC actually measured on this system was used. These assumptions (iia) lead to a value of f that is again just slightly over 2. The straight line representing $f = 2$ and the curve for $f = 2.0446$, for example, both of which fit the endpoints of the data are obviously far off from the calculated experimental points, which are on the curve determined by $f = 2.00041$, $K = 6500$. An approximate correction within the scope of assumption (iii) was made by extrapolation of the data of Fig. 5 to $M_0 = 60$ and shift of the time scale. The
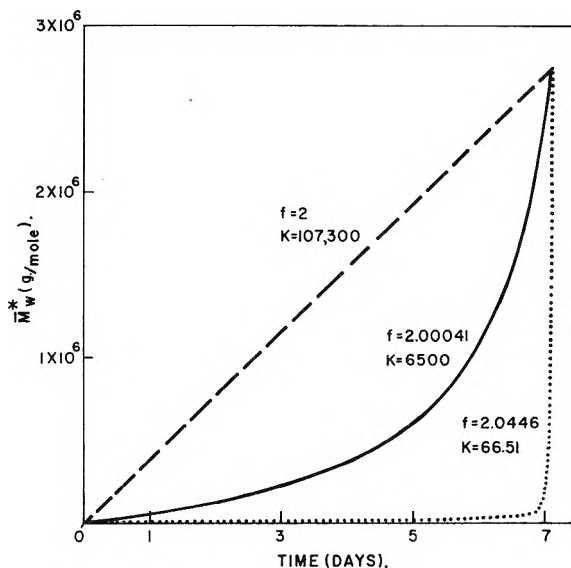
Fig. 7.—$\bar{M}_w{}^*$ vs. polymerization time calculated on the basis that the average polymer unit is

$$-\!\mathrm{O}\!-\!\overset{\displaystyle \mathrm{OH}}{\underset{\displaystyle \mathrm{OH}}{\overset{|}{\underset{|}{\mathrm{Si}}}}}\!-\!\quad(M_0 = 78)$$
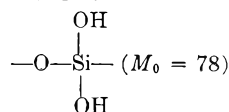
and $dn/dC = 0.065$ (for SiO_2). Curves calculated from equation 1 with values of f and K indicated. Only solid line fits all experimental points.

data are, of course, inadequate for an accurate extrapolation of this kind, but the one made, which shifts the time scale to two days prior to the observed t_0, is probably not too abrupt, since it was made by a straight line extrapolation of the last two points. Even this shift is adequate to bring down the value of f for best fit to a value less than 0.001 above that for a linear reaction, i.e., 2.
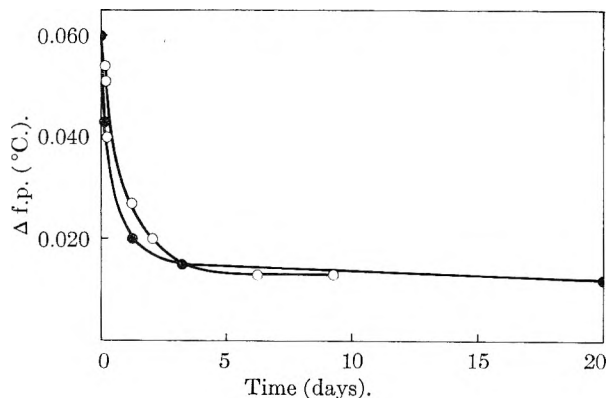
Fig. 8.—Freezing point lowering vs. polymerization time: O, 1.89% SiO_2, SiO_2/Na_2O = 760; ●, 1.845% SiO_2, SiO_2/Na_2O = 3690.

A combination of assumptions under (ii) and (iii) probably prevails over that of (i). Most importantly, all of these reduce the apparent functionality to a slight but definite value above 2, namely, 2.0004 to 2.0009, with the corresponding value of K in the range of 6500 to 3200. The values of $\bar{M}_w*$ calculated from the experimental data under various assumptions are given in Table I.

TABLE I

VALUES OF $\bar{M}_w*$ CALCULATED FROM DATA OF FIGS. 3 AND UNDER VARIOUS ASSUMPTIONS

| Time (days) | | | $\bar{M}_w*$ | |
	(i)	(ii)	(iia)	(iii)
0	(47,100)	(60)	(78)	(60)
0.111	47,800	1,140		
1.125	63,000	11,700		
2.111				47,800
3.125				63,000
3.135	147,000	110,000	240,000	
5.135				147,000
7.125	1,356,000	1,290,000	2,758,000	
9.125				1,356,000
13.125	4,093,000	4,080,000		
21.125	5,174,000			

The values of B and μ calculated from light scattering data under the various assumptions are shown in Table II.

These values of μ are in the range of 0.40 or less for $\bar{M}_w*$ values of about 100,000 or less, which is characteristic of linear polymers dissolved in good solvents. This supports the contention that the polymer is nearly linear, i.e., not highly cross-linked. The tendency of μ to approach 0.50 asymptotically at high values of $\bar{M}_w*$ indicates approach of substantial insolubility. This behavior is expected at very high molecular weights for spherical polymer molecules.

In the event the polymerization has occurred in the presence of unknown positive or negative cata-

lysts of constant total activity, the relative positions of the curves would be shifted from that of the uncatalyzed reaction. However, the value of K would be altered to accommodate this possibility, and it is not expected that the general shape or the value of f for best fit would be appreciably changed. If the upturn from an initial straight line of the curves of $\bar{M}_w*$ vs. t is caused by an increasing amount of positive catalyst (such as increasing concentration of OH^-) or by a decreasing amount of negative catalyst during polymerization, the actual value of f is, of course, nearer to 2 than to the apparent values.

The values of f, K, t_{gel} and $\bar{M}_n*_{gel}$ calculated from light scattering data are shown in Table III along with the assumed value of M_0 used.

b. $\bar{M}_n*$.—Figure 8 shows Δf.p. for typical standard effluents vs. time. The f.p. lowering decreases to about 20% of its initial value within 5 days and changes little thereafter. This behavior can be explained by assuming that the silicic acid polymerizes and that, within a short time, the residual change in $\bar{M}_n$ involves such large values of $\bar{M}_n$ that no further change in f.p. is observable by the method used. The residual Δf.p. at advanced age amounts to about 0.012°, which must be assumed to be the sum of the Δf.p. due to all silicic acids present plus the Δf.p. due to foreign particles and any systematic error. This residual Δf.p. is about 10 times that expected from the concentrations of foreign particles (H^+, Na^+, OH^-, $SO_4^=$, etc.) known to be present plus a reasonable allowance for systematic error. In view of this and conditions discussed later, an appreciable back reaction (hydrolysis) is suspected.

If the extreme assumptions are made that: (iv) all residual Δf.p. is due to siliceous materials or (v) all residual Δf.p. is due to foreign materials plus systematic error, the results shown in Table IV are obtained by calculating $\bar{M}_n*$ from Δf.p. values from the smoothed curves of Fig. 8 (up to $\bar{M}_n*$ of 10,000) and, for f and K, fitting them to equation 2. This assumes, of course, that all restrictions of equation 2 apply. The time scale was shifted by extrapolation to M_0 = 60 for t = 0. This gave a t_0 of 0.2–0.5 day prior to the apparent preparation time.

It was also shown that use of an M_0 of 78 to correspond more nearly to a linear reaction or the use of M_0 as 60 or 600 without shift in the time scale does not change appreciably the general trend of the results. Assumptions (iv) and (v) both lead to values of 11 ± 2 for the number average degree of polymerization of silicic acid in the freshly prepared effluents and (v) leads to a value of f slightly over 2 and to a reasonable gel time of 26 days for the 1.89% solutions. Assumption (iv) is absurd, if all restrictions on equation (2) prevail, because the effluent did gel (30–36 days) and this requires the actual $\bar{M}_n$ vs. t curve to be concave upwards. This situation, considered with the large residual Δf.p. observed, supports the contention of appreciable hydrolysis of the polysilicic acid.

Assumption (iv) is also of interest because it permits calculation of a minimum value of $\bar{M}_n*$ at advanced polymerization time, which for the data

TABLE II
VALUES OF B AND μ CALCULATED FROM DATA OF FIGS. 3 AND 4 UNDER VARIOUS ASSUMPTIONS

Time (days)	$B\left(\dfrac{\text{erg} \times \text{g.}^2}{\text{cm.}^2}\right) \times 10^{-7}$ (i)	(ii)	(iia)	(iii)	μ (i)	(ii)	(iia)	(iii)
0		53			-1.570			
0.111	3.85	7.5			0.350	0.210		
1.125	2.68	0.13			0.395	0.4950		
2.111				3.85				0.350
3.125				2.68				0.395
3.135	0.199	0.081	0.0545		0.4922	0.4968	0.4979	
5.135				0.199				0.4922
7.125	0.0824	0.036	0.0191		0.4968	0.4986	0.4993	
9.125				0.0824				0.4968
13.125	0.0350				0.4986			
21.125	0.00845				0.4997			

TABLE III
VALUES OF f, K, t_{gel} AND $\bar{M}_{\text{n*gel}}$ CALCULATED UNDER VARIOUS ASSUMPTIONS

	(i)	(ii)	(iia)	(iii)
M_0 used	47,100	60	78	60
f	2.88	$2 + 8 \times 10^{-4}$	$2 + 4.1 \times 10^{-4}$	$2 + 8.8 \times 10^{-4}$
$K\left(\dfrac{\text{cm.}^3}{\text{g.} \times \text{days}}\right)$	2.78	4400	6500	3206
t_{gel}	7.97	8.0	8.11	9.94
$\bar{M}_{\text{n*gel}}$	201,300	150,100	380,600	136,500

TABLE IV
ESTIMATES OF f, K AND $\bar{M}_{\text{n*}}$ FROM Δf.p.

Assumptions Effluents	$\bar{M}_{\text{n*}}$ vs. t (iv)	(v)	Initial $\bar{M}_{\text{n*}}$ (iv)	(v)	K (iv)	(v)
1.89% SiO_2	concave	concave	550	650	1.997,	2.022,
1.845% SiO_2	downward	upward	550	750	98.9	45.2

of Fig. 8 is about 2700. Since, from equations 1, 2 and 3, $\bar{M}_{\text{ngel}} = M_0[(2 - 2f)/(2 - f)]$, a maximum value of f can be calculated as follows: $(2 - 2f)/(2 - f) > 2700/60$, whence $f < 2.047$. A minimum value of f cannot be calculated from the present data in this manner but, since gelation occurs, it must be over 2. Consequently the values of 2.0008 and 2.00041 obtained by various assumptions in the independent study of $\bar{M}_{\text{w}}{}^{*}$ seem more plausible than the value of 2.88 attained by the extreme assumption of $M_0 = 47,100$.

It is of interest to calculate by equation 2 the course of $\bar{M}_{\text{n*}}$ vs. t using values of f and K obtained under the study of $\bar{M}_{\text{w*}}$. The results show much steeper rise in $\bar{M}_{\text{n*}}$ with time than is found under assumption (v). This emphasizes the need for greater precision in Δf.p., and determination of the exact contribution of siliceous and foreign materials to residual Δf.p.

c. **Gelation.**—A closer examination was made of the phenomena of gelation of silicic acid effluents in light of equations 1, 2 and especially 3. In general, the freshly prepared effluents were adjusted in pH or in polymerization catalyst content, divided into fractions, which were diluted as desired, and then gelation time was observed. Some of the results are summarized in Figs. 9 and 10. These show gel times of a few minutes to more than three months. Freezing points determined on some of the solution showed corresponding abrupt and slow changes. There is no exception to the upward curvature of all plots of t_{gel} vs. $1/C$. Straight line plots passing through the origin and t_{gel} for the most con-

centrated solution are expected, provided the restrictions on equations 1, 2 and 3 prevail and the polymerization environment is constant for all dilutions. The use of materials found to be polymerization catalysts, such as Cu^{++} and F^{-} and buffers, did not alter the upward curvature obtained. One possible explanation of this result is that cyclization is occurring and constitutes a greater percentage of the condensation in dilute solution, thus giving an apparent functionality closer to 2 than the real value of f. Another explanation would be that polymerization is essentially linear ($f = 2$) and either an impurity or a small fraction of any remaining functional groups is responsible for the crosslinking reaction leading to gelation.

An experiment showing no net change of pH during polymerization in the presence of $CuCl_2$ is shown in Fig. 10. However, the most dilute solution had a pH lower by 0.31 than the concentrated solution. Better pH control was obtained with an effluent buffered with acetic acid/sodium acetate (Fig. 10), in which the pH ranged from 5.10 to 5.17 and did not change perceptibly during polymerization. The dashed line shows the theoretical course of t_{gel}, if restrictions on equation 3 had prevailed.

Further experiments on fast-gelling, buffered solutions were made for a more direct correlation of observed gel times and gel times calculated from equations 1 and 3. The error caused by the time interval between dilution of a sample from the stock solution and the measurement of its turbidity was minimized and in addition the usual practice
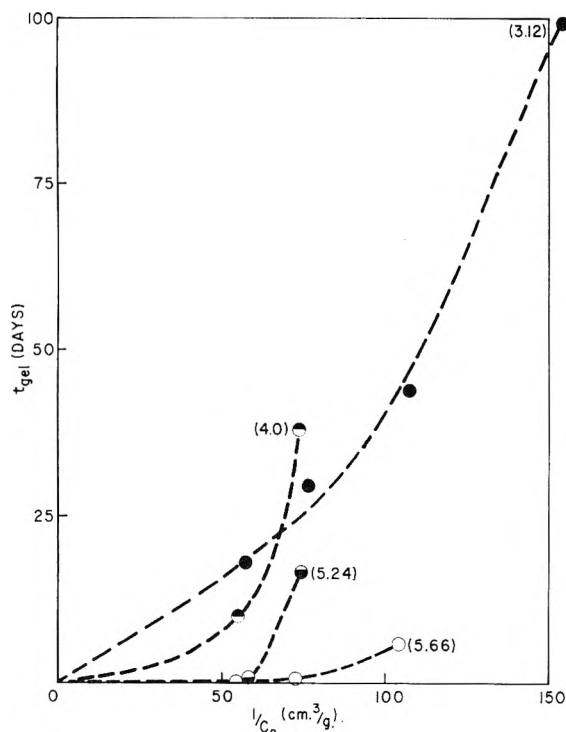
Fig. 9.—Gel time *vs.* $1/C_0$ for various silicic acid solutions (initial *p*H in paren.): ●, 1.74% SiO_2, 0.0105% Cu^{++} (*ex* $CuCl_2$); ◓, 1.79% SiO_2, adjusted to *p*H 5.12 with sodium silicate; ◕, 1.80% SiO_2; ○, 1.83% SiO_2, 0.0057% F^- (*ex* NaF).
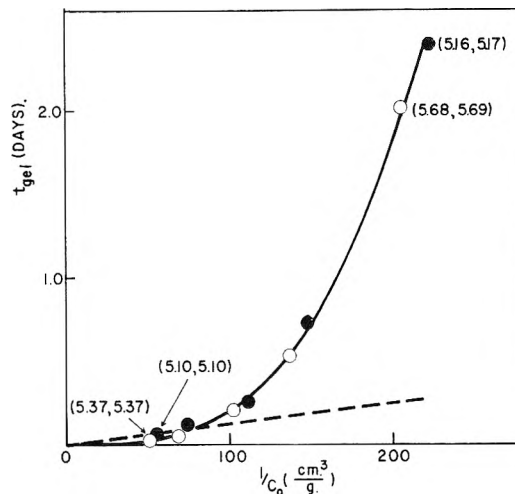

Fig. 10.—Gel time *vs.* $1/C_0$ for buffered and catalyzed silicic acid solutions (initial, final *p*H in paren.): ●, 1.80% SiO_2, acetic aid/sodium acetate buffer; ○, 1.95% SiO_2, 0.051% $CuCl_2·2H_2O$.

was followed of allowing coarse particles and bubbles in the turbidity cell to settle out or float off. Changes of turbidity due to this cause in some solutions resulted in a very slight initial decrease in turbidity with time, followed by a steady rise in turbidity due to the progress of polymerization in the solution. The turbidity of the sample at the instant of dilution was estimated by extrapolation of the turbidity *vs.* time curve (the part just after settling and flotation effects have ceased). Values of f, K and t_{gel} were calculated from the $\bar{M}_w*$ *vs.* t curves obtained. The results obtained in this manner with four solutions are summarized in Table V.

TABLE V

POLYMERIZATION AND GELATION IN FAST-GELLING, BUFFERED SILICIC ACID SOLUTIONS

Stock soln., % SiO_2	1.88	1.88	1.88	1.76
*p*H (initial)	3.60	3.60	3.60	3.35
Vol., l.	0.6	0.6	0.6	1
1 *M* NaOAc, cc.	5.4	12.6	16.2	21
1 *M* HOAc, cc.	12.6	5.4	1.8	9
*p*H	4.32	4.93	5.50	5.01
$(f - 2) \times 10^5$	23.5	0.9	...	4
$K \times 10^{-6}$	0.525	49.4	...	0.594
t_{gel} (calcd.)	0.225 d.	0.0625 d.	...	0.117 d.
t_{gel} (obsd.)	>0.33, <0.96 d.	0.135 d.	0.042 d.	0.194 d.

These results show that f is consistently greater than 2 by a very small amount and that the calculated values of t_{gel} are again about 0.5 of the observed values.

d. Titration: *p*H *vs.* Age and Gelation Time.—The titration and gelation characteristics of silicic acid effluents as a function of time were explored by additions of various amounts of strong acids and bases to several samples of the same effluent. The *p*H of each sample was taken immediately and then at advanced age. Meanwhile, its gel time was observed. The titrations performed in this way (Fig. 11 is typical) show that there is an inflection or equivalence point in the titration curve at an average *p*H = 4.65 (initial) to about 5.30 (at advanced age), that the solutions increase in *p*H with age without appreciable shift in the amount of base or acid required for titration to the inflection point, that the inflection point *p*H is independent of initial *p*H of the effluent and the nature of the base or acid added, and that the general increase in *p*H in the polymerizing solutions is greater at *p*H's higher than the equivalence point. Observations of gel time show an optimum (fastest) at an average *p*H of about 5.05 (initial) to about 5.85 at advanced age (Figs. 12, 13). Thus, the *p*H of the equivalence is about 0.5 unit lower than the optimum *p*H for rapid polymerization. To explain the sharpness of the inflection point, it seems necessary to assume that the titrations are those of a very small amount of strong acid, which might be a silicic acid species or an impurity, such as an aluminosilicic acid. The disappearance of H^+ during polymerization also appears independent of that titrated by addition of base. Estimate of the change in concentration of hydrogen ion during polymerization from the divergence of *p*H values of fresh and aged samples of effluents in the range of *p*H 3 to 4.5 lead to a value of 4×10^{-4} mole H^+/mole SiO_2, which is close to the maximum value of functionality in excess of 2 calculated from the preferred assumptions in the light scattering experiments. The existence of the inflection point and increased *p*H with age was verified by more ortho-
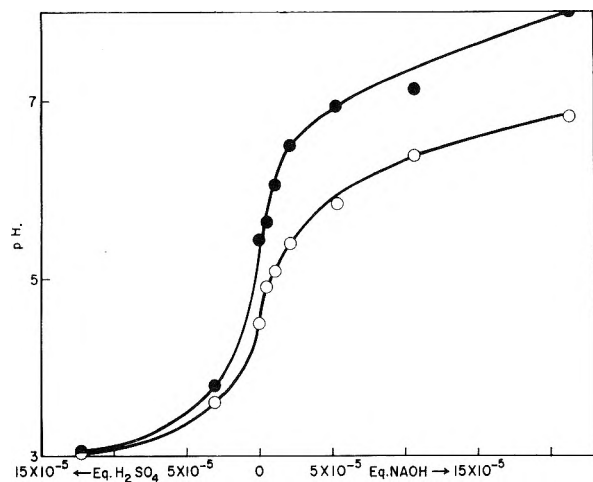
Fig. 11.—pH vs. equivalents of acid or base added to silicic acid solution; 1.80% SiO_2, SiO_2/Na_2O = 340: ○, initial pH; ●, pH after 15 days.

dox titrations in which successive additions of base were made to samples of effluent aged to various times before the start of the titrations.

Visual observations indicated that the turbidity of the effluents at gelation increases consistently with decreasing pH through the optimum pH for rapid polymerization at least down to pH values below 3. Different molecular distributions may be present even in effluents symmetrical in gel time to the optimum pH, although differences in polymer–solvent interaction could account for the turbidity difference.

e. Reactions.—A wide variety of materials including both polymers and non-polymers, organic and inorganic substances were added to the standard silicic acid effluent to alter the course of the polymerization of silicic acid by temporary or permanent reduction of the functionality or to accomplish fractionation of the siliceous molecules. After discounting the effect of pH on gelation rate, no cases of inhibition of the polymerization were observed. However, marked positive catalysis[17] was obtained by contact with metallic copper and a number of salts of bivalent metal ions (Mg^{++}, Ca^{++}, Cu^{++}, Fe^{++} and Hg^{++}), in addition to rapid gelation with NaF.

Approximately forty non-polymeric organic compounds such as alcohols, ketones, acids and amines, representing a wide range of types and functional groups were without significant effect on gel time other than that due to pH changes or on the gross physical properties of siliceous residue obtained by drying the modified effluents.

With regard to organic polymers, the combination of silicic acid effluent with polyvinyl alcohol (PVA) and with methylcellulose was examined briefly. A solution of silicic acid (1.8% SiO_2, pH 2.87) whose titration curve inflected sharply at pH 4.5 and a solution of PVA (90% hydrolyzed PVAc, 1.7%, pH 5.04) whose titration curve inflected slightly at 7 were mixed in equal volumes. The resultant solution (pH 4.28) showed no inflection in titration between 2.48 and 7.13 pH. Other mixtures of these solutions ranging from 9/1 to 1/9 by volume (pH

(17) J. F. Hazel, THIS JOURNAL, **51**, 415 (1947).
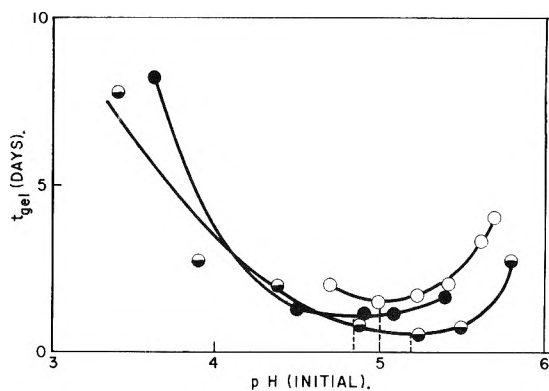
Fig. 12.—Gel time vs. *initial* pH for various silicic acid solutions: ○, 1.81% SiO_2, SiO_2/Na_2O = 518, adjusted with sodium silicate; ◑, 1.88% SiO_2, SiO_2/Na_2O = 134, adjusted with NaOH; ●, solution of Fig. 11.
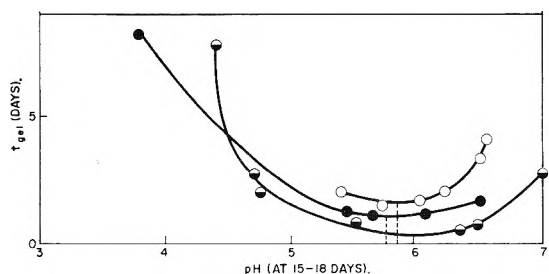
Fig. 13.—Gel time vs. pH at 15–18 days for silicic acid solutions of Fig. 12.

from 3.07 to 4.69) were examined periodically up to 16 hours. The formation of a heavy precipitate and an opaque solution (a maximum at 1/1) was apparently the result of a slow reaction or association. A similar experiment was conducted in which the silica and PVA solutions were adjusted to the same pH (4 88–4.93) before mixing; all mixed solutions after reaction were in the pH range of 4.88 to 4.92. Flakes obtained by drying the mixed solutions (1/1) at 60° were clear and insoluble in cold water compared to the partly clear, water-dispersible flakes obtained from PVA + boiled-off effluent.[1] A water-soluble film was obtained from PVA + sodium silicate under similar conditions. It appears that the silicic acid in dilute effluent reacted with PVA in water solution. The semi-gelatinous nature of the precipitate formed, as well as the fact that the reaction is not rapid, discouraged its use in fractionation of polysilicic acids.

Experiments similar to those with PVA using a methylcellulose solution (analyzing 1% total carbon) and the same silicic acid solution resulted in a more rapid precipitation reaction accompanied by a normal (for silicic acid) increase in pH during polymerization of the mixed solutions (4.67 to 5.42–5.86). The precipitate from solutions mixed at a volume ratio of 1 was insoluble in hot water, or hot 0.35 N H_2SO_4, but soluble in 0.5 N NaOH at room temperature. A similar preparation at pH 4.04 gave an immediate apparent high opacity which was measured at several dilutions and was found to correspond to a $\bar{M}_{w^*}$ of about 100,000,000. A 200-g. sample of this solution (0.87% SiO_2, 0.51% C) was centrifuged and separated into three phases: 184 g. of hazy supernatant liquid (0.0832% SiO_2, 0.26% C), 6 g. of hazy fluid gel, and

7 g. of opaque firm gel, which, after drying at 170° contained 55.56% SiO_2, 17.63% C and 3.63% H. These dry lumps were tough, were softened by hot water or hot 0.5 N NaOH, but not by hot H_2SO_4 (0.35 N). The nature of silica–methylcellulose precipitates changed with the age of the silicic acid effluent used; standard effluent mixed when first prepared in equal volume with the methylcellulose solution gave a high turbidity suspension, at intermediate age a powdery precipitate formed, but when aged, gelatinous precipitates, and, finally, only gels were obtained. Metasilicic acid effluent also gave a silica–methylcellulose precipitate.

f. Precipitation.—In the presence of certain other organic compounds of slightly basic nature, such as pyridine, dicyclohexylamine, α-picoline and nicotine, marked turbidity and even precipitation of refractory or gel-like silicic acid was observed.

Contrary to results in titration of silicic acid effluent with a strong base, titration with pyridine causes haziness and gelation in the neighborhood of pH 7, instead of accelerated gelling at pH 5. The addition of silicic acid to pyridine ($K_B = 1.8 \times 10^{-9}$) resulted in the immediate appearance of suspended particles. Sodium hydroxide, urea ($K_B = 1.5 \times 10^{-14}$), morpholine, and NH_4OH ($K_B = 1 \times 10^{-5}$), failed to show this effect. Quinoline ($K_B = 1 \times 10^{-9}$) and p-toluidine ($K_B = 2 \times 10^{-9}$) showed some precipitation or emulsion formation, but no filterable material was obtained. Coagulation of the pyridine/silicic acid precipitate with dilute H_2SO_4, for example, made the precipitate filterable. Experiments with compositions of the formula: x g. pyridine + (25 − x) g. H_2O + 25 g. standard effluent (% SiO_2 = ca. 1.8) + 10 g. of 0.35 N H_2SO_4 showed the amount of precipitate obtained to vary with the amount of pyridine, being optimum (0.76 g. dried at 75°) at x = 10. For x = 12.5, the weight obtained was not sensitive to the amount of coagulant between 5–15 cc. Metasilicic acid gave a precipitate readily, but no filterable precipitate was obtained from diluted silica sol that had been obtained by boiling water from polysilicic acid solutions. Other experiments showed that the amount of precipitate was also dependent on SiO_2 concentration. Powder precipitates were not obtained in systems of very high or very low silica concentra-

TABLE VI

PRECIPITATION OF SILICIC ACID WITH PYRIDINE

	Standard Effluent	Metasilicic Acid Effluent
Pyridine, cc.	200	100
Water, cc.	300	
Silicic acid effluent, cc.	500 (1.73% SiO_2)	700 (0.57% SiO_2)
pH after mixing	8.18	8.18
2% H_2SO_4, cc.	200	200
pH after mixing	5.81	6.55
Precipitate, g. (dried at 130°)	7.66	...
SiO_2, %	90.4	88.77
H, %	1.23	1.43
N, %	0.025	0.1
Loss on ignition, %	8.73	10.96

tion. Larger scale precipitations were made as shown in Table VI with corresponding analytical results.

Both precipitates were fine white powders and gave a diffuse X-ray diffraction pattern similar to that obtained from vitreous silicates. Electron micrographs showed them to be particles of circular cross-section, presumably spherical, with diameters of ca. 0.1 to 0.5 μ. The particles felt like talc when rubbed on the skin.

B. Cation Exchange of Other Siliceous Influents. 1. Sodium Silicate with Other Salts.—The combination of sodium silicate solutions with solutions of the salts of other polymerizable metal acids prior to cation exchange gave two results of interest. With some salts, particularly potassium niobate, large quantities of soluble or dispersed metal oxide were found in the effluent. Without the use of silicate, severe plugging of the column resulted. From influents containing sodium silicate and the salts of certain heavy metal acids, such as sodium molybdate, the effluents yielded crystals having the complex X-ray diffraction patterns characteristic of heteropolynuclear acids. One explanation of these results is that the silicic acid of low molecular weight generated in situ copolymerizes with and thus terminates or reduces the functionality of metal acids that otherwise polymerize directly to gelation. In support of this explanation, the substitution of a preformed silicic acid effluent for sodium silicate was not effective. With the heavy metal salts, the silicic acid may enter the structure of the anion in low molecular weight form to yield crystallizable products. Some of these experiments are given in detail in U.S. 2,503,991[18] and U.S. 2,657,183.[19]

Study of the ion exchanged mixtures of sodium silicate with sodium aluminate[20−22] indicates that a small amount of aluminum hydroxide has an important effect on the polymerization of silicic acid. Polymerization at room temperature in a 19/1 mole ratio SiO_2/Al_2O_3 solution concentrated by boiling to about 10% solids resulted in a clear sirup that remained highly viscous for one week before gelation. The sodium silicate/sodium aluminate ratio of the influent subjected to ion exchange for the preparation of these solutions is a major factor, since the influent gel time, as well as the minimum number average molecular weight and the percentage yield of $SiO_2 + Al_2O_3$ in the effluent are functions of this variable. Rapid changes in all three functions occur in the neighborhood of $4SiO_2/1Al_2O_3$.

2. Miscellaneous Silicates and Silicolate.—A number of other methods for the preparation of silicate and substituted silicate influents were examined briefly. A cation exchange effluent from a sodium methyl silicolate of average composition $(CH_3)_{1.5}Si(ONa)_{2.5}$ had an inflection pH of 6.5 in contrast to the inflection point near pH 4.5 for effluents from commercial 3.3/1 and 3.9/1 SiO_2/Na_2O and metasilicic acid. The silicolic acid ef-

(18) M. F. Bechtold, U. S. 2,503,991 (April 11, 1950).
(19) M. F. Bechtold, U. S. 2,657,183 (October 27, 1953).
(20) C. J. Plank and L. C. Drake, J. Colloid Sci., 2, 399 (1947).
(21) C. J. Plank, ibid., 2, 413 (1947).
(22) B. Chatterjee and A. Sen, Indian J. Agr. Sci., 15, 103 (1945).

fluent showed evidence of most rapid polymerization at pH 7 instead of pH 5 as for silicic acid. Mixtures of the silicolic acid effluent with silicic acid effluent gave extended steep inflection curves in the neighborhood of pH 5. Effluents from mixtures of sodium silicate with sodium carbonate gave decreasingly sharp inflection points characteristic of the titration of a weak acid as the proportion of carbonate increased. Effluents from the reaction of Si metal with $NaOCH_3$ and NaOH, and from reaction of tetraethyl orthosilicate with NaOH and KOH showed minimum degrees of polymerization in the range of 3.5–10 and titration inflection points at pH 4 to 5.

THE TEMPERATURE-INTERFACIAL TENSION STUDIES OF SOME HALOGENATED BENZENES AGAINST WATER

By Joseph J. Jasper and T. Donald Wood

Department of Chemistry, Wayne University, Detroit, Michigan

This paper involves the interfacial tension measurements of monochlorobenzene, monobromobenzene and monoiodobenzene against water at four temperatures over a range of 20 to 80°. The method of least squares was applied to formulate equations relating the interfacial tensions to the temperature. The equations were used to calculate the entropy, latent heat and enthalpy of formation per cm.² of interface. The results are presented in tables.

One important source of data for evaluating certain extensive properties of the transition region between two contiguous liquid phases is furnished by interfacial tension measurements. These data become all the more important if obtained over a temperature range, since most of the properties are functions of the temperature. The interfacial tension is a complex phenomenon whose magnitude is the resultant of and determined by the same forces which make the interface possible. These forces are obviously related to the molecular properties of the liquids, and if their exact nature and contribution could be established, it should be possible to evaluate the interfacial tension in terms of the molecular properties. One logical procedure is to determine how substituted groups in a given homologous series affect the interfacial tension against some arbitrarily chosen standard liquid such as water.

The purpose of this investigation was to obtain interfacial tension data for a series of monohalogenated benzenes against water over an appreciable temperature range. With these data, it was possible to evaluate the thermodynamic properties of the interfacial region and to determine how they vary with the temperature. The initial plan involved the four monohalogenated benzenes, but due to the very small density differential between the two mutually saturated liquid phases, it was found impossible to make accurate measurements on the fluorobenzene–water system.

Experimental

Purification of the Compounds.—The compounds used in this investigation were monochlorobenzene, monobromobenzene and monoiodobenzene. The best grades of Eastman Kodak Company compounds were used and each of these was further purified by vacuum fractionation. This was accomplished with the use of a 15-inch column packed with single-turn glass helices and equipped with a total reflux variable take-off head. The fractionation was carried out twice, each at a different pressure. In each case the middle third was collected for the next stage of the procedure, the final of which was the density and interfacial ten-sion measurements. The refractive indexes of the purified compounds agreed with the values given in the International Critical Tables to the fourth decimal.

Determination of the Densities.—It was important that the densities of the mutually saturated liquids be determined accurately since they appear in the interfacial tension equation as explicit variables. The densities were measured simultaneously with the corresponding interfacial tensions, with the use of a modified form of the "type D" pycnometer described by Bauer.[1] Three pycnometers, each having a volume of about 20 ml., were constructed as nearly alike as possible in dimensions and shape. These were calibrated and two reserved for the respective liquids. The third was used as a counterpoise. The halogenated benzenes and water were mutually saturated by vigorously shaking quantities of each together and then allowing the two phases to remain in contact at least 24 hours before use. The liquids were introduced into the pycnometers by means of a 30-ml., glass hypodermic syringe equipped with a 12-cm., 20-gage, stainless steel needle which could be inserted into the capillary neck of the pycnometers for their entire length. A constant volume of liquid was maintained in the pycnometers with the aid of the syringe during the temperature variation of the experiments. The densities of the two saturated liquids are shown in Table I and represent the average of not less than three independent determinations.

TABLE I

THE DENSITIES OF THE MUTUALLY SATURATED LIQUID COMPOUNDS

Compound	Temp., °C.	Density, g./ml. Water phase	Density, g./ml. Organic phase
Chlorobenzene	20.01	0.9983	1.1111
	40.20	.9922	1.0892
	59.59	.9838	1.0688
	80.02	.9727	1.0460
Bromobenzene	20.01	.9983	1.5027
	40.20	.9924	1.4750
	59.59	.9839	1.4484
	80.02	.9728	1.4201
Iodobenzene	20.01	.9983	1.8316
	40.20	.9926	1.8009
	59.59	.9842	1.7711
	80.02	.9730	1.7399

(1) N. Bauer in "Physical Methods of Organic Chemistry," Vol. 1, Interscience Publishers, Inc., New York, N. Y., 1945, p. 79.

To maintain a constant temperature during the various measurements, a specially designed glass-wool insulated water-bath was used, which was equipped with heat resistant (herculite) plate glass windows and covered with thick fiber board. Four thermoregulators were used at respective instrument settings of 20, 40, 60 and 80°. These were used interchangeably, which greatly facilitated the rechecking of data at precisely the same temperatures previously used. The stirring system was sufficiently efficient, and the thermoregulators sensitive enough, to maintain a temperature constant to 0.002° in the range 20–40° and to 0.004° up to 80°. The actual temperatures were read from NBS certified thermometers with two-degree ranges and 0.01° divisions. To maintain temperatures below ambient (about 20°) a Frigidaire refrigeration unit was used to cool a buffer bath to 10°. The cooling liquid was circulated through a coil in the main bath at such a rate that moderate additions of heat were required to maintain the set temperature.

Determination of the Interfacial Tensions.—A modification of the drop-weight apparatus of Harkins and Brown[2] was used for measuring the interfacial tensions. The method involved drop volumes instead of drop weights because of the greater experimental difficulties associated with the latter. The apparatus assembly consisted of a glass helical spring constructed of 4-mm. Pyrex tubing and this connected a calibrated measuring pipet to a flat-ground tip upon which the drops formed. The spring consisted of 7 coils 30 cm. in diameter and had a maximum uncoiling range of about 12 cm. The liquids were forced to flow from the measuring pipet through the spring, and thence to the tip by increasing the hydrostatic head. The latter was accomplished by uncoiling the spring with the aid of a screw device which actuated the spring-pipet part of the system in a vertical direction. In this way the rate of drop formation could be made extremely slow, a condition requisite for the state of virtual static equilibrium required in the final stage just before the drop becomes detached. A series of interchangeable tips and measuring pipets permitted the measurement of a wide variety of liquids representing a considerable range of densities.

Preliminary tests indicated that the aqueous phase spread much more readily on the flat surface of the tip than the organic phase. Consequently the aqueous phase was chosen as the liquid from which to form the drops. It was necessary, therefore, to arrange the tip so that the drops formed vertically upward, subsequently becoming detached and passing upward through the more dense organic phase. The pipet and tip chosen for each system depended upon the density of the organic liquid. For the bromobenzene and iodobenzene phases, the pipet and tip selected delivered 140 to 200 drops, and for the chlorobenzene, 30 to 40 drops. Twenty-four hours were required to make the measurements of each compound over the whole temperature range, and these were repeated four times.

Results and Discussion

The equation used for calculating the interfacial tensions of the organic–water systems[3] is

$$\gamma_i = vg(d_0 - d_w)/2\pi rF$$

where γ_i is the interfacial tension in ergs per cm.^{2}, v the drop volume in ml., d_0 the density of the organic phase, d_w the density of the aqueous phase, g the gravitation factor, r the radius of the tip in cm., and $F = \psi(r/V^{1/3})$ the Harkins and Brown[2] correction factor.

The thermodynamic equation of Clapeyron can be applied to liquid interfaces when written in the two-dimensional form

(2) W. D. Harkins and F. E. Brown, J. Am. Chem. Soc., **41**, 499 (1919).

(3) W. D. Harkins and Y. C. Cheng, ibid., **43**, 35 (1921).

$$-\frac{d\gamma}{dT}\mathbf{i} = \frac{l}{T} = s$$

This enables the calculation of the magnitude of the entropy of the surface s, the latent heat of the surface l, and the enthalpy h, each for unit area of the interface under isobaric and isothermal conditions. These, together with the interfacial tension values, are tabulated in Table II. Empirical equations expressing the interfacial tension as a function of the temperature were formulated by the method of least squares.

TABLE II

INTERFACIAL TENSIONS[a] AND VALUES OF SOME THERMODYNAMIC PROPERTIES OF THE INTERFACE

Compound	Temp., °C.	γ_i	$-(d\gamma_i/dt)$	l	h
Chlorobenzene	20	38.10 ± 0.20	0.03005	0.601	38.70
	40	37.22 ± .30	.05743	2.297	39.52
	60	35.80 ± .26	.08482	5.089	40.89
	80	33.83 ± .25	.11220	8.976	42.81
Bromobenzene	20	39.30 ± .10	.05898	1.180	40.48
	40	37.96 ± .12	.07487	2.995	40.96
	60	36.30 ± .08	.09077	5.446	41.75
	80	34.33 ± .08	.10666	8.533	42.86
Iodobenzene	20	41.51 ± .06	.06243	1.249	42.76
	40	40.11 ± .36	.07726	3.090	43.15
	60	38.42 ± .11	.09208	5.525	43.95
	80	36.42 ± .06	.10691	8.553	44.97

[a] Calculated.

Chlorobenzene:
$$\gamma_i = 38.42 - 2.665 \times 10^{-3}t - 6.846 \times 10^{-4}t^2$$

Bromobenzene:
$$\gamma_i = 40.32 - 4.309 \times 10^{-2}t - 3.973 \times 10^{-4}t^2$$

Iodobenzene:
$$\gamma_i = 42.61 - 4.761 \times 10^{-2}t - 3.706 \times 10^{-4}t^2$$

The form of these equations indicates that the decrease of the interfacial tension with increasing temperature is not linear but gives curves which are concave to the temperature axis. This undoubtedly results from the increasing mutual solubility of the two liquids as the temperature increases. Regardless of the increasing mutual solubility an interfacial region is maintained which possesses extensive properties unique to it alone. Table II shows that the latent heat of the interface increases with the temperature, just as it does in the case of pure liquid surfaces. The enthalpy and entropy, however, also increase, a fact contrary to the behavior of pure liquid surfaces, for which these properties are practically independent of the temperature. The empirical equations indicate that the interfacial tension decreases more rapidly than the temperature increases. Two factors are involved, namely, the influence of (a) the kinetic energy of the molecules, and (b) increasing similarity of the contiguous phases. Since the enthalpy increases, the latent heat obviously increases much too rapidly and probably approaches a value which is determined by the nature of the solution ultimately obtained when the components become completely miscible.

THE ADSORPTION OF GASES ON A GERMANIUM SURFACE

By J. T. Law

Bell Telephone Laboratories, Murray Hill, N. J.

The adsorption of hydrogen, nitrogen, carbon monoxide and carbon dioxide on a germanium surface has been studied as a function of temperature. Various methods used for cleaning the surface are discussed. The results indicate that for all the gases studied, except hydrogen, the adsorption is purely physical and might be expected to have but little effect on the electrical properties of the semiconductor.

1. Introduction

Following the work of Brattain and Bardeen[1] on the effect of various gases and vapors on the electrical properties of germanium, it was decided to carry out a systematic investigation of gas adsorption on a germanium surface. For this to be of any real value, one must have a reproducible surface. Brattain and Bardeen obtained this by cycling sparked oxygen and wet nitrogen over the germanium sample, but for adsorption work this is rather unsatisfactory as a large amount of unknown material is left adsorbed on the surface. One of the main functions of the present work was, therefore, to obtain either an atomically clean surface of germanium or to approach this condition as closely as possible. As will be described later in this report, it was found that heating the sample to a temperature close to its melting point (937°) in a vacuum of 10^{-9}–10^{-10} mm. produced what was apparently a clean surface. By the term "clean" is meant a surface which is covered with much less than a monolayer of adsorbed oxygen or oxide. It should then be possible to correlate adsorption data obtained on this surface with changes in contact potential or surface recombination velocity on a similarly treated piece of germanium.

The adsorption data were obtained by means of the "flash filament technique." This has previously been used to study adsorption on tungsten[2] and consists of measuring the pressure change in the system when previously adsorbed gas is desorbed by flashing the specimen, usually in the form of a wire or filament, to a high temperature. If the pressure is measured with an ionization gage, it is essential that no decomposition of the adsorbed gas occurs on flashing as the calibration of the gage is different for different gases. All of the gases described in this report had previously been examined using the mass spectrometer as the pressure measuring device.[3] In each case, no decomposition occurred. It was impossible to study the adsorption of water and alcohol vapors in this way as they decompose when the germanium is heated above 250°. The adsorption of hydrogen, nitrogen, carbon monoxide and carbon dioxide at 77°K. (except carbon dioxide), 195 and 300°K. has been measured. From the isotherms, heats of adsorption may be calculated, although the temperature interval between isotherms is rather large.

(1) W. H. Brattain and J. Bardeen, *Bell System Tech. J.*, **32**, 1 (1953).

(2) J. P. Molnar and C. D. Hartman, M.I.T., Physical Electronics Conference, April 1, 1950; J. A. Becker and C. D. Hartman, This Journal, **57**, 153 (1953).

(3) J. T. Law and E. E. François, *Ann. N. Y. Acad. Sci.*, **58**, Art. 6, 925 (1954).

2. Experimental

2.1. The Experimental System.—The vacuum station used consists essentially of three parts.

1. *Pumping.*—This is done by two mercury diffusion pumps in series backed by a rotary oil pump. A separate oil pump is used to pull down the mercury cut-offs.

2. *The Experimental Tube.*—This is a one-liter bulb in which a CP-4[4] etched germanium filament 2 mm. × 2 mm. × 100 mm. cut from a single crystal of high resistivity material is mounted on molybdenum leads as previously described.[3] It is connected directly to an ionization gage which is constructed entirely (apart from the filament) of molybdenum. A similar gage measures the pressure on the pump side of the system.

3. *Controllable Gas Leaks.*—The gas leaks used were of the ceramic type described by Hagstrum and Weinhart.[5] Four of these were connected in parallel so that different gases could be studied without letting the system down to air. Bulbs of spectroscopically pure gas at a pressure of 50 mm. were used. A liquid nitrogen trap prevented mercury vapor from reaching the germanium filament. The gas in the system was pumped out through a 0.165-cm. diameter hole 0.275 cm. long in the clap trap which led to a liquid nitrogen trap, mercury cut-off and the mercury diffusion pumps.

The amount of extraneous metal surfaces exposed to the gas were kept as small as possible to minimize spurious desorption.

2.2. Experimental Technique.—In order to obtain a clean surface and maintain it in that state for an appreciable length of time, it is necessary to have a vacuum of the order of 10^{-9} mm. as one cannot assume that the residual gas does not adsorb. At this pressure, it takes approximately 15 minutes for a monolayer of gas to be adsorbed, assuming a sticking coefficient of unity. Baking out the glass system is essential in order to obtain a vacuum of this magnitude. For this purpose, three separate ovens were constructed: A. The first was used for degassing the ceramic leaks and the associated liquid nitrogen trap. This was only used when new bottles of gas had been added as at all other times the ceramic leaks were covered with mercury. B. The larger of the two main ovens was used to degas the experimental tube, ionization gages and clap trap. C. A small separate oven was used around the liquid nitrogen trap closest to the diffusion pumps.

The temperature of each oven was manually controlled by a variac and measured with one or more chromel–alumel thermocouples. The bake-out procedure was as follows.

After leak checking, the system was evacuated to a pressure of 10^{-6} mm. All three ovens were then placed in position and heated to 500°. After maintaining this temperature for 6 hours, the two small ovens were turned off and allowed to cool to room temperature. Liquid nitrogen was then placed around the two traps and the ionization gages turned on. With the main oven still at 500°, the pressure was usually about 10^{-5} mm. At this stage, the main oven was turned off and the ionization gages degassed by electron bombardment. The germanium filament was then flashed. During the cooling period of the oven, these bombardments and flashes were repeated several times. When the oven reached room temperature, the pressure was usually in the range 10^{-9}–10^{-10} mm. If, for any reason it was higher, the

(4) This etch was developed by R. D. Heidenreich and has the following composition: 15 cc. of acetic acid, 25 cc. of concentrated nitric acid, 15 cc. of 48% hydrofluoric acid and 0.3 cc. of bromine.

(5) H. D. Hagstrum and H. W. Weinhart, *Rev. Sci. Inst.*, **21**, 394 (1950).

main oven was replaced and heated to 350° for 4 hours. This always produced the required high vacuum.

We have confirmed the observation made by Alpert[6] that at pressures below 10^{-8} mm. the diffusion pump ceases to be a sink. If, in this range the mercury cut-off is raised, the pressure in the system continues to decrease at approximately the same rate as when the line was open to the diffusion pumps. This is undoubtedly due to the pumping action of the ionization gages as described by Alpert[6] and by Schwartz.[7]

The vacuums obtained were sufficiently high that once the germanium surface had been cleaned, it would remain uncontaminated during a series of measurements. This was checked by leaving the cleaned surface in the high vacuum for two hours and then flashing. Less than 10^{-3} of a monolayer was desorbed. The next problem, therefore, was to produce a clean surface or at least a reproducible one.

There are four main ways of obtaining a clean surface. All have been used with varying degrees of success with different materials: (I) heating in high vacuum; (II) positive ion bombardment; (III) treating with atomic hydrogen; (IV) splitting crystals in high vacuum.

(I).—Heating metal filaments to temperatures close to their melting point in high vacuum has been used successfully to clean tungsten.[8] Clean-up by this technique depends on either dissociation of the surface oxide film or its evaporation as the oxide. It is possible to calculate the dissociation pressures of the germanium oxides thermodynamically.[9] In the case of GeO_2 this gives a value of p_{O_2} equal to 10^{-20} mm. at 1200°K. Similar calculations for GeO (which may be the stable form of the oxide at high temperatures) gives $p_{O_2} = 10^{-10}$ mm. at 1200°K. Both of these dissociation pressures are too low for us to obtain a clean surface by this means.

The vapor pressure of GeO, however, has been measured at 860°K. by Jolly,[10] and found to be greater than 10^{-3} mm. If this is the stable oxide at temperatures near the melting point of germanium one would expect to obtain a clean surface by flashing near 1200°K. in a vacuum of $10^{-9}-10^{-10}$ mm.

(II).—Positive neon ion bombardment has been used by Oatley[11] and by Eggleton and Tompkins[12] to clean surfaces of platinum and iron. It has the advantage that the wire being bombarded does not reach a very high temperature. The two main disadvantages are possible production of dislocations in the germanium (which will make measurement of electrical properties difficult) and the evaporation of appreciable quantities of germanium onto the walls of the tube (during a flash filament measurement this is heated and desorbs gas thereby producing a second peak in the pressure-time curve).

(III).—The use of atomic hydrogen has the disadvantage of the possibility of solution of hydrogen in the crystal lattice from which it is difficult to remove. When a germanium filament was exposed to a discharge in hydrogen (with a 900-v. potential on the germanium), a considerable quantity of gas was absorbed.

(6) D. Alpert, *J. Appl. Phys.*, **24**, 860 (1953).

(7) H. Schwartz, *Z. Physik*, **117**, 23 (1940).

(8) J. K. Roberts, *Proc. Roy. Soc. (London)*, **A152**, 445 (1935).

(9) The dissociation reaction for germanium dioxide is given by

$$GeO_2(s) \rightleftharpoons Ge(s) + O_2(g)$$

If $\Delta F°_f$ is the free energy change associated with this reaction and K_p the equilibrium constant, then

$$\Delta F°_f = -RT \ln K_p = -RT \ln \frac{[Ge][O_2]}{[GeO_2]} \quad (1)$$

where [Ge], [O₂] and [GeO₂] are the activities of the various entities at the temperature T. The activities of the solids are defined as being unity, therefore

$$\Delta F°_f \approx -RT \ln p_{O_2} \quad (2)$$

since the partial pressure of the gas (p_{O_2}) is equal to its activity. Using the value of $\Delta H°_f$ and $S°_{Ge(s)}$ and $S°_{GeO_2(s)}$ listed by Jolly[10] we can calculate $\Delta F°_f$ from

$$\Delta F°_f = \Delta H°_f - T [S°_{Ge(s)} + S°_{O_2(g)} - S°_{GeO(s)}]$$
$$= -131 \text{ kcal./mole} \quad (3)$$

(10) W. L. Jolly, Thesis, University of California, 1952.

(11) (a) C. W. Oatley, *Proc. Phys. Soc.*, **51**, 318 (1939).

(12) A. E. J. Eggleton and F. C. Tompkins, *Trans. Faraday Soc.*, **48**, 738 (1952).

(IV).—Splitting crystals in a high vacuum has been used for contact potential measurements on zinc,[13] but it is unsatisfactory for adsorption work as one needs to produce a new face for each measurement. The problem of surface diffusion of impurities from the remainder of the crystal is also present.

We have tried only the first two of these methods but the results indicate that the surface produced is reasonably clean.

The positive ion bombardment was carried out in 0.5 mm. of neon which was introduced over a film of freshly evaporated tungsten to remove traces of oxygen. A potential of 600 v. and a current of 25 ma. were used. After 10 minutes a visible film of germanium had formed on the walls of the tube. The quantity of hydrogen adsorbed on the filament at a fixed pressure at room temperature was used as the criterion of surface cleanliness. No difference could be detected between the amounts adsorbed before and after bombardment. Because of the disadvantages associated with positive ion bombardment, discussed above, subsequent work was confined to a surface which had been flashed several times near the melting point of germanium in a vacuum of $10^{-9}-10^{-10}$ mm. If this cleaned surface was exposed to oxygen at a pressure of 10^{-5} mm. subsequent adsorption of carbon monoxide was decreased by a factor of 2. The original adsorptive property could be recovered by flashing at 900°.

In the present work four different filaments have been used and after allowing for small differences in surface area the adsorption results are all in agreement.

2.3. Calculation of Results.—The ion current from the gage attached to the filament tube was amplified and recorded on a 5-ma. Esterline Angus recorder. From the calibration factors for the various gases the peak height on the recorder could be converted to Δp, the pressure increase in the system on flashing. If then V is the volume of the system, the number of molecules desorbed per square centimeter N_s is given by

$$N_s = \frac{KV\Delta p}{A} \quad (4)$$

K is the number of molecules per liter for $p = 1$ mm., i.e., at 300°K., $K = 3.2 \times 10^{19}$ and A is the area of the filament in cm.².

From nitrogen adsorption at 77°K. the true area was found to be 1.3 times as great as the geometrical area after a CP-4 etch. The true area figure was used in all calculations of N_s.

In the case of room temperature measurements this procedure is perfectly correct but when the filament vessel is cooled to 77 or 195°K. corrections must be made for thermomolecular flow. These must be introduced whenever the pressure gage is at a temperature different from that of the adsorbent. They will lead to changed values of both p and Δp and may markedly affect the type of isotherm obtained.

Consider a tube of diameter d cm. connecting two parts of a system at absolute temperatures T_1 and T_2 where the pressures of a gas at equilibrium are, respectively, p_1 and p_2. Knudsen[14] has shown that in general $p_1 \neq p_2$ unless λ, the mean free path of the gas molecules is negligibly small compared with d. When $d/\lambda < 1$

$$\frac{dp}{p} = \frac{3k}{8} \times \frac{1}{1 + d/\lambda} \times \frac{dT}{T} \quad (5)$$

where k is a constant equal to 4/3.

If $d/\lambda << 1$, and this will be true at pressures below 10^{-4} mm., integration of (5) gives

$$p_1/p_2 = (T_1/T_2)^{1/2} \quad (6)$$

This is the relationship that has been used to correct the data obtained in the present work. If a volume V_1 of the system is at a temperature T_1 and pressure p_1, and a volume V_2 at a temperature T_2 and pressure p_2 one can calculate the number of molecules desorbed which corresponds to a pressure change Δp_2 measured at T_2 in the system as follows. Assume $T_1 < T_2$ and $p'_2 = p_2 + \Delta p_2$. Then

$$N'_s = \frac{N}{R} \left[\frac{V_2}{T_2} (p_2' - p_2) + \frac{V_1}{T_1} p_2' \frac{(T_1)^{1/2}}{(T_2)} - \frac{V_1}{T_1} p_2 \frac{(T_1)^{1/2}}{(T_2)} \right] \quad (7)$$

(13) W. A. Zisman and H. G. Yamins, *Physics*, **4**, 7 (1933).

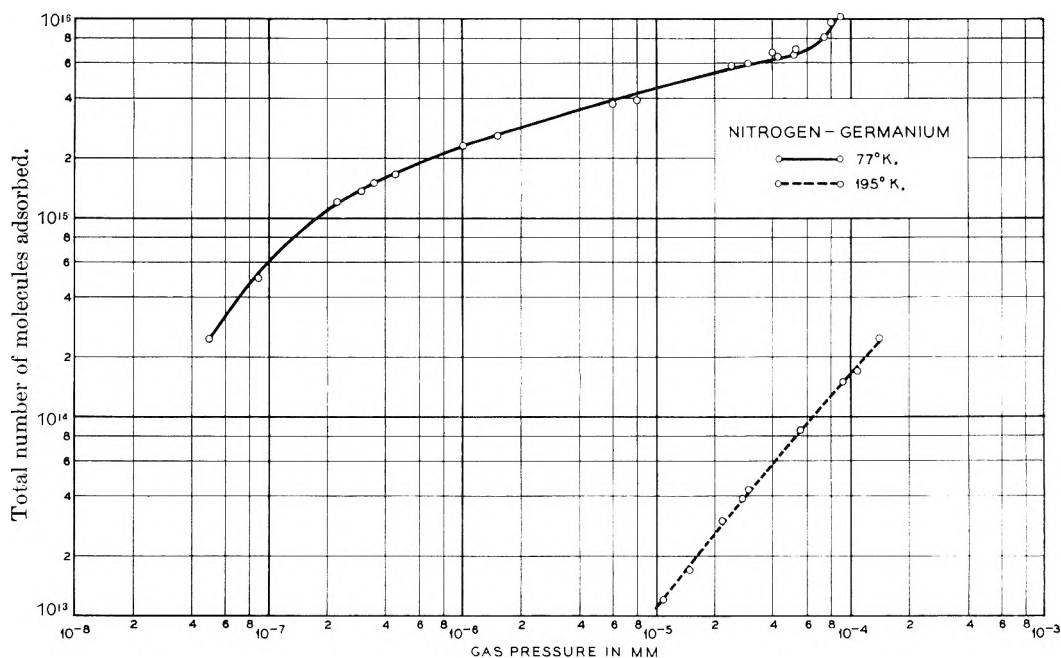(14) M. Knudsen, *Ann. Physik*, **31**, 205 (1910).

Fig. 1.—Variation of the total number of molecules of nitrogen adsorbed with pressure.

$$= \frac{N}{R}\left[\frac{V_2}{T_2}\Delta p_2 + \frac{V_1}{T_1}\frac{(T_1)^{1/2}}{(T_2)}\Delta p_2\right] \qquad (8)$$

$$= 9.65 \times 10^{21}\Delta p_2\left[\frac{V_2}{T_2} + \frac{V_1}{T_1}\frac{(T_1)^{1/2}}{(T_2)}\right] \qquad (9)$$

All the quantities on the right-hand side may be measured and N's, the total number of molecules desorbed calculated. Equation 9 reduces to equation 4 when $T_1 = T_2$.

3.0. Results

In the following figures, results are given from four different filaments used. The first two of these were mounted in a volume of 6 liters, while the other two were placed in 2.6-liter volumes. Thus the value of V in equation 4 could be varied while A was kept constant. All the measurements below room temperature were made on the latter two filaments. The geometrical area of all the filaments was the same and the total area also appeared to be practically constant as the number of molecules adsorbed per square centimeter for a given gas agreed from one filament to the next. Cross checks were made with at least two gases on each filament.

3.1. Nitrogen.—The adsorption of nitrogen on germanium is shown in Fig. 1. Results of the number of molecules desorbed against pressure at which the gas was in contact with the filament are given at two temperatures, 77 and 195°K. As previously reported[3] nitrogen does not adsorb to any appreciable extent at room temperature. The isotherms at the lower temperatures are completely reversible, indicating only a weak physical adsorption. This will be discussed further in a later section when we calculate heats of adsorption from the isotherms.

The importance of the nitrogen isotherm at 77°K. lies in the fact that from it we can calculate a true area for the filament. By inspection it seems not unreasonable to assume that the monolayer is completed at a pressure of 4–5 × 10^{-5} mm. This means that a monolayer on the filament contains 6.5 × 10^{15} molecules. Using a figure of 16.2 Å.^{2} for the

area of the nitrogen molecules[15] we now find that the total area of the filament was 10.4 cm.^{2}. This, when compared with the geometrical area of 8 cm.^{2}, gives a roughness factor of 1.3 for a CP-4 etched surface. Using this calculated value for the area the results for nitrogen may be expressed in terms of molecules adsorbed per cm.^{2}. This corrected area will be used to convert all other data to a molecules per cm.^{2} basis.

3.2. Carbon Dioxide.—The adsorption isotherms for carbon dioxide at 195 and 300°K. are shown in Fig. 2. It can be seen that the adsorption at 195°K. has not reached the monolayer region at a pressure of 10^{-4} mm. so that no check on the nitrogen area can be obtained unless the measurements are extended to a higher pressure. This would be almost impossible by the flash filament technique as the pressure changes on flashing would be a very small fraction of the total pressure. Both isotherms are only partially reversible but it is very doubtful whether this indicates any chemisorption. The heat of adsorption is quite small and even at 10^{-4} mm. the isotherm is still rising steadily. If we were in fact dealing with a chemisorbed species the amount of adsorption should be considerably greater. In the case of chemisorption of carbon dioxide it is not uncommon that dissociation to carbon monoxide occurs on desorption.[16] No evidence of this was found in our previous work[3] so that it is probable that only physical adsorption is occurring.

3.3. Carbon Monoxide.—Adsorption isotherms for carbon monoxide are shown in Fig. 3. With increasing temperature the adsorption decreases as would be expected for physical adsorption. At 77°K. a monolayer of physically adsorbed gas on the filament should contain 7.5 × 10^{14} molecules/cm.^{2}. The experimentally measured figure is 10^{15}

(15) P. H. Emmett and S. Brunauer, *J. Am. Chem. Soc.*, **59**, 1553 (1937).

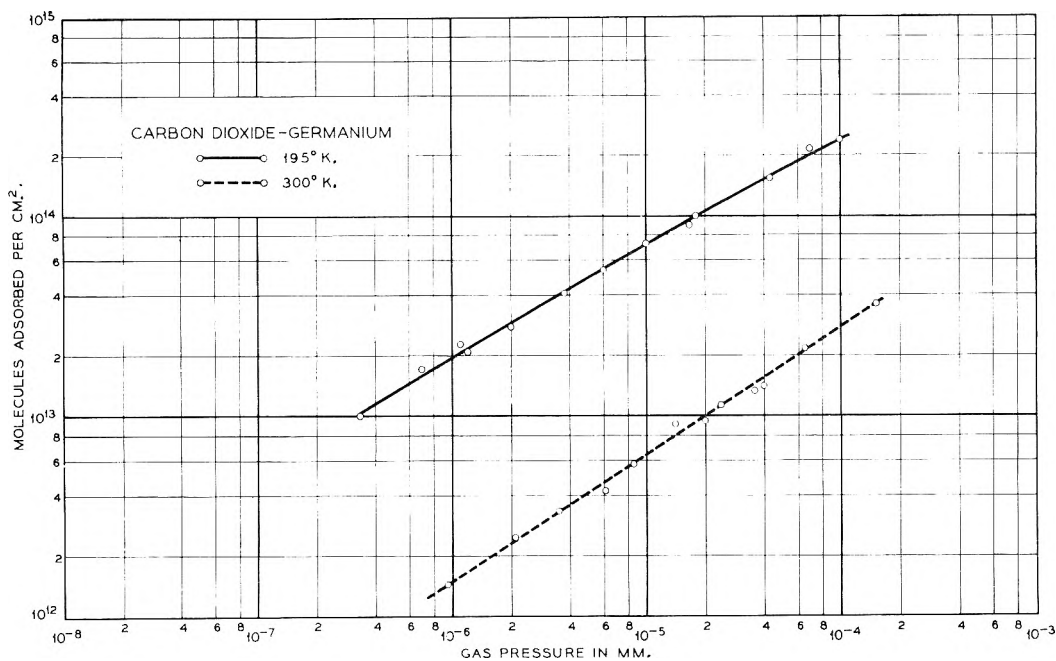(16) T. Kwan and Y. Fujita, *Nature*, **171**, 705 (1953).

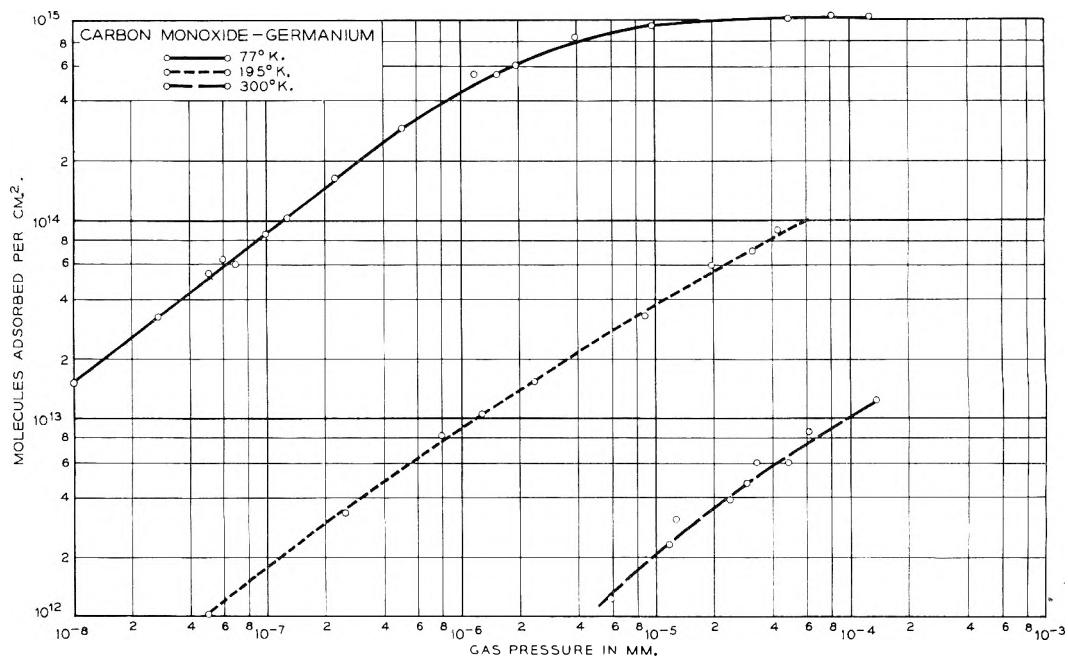Fig. 2.—Variation of the number of molecules of carbon dioxide adsorbed per square centimeter with pressure.

Fig. 3.—Variation of the number of molecules cf carbon monoxide adsorbed per square centimeter with pressure.

molecules at the point when the isotherm flattens out. The difference of 2.5×10^{14} molecules could be due to an error in the assignment of the carbon monoxide cross-section or to adsorption taking place on different sites. Unlike the nitrogen isotherm, this one is not completely reversible so that the areas obtained from nitrogen adsorption are probably more trustworthy.

3.4. Hydrogen.—Unlike the results described above for nitrogen, carbon monoxide and carbon dioxide, the amount of hydrogen adsorbed on germanium does not decrease continuously with increasing temperature. The isotherms in Fig. 4 at 195 and 300°K. are almost identical. This indi-

cates that two types of adsorption are occurring. Firstly at the lower temperatures a physical or van der Waals type, while at higher temperatures some sort of chemisorption is operative. This will be discussed further in a later section.

4.0. Calculated Thermodynamic Quantities

In a previous paper[17] details were given of the calculation of heats $(\overline{\Delta H})$ free energies (ΔF) and entropies $(\overline{\Delta S})$ of adsorption from isotherms at two or more temperatures. The equations used were as follows:
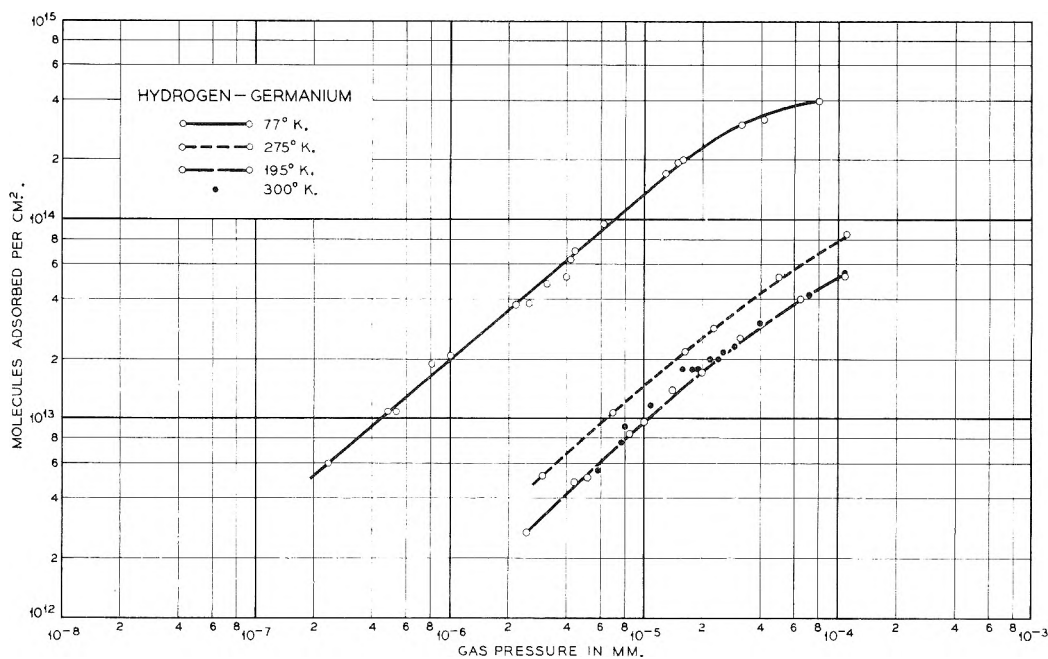
(17) J. T. Law, This Journal, **59**, 67 (1955).

Fig. 4.—Variation of the number of molecules of hydrogen adsorbed per square centimeter with pressure.

$$\overline{\Delta H} = RT^2 \frac{(\partial \ln p)}{(\partial T)v} \qquad (10)$$

$$\Delta F = RT \ln p/p_0 \qquad (11)$$

and

$$\overline{\Delta S} = (\overline{\Delta H} - \Delta F)/T \qquad (12)$$

where V is the volume of gas adsorbed at an equilibrium pressure p, T is the absolute temperature, R the gas constant and p_0 is the standard gas state pressure taken as 760 mm.

The use of equation 10 to calculate a heat of adsorption assumes that $\overline{\Delta H}$ is constant between the two temperatures at which isotherms are measured. If ΔT is small this is generally true but in the present work the temperature difference is of the order of 100°K. and accurate values of $\overline{\Delta H}$ are not possible. The order of magnitude, however, should be correct and sufficient to decide whether the adsorption is physical or chemical in nature. The heat of adsorption in the case of van der Waals type binding should never greatly exceed the heat of vaporization of the adsorbing material, in the case of gases, about 2 kcal./mole.

Values calculated for $\overline{\Delta H}_{Ads}$ for nitrogen, carbon monoxide and carbon dioxide are listed in Table I together with the heats of vaporization of the adsorbate. All the heats were calculated at a coverage of 10^{13} molecules/cm.² or $\theta = 10^{-2}$.

TABLE I[a]

	$-\overline{\Delta H}_{138°\,K.}$	$-\overline{\Delta H}_{247°\,K.}$	$+\overline{\Delta H}_{vap}$
Nitrogen	2.4	...	1.3
Carbon monoxide	2.0	3.2	1.5
Carbon dioxide	...	4.7	3.5

[a] All values in kcal./mole.

No value was calculated for hydrogen as two types of adsorption are apparently operative. Unfortunately it is not possible to calculate heats of adsorption at higher coverages as not all the isotherms extend much beyond 10^{13} moles/cm.². A

single calculation for carbon monoxide at 10^{14} moles/cm.² gave a value of 2.0 kcal./mole at 138°K., identical with the value listed in Table I at a lower coverage. All these values are sufficiently close to the heats of vaporization that we must be dealing with physical adsorption in each case.

The value obtained for the free energy, and therefore the entropy of adsorption, will depend on the degree of surface coverage at the standard surface state chosen. For the calculations to lead to any useful values we would need figures above the $\theta = 0.1$ range. With any reasonable value of free energy change, however, the low $\overline{\Delta H}_{Ads}$ figures must lead to quite small entropy changes and therefore, a picture of mobile adsorption where the gas molecules are no more localized than they are in a liquefied gas.

5.0. General Discussion of the Adsorption Results

The smallest number of adsorbed atoms that we could detect by the flash filament technique was 10^{12} cm.$^{-2}$ or about 10^{-3} of a monolayer. From this region up to 10^{14} moles cm.$^{-2}$ all the isotherms shown in Figs. 1–4 are essentially linear. This means that they are all fitted by the Freundlich equation[18]

$$\log p = n \log v + n \log k \qquad (13)$$

where v is the volume adsorbed at a pressure p and k and n are constants. The number of molecules adsorbed N_S is of course proportional to v.

Zeldowitsh[9] derived this isotherm many years ago but it is frequently dismissed as the central region of the Langmuir isotherm. This explanation would only apply over a limited pressure range while the results obtained show good agreement with the equation over many decades of pressure.

Halsey and Taylor[20] have derived the Freundlich

(18) H. Freundlich, "Colloid and Capillary Chemistry," London, 1926.

(19) J. Zeldowitsh, Acta Physicochim. U.R.S.S., 1, 961 (1934).

(20) G. Halsey and H. S. Taylor, J. Chem. Phys., 15, 624 (1947).

equation by assuming an exponential distribution of adsorption energies, i.e., a heterogeneous surface and shown that it fits the data obtained by Frankenburg[21] for the adsorption of hydrogen on tungsten. Assumptions of strong repulsive interactions do not lead to the Freundlich equation but to an isotherm of the type $\log p = a\theta + b$. However, as Halsey and Taylor point out it is proper to assume non-interactive adsorption when the surface is strongly non-uniform as the sites are so dispersed that the number of nearest neighbors of a given energy is almost zero. It is therefore reasonable to conclude that the adsorption measured in the present work is occurring on a heterogeneous surface. In the region of very low coverage the slopes shown in Figs. 3-5 are unity for nitrogen and hydrogen and approach this value in the other two cases so that the Langmuir equation is applicable. The number of Langmuir sites however is a very small percentage of the total number.
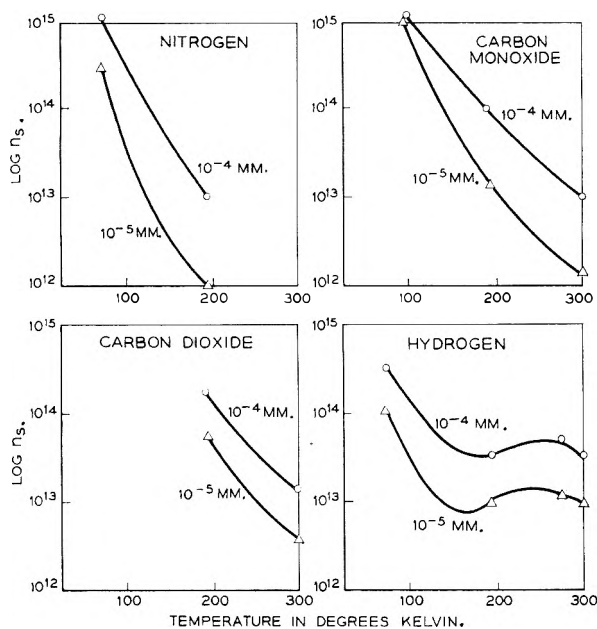

Fig. 5.—Adsorption isobars for nitrogen, carbon monoxide, carbon dioxide and hydrogen.

It should be noted that the Freundlich isotherm predicts steadily increasing adsorption with pressure. This is only possible if the number of available sites is infinite. The data for nitrogen, carbon monoxide and hydrogen all show some levelling off at higher pressures (as one would expect for a finite number of sites). Sips[22] has investigated the type of site distribution required to give an equation of the form

$$\theta = \frac{Ap^c}{1 + Ap^c}$$

which reduces to the Freundlich equation at low pressures but reaches a saturation value of $\theta = 1$ when p is large. He finds that the distribution is almost Gaussian in form. With suitably large values of A this equation will represent the low temperature isotherms obtained for carbon monoxide and hydrogen.

(21) W. G. Frankenburg, J. Am. Chem. Soc., 66, 1827, 1838 (1944).
(22) R. Sips, J. Chem. Phys., 16, 490 (1948).

In the case of hydrogen adsorption at 300°K. we have the complicating factor of chemisorption on a semi-conductor. If this process is accompanied by an electronic charge transfer between the hydrogen and the germanium a space charge region analogous to that of a rectifying junction may develop and limit the amount of chemisorption because of the raising of the Fermi level of the semiconductor as suggested by Boudart[23a] and Weisz.[23b]

In Fig. 5, the amount of gas adsorbed at a given pressure is plotted as a function of the absolute temperature. It can be seen that for nitrogen, carbon monoxide and carbon dioxide the adsorption decreases with increasing temperature as would be expected for physical adsorption. The results for hydrogen do not show this monotonic change. The isotherms measured at 195 and 300°K. were almost identical so that a further set of measurements were made at 275°K. The adsorption at 275°K. was slightly higher than that at either 195 or 300°K. If a gas can be adsorbed in two forms, i.e., in the form of van der Waals or physical adsorption at low temperatures and in the chemisorbed form at high temperatures, one finds that the adsorption first decreases with increasing temperature, due to decreasing physical adsorption and then begins to increase when the chemisorption becomes appreciable. Langmuir first noticed this phenomenon during the adsorption of carbon monoxide on platinum. In the ascending region of the isobar, the adsorption is composite and the adsorption is not reversible with respect to temperature. As the temperature is lowered the amount of adsorption increases steadily.

6.0. Comparison with Previous Work

The only previous adsorption measurements on germanium were made using the flash filament technique and the mass spectrometer as a pressure measuring device.[3] Two main criticisms can be levelled at this earlier work:

1. The germanium surface was not cleaned in a very high vacuum. At this pressure ($\sim 10^{-7}$ mm.) it would be almost impossible to maintain a clean surface for sufficient time to make a measurement.

2. The more serious source of error was introduced by the method of evacuation before flashing. The gas was left in contact with the filament for some time and then pumped out before the filament was flashed. This was necessary as the mass spectrometer is only capable of measuring very low pressures. If the isotherm is at all reversible, however, the final measured value of adsorption will not correspond to the pressure at which the gas was initially in contact with the germanium. The present work has shown that all the gases are to some extent reversibly adsorbed. For this reason we can only say that the original adsorption measurements correspond to some pressure between the initial and final gas pressures. The comparison with the present work is shown in Table II.

The results for hydrogen and carbon dioxide are in reasonable agreement with the previous work but the adsorption of carbon monoxide is much less.

(23) (a) M. Boudart, J. Am. Chem. Soc., 74, 1531 (1952); (b) P. B. Weisz, J. Chem. Phys., 21, 1531 (1953).

Gas	Present work	Previous work
Hydrogen	2×10^{-6} mm.	1×10^{-6}–3×10^{-5}
Carbon monoxide	4.5×10^{-4} mm.	3×10^{-6}–6×10^{-5}
Carbon dioxide	6.5×10^{-6} mm.	3×10^{-6}–3×10^{-5}

This was checked on each of the four filaments used, with different samples of gas but the same values were obtained in each case.

7.0. Summary

7.1.—The adsorption of carbon monoxide, carbon dioxide, nitrogen and hydrogen on a germanium filament has been measured at several temperatures and at pressures between 10^{-8} and 10^{-4} mm.

7.2.—Calculated heats of adsorption show that all except hydrogen are physically adsorbed.

7.3.—A roughness factor of 1.3 for a CP-4 etched surface was measured.

7.4.—Various methods for cleaning the surface have been investigated.

THE MEASUREMENT OF TRANSPORT NUMBERS IN PURE FUSED SALTS[1]

BY FREDERICK R. DUKE AND RICHARD W. LAITY

*Contribution No. 374, Institute for Atomic Research and Department of Chemistry,
Iowa State College, Ames, Iowa*

Transport numbers are here defined as the fractions of current carried by the ions when their motions relative to the bulk of the liquid, rather than to the electrodes, are considered. They are measured by means of a cell which has two electrode compartments separated by a porous membrane. The displacement of an air bubble in a capillary tube connecting the two compartments serves to indicate the volume changes occurring on electrolysis. These data combined with known density data are used to calculate the transport numbers, assuming the simplest formulas for the current-carrying ions. The use of the membrane is justified for fused $PbCl_2$ by showing that three very different membranes, of porous glass, porcelain and asbestos, give substantially identical results, the indicated value of t_- being 0.75.

In one sense the concept of transport numbers in pure fused salts is meaningless.[2] Thus, if molten lead chloride is electrolyzed between lead electrodes, the requirement of over-all electrical neutrality within all parts of the liquid permits no concentration changes to occur, so that relative to the two electrodes the chloride ions do not move. Using chlorine electrodes, on the other hand, it would appear from similar reasoning that the chloride ions carry all the current, while the lead ions stand still. It is clear, then, that taking the electrode surfaces as reference points from which to compare the relative velocities of the ions the transport numbers depend on the particular electrode processes taking place.

Consider, however, an ionic liquid subject to neither gravitational nor atmospheric restoring forces, so that its surface is not constrained to lie flat and horizontal. Let the liquid be lead chloride and once again use lead electrodes. As electrolysis is begun, an excess of lead ions is formed momentarily around the anode, while an equal number are removed from the liquid surrounding the cathode. This gives rise to a very slight increase in the volume of the anolyte and, of course, a corresponding decrease in the catholyte. Now the ions that comprise the liquid begin to move in order to re-establish electrical neutrality. If the lead ions carry all the current, the original volume changes in the liquid will be exactly nullified, but any conductivity by chloride ions will lead to a net gain in the quantity of lead chloride around the anode and a corresponding loss from the catholyte. Here the motion of the current-carrying ions relative to the bulk of the liquid might be used to define transport numbers which are properties of the salt alone and do not depend on the electrode processes. In the situation described this would mean letting t_- (the transport number of the chloride ion) be the fraction of an equivalent of lead chloride transferred from catholyte to anolyte during the passage of one faraday of electricity.

Since the conditions suggested above cannot, of course, be realized experimentally, Karpachev and Pal'guev[3] tried inserting a membrane between the anode and cathode compartments which would restrain the flow of the bulk of the liquid under a small gravitational gradient, but permit the passage of ions under an appreciable potential gradient. For this purpose they used a plug of tightly packed asbestos. Their tedious procedure of breaking open the cell following each electrolysis to determine the changes in weight of anolyte and catholyte gave results of poor reproducibility, but indicated that transport numbers independent of the electrode reactions might be obtained by such a method. They failed to show with any conclusiveness, however, that the use of such a membrane was not introducing surface effects which would cause the ions to behave differently than in the bulk of the liquid.

The present work was an attempt to establish the validity of using such a membrane, and to develop a method of greater sensitivity than that employed by the Russian workers. A preliminary report of the results appeared in an earlier communication.[4]

(1) Work was performed in the Ames Laboratory of the Atomic Energy Commission.

(2) K. Schwarz, *Z. Elektrochem.,* **45**, 740 (1939).

(3) S. Karpachev and S. Pal'guev, *Zhur. Fiz. Khim.,* **23**, 942 (1949).

(4) F. R. Duke and R. Laity, *J. Am. Chem. Soc.,* **76**, 4046 (1954).

Experimental

Materials.—Fisher certified reagent lead chloride was used. Further purification did not seem necessary, since small amounts of impurities had no apparent effect on the results.

The lead metal was "Baker Analyzed" reagent grade. The metal itself acts as an impurity by dissolving to some extent in the molten salt. The reasons for not considering this to be a significant factor in the experimental results will be discussed.

Apparatus.—The important features in the design of the cell which proved to be most practical have already been described.[4] The dimensions of the cell were chosen to permit convenient use in the particular muffle furnace to be used and are not critical. It is about 5 inches high and 4 inches wide. The piece of tungsten wire sealed through the bottom of each vertical compartment emerges into a hollow glass foot, where it is fused to a more flexible piece of nickel wire. The nickel wire projects from the cell where it can be connected to a power source. In this work the following different membranes were used to separate the two compartments: fritted glass disks of "coarse," "medium," "fine" and "ultrafine" porosity; a plug of finely shredded asbestos, tightly packed between "coarse" porosity fritted glass disks; a porcelain disk cut from an unglazed plate.

The power supply used was a pair of standard six-volt storage batteries connected in parallel. The current was measured by noting the scale deflection on a Leeds and Northrup galvanometer connected in the circuit with appropriate resistors after careful calibration.

A Hoskins electric furnace was used to maintain the cell and salt at the desired temperature, this being determined with a chromel–alumel thermocouple the tip of which was located near the center of the cell. A hole in the rear of the oven serves to allow light from a bulb hung behind the furnace to fall upon the capillary of the cell inside. A hole in the door at the front allows the capillary of the cell to be observed with a cathetometer located about one foot away.

Procedure.—Sufficient molten lead was added to each compartment of the cell to form pools which covered the tungsten wires and thereby served as lead electrodes. Care was taken to prevent atmospheric oxidation of the lead, either by melting it under nitrogen, or by dropping solid pieces of lead into molten lead chloride. The remainder of the cell was filled to a point just above the level of the capillary with fused lead chloride. This was done in such a way that an air bubble about 0.5 cm. long was trapped in the horizontal capillary. Observation of the bounding surfaces of this bubble through the telescope showed that there would be no tendency for any liquid to flow around the bubble, and hence that the bubble would move along with the column of liquid in the capillary.

On passing a current of about 0.5 amp. through the cell, the bubble was observed to move slowly in the direction of the cathode compartment. As the trailing edge of the bubble passed the vertical crosshair of the cathetometer, a timer was started and the exact current noted. About 0.5 g. of powdered lead chloride was then weighed onto a deflagrating spoon. This was inserted into the oven and emptied into the flared top of the cathode compartment, causing the bubble to move rapidly back to the other side of the crosshair. As the trailing edge of the bubble once more arrived at the crosshair the timer was stopped. The current was again observed, and the exact time of the run noted. During each run the temperature also was noted. Such an experiment took about 700 seconds. After each two or three runs the direction of current flow was reversed. This procedure could be continued as long as the level of liquid in each vertical compartment remained within the uniform section of the column.

Results and Discussion

The equation relating transport numbers to measured experimental quantities is derived as follows. We first assume that the only current-carrying species in the melt are Pb^{++} and Cl^-. Although it has been suggested that there may be an appreciable amount of complexing in fused lead chloride,[5]

(5) (a) G. Wirths, *Z. Elektrochem.*, **43**, 486 (1937); (b) H. Bloom and E. Heymann, *Proc. Roy. Soc. (London)*, **188A**, 392 (1947).

this has never been adequately shown by experiment. Radiotracer experiments are presently under way to determine whether any appreciable fraction of the current is carried by complex ions. If positive results are obtained, the data can readily be reinterpreted in terms of the entities involved. On passing n faradays of electricity, then, we assume that nt_+ equivalents of Pb^{++} ion migrate from the anode into the cathode compartment, and nt_- equivalents of Cl^- ion pass through the membrane in the opposite direction. At the same time n equivalents of Pb^{++} ion are being formed from the lead of the anode, and a like quantity discharged at the cathode. The net result is thus the transfer of nt_- equivalents of $PbCl_2$ from cathode to anode compartment, and a transfer of n equivalents of Pb from anode to cathode compartment. Letting d_{PbCl_2} and d_{Pb} be the respective densities of the two liquids, this amounts to a transfer of $(nt_- \times$ eq. wt. $PbCl_2/d_{PbCl_2}) - (n \times$ eq. wt. $Pb/d_{Pb})$ cc. of liquid from cathode to anode compartment, so that the bubble must be displaced by an equal volume in the direction of the cathode. Since the bubble is in the same place at the beginning and end of one experiment, the addition of the powdered lead chloride to the cathode compartment must have exactly nullified this displacement. And since both compartments are of the same diameter and uniform at the surface of the liquid, one-half of the volume of the added liquid must flow through the capillary from the cathode toward the anode compartment in causing this counterdisplacement of the bubble. (Reversing the direction of current frequently and averaging the results takes care of any lack of symmetry in the cell.) The former volume may therefore be equated with one-half the latter

$$\frac{nt_- \times \text{eq. wt. } PbCl_2}{d_{PbCl_2}} - \frac{n \times \text{eq. wt. Pb}}{d_{Pb}} = \frac{\frac{1}{2} \text{ wt. } PbCl_2 \text{ added}}{d_{PbCl_2}}$$

Solving for the transport number gives

$$t_- = \frac{\left(\dfrac{\text{wt. } PbCl_2 \text{ added}}{2n}\right) + \left(\text{eq. wt. Pb} \times \dfrac{d_{PbCl_2}}{d_{Pb}}\right)}{\text{eq. wt. } PbCl_2} \quad (1)$$

The current remained very nearly constant during the course of a run, usually showing a slight drift in one direction. In view of this, an accurate measure of the number of coulombs passed was obtained by merely taking the product of the time and the average current. The ratio R_{PbCl_2} of (wt. $PbCl_2$ added/coulombs passed) determined in each experiment should be a constant. Multiplication of R_{PbCl_2} by $96,500/2$ gives the first term of the numerator in equation 1. In principle it should be possible to measure the ratio of densities required in the second term using the same cell. Thus, if lead were added to the cathode compartment during an experiment instead of lead chloride, a new ratio R_{Pb} would be obtained. The desired density ratio would then, of course, be given by

$$\frac{d_{PbCl_2}}{d_{Pb}} = \frac{R_{PbCl_2}}{R_{Pb}}$$

It was found, however, that the addition of lead gave results of poor reproducibility, due to the

TABLE I

SUMMARY OF RESULTS OF TRANSPORT NUMBER EXPERIMENTS ON FUSED PbCl$_2$ AT 565° USING VARIOUS MEMBRANES

Membrane	No. of expts.	RPbCl$_2$ × 10³ (av.)	Av. dev. of RPbCl$_2$	t_- (av.)
"Coarse" porosity fritted glass disk	1	0[a]	. . .	0.336
"Medium" porosity fritted glass disk	11	0.958	±0.045	0.669 ± 0.016
"Fine" porosity fritted glass disk	26	1.079	± .048	0.711 ± .017
"Ultrafine" porosity fritted glass disk	22	1.213	± .039	0.758 ± .014
Asbestos packed between two "coarse" porosity disks	20	1.165	± .060	0.742 ± .020
Porcelain disk cut from unglazed plate	25	1.190	± .064	0.750 ± .022

[a] Bubble did not move.

tendency of the metal to cling to the glass and oxidize there, rather than run freely into the melt. Comparison of the density ratio obtained in this way nevertheless showed good agreement with the literature value, but considerably poorer accuracy. The density figures in the literature were therefore used in calculating the transport numbers reported here.[6,7]

The results for six different membranes are summarized in Table I. It will be seen that, except for that obtained with the "coarse" porosity fritted disk in which case the bubble failed to move, they are all in qualitative agreement. The last three results show excellent agreement with each other, all lying within the same range. The membranes used in these cases were the least porous, and hence least likely to permit any of the accumulating liquid to flow back through them rather than through the capillary. Such backflow was certainly the cause of the first result, and hence appears most likely to have contributed to the next two low results. The agreement among the last three results therefore appears to justify two conclusions: (1) in view of the small probability that the three very different membranes have identical resistances to flow of the liquid, the contribution of backflow in these experiments must have been small enough to be considered negligible; (2) in view of the fact that the membrane pores through which the conductivity took place were in the three cases of different size, shape and length, and that the membranes themselves were of entirely different materials, the influence of surface effects in defining the transport numbers must also be very nearly negligible. In this latter connection it might be recalled that most electrokinetic phenomena are so sensitive to the nature of the surface that it is difficult to reproduce results from one glass capillary to the next.

Although the temperature was not too carefully controlled in these experiments and was probably not uniform throughout the cell, it is doubtful that this had any effect on the measured transport numbers. On carrying out a series of runs at 635° the only apparent effect was on the relative densities of the liquids. The average t_- for seven experiments, using the "ultrafine" fritted disk as mem-

brane, was 0.757 ± 0.009, which is identical with the result of 565°. Further discussion of the significance of this temperature effect will appear in a subsequent paper.

The above results are also in good agreement with those of the Russian workers cited earlier.[3] In 14 experiments of the type described carried out over a temperature range of 520–680°, they observed no temperature effect and an average t_- of 0.78 ± 0.03. These workers also tried methods using a radioactive isotope of lead, but the results, while showing qualitative agreement with the above, were too erratic to be conclusive.

The dissolving of lead metal from the electrodes in the salt changes the color of normally yellow fused PbCl$_2$ almost to black at higher temperatures (above 600°). It is reported, nevertheless, that the solubility of the metal in the salt at 550° is 0.0002 mole per cent., increasing to 0.0005 mole per cent. at 610°.[8] To determine the influence of this metal on ionic migration in the salt the following experiment was carried out. A cell was filled with pure lead chloride so that the tungsten wires served as electrodes. Its resistance was measured as a function of temperature from 520 to 600° using a 1000 cycle conductivity bridge. The salt was then poured over an excess of lead metal and allowed to stand at 600° until its very dark color indicated probable saturation. The solution was decanted back into the cell and its resistance again measured. At every temperature the readings were found to be identical to those for the pure salt within the accuracy of the instrument (about one part in 300). It seems very unlikely that the mechanism of conductivity could have changed significantly while both the conductivity and its temperature dependence remained unchanged. It was therefore felt that transport numbers measured in the presence of dissolved metal are ascribable to the pure salt.

In conclusion it is recommended that "ultrafine" porosity fritted glass disks be used in future work of this type, although, strictly speaking, the use of such a membrane should be justified in each specific case. An adequate justification for ignoring possible surface effects in such a membrane might be obtained by measuring the temperature dependence

(6) R. Lorenz, H. Frei and A. Jabs, Z. physik. Chem., 61, 468 (1907).

(7) P. Pascal and A. Jouniaux, Compt. rend., 158, 414 (1911).

(8) R. Lorenz, G. Hevesy and E. Wolff, Z. physik. Chem., 76, 732 (1911).

of the conductivity in cells with and without the membrane. The "activation energy of ionic migration" computed from such data is very sensitive to changes in the conductivity mechanism, and hence may be used to indicate the validity of the method.

NON-EQUILIBRIUM INHIBITION OF THE CATALASE–HYDROGEN PEROXIDE SYSTEM

By ROLAND F. BEERS, JR.

Division of Biochemistry, Department of Biology, Massachusetts Institute of Technology, Cambridge 39, Massachusetts
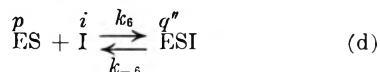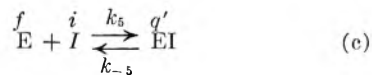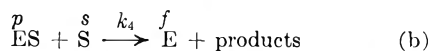
The kinetics of the catalase–hydrogen peroxide system during the period it is undergoing progressive inhibition has been examined analytically. It has been shown that because the steady state ratio, free enzyme/primary complex, is independent of the substrate concentration, it is possible for this ratio to remain constant even though both terms may be changing continuously during the inhibitory reaction. Consequently, it is a relatively simple matter to determine the concentration of active enzyme from tangents drawn along the semi-log slope of substrate vs. time, *i.e.*, transient first-order constants. The kinetic data of the conversion of the primary complex to the inactive secondary complex published by Chance have been examined and found to follow the theoretical predictions of this paper. Azide inhibition is believed to involve a competitive reaction between azide and hydrogen peroxide for the primary complex, following a simple reversible first-order equation, independent of substrate concentration.

Introduction

In an earlier paper[1] the author examined equilibrium inhibition of the catalase–hydrogen peroxide system during the steady state, *i.e.*, when the concentrations of the various enzyme forms are time invariant. In this instance we were concerned with analytical methods for calculating dissociation constants of the enzyme–inhibitor complexes. In the present paper we will consider the alternate situation in which the enzyme–substrate system is being progressively inhibited, *i.e.*, non-equilibrium inhibition. In particular we will explore the analytical methods for calculating the individual velocity constants. Some of the published experimental results and interpretations can profitably be examined in the light of the concepts developed in this paper.

Theory

The reaction scheme is

$$\overset{f}{E} + \overset{s}{S} \xrightarrow{k_1} \overset{p}{ES} \qquad (a)$$

$$\overset{p}{ES} + \overset{s}{S} \xrightarrow{k_4} \overset{f}{E} + \text{products} \qquad (b)$$

$$\overset{f}{E} + \overset{i}{I} \underset{k_{-5}}{\overset{k_5}{\rightleftarrows}} \overset{q'}{EI} \qquad (c)$$

$$\overset{p}{ES} + \overset{i}{I} \underset{k_{-6}}{\overset{k_6}{\rightleftarrows}} \overset{q''}{ESI} \qquad (d)$$

In conformity with previous papers[1-3] the quantities f, p, q', and q'', refer to the concentrations of the various components of the system. We continue the assumption[1] that the free inhibitor concentration is equal to the total inhibitor concentration and, therefore, is constant.

Two mechanisms may produce a state of non-equilibrium between the inhibitor and the enzyme. The first, discussed briefly in the previous paper,[1] is found if either inhibitor–enzyme complex, *i.e.*,

EI or ESI, but not both, reacts to an appreciable degree with the substrate. It was shown that the enzyme–substrate system cannot approach or be in a steady state. Furthermore, the degree of inhibition, reflected in the transient first-order velocity constant, becomes a function of the substrate concentration. However, these characteristics have not been observed in the catalase–hydrogen peroxide system. Nevertheless, Theorell and Ehrenberg[4] have recently proposed that hydrogen peroxide reacts directly with the catalase–azide compound to form the catalase–azide–peroxide compound. We shall return to this point later (see Discussion).

The second mechanism for non-equilibrium between enzyme and inhibitor is obviously an enzyme–inhibitor reaction approaching equilibrium. The concentration of the active enzyme species decreases to a finite value during which period the time decay of the substrate is greater than first order. At equilibrium the rate of catalysis returns to first order. Since the concentrations of active enzyme species during this transient period are varying with time we must ascertain what effects this progressive inhibition has on the steady state of the catalase-hydrogen peroxide system. This has been defined by (a) $dp/dt = 0$ and (b) the equation[5]

$$f/p = k_4/k_1 = R_k \qquad (1)$$

Under what conditions when $dp/dt \neq 0$ can we assume that equation 1 is correct or at least a satisfactory approximation?

The rates of change, dp/dt and df/dt, are

$$dp/dt = (k_1 f - k_4 p)s - (k_6 pi - k_{-6} q'') \qquad (2)$$

$$df/dt = -(k_1 f - k_4 p)s - (k_5 fi - k_{-5} q') \qquad (3)$$

Equation 1 is an exact solution (within the limits of the steady state approximation) when the rates in equations 2 and 3, specifically, $(k_6 pi - k_6 q'')$ and $(k_5 fi - k_{-5} q')$, are zero. The inhibitor reactions are at equilibrium. This represents the mini-

(1) R. F. Beers, Jr., THIS JOURNAL, **59**, 25 (1955).

(2) R. F. Beers, Jr., *ibid.*, **58**, 197 (1954).

(3) B. Chance, D. S. Greenstein and F. J. W. Roughton, *Arch. Biochem. Biophys.*, **37**, 301 (1952).

(4) H. Theorell and A. Ehrenberg, *ibid.*, **41**, 462 (1952).

(5) R. F. Beers, Jr., and I. W. Sizer, THIS JOURNAL **57**, 290 (1953).

mum error introduced into equation 1. The maximum error may be found when these quantities are maximum, *i.e.*, when q' and q'' are zero during the initial phase of the inhibitory reactions. Using the relationship $R_k dp/dt = df/dt$, we can show that

$$k_1 f - k_4 p = \left[\frac{R_k(k_6 - k_5)}{(R_k + 1)^2}\right]\left[\frac{iE}{s}\right] \quad (4)$$

Equation 1 is valid provided the quantity in the right-hand side of (4) is much smaller than either $k_1 f$ or $k_4 p$. Since the substrate has no effect on the concentrations of the various enzyme species[5] we are free to make the quantity, s, large enough to assure that equation 4 is for all practical purposes zero.

For example, the maximum value of $R_k/(R_k + 1)^2$ is 0.25 ($R_k = 1$). In the usual inhibition studies $E = 10^{-10}M$ and $s = 10^{-3}M$. Let $(k_6 - k_5)i$ have some reasonable value (determined in part by the allowable range of i), say 10^{-1} sec. With these values the right-hand member of (4) is approximately 2×10^{-9} sec.$^{-1}$. The magnitude of the left-hand member is the difference between two relatively large numbers, *viz.*, $(10^7) (10^{-10}) = 10^{-3}$. Therefore, compared to either $k_1 f$ or $k_4 p$, the right-hand term is negligible. This is true even if the substrate concentration decreases by a factor of 10^2. It is obvious that under these conditions equation 1 is valid. We may now proceed with the derivation of rate equations describing the inhibition kinetics.

Case I.—At $t = 0$ let $q' = 0$ and $q'' = 0$. The total rate of inactivation of the enzyme is the sum of the rates of inactivation of the free enzyme and of the primary complex

$$de/dt = (df + dp)/dt = -k_5 fi + k_{-5} q' - k_6 pi + k_{-6} q'' \quad (5)$$

Substituting the term pR_k for f from (1) and replacing q'' by $E - p(R_k + 1) - q'$ yields

$$(R_k + 1)dp/dt = -p[i(k_6 + R_k k_5) + k_{-6}(R_k + 1)] + q'(k_{-5} - k_{-6}) + k_{-6}E \quad (6)$$

Since $R_k dp/dt = df/dt$, then we may find q' in terms of p

$$q' = \frac{k_{-6}E - p[i(k_6 - k_5) + k_{-6}(R_k + 1)]}{k_{-6} + k_{-5}/R_k} \quad (7)$$

Substitute this value for q' into equation 6

$$(R_k + 1)dp/dt = p\left[\frac{\{i(k_6 - k_5) + k_{-6}(R_k + 1)\}\{k_{-6} - k_{-5}\}}{k_{-6} + k_{-5}/R_k}\right] + \frac{k_{-6}k_{-5}E}{k_{-6}R_k + k_{-5}} \quad (8)$$

Equation 8 is integrated between the limits of t to yield

$$\ln\left(\frac{p - p_e}{p_0 - p_e}\right) = \frac{d\ln(p - p_e)}{dt} = K_0 = \frac{i[K_5 + R_k K_6 + K_5 K_6(R_k + 1)/i]}{\left[\frac{K_6 R_k}{k_5} + \frac{K_5}{k_6}\right](R_k + 1)} \quad (9)$$

where $K_5 = k_{-5}/k_5$, $K_6 = k_{-6}/k_6$, and p_0 and p_e are the values of p at $t = 0$ and at equilibrium, respectively. K_0 is the observed first-order velocity constant of the inhibition reaction.

We note, of course, that as in the case of equilibrium inhibition[1] the substrate concentration does not appear as a term in equation 9. The constant,

K_0, given in the form above has little kinetic or thermodynamic significance aside from its order with respect to p. By experimental and analytical methods previously described[1] we can determine K_5 and K_6. Presumably, in certain cases it is possible to determine k_5 in the absence of the substrate by means of rapid kinetic methods, and, indeed, this has been done.[6] Consequently, from known values of K_0, K_5, K_6, k_5 and R_k it becomes possible to determine k_6 by means of equation 9. A simpler and more accurate method experimentally is discussed below (Case II).

Calculation of K_0 from the rate of catalysis of the substrate is in the case of catalase an extremely simple procedure. At any given instant, dt, when $dp/dt = 0$, the rate of catalysis is given by the usual expression[7]

$$d\ln s/dt = -k_s e = -k_0 = -k_s(f + p) = -k_s(R_k + 1)p \quad (10)$$

where k_s is the specific reaction rate of one mole of enzyme. In other words, at any point t along the slope, $d\ln s/dt$, the concentration of active enzyme, e, is proportional to the tangent, $d\ln s/dt$, drawn at that point. Rearranging (10) gives us p in terms of k_0 and k_s

$$p = \frac{k_0}{k_s(R_k + 1)} \quad (11)$$

If, now, we substitute this value of p into equation 9 we obtain

$$\frac{\ln\left[\frac{k_0^t - k_0^e}{k_0^0 - k_0^e}\right]}{t} = \frac{d\ln(k_0^t - k_0^e)}{dt} = K_0 \quad (12)$$

where k_0^t, k_0^0 and k_0^e are the observed velocity constants at $t = t$, $t = 0$ and at equilibrium, respectively.

Case II.—At $t = 0$, $q' = fi/K_5$ and $q'' = 0$. In other words, q' is in equilibrium with the free enzyme. This necessitates two assumptions: (a) the addition of substrate does not upset this equilibrium; (b) the progressive decline of f does not alter the fundamental relationship between the equilibrium and R_k. Both assumptions are, in fact, approximations but within the limits of the experimental error they are valid. This condition can be met by specifying that $k_5 \gg k_6$ and $k_{-5} \gg k_{-6}$. The rate of formation of the inactive enzyme, ESI, has the solution

$$d\ln(q'' - q''_e)/dt = k_6 p_0 i/q''_e \quad (13)$$

where q''_e is the equilibrium concentration of ESI. The expanded expression corresponding to equation 12 is

$$\frac{d\ln(k_0^t - k_0^e)}{dt} = \frac{k_6 k_0^0 i}{(k_0^e - k_0^e)(R_k + 1) - k_5^e R_k i/K_5} \quad (14)$$

In (14) k_0^c is the observed first-order velocity constant for the destruction of hydrogen peroxide in the absence of any inhibitor (control).

In the event that i/K_5 is very small, *i.e.*, reaction c is non-inhibitory at the concentration of inhibitor present, equation 14 reduces to

$$d\ln(k_0^t - k_0^e)/dt = \frac{k_6 k_0^0 i}{(k_0^e - k_0^e)(R_k + 1)} \quad (15)$$

where now $k_0^0 = k_0^c$. (15) could also have been

(6) B. Chance, *J. Biol. Chem.*, **179**, 1299 (1949).

(7) R. F. Beers, Jr., and I. W. Sizer, *ibid.*, **195**, 133 (1952).

derived directly from equation 9. From known values of K_5, K_6, K_0 and equation 14 we can calculate k_5 with reasonable accuracy provided it is of the same order of magnitude as k_6.

Case III.—At $t = 0$ let $q'' = pi/K_6$ and $q' = 0$. i.e., $k_5 << k_6$ and $k_{-5} << k_{-6}$. Following the same procedure as above, the graphic solution for k_5 is found to be

$$\frac{d \ln (k_0{}^t - k_0{}^e)}{dt} = \frac{k_5 k_0{}^0 R_k i}{(k_0{}^e - k_0{}^e)(R_k + 1) - k_0{}^e i/K_6} \quad (16)$$

When $K_5 << K_6$, then equations 9 and 16 reduce to

$$\frac{d \ln (k_0{}^t - k_0{}^e)}{dt} = \frac{k_5 k_0{}^0 R_k i}{(k_0{}^e - k_0{}^e)(R_k + 1)} \quad (17)$$

There has been no evidence published that this type of inhibition occurs with catalase.

Discussion

A clear distinction must be made between inhibition of catalase by the substrate directly and by the substrate indirectly through the reaction of an inhibitor with the primary complex. The former, "substrate inhibition," has been the subject of extensive kinetic studies in the past.[8] A more recent study by Lemberg and Legge[9] has shown that under conditions where the change in substrate concentration during the catalysis by catalase is small, the rate of inhibition obeys the equation

$$\frac{d \ln e}{dt} = -k' \quad (18)$$

but if there are large changes in the substrate concentration then the following equation applies

$$de/dt = -k''es \quad (19)$$

This inhibition is reported to be irreversible. In contrast to this "substrate-inhibition" the present paper has considered the kinetics of what we might call "inhibitor-inhibition." Some manifestations of this described in the literature will now be reviewed.

Inactive Secondary-complex Formation from the Primary Complex.—Chance[10] has shown that an inactive catalase, complex II, can be formed reversibly from the active enzyme substrate complex I, ES. Complex II has a light absorption spectrum and magnetic susceptibility characteristic of an Fe^{+++} complex with 6 d^2sp^3 covalent bonds in an octahedral array. Using the glucose–glucose-oxidase system for a constant supply of hydrogen peroxide (est. $10^{-9}M$), from changes in the spectrum of catalase, Chance[10] was able to measure the rate of formation of complex II. This rate increased with an increase in the steady-state concentration of hydrogen peroxide. These kinetics suggest that the substrate is acting directly on the primary complex. However, the final concentration of complex II was found to be un-

(8) S. Yamasaki, *Science Rept. Tôhoku Imp. Univ.* **9**, 13 (1920); S. Morgulis, *J. Biol. Chem.*, **47**, 341 (1921); J. H. Northrop, *J. Gen. Physiol.*, **7**, 373 (1924); J. Williams, *ibid.*, **11**, 309 (1927); S. M. Maximovich, *Z. physiol. Chem.*, **174**, 233 (1928); K. Nosaka, *J. Biochem. (Japan)*, **8**, 331 (1928); J. Matsuyama, *J. Faculty Agr. Hokkaido Imp. Univ.*, **32**, 109 (1933); G. W. Marks, *J. Biol. Chem.*, **115**, 299 (1936); E. H. Hinshelwood, *Trans. Faraday Soc.*, **43**, 266 (1947).

(9) R. Lemberg and J. W. Legge, *Biochem. J.*, **37**, 177 (1943).

(10) B. Chance, *ibid.*, **46**, 387 (1950).

affected by the addition of excess hydrogen peroxide.

An alternate mechanism for the formation of Complex II is suggested by the analysis above. We have shown that in order for the rate of inhibition to have no effect on the ratio f/p and, therefore, the rate of inhibition to be independent of the substrate concentration, the magnitude of the right-hand term in equation 4 must be approximately zero. This follows whether s is large or small so long as in the latter case s remains constant. In the formation of complex II there is no evidence that the free enzyme is directly involved. Therefore, we may neglect k_5 and consider only $k_6 i$.

At pH 7.5 with a horse liver catalase (3.3 hemes) concentration of $5.28 \times 10^{-7} M$ heme, Chance quotes a half time of 780 sec. for the formation of complex II. This corresponds to an observed first-order constant, $d \ln(q'' - q''_e)/dt$, of 8.9×10^{-4} sec.$^{-1}$. At equilibrium the fraction of hemes converted to complex II is given as $1.4/3.3$. Initially the fraction of enzyme as the primary complex was $p_0/E = 1/(R_k + 1) = 0.333$. Substituting these quantities into equation 13 gives a value of 1.13×10^{-3} sec.$^{-1}$ for $k_6 i$. The estimated substrate concentration is $10^{-9} M$. The right-hand member of equation 4 is

$$\frac{(2)(1.13 \times 10^{-3})(5.28 \times 10^{-7})}{(9)(10^{-9})} = 0.132$$

$$(k_1 f \cong 10^7 \times 10^{-7} \cong 1)$$

Although this number is not large it suggests that equation 1 may not be a good approximation for determining $k_6 i$.

A further check may be had by comparing the observed ratio of q''_e/p_e with the observed value of $k_6 i/k_{-6}$. In the presence of methanol the primary complex rapidly disappears by the following mechanism

$$\text{ES} + \text{MeOH} \xrightarrow{k_4{}^*} \text{E} + \text{formaldehyde} \quad (e)$$

where $k_4{}^*$ is approximately 10^3 liters mole^{-1} sec.$^{-1}$. Complex II disappears concurrently, presumably by the mechanism

$$\text{Complex II} \xrightarrow{k_{-6}} \text{ES} \xrightarrow{\text{MeOH}} \text{E} \quad (f)$$

The half time for this reaction at pH 7.5 is quoted as 600 seconds, corresponding to a first-order constant of 1.15×10^{-3} sec.$^{-1}$. The first-order constant for the disappearance of the primary complex, assuming MeOH is constant, is $(k_4{}^*)(\text{MeOH}) = 1.7 \times 10^{-2}$ sec.$^{-1}$. In view of the fact that the reaction with methanol is irreversible and the rate is 10^5-fold greater than the rate of disappearance of complex II we may safely assume that this observed rate of disappearance of complex II is rate determining and, therefore, is the true rate. We obtain for $k_6 i/k_6$ a value of $1.13 \times 10^{-3}/1.15 \times 10^{-3} \cong 1.0$. The ratio, q''_e/p_e, is determined as

$$R_k = f_e/p_e = \frac{E - q''_e - p_e}{p_e}; \quad \frac{q''_e}{p_e} = \frac{1 + R_k}{\frac{1/q''_e}{E} - 1} \quad (20)$$

For values for q''_e/E of $1.4/3.3$ and for R_k of 2.0 we find from equation 20 that $q''_e/p_e = 2.2$. The dis-

crepancy between the respective values of k_6i/k_6 and q''_e/p_e can with considerable certainty be attributed to experimental errors. In fact, considering the possible range of errors one might anticipate, these values are in remarkably close agreement. We may conclude, therefore, that under these conditions at pH 7.5, the approximation of equation 1 is valid. The experimental data of Chance can be accounted for by the mechanism on which is based this analysis.
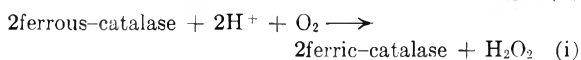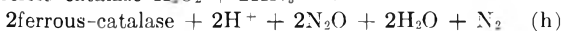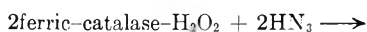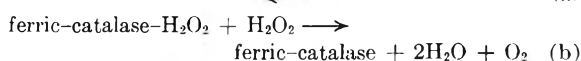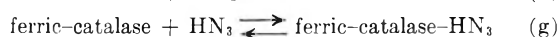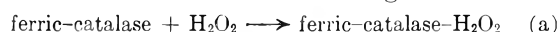
A different picture is found at pH 3.5. At a heme concentration of 2.4×10^{-7} M horse erythrocyte catalase (4 hemes) has a k_6i value of 8.16×10^{-2} sec.$^{-1}$. The right-hand member of equation 4 is 3.66; $k_6i/k_{-6} = 7.63$ and $q''_e/p_e = 28.3$. The large discrepancy between these values is predicted by the correspondingly large magnitude of equation 4. Therefore, equation 1 is no longer a correct approximation. Physically this means that the primary complex is being removed from the active enzyme system faster than the underlying catalytic mechanism can convert the free enzyme to the primary complex at a rate sufficient to keep the ratio f/p a constant. Because of this lag in the formation of the primary complex the value of f/p increases or p falls. We would expect, therefore, that the rate of formation of the secondary complex is slower the lower the substrate concentration. As the inhibitory reaction reaches equilibrium $k_6ip = k_{-6}q''$ and $dp/dt = 0$. Therefore, $f/p = R_k$ and the secondary complex becomes independent of the substrate concentration. These predictions are confirmed by the findings of Chance.[11]

Azide Inhibition.—Lemberg and Foulkes[13,14] and independently, Ogura, et al.,[15] observed at low temperatures that the rate of inhibition of the catalase–hydrogen peroxide system by azide is sufficiently slow to be detected during the initial phase of the catalysis of the substrate. This inhibition of the catalysis of hydrogen peroxide manifests itself by a rapid drop in the first order time decay of the substrate to a finite or equilibrium value. No characterization of the kinetics was attempted by these investigators, but the graphs published by Lemberg and Foulkes[13,14] show rate curves approximating a reversible first-order reaction. They were able to reverse this inhibition by dilution of the reaction system and made the important observation that the rate and final extent of inhibition is greater in an atmosphere of carbon monoxide.

Studies by Beers[16] and Beers and Sizer,[17] based on the more accurate tracking procedure in the spectrophotometric method for following the rate destruction of hydrogen peroxide,[7] have confirmed

these findings and, in addition, have shown that[17] in aerobiosis the rate of inhibition by azide obeys a reversible first-order equation over 90% of the time. The rate of inhibition in preliminary studies appears to be proportional to the concentration of azide but independent of the substrate concentration. The degree of inhibition can be reversed by dilution of the system, pH rise and dialysis.[16] These findings, in addition to the well-known fact that at equilibrium (observed at higher temperatures) the time decay of the substrate obeys an irreversible first-order equation, are strong evidence in favor of the proposal[18] that the mechanism of inhibition by azide is through the reaction of azide with the primary complex. (See discussion in previous paper.[1]) The experimental results of Theorell and Ehrenberg[4] do not in our opinion conflict with this argument, despite the fact that they have suggested an alternate proposal, namely, that the hydrogen peroxide reacts with the azide–catalase compound to yield the inactive ferrous-catalase compound. However, at equilibrium such a mechanism would show a dependence of the degree of inhibition on the concentration of the substrate.[1]

The experimental data of Theorell and Ehrenberg[4] are susceptible to a different set of interpretations. We have the following set of reactions

ferric–catalase + $H_2O_2 \longrightarrow$ ferric–catalase–H_2O_2 (a)

ferric–catalase + $HN_3 \rightleftharpoons$ ferric–catalase–HN_3 (g)

ferric–catalase–H_2O_2 + $H_2O_2 \longrightarrow$
  ferric–catalase + $2H_2O$ + O_2 (b)

2ferric–catalase–H_2O_2 + $2HN_3 \longrightarrow$
  2ferrous–catalase + $2H^+$ + $2N_2O$ + $2H_2O$ + N_2 (h)

2ferrous–catalase + $2H^+$ + $O_2 \longrightarrow$
  2ferric–catalase + H_2O_2 (i)

We have replaced with reaction h the following reaction given by Theorell and Ehrenberg

2ferric–catalase–HN_3 + $2H_2O_2 \longrightarrow$
  2ferrous–catalase + $2H^+$ + $2N_2O$ + $2H_2O$ + N_2 (j)
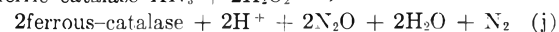
The sum of reactions a and b, the catalytic reactions, is

$$2H_2O_2 \longrightarrow 2H_2O + O_2 \qquad \text{(k)}$$

and of reactions h and i (or j and i), the peroxidatic reactions, is

$$O_2 + H_2O_2 + 2HN_3 \longrightarrow 2N_2O + 2H_2O + N_2 \qquad \text{(l)}$$
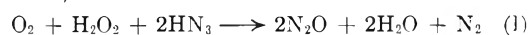
At low concentrations of azide only reaction k takes place; the ratio of mole fraction of gas produced to mole fraction of hydrogen peroxide destroyed is 0.5. At high concentrations of azide only reaction l can take place; the corresponding mole fraction ratio is 2.0. These as well as intermediate values for moderate azide concentrations have been observed by Theorell and Ehrenberg.[4] From the given ratio of gas produced to hydrogen peroxide destroyed we can determine what fraction of hydrogen peroxide has been decomposed catalytically or used in the peroxidatic reaction with azide.

Let $x =$ mole fraction (MF) of H_2O_2 destroyed catalytically and $1 - x =$ MF of H_2O_2 consumed in reaction 1. Then $x/2 =$ MF of gas produced in

(11) Recently Keilin and Hartree[12] have suggested that the "secondary complex" described by Chance[10] actually consists of two inactive complexes. This possibility complicates the simple picture given above but does not necessarily invalidate the general conclusions or interpretations reached. More information is needed about the exact mechanism by which Complex III is generated.

(12) D. Keilin and E. F. Hartree. *Biochem. J.*, **49**, 88 (1951).
(13) R. Lemberg and E. C. Foulkes, *Nature*, **161**, 131 (1948).
(14) E. C. Foulkes and R. Lemberg, *Enzymologia*, **13**, 302 (1949).
(15) Y. Ogura, Y. Tonomura, S. Hino and H. Tamiya, *J. Biochem. (Japan)*, **37**, 153 (1950).
(16) R. F. Beers, Jr., Ph.D. Thesis, Mass. Inst. Tech., 1951.
(17) R. F. Beers, Jr., and I. W. Sizer, in preparation.

(18) D. Keilin and E. F. Hartree, *Nature*, **173**, 720 (1954).

reaction k and $2(1 - x) =$ MF of gas produced in reaction 1. The ratio, R, of substrate destroyed to gas produced is

$$R = \frac{H_2O_2}{gas} = \frac{x + (1 - x)}{\frac{x}{2} + 2(1 - x)} = \frac{2}{4 - 3x} \quad (21)$$

In one aerobic experiment (azide $6.67 \times 10^{-2} M$, catalase–heme $1.3 \times 10^{-7} M$) Theorell and Ehrenberg obtain an R value of approximately 1.0. From equation 21 we find that 66% H_2O_2 was destroyed catalytically, 33% peroxidatically. They point out that when $R = 1$ the net production of O_2 should be zero. This was observed in another experiment using 10^{-3} mole of H_2O_2 and 5×10^{-3} moles of HN_3, but unfortunately the R value was not determined. Increasing azide concentration or decreasing pH increased the final R value but had little effect on the rate of gas production. The reaction was simply prolonged. The rate was zero order during the major portion of the reaction and independent of hydrogen peroxide concentration. Since these ratio values are the final values at the end of the reaction we know very little about the change of R during the course of the reaction. It should be emphasized that the time course of these reactions was of the order of an hour.

A complete explanation of these findings on the basis of the theories presented in this paper or by others does not appear to be possible at present. Particularly difficult to account for is the absence of any effect of hydrogen peroxide concentration on the rate of gas production. It appears very likely that a competition exists between azide and hydrogen peroxide for the primary complex. We may assume, therefore, that f/p does not remain constant or equal to R_k. Thus, we need not expect the rate of catalytic destruction of the substrate to be at all times proportional to its concentration. A reasonable guess to make is that initially the catalytic reaction dominates, yielding initial R values less than unity. Then, as the substrate diminishes the azide reaction increases producing R values greater than unity. The value of R at the end of the reaction represents an average over the entire period. One consequence of this could be as follows. As the rate of oxygen evolution decreases the rate of N_2O and N_2 evolution increases. The net effect is a zero-order rate of gas evolution. It mut be emphasized that under aerobic conditions the small increment of oxygen produced in the catalytic reaction probably has no appreciable effect on the oxidation of ferrous catalase. More-

over in view of the fact that the reaction persists for an hour or more and the initial ratio of hydrogen peroxide to catalase was only 69, we must conclude that at all times the major fraction of the enzyme is in the inactive ferrous form.

Conclusions

In the majority of enzyme systems the extent of inhibition is determined from the rates at which the products appear in the catalyzed reaction. Usually these rates are zero order and in addition to the enzyme are often dependent upon the substrate concentration. The classical illustration of this is the Michaelis–Menten enzyme–substrate system wherein the substrate during the observed time course of the reaction is constant. The concentration of active enzyme is measured directly from the linear rate slope

$$v = kSE$$

where S is constant, E is one of the enzyme forms and k is the composite constant for the Michaelis–Menten equation which usually contains S as a function. In the presence of an inhibitor this equation becomes

$$v_i = kS(E - E_i)$$

Thus the fraction of enzyme inhibited becomes

$$\frac{v - v_i}{v} = \frac{E_i}{E}$$

The important point to note is that S must be the same in both the inhibited and uninhibited reactions.

In contrast with the above, the kinetics of inhibition of the catalase–hydrogen peroxide system is independent of the substrate concentration (except under certain given restricted conditions) even during non-equilibrium states of inhibition. Thus, although the kinetics of the catalase hydrogen peroxide system is more complicated than that of the Michaelis–Menten system in practice the determination of the concentration of active (or inactive) enzyme concentrations is a relatively simple matter easily found from observed first order constants of the time decay of the substrate. With the aid of the analytical solutions of this and the previous paper we can obtain information on free energies, heats and entropies of these inhibitory reactions as well as their corresponding activation energies, entropies and free energies of activation. The experimental problems suggested in these studies will be the subject of future papers.

SURFACE TENSION AT ELEVATED TEMPERATURES. II. EFFECT OF C, N, O AND S ON LIQUID IRON SURFACE TENSION AND INTERFACIAL ENERGY WITH Al₂O₃

By F. A. HALDEN AND W. D. KINGERY

Ceramics Division,[1] Department of Metallurgy,
Massachusetts Institute of Technology, Cambridge, Massachusetts

The effect of additions of C, N, O and S on the surface tension of liquid iron and its interfacial energy with Al₂O₃ have been determined at 1570°. Surface tension of pure iron was found to be 1720 dynes cm.⁻¹. Oxygen and sulfur form monolayers on the surface at concentrations below 0.1%. Surface activity decreases in the order S > O > N > C.

Introduction

Previously it was qualitatively observed that small amounts of oxygen markedly lowered the surface tension of liquid metals.[2] Similarly, sulfur has been reported as surface-active in liquid copper,[3] and silicon has been found to be selectively adsorbed at a liquid iron–aluminum oxide interface.[4] In general, reported data for liquid metal surface tension at elevated temperatures have concerned systems in which minor impurities were not eliminated.

There have been no previous investigations of the quantitative effects of O, N and S in liquid iron. Reported data for C are not in agreement. Data for pure iron vary from 1580[2] to 1380[5] dyne/cm. Data for about 4–5% C vary from 1720[6] and 1100[7] to 600[8] dyne/cm. In the present investigation, the effects of these materials on surface and interface energy for liquid iron in contact with Al₂O₃ have been determined.

Experimental

The sessile drop method previously described[2] has been employed to measure both surface tension and contact angle. The calculated uncertainty of results due to uncertainty of measurements is ±2%. Experimentally, it is found that maximum deviations obtained vary between 1 and 3% for a given composition.

High-purity, vacuum-melted iron (Vacuum Metals Corporation Ferrovac E Ingot) was employed as the base metal for all compositions prepared. This material has the following impurities: 0.0031% C; 0.0072 O; 0.00051 N; 0.005 S; < 0.003 Al; < 0.006 Co; < 0.001 Cu, Mn; < 0.01 Ni, Pb; 0.01 Si; < 0.003 Sn; < 0.003 Mo. Iron alloys with C, O and S were prepared by melting in purified helium after outgassing at red heat *in vacuo*. The alloying agents were placed in the center of iron ingots machined to the shape of the alumina crucible in order to prevent reaction with the container. Alloying additions were spectroscopic grade carbon (National Carbon Corporation), ferric oxide (Baker & Adamson reagent grade), and ferrous sulfide prepared in this Laboratory by passing sulfur vapor (Mallinckrodt, ppt. sulfur) over pure iron turnings in a purified atmosphere. From the resulting alloy ingots, samples (2 g.) were prepared in approximately spherical shape (to

ensure a uniform advancing contact angle), weighed, rinsed with acetone and placed with glass tongs on an Al₂O₃ plaque prepared by calcining aluminum hydroxide (J. T. Baker, reagent grade), pressing and firing at 1850°. Plaque surfaces were polished with a fine diamond lap, washed, dried and used without touching the surfaces, in order to avoid any possible contamination. After placing in the furnace and leveling, the system was heated to 1000° under vacuum (0.005 μ) and then heated to 1570° for measurements in 0.5 atm. of helium. Hospital grade helium was purified with a liquid nitrogen cold trap, Cu₂O at 400° to oxidize any reduced gases, Mg chips at 600° and sponge Ti at 1000° to remove oxidized gases, and activated charcoal at −200°.

Iron–nitrogen compositions were studied using a flow system of purified nitrogen and argon mixed in a flow-meter with a total flow rate giving a displacement of one foot per minute in the furnace. Measurements were made with both increasing and decreasing nitrogen partial pressure in order to ensure that equilibrium was obtained. Nitrogen activity was determined from the partial pressure and Sievert's law

$$a = 0.0393\sqrt{P_{N_2}} \qquad (1)$$

In view of the effect of small amounts of oxygen and sulfur, alloys were analyzed for O, S, N and C before and after surface tension measurements. Compositions and experimental measurements are shown in Table I. No change was found before and after measurements except in the one case indicated.

TABLE I

RESULTS FOR SURFACE TENSION AND CONTACT ANGLE MEASUREMENTS

Composition, %			Surface tension, dyne cm.⁻¹	Contact angle, degree	Interface energy, erg cm.⁻²
Oxygen	Carbon	Sulfur			
0.0006	0.027	0.005	1717	...	...
.0077	0.009	0.005	1632	147.5	2313
.020	...	0.005	1541	121.7	1745
.041	0.009	...	1362	110.2	1406
.07[a]	...	0.010	1151	109.0	1278
.0006	0.027	...	1717	104.5	1365
.0007	0.47	...	1701	106.2	1407
.0016	3.39	...	1708	111.6	1563
.0205	0.003	0.065	1281	127.4	1713
.0215	.004	0.36	976	133.7	1609
.0398	.004	2.00	707	100.8	1067
.0079	.004	1.70	707	119.8	1268

Nitrogen series

Nitrogen, %			Surface tension	Contact angle	Interface energy
0.0004			1731	136	2178
0.0176			1632	136	2110
0.0078			1683	136	2145
0.0278			1578	136	2070
0.0340			1568	136	2063
0.0393			1530	136	2036

[a] 0.092 before testing, 0.060 after testing.

(1) With funds from the U. S. Atomic Energy Commission under Contract Number AT(30-1)-1192.

(2) W. D. Kingery and M. Humenik, Jr., THIS JOURNAL, **57**, 359 (1953).

(3) C. F. Baes and H. H. Kellogg, *J. Metals*, May, 643 (1953).

(4) W. D. Kingery, *J. Am. Cer. Soc.*, **37**, 42 (1954).

(5) F. Becker, F. Harders and H. Kornfeld, *Arch. Eisenhüttenwesen*, **20**, 363 (1949).

(6) J. Kevarian, Thesis, Metallurgy Department, M. I. T., 1954.

(7) P. Kozakevitch, S. Chatel and M. Sage, *Compt. rend.*, **255**, 2064 (1953).

(8) R. V. Stack and S. I. Filippov, *Izvestia Akad. Nauk. S.S.S.R., Otd. Tekh. Nauk.*, No. 3, 413 (1949); Brutcher Translation No. 2476.

Some care was taken to establish a satisfactory value for the density of liquid iron at 1570° since the calculated value of surface tension is directly proportional to density. The mean value found was 7.12 g./cc. with a maximum deviation of 2%. The small additions employed did not affect this value except for the highest carbon concentration where a slight decrease was noted.

Interface energies were calculated from the relation

$$\gamma_{LS} = \gamma_{SV} - \gamma_{LV} \cos \theta \qquad (2)$$

taking a value of 935 ergs/cm.^{2} for the surface energy of Al$_2$O$_3$.[4] An error in this value, or a change due to the presence of liquid iron, will shift the values calculated by a fixed amount, but will not change the slope of the curves.

Discussion

Surface tension and interface energy are plotted as a function of log weight per cent. addition in Fig. 1 and Fig. 2. At these concentrations, the
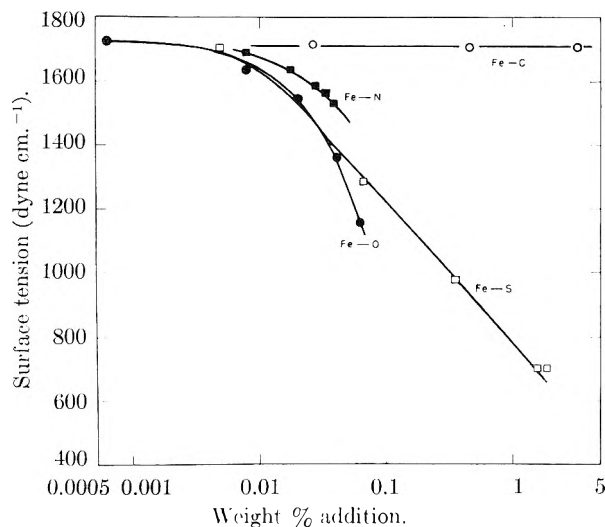
Fig. 1.—Effect of C, N, S and O on the surface tension of liquid iron.
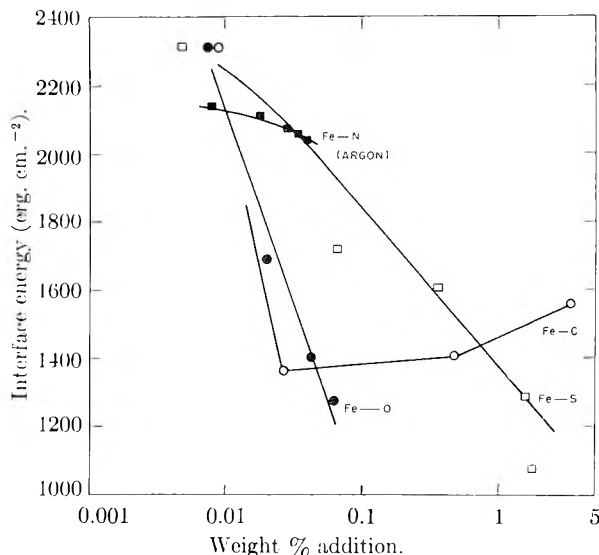
Fig. 2.—Effect of C, N, S and O on the interfacial energy between liquid iron and Al$_2$O$_3$.

activity is essentially equal to concentration for all materials except carbon. Activity coefficients

are available in the literature.[9-12] The excess surface concentration of surface-active materials can be calculated from Gibbs' isotherm

$$\Gamma = \frac{-d\gamma}{RT \, d \ln a} = \frac{-d\gamma}{RT \, d \ln c} \qquad (3)$$

The excess surface concentrations have been determined from the slopes of the curves in Fig. 1 and are plotted in Fig. 3. The excess surface concentration of oxygen rapidly increases until a value of 21.8 × 10^{-10} mole cm.$^{-2}$ is reached at about 0.04%. The area per oxygen atom at the surface is 7.62 Å.^{2}. This is in reasonable agreement with the value of 8.12 Å.^{2} per atom in the plane of maximum packing in FeO[13] (and the value of 6.78 Å.^{2} calculated from Pauling's[14] radius of 1.40 for O$^=$).
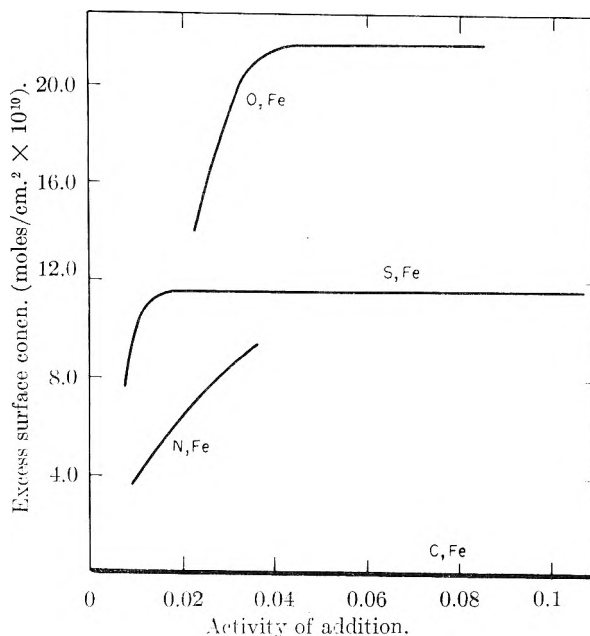

Fig. 3.—Excess surface concentration of additions to iron at 1570°.

The excess surface concentration of sulfur rapidly increases until a value of 11.6 × 10^{-10} mole cm.$^{-2}$ is reached. This concentration corresponds to an area of 14.4 Å.^{2} per atom which is somewhat larger than the value of 11.56 Å.^{2} per atom in the plane of maximum packing in FeS[13] (and the value of 10.49 Å.^{2} calculated from Pauling's[14] radius of 1.84 for S$^=$). At low concentrations, sulfur is seen to be more highly surface active than oxygen due to its large ionic size, leading to the ion becoming highly polarized by the iron ionic potential. However, with complete surface coverage, the rate of surface tension lowering with concentration be-

(9) J. Chipman, Faraday Soc. Discs., 4, 44 (1948).

(10) C. W. Sherman, H. J. Elvander and J. Chipman, Trans. A. I. M. E., 188, 334 (1950).

(11) C. W. Sherman and J. Chipman, J. Metals (June, 1952); Trans. A. I. M. E.

(12) J. A. Kitchener, J. O'M. Bockris and A. Liberman, Faraday Soc. Discs., 4, 49 (1948).

(13) R. G. Wyckoff, "Crystal Structures," Interscience Publishers Co., New York, N. Y., 1948.

(14) L. Pauling, "The Nature of the Chemical Bond," Cornell Univ. Press, Ithaca, N. Y., 1945.

comes greater for oxygen than is the case for sulfur. Nitrogen has a smaller effect on surface tension, decreasing the surface tension by only 200 dyne cm.$^{-1}$ at 1 atm. pressure of nitrogen. At this concentration, the excess surface concentration was 8.3×10^{-10} mole cm.$^{-2}$, which is only a small fraction of a hexagonal close-packed monolayer (95×10^{-10} mole cm.$^{-2}$). Carbon has no effect on the surface tension of pure iron at 1570°.

Results for interface energy shown in Fig. 2 give values for the excess surface concentration of oxygen, sulfur and nitrogen, which are in good agreement with surface adsorption except that a complete layer of oxygen is formed at a somewhat lower concentration. The experimental points for sulfur show more scatter, which is probably due to the increased effects of small amounts of oxygen on the interface energy. While carbon has no effect on the surface energy, it does have a considerable effect in lowering the interface energy. Increases in carbon content above 0.1% increase the value, however. Observation of the interface indicates a marked discoloration, and the probable effect of carbon is to react with the Al_2O_3. Attempts to identify a new phase at the surface by X-ray techniques were unsuccessful. Increasing carbon content may cause a slight increase in interface energy due to the lowering of oxygen activity.

The effects of minor additions of oxygen and sulfur on the surface tension of pure iron and its interface energy with Al_2O_3 are considerable with amounts below 0.1% forming approximately a monolayer at the surface. Nitrogen has considerably less effect, and carbon has no effect. The surface activity decreases in the order: S > O > N > C, which is the order of decreasing atomic size and polarizability. Surface activity measured as atoms entering the surface layer per wt. per cent. addition at low concentrations (see Fig. 3) are directly proportional to the polarizability.

The surface tension of 1720 dyne cm.$^{-1}$ for pure iron at 1570° found here is somewhat higher than previous values reported. The higher value is due to decreased surface contamination by atmosphere and impurities. Surface tension–concentration curves for small additions indicate that 1720 dyne cm.$^{-1}$ can be accepted as a true surface tension result for pure liquid iron at 1570°.

METAL–POLYELECTROLYTE COMPLEXES. III. ENTROPY AND ENTHALPY OF COMPLEXATION FOR POLYACRYLIC ACID–COPPER SYSTEMS

By Ernst M. Loebl, Lionel B. Luttinger[1] and Harry P. Gregor

Contribution from the Department of Chemistry of the Polytechnic Institute of Brooklyn, New York

Entropy and enthalpy changes in complexation reactions between linear and cross-linked polyacrylic acid and copper(II) were studied by measuring temperature dependence of the equilibrium constants. It appears that, as in the case of other chelation reactions, the main contribution to the complex stability is that of the entropy. The differences between the linear and cross-linked material are small; however, it appears that the entropy factor is more favorable in the case of the linear polymer, reflecting probably its greater flexibility.

Introduction

In the course of investigations of the complexation equilibria between polyelectrolytes and copper reported on previously,[2,3] it was felt desirable to study also the temperature dependence of some of these equilibria so as to measure the enthalpy and entropy change in these reactions, and compare them if possible with corresponding values for reactions involving similar non-polymeric systems.

Complexation constants of linear polyacrylic acid (PAA) and of cross-linked polyacrylic acid (resin XE 89. see ref. 3 for description) with copper were accordingly measured at three different temperatures.

Experimental

The experimental details were essentially as described before.[2] Data were obtained both in the absence and in the presence of copper; however, the temperature was now controlled to ±0.5°. The XE 89 resin was measured at 3, 25 and 40° and the linear material at 10, 25 and 40°. The readings were repeated until the pH remained constant. Intermittent shaking was performed manually on the samples at frequent intervals, between which they were kept at the temperature of choice. Experiment showed that the equilibria were reached in only a moderately longer period of time than before.

To facilitate the calculations, exactly 0.300 g. of resin was taken for each sample, and the same samples were used at each of the three temperatures of measurement. No colorimetric determinations of the solution phase were performed with the resin systems. The pH readings of the resin systems were performed as follows. A 50-ml. sample of supernatant solution was pipetted off into a dry beaker, allowed to reach room temperature, and the pH read. The sample was then returned to the system. In this way the pH was measured without disturbing the equilibrium of the system. For the linear material, this procedure could not be followed and the pH of the system was read directly. Appropriate temperature corrections were made, including that for changes in the pH of the standard buffer.

Results and Discussion

The complexation constants B_2 were calculated at each temperature by the method described previously.[2] From the slope of the plot of ln B_2 vs. $1/T$, ΔH for the reaction was obtained; ΔF was

(1) A portion of this work is abstracted from the Dissertation of Lionel B. Luttinger, submitted in partial fulfillment of the requirements for the degree of Doctor of Philosophy in Chemistry, Polytechnic Institute of Brooklyn, June, 1954.

(2) H. P. Gregor, L. Luttinger and E. M. Loebl, This Journal, **59**, 34 (1955).

(3) H. P. Gregor, L. Luttinger and E. M. Loebl, *ibid.*, **59**, 366 (1955).

Table I

System	B_2 ΔH, kcal./mole	ΔF, kcal./mole	ΔS, e.u.	K_2 ΔH, kcal./mole	ΔF, kcal./mole	ΔS, e.u.	K_a ΔH, kcal./mole	ΔF, kcal./mole	ΔS, e.u.
PAA in 1 M KCl	3.7	4.8	−3.9	0.5	−8.0	28	1.6	6.4	−16
XE 89 in 2 M NaNO₃	0.8	4.6	−13	0.4	−9.5	33	0.2	7.1	−23

obtained from the value of ln B_2 at 25° and ΔS was calculated from the difference $\Delta H - \Delta F$.

The constants K_2 were also calculated from the B_2's and the acid dissociation constants K_a which were also determined at each temperature. From these the ΔH, ΔF and ΔS values for the reactions characterized by the derived constant K_2 were also obtained.

Table I summarizes the results.

Bearing in mind that the constant B_2 refers to the displacement of the bound hydrogen ion by the copper ion, and the constant K_2 to the combination of the carboxylate ion with copper ion, *i.e.*, B_2 refers to the reaction

$$2RCOOH + Cu^{++} \longrightarrow (RCOO)_2Cu + 2H^+$$
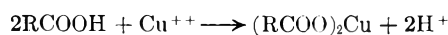
and K_2 to the reaction

$$2RCOO^- + Cu^{++} \longrightarrow (RCOO)_2Cu$$
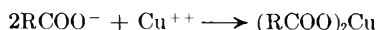
the following general conclusions can be drawn from the data obtained.

For the combination reaction it appears here as in the case of other complexation or chelation reactions[4,5] that the main contribution to the complex stability is the entropy contribution.

The values for the linear and cross-linked polyacrylic acid are very similar and especially the enthalpy values are practically identical, showing that the difference between the heats of hydration of the carboxylate ion and the metal ion and the heat of formation of the carboxylate–metal bond is quite independent of the nature and structure of the chain.

(4) C. G. Spike and R. W. Parry, *J. Am. Chem. Soc.*, **75**, 2726, 3770 (1953).

(5) A. E. Martell and M. Calvin, "Chemistry of the Metal Chelate Compounds," Prentice–Hall, Inc., New York, N. Y., 1952.

For the displacement reaction (characterized by B_2) the enthalpy term is again rather small and positive while the entropy term is now negative reflecting the tremendous loss in entropy concomitant with the displacement of the hydrogen ion which is only partially compensated by the entropy gain through the attachment of the metal ion. It appears here that the closeness of the complexation constants for linear and cross-linked PAA as shown by the ΔF values is due to a cancellation of two opposing factors: while the net enthalpy change ΔH is less favorable in the linear than in the cross-linked case, the reverse is true for the entropy factor. Nothing can be said about the former since the net enthalpy change represents certainly a small difference between large quantities; however, the latter probably shows the influence of the greater flexibility of the linear polymer chain which makes possible a smaller entropy loss upon complexation than in the case of the cross-linked polymer.

The differences between the respective values referring to B_2 and K_2 refer to the dissociation reaction

$$RCOOH \longrightarrow RCOO^- + H^+$$

It is seen that the linear polymer shows a larger heat of reaction and smaller (negative) entropy effect than the cross-linked polymer. No simple explanation can be advanced.

SOLID SOLUTIONS OF THE ALKALI HALIDES. III. LATTICE CONSTANTS OF RbBr–RbCl AND RbBr–KBr SOLID SOLUTIONS[1]

BY GEORGE S. DURHAM, LEROY ALEXANDER, DOUGLAS T. PITMAN, HELEN GOLOB AND HAROLD P. KLUG

Contribution from the Department of Research in Chemical Physics, Mellon Institute, Pittsburgh, Pa., and the Department of Chemistry, Smith College, Northampton, Mass.

Lattice constants in the solid-solution systems RbBr–RbCl and RbBr–KBr have been determined at 25° by means of X-ray diffraction measurements, with an average estimated probable error of ±0.01%. Theoretical values previously calculated through a consideration of ionic displacements are found to be in reasonably satisfactory agreement.

Introduction

In paper II of this series,[2] lattice constants, heats of mixing and distributions between aqueous and solid solutions were calculated for four alkali-halide solid-solution systems, on the basis that the ions in a given solution are not at a constant nearest neighbor distance, but may be displaced from normal lattice points to positions of minimum potential energy. Comparison of the theoretical heats of mixing and distributions with available experimental values showed good agreement. Since, however, no dependable data existed for lattice distances,[3] it was not possible at the time to draw any conclusions regarding the theoretical values for these, other than that they appeared to be more reasonable than any previously obtained.

For two of the systems, RbBr–RbCl and RbBr–KBr, studied in paper II, solid-solution samples were available. In order to gain further information about solid-solution relationships, as well as to make possible comparison with theoretical values, it seemed worth while to obtain experimental lattice-constant data for these.

Experimental

The solid solutions used were prepared by Durham, Rock and Frayn[4] in their study of the ternary aqueous systems. In addition to the analyses reported in the original study, the rubidium salts used for preparation of the solid solutions have been analyzed flame-spectrophotometrically for their Li$^+$, Na$^+$, K$^+$ and Cs$^+$ ion contents, and the Rb-Br–RbCl solid-solutions for their K$^+$ ion content. Emission-spectrographic analyses of the salts disclosed that no other cations were present in significant amounts. In the three original salts the potassium content ranged from 0.43 ± 0.02% to 1.09 ± 0.03% and the cesium from 0.17 ± 0.01% to 1.84 ± 0.03%, by weight; lithium and sodium were found in negligible amounts, less than 0.01 and 0.02%, respectively. These results are shown in Tables I and II, expressed in units of mole per cent. In the K$^+$ and Cs$^+$ ion determinations the enhancing effect of a large excess of Rb$^+$ ions was allowed for by careful preparation of calibration standards containing amounts of Rb$^+$ ions comparable to the unknown solutions being analyzed.

The original bromide–chloride compositions for the Rb-Br–RbCl solid solutions, which were obtained indirectly by determination of total halide, have been recalculated to take into account the effects of the potassium actually found present (from 0.43 to 1.00% by weight), and these corrected compositions are used in the present paper. The possible effects of the K$^+$ and Cs$^+$ ion contamination are brought out later in the discussion of the results.

The coarsely-crystalline solid-solution samples were reduced to sufficient fineness for diffraction analysis by grinding each in an agate mortar for a few minutes. Suitable specimen mounts were then prepared by mounting a thin layer of powder on the outside of a fine Pyrex capillary tube (about 0.3-mm. outside diameter) with Duco cement, the total diameter of the cylindrical mount being about 0.4 mm. The powder patterns were prepared in an improved Norelco Debye–Scherrer camera of 114.6-mm. diameter using nickel-filtered CuK radiation. In order to obtain optimum definition of lines a 0.5-mm. pinhole collimator was employed, which necessitated exposures of 12 to 15 hours. The film was placed in the camera in the asymmetric, or Straumanis, position,[5] which is superior for precision measurements because it permits the determination of the film radius directly from the diffraction data. All diffraction patterns were prepared at laboratory temperature, the mean temperature of each exposure being ascertained with an accuracy of ±0.4° or better. The lattice constants as measured at laboratory temperature were finally corrected to 25° using the previously determined linear thermal expansion coefficient, α, which for the three salts involved, lies between 37 and 38 × 10^{-6}/degree.[6] Because of the close agreement of α for the pure salts, it seemed very unlikely that the coefficients of the solid solutions formed from the compounds could differ much from these same values.

The extrapolation method of Bradley and Jay[7] was used to obtain the best value of each lattice constant from the several values calculated for lines between $\theta = 60$ and $90°$. The efficacy of this method has been established by time, and it has the advantage over Cohen's analytical method[8] that the relative quality of the various lines can be taken into account in performing the extrapolation. The number of lines utilized in the extrapolations ranged from 4 to 11 depending upon the quality of the pattern. In three cases (samples No. 4A, 4B and 6A of the RbBr–KBr series, Table II) these back-reflection lines were so poorly defined that satisfactory extrapolations against cos^2 θ could not be made; instead the extrapolations were performed using the function cos^2 θ (1/sin θ + 1/θ), which makes use of reflections in the larger angular range $\theta = 30$ to $90°$.[9]

Results

The lattice constants for the two solid-solution series RbBr–RbCl and RbBr–KBr are listed in Tables I and II, respectively. The values are given in true ångström units. It should be mentioned that the lattice constants given have not been corrected for the refraction of the X-rays, since the magnitude of this correction is much

(1) The flame-spectrophotometric analyses of the study were done by Helen Golob, and the X-ray diffraction measurements were made by L. E. Alexander, D. T. Pitman and H. P. Klug, all of the Department of Research in Chemical Physics, Mellon Institute. Comparison of the theoretical and experimental results is by G. S. Durham of the Department of Chemistry, Smith College.

(2) G. S. Durham and J. A. Hawkins, *J. Chem. Phys.*, **19**, 149 (1951).

(3) F. Oberlies, *Ann. Physik*, **87**, 238 (1928), has measured lattice constants for KBr–KCl solid solutions; however, no temperatures are given, and the average deviation of her results is large, ±0.06%. R. J. Havighurst, E. Mack, Jr., and F. C. Blake, *J. Am. Chem. Soc.*, **47**, 29 (1925), have obtained a value for 50 mole % KBr–KCl and two values for the RbCl–KCl system, but the small number and poor overall accuracy of these results made them useless for our purpose.

(4) G. S. Durham, E. J. Rock and J. S. Frayn, *ibid.*, **75**, 5792 (1953).

(5) M. E. Straumanis, *J. Appl. Phys.*, **20**, 726 (1949).

(6) "Physikalisch-Chemische Tabellen," Vol. II, Verlag von Julius Springer, Berlin, 1923, p. 1223.

(7) A. J. Bradley and A. H. Jay, *Proc. Phys. Soc.*, **44**, 563 (1932).

(8) M. U. Cohen, *Rev. Sci. Instruments*, **6**, 68 (1935); **7**, 155 (1936).

(9) A. Taylor and H. Sinclair, *Proc. Phys. Soc.*, **57**, 126 (1945); J. B. Nelson and D. P. Riley, *ibid.*, **57**, 160 (1945).

TABLE I

EXPERIMENTAL LATTICE CONSTANTS OF RbBr–RbCl SOLID SOLUTIONS

Sample	Mole % RbBr	Mole % RbCl	K(Br, Cl)	Mean temp. of measurement (°C.)	a_0 in Å. (25°)	Estimated probable error (Å.)	$\Delta r = \frac{1}{2}[a_0(\exp.) - a_0(\text{Veg.})]^d$
1 (RbCl)[a]	0.00	95.0	3.39	29.2	(6.5914)[b] 6.5869	±0.0004	0.0000
2	3.78	93.1	3.09	27.4	6.5946	.0004	+ .0007
3A	15.8	81.6	2.61	28.0	6.6298	.0004	− .0018
3B	15.5	81.6	2.95	28.3	6.6304	.0004	− .0003
4	34.2	63.5	2.36	28.1	6.6915	.0004	+ .0007
5	47.7	50.1	2.28	27.9	6.7357	.0006	+ .0021
6A	77.8	20.4	1.88	27.1	6.8290	.0006	+ .0014
6B	77.9	20.0	2.11	28.1	6.8259	.0010	− .0002
7	93.2	5.05	1.79	26.7	6.8700	.0006	− .0014
8 (RbBr No. 1)[c]	95.3	0.00	3.18	26.1	(6.8946)[b] 6.8900	.0004	

[a] This sample also contained 1.66 mole % CsCl. [b] These values were obtained by extrapolation to zero % impurity, using Vegard's law. [c] This sample also contained 1.52 mole % CsBr. [d] Values of a_0(Veg.) were calculated using a_0(RbBr) = 6.8936 Å.

TABLE II

EXPERIMENTAL LATTICE CONSTANTS OF RbBr–KBr SOLID SOLUTIONS

Sample	Mole % RbBr	Mean temp. of meas. (°C.)	a_0 in Å. (25°)	Estimated probable error (Å.)	$\Delta r = \frac{1}{2}[a_0(\exp.) - a_0(\text{Veg.})]^f$
1 (KBr)[a]	0.0	26.6	6.5982 (6.5988)[b]	±0.0004	0.0000
2A	10.0	25.4	6.6284	.0004	.0000
2B	9.9	23.1	6.6291	.0004	+ .0006
3A	26.7	23.5	6.6766	.0004	− .0006
3B	26.8	26.6	6.6768	.0004	− .0006
4A	50.8	25.4	6.7493	.0010	+ .0004
[4B	50.8	26.2	6.7433	.0006	− .0026
5A[c]	65.8	24.4	6.7932	.0010	+ .0007
5B	67.8	23.9	6.8005	.0008	+ .0009
6A[c]	79.7	22.0	6.8341	.0008	+ .0002
6B	82.0	23.4	6.8393	.0006	− .0006
7A[c]	90.8	23.0	6.8591	.0008	− .0036
7B	91.7	21.9	6.8640	.0006	− .0025
8 (RbBr No.1)[d]	95.3	26.1	6.8900 (6.8946)[b]	.0004	
9 (RbBr No. 2)[e]	98.0	25.9	6.8884 (6.8936)[b]	.0005	.000

[a] This sample contained 0.2 mole % KCl. [b] These values were obtained by extrapolation to zero % impurity, using Vegard's law. [c] RbBr No. 1 was used in making up these solid solutions. The others were prepared from RbBr No. 2. [d] RbBr No. 1 contained 3.18 mole % KBr and 1.52 mole % CsBr. [e] RbBr No. 2 contained 1.79 mole % KBr and 0.21 mole % CsBr. [f] Values of a_0(Veg.) were calculated using a_0(RbBr) = 6.8936 Å.

smaller than the errors of measurement. Allowance for refraction would increase all the values by 0.0001 Å.

Discussion

For purposes of comparison, both the experimental results of this paper and the theoretical values of reference (2) have been converted into differences from the corresponding nearest-neighbor lattice spacings calculated according to the Vegard's-law relationship of additive lattice constants. Values of the pure-salt lattice constants required for calculating Vegard distances were obtained by algebraically extrapolating the experimental values for the original salts to zero % K+ and Cs+ ion, according to Vegard's law. The interionic distances used for the face-centered forms of CsCl and CsBr were those calculated by Pauling.[10] Some indication of the validity of this

(10) L. Pauling, "The Nature of the Chemical Bond," 2nd Edition, Cornell University Press, Ithaca, N. Y., 1942, p. 358.

procedure in the case of small impurity concentrations is given by the close agreement (within 0.0005 Å.) of the extrapolated values for the nearest-neighbor distances obtained from two samples of RbBr which differed widely in the amounts of K+ and Cs+ ion present. Since RbBr No. 2 was considerably purer, its value was used in the subsequent calculations.

The Vegard values for the RbBr–RbCl system were calculated to include the effects of the potassium impurity content, which was known for each sample by direct analysis. It is interesting to note that almost exactly the same results are obtained here whether or not the potassium impurity in the solid solutions is considered. The effect on the analytical calculations of taking the potassium into account is to increase the percentage of bromide. However, when the Vegard lattice distances are calculated, the effect of a greater proportion of large bromide ion is counterbalanced by the effect of the small K+ ion.

Due to a similar size–weight relationship for the Cs+ ion, whether or not it is taken into account is immaterial as far as the Vegard interionic distances in the solid solutions are concerned. For this reason it was not thought worth while to analyze the solid solutions for cesium, particularly since the distribution ratio obtaining for small Cs+ ion concentrations would be such that most of the Cs+ ion would remain in the aqueous phase during the preparation of the solid solutions. Evidence for the correctness of these conclusions is given by the excellent agreement in the RbBr–KBr system between |r(exp.) − r(Veg.)| values for duplicates made up using two RbBr samples which varied widely in cesium content.

Differences between Vegard values and those calculated according to the ninth-power mixing rule have also been obtained, since they are closely comparable to the theoretical values which result when ionic displacements are not considered. The use of deviations from Vegard's law for comparisons obviates any inconsistencies due to slight differences in the pure-salt values taken for the theoretical calculations.

The derived experimental data described above are included in Tables I and II, and the theoretical data are listed in Table III; for comparison both

TABLE III

THEORETICAL NEAREST-NEIGHBOR DISTANCES IN ALKALI–
HALIDE SOLID SOLUTIONS

N_{RbBr}	r (theor.),[a] Å.	Δr (theor.-Veg.)	r (9th power), Å.	Δr (9th pow.-Veg.)
		I. RbBr–RbCl		
0.0	(3.2935)	0.0000	(3.2935)	0.0000
.1	3.3108	+ .0022	3.3113	+ .0027
.3	3.3416	+ .0028	3.3448	+ .0060
.5	3.3722	+ .0031	3.3757	+ .0066
.7	3.4018	+ .0025	3.4046	+ .0053
.9	3.4304	+ .0009	3.4317	+ .0022
1.0	(3.4446)	.0000	(3.4446)	.0000
		II. RbBr–KBr		
0.0	(3.2997)	0.0000	(3.2997)	0.0000
.1	3.3146	+ .0004	3.3167	+ .0025
.3	3.3442	+ .0011	3.3487	+ .0056
.5	3.3735	+ .0013	3.3783	+ .0061
.7	3.4019	+ .0007	3.4061	+ .0049
.9	3.4298	− .0003	3.4322	+ .0021
1.0	(3.4446)	.0000	(3.4446)	.0000

[a] Taken from ref. (2).

are plotted in Fig. 1. In the graph, the average has been used for near-duplicate experimental values, except for one point in the RbBr–KBr system, where an extremely low value was discarded.

In the RbBr–RbCl system, the theoretical points are seen to fall somewhat higher than the experimental, although the over-all agreement is far better than for the old ninth-power values. In the RbBr–KBr system, the agreement is in general excellent, with the exception of the solid solution richest in rubidium bromide.

It was at first thought that the negative deviations which occur in both systems might be due to use of too high lattice constants for the pure salts. However, with the exception of cesium, which was corrected for, the only impurity which might be expected to give rise to such high values was iodide, and this element was shown to be absent. It is interesting to note that in the systems KBr–
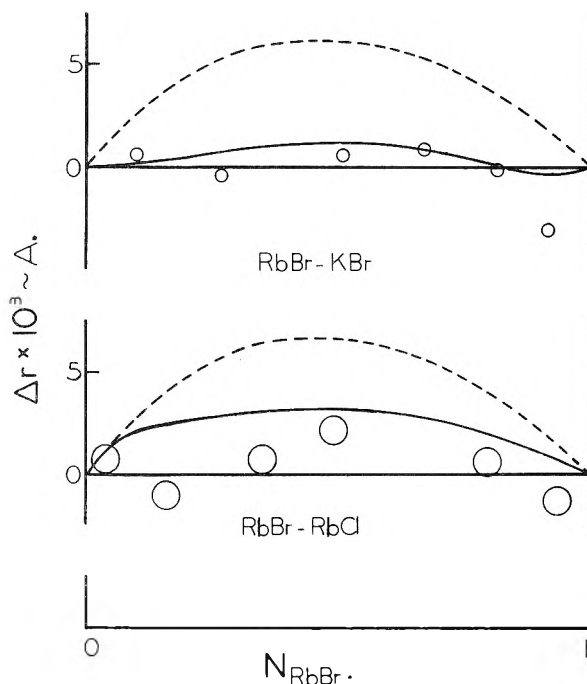

Fig. 1.—Experimental and theoretical nearest-neighbor distances in alkali–halide solid solutions, expressed as deviations from Vegard's-law values: O, exptl.; —, theor., ---, 9th power.

KCl[3] and thallium alum–ammonium alum,[11] negative deviations have also been found to occur; however, the deviations fall within the possible experimental error and hence, in their cases, no definite conclusions can be drawn.

It is felt that the present experimental curves, which are doubly sigmoidal in shape, with the greatest tendency toward negative deviations from Vegard's law being found at high mole fractions of rubidium bromide, give a valid picture of the lattice-constant relationships in such alkali–halide solid solutions. Although the theoretical methods of reference (2) are not sufficiently sensitive to give detailed agreement with the experimental, they lead on the whole to lattice constants of the correct magnitude.

(11) H. P. Klug and L. E. Alexander, *J. Am. Chem. Soc.*, **62**, 2993 (1940).

THE STRUCTURE OF SILICA-ALUMINA CRACKING CATALYSTS[1]

By Joseph D. Danforth

Contribution from the Department of Chemistry, Grinnell College, Grinnell, Iowa

Received January 21, 1955

A study of the acidity developed in condensation products of certain methylsiloxanes and aluminum hydroxide indicated that compounds of definite atomic ratios of silicon to aluminum were formed as a function of the number of the available hydroxyl groups on the silicon. A logical extension of these data indicates that the active centers of the silica–alumina catalyst can be represented as a combination of a Lewis acid (three coördinated aluminum) and a Brönsted acid. The proposed structure permits correlation of much of the known data on cracking catalysts.

The structure of silica alumina cracking catalysts has been deduced from information obtained in a study of the reactions between the hydrolysis products of methyltriethoxysilane, dimethyldiethoxysilane, trimethylethoxysilane and hydrolyzed aluminum isopropoxide. The acidity which was developed in mixtures of the hydrolyzed products as a function of the added aluminum isopropoxide indicated specific silicon to aluminum ratios which can be represented by chemical structures. Geometric considerations, involving the number of hydroxyl groups condensing per silicon atom, lead to plausible structures for the atomic ratios of silicon to aluminum which have been suggested. The proposed catalyst structure has been found to be consistent with a vast amount of physical and chemical data which have been compiled on silica–alumina composites.

Experimental

Materials.—Methyltriethoxysilane, dimethyldiethoxysilane and trimethylethoxysilane were purchased from Dow Corning Corporation. Aluminum isopropoxide obtained from Matheson–Coleman and Bell was redistilled before use.

Procedure.—Into 250-ml. clear glass bottles were introduced 50-ml. samples of a 3 to 1 isopropyl alcohol–water solution containing 10 mmoles of the desired methylsiloxane. The bottles were stoppered and allowed to stand at room temperature for 48 hours to assure hydrolysis of the ethoxyl groups. The desired amount of a 0.50 molar solution of aluminum isopropoxide in benzene and isopropyl alcohol solution was added from a buret, each bottle stoppered, shaken and allowed to stand for 24 hours. Phenolphthalein was added and the acidity determined by titration with standard sodium hydroxide. The first portions of sodium hydroxide were neutralized rapidly in those bottles where

Fig. 1.—Developed acidity as a function of aluminum content for 10-mmole portions of the siloxane: O, trimethylethoxysilane; △, dimethyldiethoxysilane; ●, methyltriethoxysilane.

(1) Presented before the Petroleum Division of the American Chemical Society, April, 1955.

acidity developed, while neutralization became slow as the end-point was approached. Sodium hydroxide was added in small increments until a pink color persisted on standing overnight. The small excess of base was back titrated with standard acid.

Results

The millimoles of acid are plotted as a function of the added aluminum for 10 mmoles of each siloxane in Fig. 1. The hydrolyzed products of trimethylethoxysilane and aluminum isopropoxide did not develop acidity as a function of the aluminum content. There was developed one mole of acid for each added aluminum up to two millimoles of acid per 10 mmoles of dimethyldiethoxysilane which corresponds to an atomic ratio of 5Si to 1Al. A clear solution was obtained on neutralization up to the point at which the addition of aluminum isopropoxide caused no additional acid. Beyond this point a floc, presumed to be aluminum hydroxide, remained undissolved at the phenolphthalein end-point.

Methyltriethoxysilane gave slightly less than one hydrogen ion per aluminum up to a value of 3.32 to 3.39 mmoles of aluminum isopropoxide per 10 mmoles of the siloxane, which corresponds to an atomic ratio of 3Si to 1Al.

Incomplete hydrolysis, high concentrations of solutions and short reaction times tend to give less acidity per aluminum than is indicated in Fig. 1. Since it was not the purpose of this work to investigate the effect of these variables, conditions were chosen so that higher dilution, longer times of hydrolysis and longer reaction times did not alter significantly the data of Fig. 1.

Studies of base exchange capacity and acidity of silica–alumina composites as a function of the alumina content have indicated maximum values at 30 wt. % alumina[2] which correspond to an atomic ratio of 2Si to 1Al.

The atomic ratio of silicon to aluminum appears to be a function of the number of hydroxyl groups on each silicon atom which is available to form siloxane linkages. Thus, two hydroxyl groups gave a ratio of 5Si to 1Al; three hydroxyl groups, a ratio of 3Si to 1Al; and four hydroxyl groups, as in the cracking catalyst, a ratio of 2Si to 1Al. A single hydroxyl group on a silicon did not develop acidity as a function of the added aluminum isopropoxide.

If a single hydroxyl group on the silicon gives no acidity, while two hydroxyl groups produce acidity, the aluminum must be involved in a reaction with two hydroxyl groups in order to produce acidity.
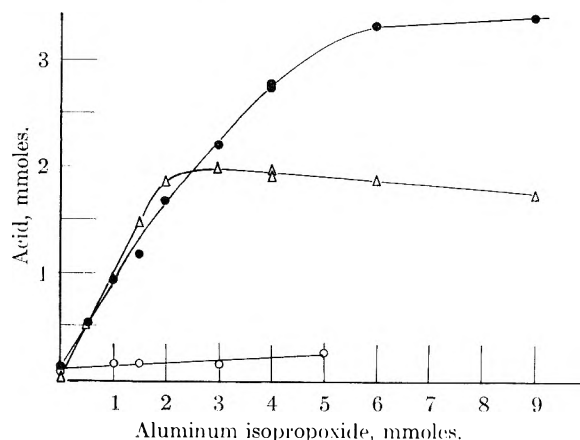
(2) A. G. Oblad, T. H. Milliken, Jr., and G. A. Mills, "Advances in Catalysis," Vol. III, Academic Press, Inc., New York, N. Y., 1951, pp. 221–223.

Bond angles, the exact 5 to 1 ratio, and other factors overwhelmingly favor the cyclic structure shown as A of Fig. 2. Structure A may be dehydrated to structure B which may be further dehydrated to structure C.

The structure resulting from methyltriethoxysilane differs from structure A in that a methyl group has been replaced by a hydroxyl group which can undergo further condensation. Utilization of 4 of the 5 available hydroxyl groups leads to the polymeric structure shown diagrammatically as D of Fig. 2. When infinitely extended, structure D predicts an atomic ratio of 3Si to 1Al. Calcination results in the dehydration of the acid as shown in A and B, and probably leads to the formation of siloxane linkages between adjacent surfaces of the structure, D.

A structure representing that which obtains when four hydroxyl groups are available is shown as E. Extension of this structure leads to an atomic ratio of 2Si to 1Al. It would be expected to undergo dehydrations similar to those discussed, and in this form be representative of a calcined cracking catalyst. Representations have been made on a plane surface to illustrate the structures. Atomic models better represent the structures in three dimensions and indicate that a number of isomers may form, in structures D and E, depending on the direction and the position of the hydroxyl groups which form the siloxane linkages.

The proposed structure is consistent with many observations regarding the nature of the cracking catalyst. It accounts for the acidity and base exchange capacity of cracking catalysts. The dehydrated structure similar to B, when present in the calcined structure, E, can be represented as

$>$Al–OH and appears to this writer to represent the active component of the cracking catalyst. The reaction of hydrocarbons, or traces of moisture with the structure C, is believed to lead to the regeneration of the structure B. The active structure represents a Lewis acid as it reverts from three to four coördination by reaction with water or hydrocarbon, and, at the same time, is a Brönsted acid by virtue of the available proton. This combination appears essential to the cracking reaction, and is analogous to the use of anhydrous hydrogen chloride (Brönsted acid) in conjunction with anhydrous aluminum chloride (Lewis acid) in reactions of isomerization. This dual nature of the cracking catalyst may account for the results of Stright[3] in which olefins were extensively decomposed by catalysts which had undergone sufficient base exchange that they were no longer active for cetane cracking. It would appear that the Lewis acid, alone, catalyzed olefin decomposition, while the combination of the Lewis acid and Brönsted acid was necessary for the cracking of cetane.

The work of Tamele,[4] in which it was shown that in the presence of an excess of silica sol, no free aluminum hydroxide was precipitated by a base, is easily explained by the proposed catalyst structure.

(3) Paul Stright and Joseph D. Danforth, This Journal, **57**, 448 (1953).

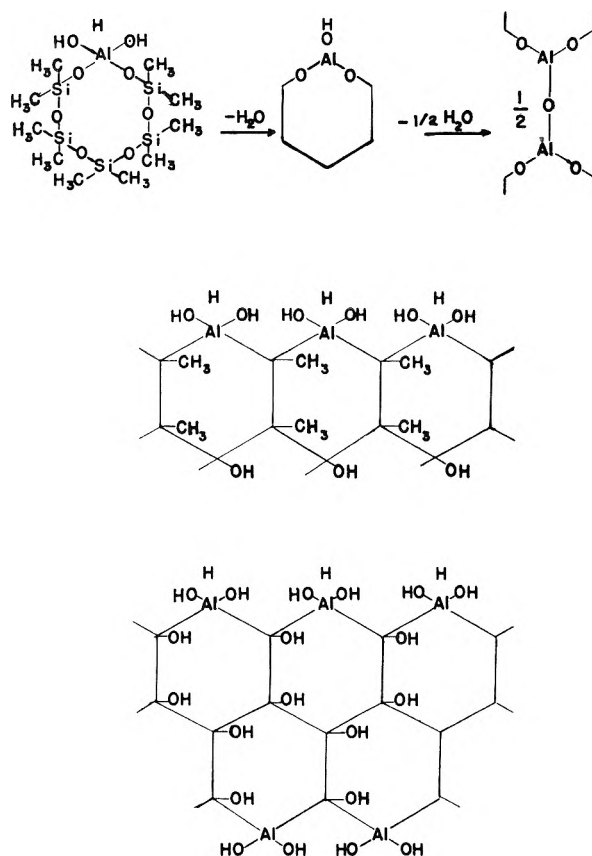(4) M. W. Tamele, "Heterogeneous Catalysis," Faraday Society, April, 1950, p. 270.

Fig. 2.—Structural representation of products: A, dimethyldiethoxysilane, hydrated form; B, dehydrated form of A; C, dehydrated form of B; D, methyltriethoxysilane, hydrated form; E, hydrated structure of silica-alumina catalyst.
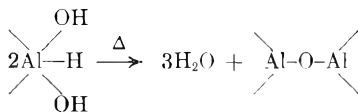
It is significant that "the reaction of aluminum hydroxide proceeds rapidly with fresh silica gel, less readily with aged gel, and only very slowly with thoroughly aged gel." This observation implies that silica rings or chains of some stability can form in the absence of alumina. On aging, the number of stable siloxane linkages between the silica increases and makes it more difficult to introduce an aluminum into the silica ring.

The work of Oblad[5] in which it is shown that dried silica alumina gels, which had been exchanged with ammonia, evolved one mole of water per mole of ammonia on calcination, is exactly what would be predicted on the basis of the proposed structure as shown by the equation
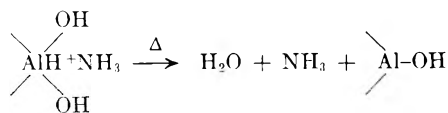
The discrepancies observed by Oblad above 20% alumina indicate incomplete utilization of alumina in catalyst formation in this range. When the ammonium salt is converted to the acid, and completely dehydrated, there would be exactly 1.5 waters per aluminum as suggested by Oblad and shown below

(5) Reference 2, pp. 223–225.

$$2Al{\overset{OH}{\underset{OH}{\diagdown\diagup}}}H \overset{\Delta}{\longrightarrow} 3H_2O + {\overset{\diagdown}{\underset{\diagup}{}}}Al-O-Al{\overset{\diagup}{\underset{\diagdown}{}}}$$

The proposed catalyst structure is consistent with the idea of linear arrangements of active centers as suggested from the poisoning studies with alkali metal ions.[6]

It is consistent with the presence of both NH_3 and $NH_4{}^+$ as reported by Mapes and Eischens.[7]

The present report has been limited to the inorganic structure of the silica–alumina catalyst. Many additional pieces of information about the cracking catalyst can be explained on the basis of the proposed structure. Correlation of reaction

mechanisms and deuterium exchange data with the suggested structure will be the subject of another paper. The extension of the present techniques to other cracking composites, and the general application of this technique to the study of inorganic structures other than catalysts remains to be investigated.

Summary

A study of the acidity developed in the condensation products of aluminum hydroxide and silicon compounds containing one, two and three available hydroxyl groups, leads to the suggestion of a plausible structure for the silica–alumina cracking catalyst.

(6) Joseph D. Danforth, THIS JOURNAL, **58**, 1030 (1954).
(7) J. E. Mapes and R. P. Eischens, *ibid.*, **58**, 1059 (1954).

THE OXIDATION OF CARBON MONOXIDE OVER CHROMIC OXIDE

BY STERLING E. VOLTZ AND SOL W. WELLER

Contribution from the Houdry Process Corporation, Marcus Hook, Pa.

The oxidation of carbon monoxide has been studied at 100° over both oxidized and reduced chromia catalysts. The preconditioned state of the reduced catalyst, which was established by pretreatment at 500°, is altered during the oxidation reaction. Both elemental material balances and electrical resistivity measurements show that considerable reaction occurs between gaseous oxygen and adsorbed hydrogen on the reduced catalyst. The preconditioned state of oxidized chromia is not altered to any appreciable extent during the carbon monoxide oxidation. The reaction rates over both catalysts are too similar for any conclusions to be drawn concerning the effects of pretreatment on activity. The reaction of gaseous oxygen and adsorbed hydrogen on the reduced catalyst results in the formation of water, most of which remains on the catalyst at 100°.

Introduction

Chromia is more active in the reduced state for hydrogen-deuterium exchange and ethylene hydrogenation, whereas the electrical conductivity is higher in the oxidized state.[1,2] The state of the chromia (oxidized or reduced) which results from pretreatment at 500° is not changed during hydrogen–deuterium exchange at −78° or lower.[1]

In preliminary experiments, oxidized chromia appeared to be slightly more active for the oxidation of carbon monoxide than the reduced catalyst. This suggested that oxidized chromia might be more active as an oxidation catalyst and the reduced catalyst more active for the activation of hydrogen. Chromia has characteristics of a p-type (oxygen excess) semiconductor,[1,3] and oxides of this type generally adsorb oxygen in a labile form and are good catalysts for reactions involving chemisorbed oxygen, such as the oxidation of carbon monoxide and the decomposition of nitrous oxide.[4] Chromia exhibits a much lower activity for the decomposition of nitrous oxide than most p-type semiconductors.[5,6] It has been recognized

recently that chromia can become an n-type semiconductor in a reducing atmosphere.[7,8]

At 100° chromia may be partially reduced or oxidized during the oxidation of carbon monoxide. The results presented in this paper are concerned with the effects of the reaction mixture on the preconditioned state of the catalyst.

Experimental

The chromic oxide was prepared from chromic nitrate and ammonia hydroxide; it was stabilized by consecutive oxidation–reductions at 500°. The detailed procedures have been described previously.[1,2]

Carbon monoxide (99.9+%) was prepared from formic acid and purified by passage through Ascarite and phosphoric anhydride. Purified oxygen was dried with calcium sulfate and magnesium perchlorate. A 2:1 mixture of carbon monoxide–oxygen was prepared from these gases. The oxidations were carried out in a high vacuum system equipped with an all-glass circulating pump. The product carbon dioxide was frozen out of the reaction mixture by a −196° trap in series with the circulating pump and reactor. In each experiment, the catalyst was oxidized or reduced at 500°, evacuated for 16 hours, and cooled under helium to 100°; the reaction mixture was then admitted. The reaction rate was followed by measuring the decrease in pressure with time.

When electrical resistance measurements were made, the catalyst was placed between platinum electrodes; the upper electrode was weighted with a perforated stainless steel cylinder. Resistance measurements (d.c.) were made with a Shallcross No. 635-A Wheatstone Megohm Bridge. The

(1) S. E. Voltz and S. W. Weller, *J. Am. Chem. Soc.*, **75**, 5227 (1953).
(2) S. W. Weller and S. E. Voltz, *ibid.*, **76**, 4695 (1954).
(3) D. J. M. Bevan, J. P. Shelton and J. S. Anderson, *J. Chem. Soc.*, 1729 (1948).
(4) R. M. Dell and F. S. Stone, *Trans. Faraday Soc.*, **50**, 501 (1954).
(5) R. M. Dell, F. S. Stone and P. F. Tiley, *ibid.*, **49**, 201 (1953).
(6) C. B. Amphlett, *ibid.*, **50**, 273 (1954).

(7) S. E. Voltz and S. W. Weller, unpublished results.
(8) P. R. Chapman, R. H. Griffith and J. D. F. Marsh, *Proc. Royal Soc. (London)*, **A224**, 419(1954).

measuring voltage was only momentarily applied during a resistance measurement in order to minimize polarization effects.

Results

Preliminary Experiments.—During a study of the effects of certain additives on chromia catalysts, it was observed that both oxidized and reduced chromia catalysts were active for the oxidation of carbon monoxide at 100°. According to pressure measurements, oxidized chromia appeared to be more active than reduced chromia. However, the difference in rates between the two catalysts was approximately equal to the amount of carbon monoxide which could react with the excess oxygen on the oxidized, evacuated catalyst.[2] In view of the possible oxidation or reduction of the catalysts by the carbon monoxide–oxygen mixture at 100°, the effects of the reactants on the oxidation–reduction states of the catalysts were more fully investigated.

Interaction of Reactants and Catalyst.—One of the simplest and most direct methods of determining whether the gaseous reactants interact with a solid catalyst in a heterogeneous reaction is to examine the elemental material balances. Any loss or gain of reactants, which results from irreversible reactions with the catalyst, can be amplified by using a relatively large catalyst concentration.

A series of experiments was carried out in which 5.0 cc. (5.6 g.) of chromic oxide was used and 3.1 mmoles of the carbon monoxide–oxygen mixture (70.9% CO, 29.1% O₂) were charged in each run. This corresponds to 0.55 mmole reactants/gram catalyst. From other work[2] it is known that catalyst of this type contains about 0.1 mmole excess oxygen per gram in the oxidized condition, and the equivalent of 0.3 mmole hydrogen per gram in the reduced condition.

Triplicate experiments were carried out over both oxidized and reduced chromia samples. Typical pressure curves are given in Fig. 1. The pressure decreased more rapidly initially over the reduced catalyst, but the rate of reaction also decreased more rapidly with time over this catalyst.

At the end of each experiment (when the pressure had decreased from 400 to 100 mm.), the non-condensable gases were analyzed by mass spectrograph. The amount of product carbon dioxide was determined by allowing it to sublime into a calibrated volume. The non-condensable gas mixture over the oxidized chromia had the same composition as the charge stock, while the residual gas over the reduced catalyst was 99+% carbon monoxide. Detailed elemental material balances are given in Table I. These results make it clear that the catalyst participated in the reaction to a significant extent. The loss of carbon from the gas phase means that carbon monoxide was adsorbed by the catalyst in each case. The large disappearance of oxygen with the reduced catalyst implies reaction of gaseous oxygen with the catalyst. In the case of the oxidized catalyst, however, the fact that the total oxygen content of the gas remains essentially constant, in spite of the adsorption of carbon monoxide, means that some catalyst oxygen has reacted with carbon monoxide
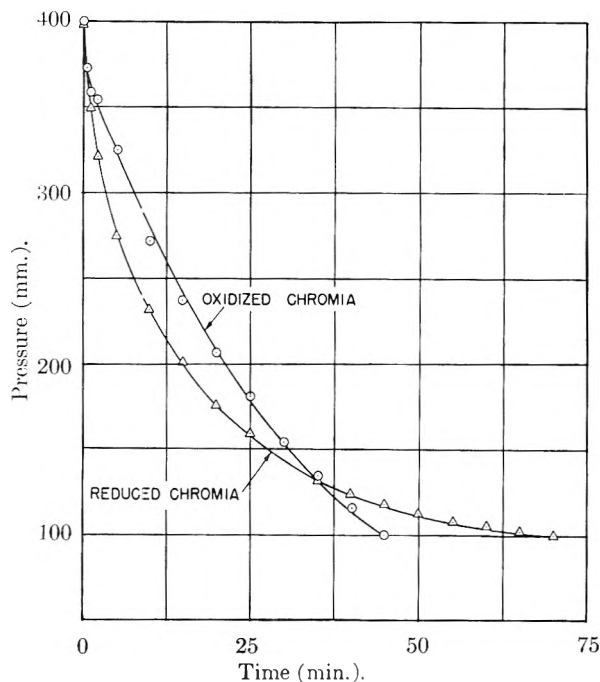

Fig. 1.—Oxidation of carbon monoxide at 100° at high catalyst concentrations.

to produce carbon dioxide (gas). In view of these complicating factors, it is doubtful that rigorous conclusions can be drawn concerning the purely catalytic effect of chromia for carbon monoxide oxidation as a function of pretreatment.

TABLE I
ELEMENTAL MATERIAL BALANCES[a]

State of catalyst	Initial gases (mmoles) CO	O₂	Final gases (mmoles) CO	O₂	CO₂	Δ Carbon (mmoles)	Δ Oxygen (mmoles)
Oxidized, evac.	2.21	0.91	0.55	0.23	1.52	−0.14	+0.01
Reduced, evac.	2.19	.90	.77	.0	1.26	− .16	− .35

[a] 5.6 g. catalyst used in each run.

Effects of Reactants on Electrical Properties of Chromia.

—The effects of exposure to the carbon monoxide–oxygen mixture at 100° on the electrical resistivity of the catalyst at 500° have been investigated. The resistivity of the reduced catalyst is decreased, which is consistent with the large disappearance of oxygen noted in the preceding section. The electrical resistivity of oxidized chromia is not significantly altered. The resistivity data for 500° are summarized in Table II.

TABLE II
EFFECTS OF CARBON MONOXIDE OXIDATIONS ON THE ELECTRICAL RESISTIVITY

State of catalyst	Resistivity at 500° (ohm-cm.) Oxidized	Reduced
In pretreating gas	1700	16.5 × 10⁷
After pretreating evacuation	2600	3.2 × 10⁷
After evacuation following CO oxidation[a]	2750	1.4 × 10⁶

[a] The catalysts were evacuated at 100° and then at 500° for 16 hours.

The resistivity and pressure measurements observed during the oxidation of carbon monoxide at 100° are shown in Figs. 2 and 3. The resistivity
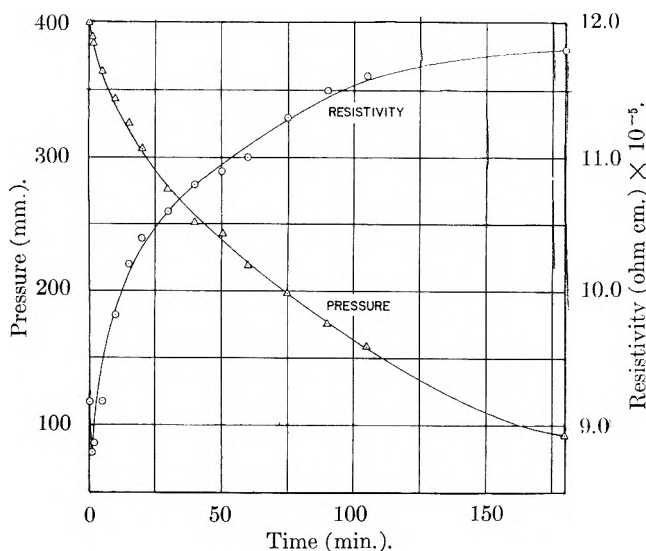
Fig. 2.—Pressure and resistivity data for the oxidation of carbon monoxide over oxidized chromia at 100°.
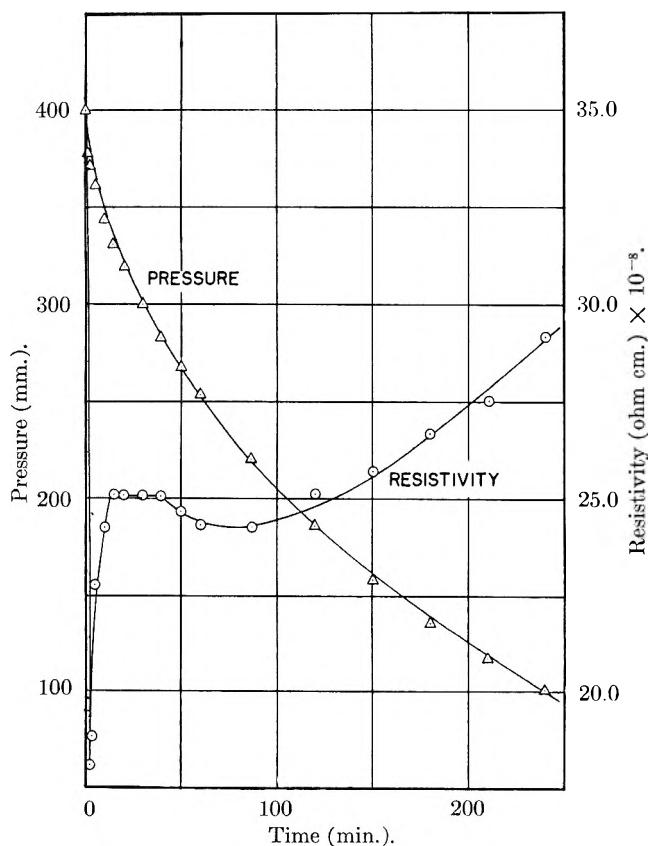

Fig. 3.—Pressure and resistivity data for the oxidation of carbon monoxide over reduced chromia at 100°.

of the reduced, evacuated catalyst at 100° was very high; it decreased to a measurable value when the reaction mixture was added.

In these experiments 3.0 cc. of catalyst was used and 5.8 mmoles of carbon monoxide-oxygen charges. This is equivalent to 1.7 mmoles reactants/g. catalyst, which represents a lower catalyst concentration than employed in the preceding section. Even under these conditions the pressure decreased more rapidly over the reduced catalyst.

The ratio of carbon monoxide to oxygen in the gaseous charge used in these experiments was 2:1. The ratios in the residual gases from the oxidized and reduced catalysts were 1.8 and 2.8, respectively. These results imply that even at this lower catalyst concentration, the amounts of reactants that disappear from the gas phase due to interaction with the catalyst are sufficient to have a pronounced effect on the pressure measurements.

Other Oxidation Reactions.—Several attempts were made to relate pretreatment and electrical conductivity to the activity of chromia catalysts for other inorganic oxidations. The oxidation of sulfur dioxide did not take place over chromia in a flow system at 300° or lower. The oxidation of nitric oxide was studied between −78 and 30°, but the uncatalyzed reaction was too rapid for the determination of catalytic effects.

Discussion

The oxygen balances and electrical resistivity measurements show that considerable amounts of oxygen react with the catalyst during the oxidation of carbon monoxide over reduced, evacuated chromia. Reduced chromia contains appreciable quantities of adsorbed hydrogen; evacuation at 500° only removes a fraction of this hydrogen, i.e., that which is reversibly chemisorbed.[2] The interaction between gaseous oxygen and catalyst hydrogen leads to the formation of water, which presumably is not effectively removed from the chromia surface at 100°. Water is known to be an effective poison of oxide catalysts such as chromia for many reactions.

At low catalyst concentrations, the small quantities of reactants removed from the gas phase by reaction with the catalyst have only a negligible effect on the total pressure of the system. Under these conditions, the change in pressure is a reliable measure of the rate of reaction. Oxidized chromia is more active than the reduced catalyst at relatively low catalyst concentrations; however, the formation of water on the surface of the reduced catalyst seriously complicates the interpretation of this result.

At high catalyst concentrations, the removal of reactants by interaction with the catalyst has a pronounced effect on the total pressure, and the change in pressure is no longer an accurate measure of the rate of the catalyzed reaction. Under these conditions, reduced chromia appears to be initially more active than oxidized chromia, since gaseous oxygen is being consumed by the reduced catalyst. As water is formed on the catalyst surface, however, the rate of carbon monoxide oxidation decreases.

The removal of large quantities of gaseous oxygen over reduced chromia at high catalyst concentrations also has a marked effect on the rate of carbon monoxide oxidation. No oxygen was present in the gas phase over reduced chromia (at the higher catalyst concentration) when the reaction stopped at 100 mm. The oxygen removal leads to a large excess of carbon monoxide in the gas phase, which also complicates any interpretation of the kinetic results.

In view of the reaction of the reduced catalyst with gaseous oxygen to form water, it is not possible to fairly compare the activities of reduced chromia and oxidized chromia for carbon monoxide oxidation at 100°. These results further emphasize that in fundamental studies of the relation between electrical properties and catalytic activity, the chemical changes that occur on the catalyst surface must be carefully considered. Failure to observe this precaution may lead to meaningless conclusions.

THE EFFECTS OF POTASSIUM ON CHROMIA CATALYSTS

By Sterling E. Voltz and Sol W. Weller

Contribution from the Houdry Process Corporation, Marcus Hook, Pa.

The influence of potassium oxide on the surface properties and catalytic activities of chromia and chromia–alumina has been investigated. The presence of potassium increases the surface oxidation of chromia catalysts and partially stabilizes the oxidized catalyst against reduction. Apparent catalyst acidities are dependent on the methods of determination. Potassium decreases the activities of chromia catalysts for ethylene hydrogenation, cyclohexane dehydrogenation, double bond isomerization, and carbon monoxide oxidation; it increases the activity for the decomposition of aqueous hydrogen peroxide. The effect of potassium on the surface chemistry can be accounted for by postulating the formation of chromate, dichromate or their equivalents on the surface.

Introduction

Chromia catalysts are of great practical importance and theoretical interest. The properties of such catalysts are markedly changed by the incorporation of small amounts of oxides of other metals, such as the alkali metals. Although isolated descriptions have appeared of alkali-containing chromia catalysts,[1–6] no systematic study seems to have been made of the changes in catalyst properties caused by addition of alkalies. This paper is concerned with the effect of potassium oxide addition on certain physical, chemical and catalytic properties of chromia and chromia–alumina catalysts.

Experimental

Catalyst Preparation.—The catalysts employed in this study were prepared by impregnating an unsupported chromia catalyst (stabilized by cycling in hydrogen and oxygen at 500°)[7] and a commercial chromia–alumina (20:80) catalyst (Houdry Type R) with potassium oxide. The base catalysts were dipped in solutions of potassium nitrate or hydroxide for one hour; the solutions were then decanted. The catalysts were dried in air at 110° overnight and then at 500° for eight hours. Impregnation with potassium nitrate or potassium hydroxide had the same effect on the surface properties and catalytic activities.

Procedures.—The surface oxidations, titratable acidities, pH values of aqueous suspensions and activities for the decomposition of aqueous hydrogen peroxide were determined by methods previously described.[8] The quinoline adsorption data were determined by a method similar to that used for silica–alumina cracking catalysts.[9] The procedure and apparatus for the hydrogen–deuterium exchange experiments have been described previously.[7] The analyses for aldehydes and ketones were carried out by standard procedures.[10] Potassium contents of catalysts were determined by a modified flame photometric method.

A flow system was employed in the dehydrogenation of cyclohexane, oxidation and decomposition of ethanol, and the isomerization of pentene-1. Five cc. of fresh catalyst was used for each experiment and the pretreatments were at 500° (538° in the cyclohexane runs). After pretreatment the catalyst temperature was adjusted to that desired for the particular run, and the reaction mixture was passed through. In each case, a carrier gas was bubbled through a thermostatted reservoir of liquid feed. The LHSV was 1 volume/volume/hour for cyclohexane and pentene-1 and 0.05 for ethanol.

The oxidation of carbon monoxide and the hydrogenation of ethylene were studied in high vacuum systems; the one used for the oxidation contained an all-glass circulating pump. In each experiment, the catalyst was treated with oxygen or hydrogen at 500° and then evacuated for at least 16 hours. The catalyst temperature was then adjusted, and a 2:1 mixture of carbon monoxide–oxygen or a 1:1 mixture of ethylene–hydrogen was admitted. In the carbon monoxide oxidation, the product carbon dioxide was continuously frozen in a −196° trap.

Results

Catalyst Characterization.—The effect of potassium on the surface properties of chromia is illustrated in Table I. These data show that the presence of potassium increases the surface oxidation, activity for hydrogen peroxide decomposition and aqueous titratable acidity of oxidized chromia. It has been previously established that the activity of chromia catalysts for hydrogen peroxide decomposition is proportional to the surface oxidation,[7] and it is not surprising, therefore, that potassium has the same effect on both of these properties.

The surface oxidations of the reduced catalysts containing potassium are about one-third of those in the oxidized state, and increase with increasing alkali content. Impregnation with alkali thus partially stabilizes surface-oxidized chromia against reduction. The activities of the reduced catalysts for the decomposition of aqueous hydrogen peroxide also increase with increasing surface oxidation.

The conventional method of determining titrat-

(1) G. H. Visser and W. F. Engel, U. S. Patent 2,271,751 (February 7, 1941).

(2) B. S. Greenfelder and R. C. Archibald, British Patent 572,251 (Sept. 28, 1945).

(3) H. Hoog, *Chemistry and Industry*, No. 42, 873 (1951).

(4) J. Varga, G. Rabo and A. Zalai, *Acta Chim. Hung.*, 1, 137 (1951).

(5) J. R. Coley and V. I. Komarewsky, *J. Am. Chem. Soc.*, 74, 4448 (1952).

(6) A. Clark, *Ind. Eng. Chem.*, 45, 1476 (1953).

(7) S. E. Voltz and S. W. Weller, *J. Am. Chem. Soc.*, 75, 5227 (1953).

(8) S. E. Voltz and S. W. Weller, *ibid.*, 76, 1586 (1954).

(9) G. A. Mills, E. R. Boedeker and A. G. Oblad, *ibid.*, 72, 1554 (1950).

(10) S. Siggia, "Quantitative Organic Analysis via Functional Groups," John Wiley and Sons, Inc., New York, N. Y., 1949, pp. 10–16.

TABLE I

EFFECT OF POTASSIUM ON THE SURFACE PROPERTIES OF CHROMIA

Catalyst	K₂O (wt. %)	Excess oxygen (μmoles/g.) Oxidized	Reduced	Activity for hydrogen peroxide decompn. (cc. O₂/sec.) Oxidized	Reduced	Titratable acidity (meq./g.) Oxidized	Reduced	pH of aqueous suspension Oxidized	Reduced
Cr₂O₃	0	112	0	0.04	0.03	0.10	0.05	2.7	6.7
Cr₂O₃ + K₂O (ex KNO₃)	0.25	136	33	.12	.05	.16	.03	2.9	7.6
Cr₂O₃ + K₂O (ex KNO₃)	.55	158	56	.33	.09	.20	.01	3.1	9.5
Cr₂O₃ + K₂O (ex KNO₃)	.81	239	89	.39	.14	.28	.00	3.3	10.0

able acidity, which involves titration to a phenolphthalein end-point, gives erroneous results with these catalysts. Reduced catalysts containing alkali, for example, show finite values for titratable acidity, although the aqueous suspensions are actually alkaline. Furthermore, the titratable acidities of oxidized catalysts increase with increasing potassium content, while the pH values increase in the same order. The origin of these discrepancies was found to lie in the shape of the neutralization curve. The change in pH with titrant volume for these catalysts is quite gradual near the equivalence point, and it is impossible to represent adequately the equivalence point by simply noting the volume at which a single indicator changes color.

The influence of potassium on chromia-alumina was similar to that on chromia. Potassium was not as effective, however, in stabilizing the surface oxidation of reduced chromia–alumina as of reduced chromia. This was evidenced by the lower surface oxidations and lower activities for hydrogen peroxide decomposition of reduced chromia–alumina catalysts containing potassium compared to the corresponding unsupported chromia samples with potassium.

X-Ray diffraction patterns were obtained for most of the catalysts. All of the potassium-impregnated unsupported chromia catalysts gave patterns corresponding to α-chromia only. There was no evidence (from the X-ray patterns) for the formation of K₂CrO₄, K₂Cr₂O₇, KCr₃O₈ or other oxides of chromium.[11-13]

The X-ray diffraction patterns of the chromia-alumina catalysts with and without potassium, corresponded to α-chromia and γ-alumina. In the oxidized state, however, there was a line at d/n = 2.55 Å. that does not belong to the patterns for either chromia or alumina. In the reduced state this line was either absent or of much lower intensity. This line may be due to the presence of the cubic oxide reported by Laubengayer and McCune,[12] for which the strongest diffraction line is at d/n = 2.52 Å.

The surface areas of the stabilized chromia catalyst and the chromia–alumina were 11 and 40 m.²/g., respectively, as measured by nitrogen adsorption at −196°. Impregnation with potassium oxide and calcination in air at 500° had no effect on the areas. The areas of the reduced catalysts were the same as the oxidized ones.

The amount of quinoline chemisorbed by chromia

(11) L. Suchow, I. Fankuchen and R. Ward, *J. Am. Chem. Soc.*, **74**, 1678 (1952).

(12) A. W. Laubengayer and H. W. McCune, *ibid.*, **74**, 2362 (1952).

(13) R. S. Schwartz, I. Fankuchen and R. Ward, *ibid.*, **74**, 1676 (1952).

catalysts at 316° was found to be decreased by the presence of potassium. The results for a few catalysts are given in Table II. Quinoline adsorption is a measure of catalyst acidity, and these data show that acidity decreases with increased potassium concentration. This is in agreement with the pH measurements of the aqueous suspensions.

TABLE II

QUINOLINE ADSORPTION

Catalyst	K₂O (wt. %)	Quinoline adsorbed (meq./g.)
Cr₂O₃–Al₂O₃	0	0.078
Cr₂O₃–Al₂O₃–K₂O	1.49	.041
Cr₂O₃–Al₂O₃–K₂O	1.72	.014
Al₂O₃	0	.016

Effect of Potassium on Catalytic Activity. Low Temperature H₂–D₂ Exchange.—The effects of potassium on the activities of chromia and chromia–alumina for the hydrogen–deuterium exchange reaction are illustrated in Table III. The activity of oxidized chromia decreases with increasing potassium concentration, whereas potassium has very little effect on the activity of reduced chromia. The activities of the various chromia–alumina catalysts are similar to the corresponding unsupported chromia catalysts.

TABLE III

HYDROGEN–DEUTERIUM EXCHANGE

Catalyst	K₂O (wt. %)	Temp., °C.	Activity
Oxidized Cr₂O₃	0	−78	Equil. in about 0.5 hr.
Reduced Cr₂O₃	0	−195	5.6% HD in 6 hr.
Oxidized Cr₂O₃–K₂O	0.25	−78	Equil. within 5 hr.
Oxidized Cr₂O₃–K₂O	.55	−78	4.4% HD in 6 hr.
Oxidized Cr₂O₃–K₂O	.81	−78	Inactive
Reduced Cr₂O₃–K₂O	.81	−195	7.3% HD in 6 hr.
Reduced Cr₂O₃–K₂O	.99	−195	2.2% HD in 6 hr.
Oxidized Cr₂O₃–Al₂O₃–K₂O	.29	−78	Equil. within 5 min.
Oxidized Cr₂O₃–Al₂O₃–K₂O	.46	−78	Equil. within 6 hr.
Oxidized Cr₂O₃–Al₂O₃–K₂O	1.49	−78	26.3% HD in 6 hr.
Oxidized Cr₂O₃–Al₂O₃–K₂O	1.72	−78	1.4% HD in 6 hr.

Dehydrogenation of Cyclohexane.—Potassium impregnation of chromia–alumina decreases the activity of the catalyst for the dehydrogenation of cyclohexane. The results obtained at 538° are given in Table IV. The conversion to benzene decreased with increasing potassium concentration. Analyses of the exit gas showed no appreciable amounts of cracking occurred.

TABLE IV

DEHYDROGENATION OF CYCLOHEXANE

Catalyst	K₂O (wt. %)	Benzene in liq. product (vol. %)
Cr₂O₃–Al₂O₃	0	19.3
Cr₂O₃–Al₂O₃–K₂O	0.46	17.0
Cr₂O₃–Al₂O₃–K₂O	0.81	13.2
Cr₂O₃–Al₂O₃–K₂O	1.72	7.0

Oxidation and Decomposition of Ethanol.— The oxidation of ethanol in oxygen was studied over oxidized chromia–alumina. At 100° there was no reaction, while at 300 and 500° the ethanol was completely converted to water, carbon dioxide and carbon monoxide.

The decomposition of ethanol, using a nitrogen carrier stream, was also studied at 300 and 500° over oxidized chromia–alumina. At 300° there was no reaction, but at 500° reaction occurred over this catalyst and over chromia–alumina containing potassium (1.72%). In the experiments at 500°, the liquid product consisted of two layers; the top was a yellow oil of high refractive index, while the lower was colorless with a refractive index near that of water. Infrared analyses indicated that the bottom layer was essentially water and that the top layer contained a compound probably having a carbonyl group but no hydroxyl group. The top layer could not be identified more specifically from the infrared absorption curve and all attempts to prepare aldehyde or ketone derivatives were unsuccessful. Analysis of the gaseous products showed that much more dehydrogenation than dehydration of the ethanol had occurred.

Isomerization of Pentene-1.—Typical data for the double-bond isomerization of pentene-1 over chromia catalysts at 300° are given in Table V; very little isomerization took place at 250°. All of the catalysts were more active in the reduced state than in the oxidized state, and impregnation with potassium decreased the isomerization activity. Under the experimental conditions employed in this work, no structural isomerization took place. This was evidenced by the absence of appreciable quantities of methyl butenes in the liquid product.

TABLE V

ISOMERIZATION OF PENTANE-1 AT 300°

Catalyst	K_2O (wt. %)	Pentene-2 in liq. product[a] (vol. %)
Oxidized Cr_2O_3–Al_2O_3	0	30.2
Reduced Cr_2O_3–Al_2O_3	0	62.8
Oxidized Cr_2O_3–Al_2O_3–K_2O	1.49	5.1
Reduced Cr_2O_3–Al_2O_3–K_2O	1.49	15.7

[a] Includes both *cis* and *trans* forms.

Oxidation of Carbon Monoxide.—Both oxidized and reduced chromia catalyze the oxidation of carbon monoxide in a closed system at 100°. Impregnation with potassium completely deactivates the catalyst for this oxidation.

Hydrogenation of Ethylene.—Both chromia and chromia–alumina are active catalysts, in the reduced state, for the hydrogenation of ethylene at −78°; these catalysts are completely inactive in the oxidized state. The presence of potassium, however, completely inactivates both chromia and chromia–alumina even in the reduced state.

Discussion

Chromia catalysts contain considerable amounts

of surface excess oxygen in the oxidized state.[14,15] It is reasonable to postulate that the incorporation of potassium results in the formation of appreciable amounts of potassium chromate, potassium dichromate or their equivalents on the oxidized surface.

Table VI contains a comparison of the increase in surface oxidation, which results from the incorporation of potassium in the chromia, and the concentration of potassium oxide. These results are based on the data in Table I. The increase in surface oxidation was determined by subtracting the surface oxidation of the chromia without any potassium from the observed value in each case. The corresponding amounts of potassium (as K_2O) calculated from the increase in surface oxidation, were deduced from the equations

$$Cr_2O_3 + 2K_2O + 3/2O_2 \longrightarrow 2K_2CrO_4$$
$$Cr_2O_3 + K_2O + 3/2O_2 \longrightarrow K_2Cr_2O_7$$
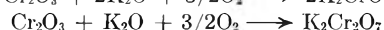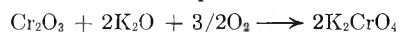
Comparison of the calculated with the actual values of the potassium oxide contents shows that the increases in surface oxidation correspond reasonably well to the formation of chromate or dichromate. The stabilization of part of the surface oxidation by potassium against reduction undoubtedly results from the higher stability of potassium chromate or dichromate compared to that of the higher chromium oxides.

TABLE VI

RELATION BETWEEN SURFACE OXIDATION AND POTASSIUM CONCENTRATION

Increase in surface oxidation (μmoles/g.)	Calcd. K_2O (μmoles/g.) K_2CrO_4	$K_2Cr_2O_7$	Actual K_2O concn. (μmoles/g.)
24	32	16	27
46	61	31	58
127	169	85	86

Both potassium chromate and dichromate are catalysts for the decomposition of aqueous hydrogen peroxide.[16] Thus, the increase in activity for this reaction can be accounted for by the formation of chromate or dichromate. For all of the other catalytic reactions studied, added potassium either had no effect or inhibited the reaction. The decreased activity of potassium-containing catalysts for pentene isomerization, a reaction normally considered to be acid catalyzed, is consistent with the decrease in catalyst acidity as measured by quinoline chemisorption or the pH of aqueous suspensions. The decrease in acidity is consistent with the observation of Clark[6] that alkali lowers the deposition of coke on chromia during butane dehydrogenation. The standard method for determining titratable acidity appears to be inherently inaccurate for materials such as chromia, which show broad pH changes during acid–base titration.

(14) S. W. Weller and S. E. Voltz, *J. Am. Chem. Soc.*, **76**, 4695 (1954).

(15) S. E. Voltz and S. W. Weller, *ibid.*, **76**, 4701 (1954).

(16) J. H. Baxendale, "Advances in Catalysis," Vol. IV, Academic Press, Inc., New York, N. Y., 1952, pp. 75–80.

NOTES

POTENTIAL BARRIERS ABOUT DOUBLE BONDS

By N. W. Luft

52 Lady Bridge Road, Cheadle Hulme, Cheshire, England

A review of the literature seems to indicate that of all the torsional assignments those for twisting oscillations about double bonds are particularly complicated and uncertain. If the torsional mode is separable from the other oscillations then, to the harmonic oscillator approximation, the torsional fundamental is given by

$$\delta_t = (1/2\pi c)(k_\phi/I_r)^{1/2} \qquad (1)$$

where k_ϕ is the force constant and I_r the reduced moment of inertia of rotating groups about the torsional axis.

In ethylene derivatives the torsional mode can be strictly separated[1] from the other two out-of-plane oscillations only if the torsional axis is a symmetry axis for the whole molecule, *i.e.*, in $X_2C{=}CY_2$ and $X_2C{=}CX_2$. With *cis* and *trans* $XYC{=}CYX$ the torsional vibration arises from a quadratic, with $X_2C{=}CXY$, etc., from a cubic factor in the secular equation, so that the non-planar oscillations concerned (of species A_2, A_u and A'', respectively) may interact with each other and render the expression for the torsional δ_t less simple in form. These formal difficulties have been discussed, in some detail, by Torkington.[2] An important practical conclusion of his is the observation that even with the less symmetrical ethylene derivatives certain non-planar bending frequencies, δ_{CX} and δ_{CX_2}, behave often as typical group frequencies inasmuch as in a series of homologs they are almost completely independent of the nature of other substituents Y. This, however, indicates that the corresponding elements in the secular equation factorize approximately linearly, and this must consequently also apply to the remaining factor yielding δ_t, again in good agreement with eq. 1. Formally this result may always be expected if the force constant or kinetic energy matrices or both satisfy certain requirements. But whereas for the kinetic energy matrix the necessary restrictions are simply expressed in terms of mass ratios, etc., the influence of the force and interaction constants is rather uncertain[2] because of the lack of reliable experimental data.

On the whole the error incurred by using the simple eq. 1 as a first approximation is, in most cases, small compared with these uncertainties of force constants and the inaccuracies of many a k_ϕ value reported in the literature. Whilst Torkington[2] tried to discover an empirical correlation for k_ϕ values of substituted ethylenes, sometimes the torsional force constant of ethylene appears to have been used indiscriminately in order to estimate torsional fundamentals for its derivatives, *e.g.*, recently[3] for $H_2C{=}CF_2$. Such procedure is bound to lead to serious errors as can be shown by reference to the torsional barrier heights, V_0, corresponding to these k_ϕ values. In many cases it is indeed only necessary to obtain, from eq. 1, an approximate value of k_ϕ and V_0 in order to select the correct δ from a set of alternative experimental values. On this basis a number of proposed torsional fundamentals can be rejected simply because the orders of magnitude of the corresponding barriers are unreasonable.

As outlined earlier[4,5] the torsional potential barriers, $V(\phi)$, about double bonds arise from: (i) contributions of the two π-electrons, with minima for $\phi = 0$ and π (planar *cis* and *trans* configuration, respectively); (ii) repulsive interactions between non-adjacent bonds (i, k . . .) and lone electron pairs (p) on different sides of the double bond; (iii) interactions of these charge clouds with the π-electrons. The contributions (ii) may be taken into account by their Fourier coefficients c_n^{ik} as explained previously.[4,6] They satisfy the same symmetry conditions but, mainly because of differences in bond lengths and angles, their actual values differ from c_n^{ik} values about CC single bonds. According to M.O.[7,8] and V.B.[8] calculations for ethylene the π-electron contributions (i) possess very nearly twofold symmetry so that

$$2c_2^\pi \rightleftharpoons E_N(\pi/2) - E_N(0) \rightleftharpoons E_T(0) - E_N(0) - V_T^\pi \qquad (2)$$

where $E(\phi)$ is the energy of the ethylene molecule, for azimuthal angles ϕ, in its N($^1A_{1g}$) and T-($^3B_{1u}$) states, respectively. The term V_T^π is that part of the potential barrier in the T-state, which is due to the unshared electrons on either carbon atom ($\sim 20 - 25$ kcal./mole).[7,8] The over-all barrier, however, contains additional contributions arising from CH bond interactions and should thus be comparable to the barrier structure of the similar $H_2N{-}NH_2$ molecule.

The interactions (iii), representing polarization and resonance effects, become apparent in the known $C{=}C$ bond shortening of some halogenated ethylenes and may be included, at least to some approximation, in the c_2^{ik}'s or in a modified c_2^π. On the other hand the reduced $C{=}C$ bond energy in $F_2C{=}CF_2$ (<112 kcal./mole[11]) seems to indicate that repulsion still outweighs resonance effects considerably.

In the Fourier expansions of potential barriers about double bonds c_3 vanishes on symmetry grounds and higher terms are usually negligible, in comparison with c_2, since both c_4^{ik} and c_4^π are small (*cf.* refs. 4, 5 and 7, 8, respectively). Therefore we

(1) G. Herzberg, "Infrared and Raman Spectra of Polyatomic Molecules," D. van Nostrand, New York, N. Y., 1946.

(2) P. Torkington, *Proc. Roy. Soc. (London)*, **206A**, 17 (1951).

(3) D. C. Smith, J. R. Nielsen and H. H. Claassen, *J. Chem. Phys.*, **18**, 326 (1950).

(4) N. W. Luft, *ibid.*, **22**, 1814 (1954).

(5) N. W. Luft, *Z. Elektrochem.*, **57**, No. 1 (1955).

(6) N. W. Luft, *J. Chem. Phys.*, **21**, 179 (1953).

(7) W. G. Penney, *Proc. Roy. Soc. (London)*, **144A**, 166 (1934).

(8) R. G. Parr and B. L. Crawford, *J. Chem. Phys.*, **16**, 526 (1948).

may approximate the torsional barrier by

$$V = c_1(1 - \cos \phi) + c_2(1 - \cos 2\phi) \qquad (3)$$

then for molecules symbolized by $i_2 = kl$ and $ik = ik$, e.g., $H_2C{=}CFCl$ and $ClHC{=}CHCl$, simple formulas for internal potential barriers can be set up (Table I, cf., refs. 4, 5), which may serve to determine c_2's and differences of c_2^{ik}'s from experimental torsional barriers. These increments may be used to estimate unknown barrier heights.

Equation 3 again implies that torsion can be separated from other non-planar oscillations. Although this was shown to be feasible at least to a first approximation, it may here be justified also in a slightly different manner. Obviously separability applies rigorously, to the harmonic oscillator approximation, if $k = l$ and $k = i$, respectively, in Table I. Therefore eq. 3 may be regarded as a good approximation as long as the bond k is not too different from l and i, respectively. This means

$$2(c_2^{ik} - c_2^{il}) \sim 2c_2^{ik} - c_2^{ii} - c_2^{kk} \sim 2c_2^{il} - c_2^{ii} - c_2^{ll} \ll c_2^{\pi} \qquad (4)$$

conditions which are satisfied sufficiently for present purposes.

TABLE I
TORSIONAL BARRIERS ABOUT DOUBLE BONDS
$(\alpha \equiv c_1/4c_2)$

Structure	$i_2 = kl$	$ik = ik$
c_1	0	$2c_1^{ik} - c_1^{ii} - c_1^{kk}$
c_2	$c_2^{\pi} - 2c_2^{ik} - 2c_2^{il}$	$c_2^{\pi} - 2c_2^{ik} - c_2^{ii} - c_2^{kk}$
V_0	$2c_2$	$2c_2(1 - \alpha)^2$
$\Delta E = V(0) - V(\pi)$	0	$-2c_1$
$k_\phi, (\phi = 0, \pi)$	$4c_2$	$4c_2(1 \pm \alpha)$

Figures reported in the literature[8-11] for the separation of the T and N states in ethylene give $c_2^{\pi} \sim$ 20 to 30 kcal./mole from eq. 2. A slightly preciser value may be derived by using the barrier heights $V_0 = 39.3$ and 27.2 kcal./mole for ethylene (E) and allene (A), as obtained from their recently observed[12,13] twisting frequencies $\delta_t = 1027$ and 865 cm.$^{-1}$, in combination with $c_2^{\pi}(E)/c_2^{\pi}(A) = 1.71$ (cf. refs. 9, 8) and $c_2^{HH}(E) \gg c_2^{HH}(A) \sim 0$ because of larger H . . . H distances in allene one finds $c_2^{\pi} = 23.3$ kcal./mole in ethylene and $c_2^{HH} = 1.0$ kcal./mole.

Substitution of D for H should leave the potential barriers unchanged, thus $V_0 \sim 39.5$ kcal./mole is expected for all deuteroethylenes. To achieve this certain assignments have to be revised or interchanged as suggested in Table II.

With some halogenated and methylated ethylenes up to three greatly differing values of torsional frequencies have been proposed by different investigators. High values quoted for $H_2C{=}CCl_2$,[14] $Cl_2C{=}CClH$,[14] $F_2C{=}CHCl$,[15] $H_2C{=}CH(CH_3)$,[16]

(9) J. D. Dunitz and L. E. Orgel, *J. Chem. Phys.*, **20**, 1328 (1952).

(10) E. C. Baughan and M. Polanyi, *Nature*, **146**, 685 (1940).

(11) B. Atkinson, *J. Chem. Soc.*, 2684 (1952).

(12) R. L. Arnett and B. L. Crawford, *J. Chem. Phys.*, **18**, 118 (1950).

(13) R. C. Lord and P. Venkateswarlu, *ibid.*, **20**, 1237 (1952).

(14) Landolt-Börnstein, "Zahlenwerte und Funktionen," Parts 2/3, Springer, 1951.

(15) J. R. Nielsen, C. Y. Liang and D. C. Smith, *J. Chem. Phys.*, **20**, 1090 (1952).

(16) J. E. Kilpatrick and K. S. Pitzer, *J. Research Natl. Bur. Standards*, **38**, 191 (1947).

TABLE II
TORSION IN ETHYLENE AND ITS DEUTERIDES

Molecule	δ_t (cm.$^{-1}$) Previous	Present
$H_2C{=}CH_2$	$1027^{a,b}$	1027
$D_2C{=}CD_2$	$726,^{a,b}$ 780^c	726
$H_2C{=}CHD$	1000^b	943^d
$H_2C{=}CD_2$	$(889)^b$	889
$HDC{=}CDH$	988^b	843^d

^{a} Ref. 12. ^{b} B. L. Crawford, J. E. Lancaster and R. G. Inskeep, *J. Chem. Phys.*, **21**, 678 (1953). ^{c} Ref. 2. ^{d} Proposed re-assignment based on Crawford's data.^{b}

and $H_2C{=}C(CH_3)_2$,[14] viz., 860, 211, 243, 990 and 878 cm.$^{-1}$, respectively, can almost certainly be ruled out since the corresponding barrier heights are well in excess of 50 kcal./mole and, with some, more than twice the expected value. For vinyl and vinylidene compounds alternative values have been given by Torkington,[2] though his figure $\delta = 578$ cm.$^{-1}$ for $H_2C{=}CH(CH_3)$, resulting in $V_0 \sim 24$ kcal./mole, appears to be somewhat low. Recently[14] low Raman shifts at 62 and 174 cm.$^{-1}$ have been observed, in solid $Cl_2C{=}CClH$ at $-150°$, which however are unlikely to be torsional fundamentals since the corresponding barriers are somewhat too low and too high, respectively. As a last possibility one might interpret the frequency of 211 (or 174) cm.$^{-1}$ in $Cl_2C{=}CClH$, and similarly 243 cm.$^{-1}$ in $F_2C{=}CHCl$, as first overtones of the torsional fundamental. Whilst this yields reasonable barrier heights (15–20 kcal./mole) for these two molecules it would call for modifications of torsional fundamentals of other polyhalogenated ethylenes, including $F_2C{=}CF_2$ and $F_2C{=}CFCl$. The assignment[17] for the former, $\delta_t = 210$ cm.$^{-1}$ (i.e., $V_0 \sim 43$ kcal./mole), seems to be well supported by measured entropy data,[18] whereas a recent re-assignment[19] of frequencies for $F_2C{=}CFCl$, with $\delta_t = 194$ instead of the earlier[20] doubtful value $\delta_t \sim 158$ cm.$^{-1}$, still leaves an entropy difference of about 0.6 cal./mole deg. unaccounted for. Also the barrier height $V_0 \sim 52$ kcal./mole which obtains by use of eq. 1, though approximate, appears to be too high. The difficulties might be resolved by regarding the frequency of 215 cm.$^{-1}$ as the overtone $2\delta_t$ and assigning 739 cm.$^{-1}$ as fundamental and $369 \sim 2 \times 194$ cm.$^{-1}$.

It appears from Table I that c_1's of molecules $ik = ik$ represent differences of c_1^{ik}'s. Even if the c_1^{ik}'s are big c_1 and therefore ΔE is expected to be comparatively small and thus

$$\alpha = c_1/4c_2 = -(\Delta E/4V_0)(1 - \alpha)^2 \qquad (5)$$

is insignificant as long as V_0 is large. This however implies that the torsional force constants for cis and trans configurations are almost identical, and

$$V_0(ik = ik) \simeq \tfrac{1}{2}V_0(i_2 = ik) + \tfrac{1}{2}V_0(k_2 = ki) \qquad (6)$$

(17) J. R. Nielsen, H. H. Claassen and D. C. Smith, *J. Chem. Phys.* **18**, 812 (1950).

(18) G. T. Furukawa, R. E. McCoskey and M. L. Reilly, *J. Research Natl. Bur. Standards*, **51**, 69 (1953).

(19) J. A. Rolfe and L. A. Woodward, *Trans. Faraday Soc.*, **50**, 1030 (1954).

(20) D. E. Mann, N. Acquista and E. K. Plyler, *J. Chem. Phys.*, **21**, 1949 (1953).

For these reasons $\nu_7 = 406$ cm.$^{-1}$, recently[21] proposed as the torsional fundamental of *cis* ClHC= CHCl, is certainly ruled out and $\delta_t(cis) \simeq \delta_t(trans)$ < 200 cm.$^{-1}$ corresponding to $V_0 < 56$ kcal./mole is expected. Thus the faint infrared band at about 150 cm.$^{-1}$ which Pitzer and Hollenberg[21] recorded for *trans* ClHC=CHCl but discarded as fundamental frequency may well be the twisting fundamental and 278 cm.$^{-1}$, previously explained[21] as the ternary combination $2\nu_{12} - \nu_7$, its first overtone. Then $\delta_t \sim 140$ cm.$^{-1}$ gives $V_0 \sim 28$ kcal./mole in good agreement with the value of 30 kcal./mole from rates of isomerization.[22] On the other hand, because of eq. 6, this would support the lower value $V_0(Cl_2C=CHCl) \sim 20$ kcal./mole as given above.

Similar considerations apply to torsional oscillations about CN and NN double bonds. The values of $c_2{}^\pi$, however, and the influence of lone electron pairs on the nitrogen atoms are not known to any degree of accuracy, although Birnbaum and Style,[23] in a schematic diagram for the torsional potential energy of the various electronic states of azobenzene, indicate $V_0 \sim 2c_2 \sim 50$ and $\Delta E \sim 12$ kcal./ mole for its ground state. Since the N=N bond is shorter than the C=C bond, repulsion between the substituents is expected to be stronger and, in the *cis*-form, of a "steric nature." Thus the values by Birnbaum and Style would suggest that $c_2{}^\pi$ is larger for N=N than for C=C bonds, a view not inconsistent with the tendency of nitrogen to form stronger bonds.

(21) K. S. Pitzer and J. L. Hollenberg, *J. Am. Chem. Soc.*, **76**, 1493 (1954); *cf.* H. J. Bernstein and D. A. Ramsay, *J. Chem. Phys.*, **17**, 556 (1949).

(22) R. E. Wood and R. G. Dickinson, *J. Am. Chem. Soc.*, **61**, 3259 (1939); *cf.* McConnel, *J. Chem. Phys.*, **20**, 1043 (1952).

(23) P. P. Birnbaum and D. W. G. Style, *Trans. Faraday Soc.*, **50**, 1192 (1954).

INSTABILITY OF SELF-EXCITED SYSTEMS

By G. Narsimhan

Department of Chemical Engineering, Laxminarayan Institute of Technology, Nagpur University, Nagpur, India

The partial differential equation which defines the vibration of a stretched membrane may be written as

$$\frac{\partial^2 y}{\partial \theta^2} = \frac{T}{m}\left[\frac{\partial^2 y}{\partial x^2} + \frac{\partial^2 y}{\partial z^2}\right] \quad (1)$$

If the assumption is made that either the width of the membrane is very small or dy/dz is constant, the equation reduces to

$$\frac{\partial^2 y}{\delta \theta^2} = \left(\frac{T}{m}\right)\frac{\partial^2 y}{\partial x^2} \quad (2)$$

Under the added influence of an internal pressure of a system of which the stretched membrane forms a part, *viz.*, gas flow through a pipe line, an additional term in y is to be included in the general equation. The effect of the internal pressure is to displace the membrane in the y direction and this displacement is proportional to the pressure. The final equation reduces to

$$\frac{\partial^2 y}{\partial \theta^2} = \left[\frac{T}{m}\frac{\partial^2 y}{\partial x^2} + ky\right] \quad (3)$$

The solution of the above equation is conveniently obtained by the following method. Defining two new functions, Θ, which is a function of θ only and independent of x, and X, which is a function of x only and independent of θ, let

$$y = \Theta(\theta)X(x) \quad (4)$$

Equation 3 can now be written as

$$X\frac{\partial^2 \Theta}{\partial \theta^2} = \left[\alpha\Theta\frac{\partial^2 x}{\partial x^2} + k(\Theta X)\right] \quad (5)$$

Dividing throughout by (ΘX).

$$\left[\frac{1}{\Theta}\times\frac{\partial^2 \Theta}{\partial \theta^2} - k\right] = \left[\frac{\alpha}{X}\times\frac{\partial^2 X}{\partial x^2}\right] = -\beta^2 \quad (6)$$

Or splitting the above equation into two ordinary second order differential equations

$$\frac{d^2\Theta}{d\theta^2} = \Theta(k - \beta^2) \quad (7)$$

$$\frac{d^2 X}{dx^2} = \left(\frac{-\beta^2}{k}\right)X \quad (8)$$

The solution of eq. 7 is

$$\Theta = [A_1 e^{-\sqrt{k - \beta^2}\theta} + A_2 e^{+\sqrt{k - \beta^2}\theta}] \quad (9)$$

The solution of eq. 8 is

$$X = \left[A_3 \sin\frac{\beta}{\sqrt{\alpha}}x + A_4 \cos\frac{\beta}{\sqrt{\alpha}}\right]x \quad (10)$$

The general solution of eq. 3 is hence

$$y = \left[A_3 \sin\frac{\beta}{\sqrt{\alpha}}x + A_4 \cos\frac{\beta}{\sqrt{\alpha}}x\right]$$
$$[A_1 e^{-\sqrt{k - \beta^2}\theta} + A_2 e^{+\sqrt{k - \beta^2}\theta}] \quad (11)$$

The boundary conditions are

(1) when $x = L$, $y = 0$ for all θ
$$\therefore A_1 = 0 \text{ and } \frac{\beta}{\sqrt{\alpha}}L = 2\pi$$

(2) when $\theta = \Theta$, $y = 0$ for all x
$$\therefore A_2 = 0$$

(3) If the initial displacement at $x = L/2$, is y_0, when $\theta = 0$ the final solution reduces to

$$y = \left[y_0 \sin\frac{2\pi x}{L} e^{-\sqrt{k - \beta^2}\theta}\right] \quad (12)$$

For self excited instability, $k = \beta^2$ or

$$k = 4\pi^2\alpha/L^2 \quad (13)$$

or

$$L = [2\pi\sqrt{\alpha/k}] \quad (14)$$

NOMENCLATURE

A = reactant
A_1, A_2, A_3, A_4 = constants
C = concentration, moles/unit vol.
k = constant
k_1 = reaction velocity constant
m = mass of stretched membrane, g./cm.
p = pressure
T = tension in membrane, dynes
x = coördinate along length of the membrane
y = displacement in y-direction, cm.
y_0 = initial displacement, cm.
z = coördinate along with width of the membrane
α = T/m
β = constant
γ = no. of moles
Θ X = functions defined by eq. 4
θ, x = independent variables in eq. 1

Application of Eq. 12 for the Measurement of Irreversible Fast Flow Reactions.—Under the condition of self-excited instability, imposition of eq. 13 eliminates the damping effect of the exponential

term, and at the middle of the membrane the amplitude becomes y_0 which is a characteristic of the internal pressure provided k and α are held constant. Hence it is possible to measure the effect of change in the internal pressure by adjusting L for self-excited instability and measuring the new amplitude at $x = L/2$. The amplitude or displacement is a function of pressure. Therefore, it is possible to calibrate a stretched membrane for initial reactant pressure and as the flow reaction progresses resulting in the increase or decrease of pressure, the new displacement can be measured and hence the pressure. Once the pressure is known, the reaction velocity can be estimated.

Consider the general unimolecular reaction at constant volume

$$A \longrightarrow \gamma\beta \qquad (15)$$

where γ is the number of moles of products formed from the reaction of one mole of A. Ideal gas laws are assumed. Let n_{A0} moles of A continuously enter the reaction zone per unit time, n_A, the number of moles unreacted after time θ and passing any given point in the zone per unit time and V, the total volume.

Under isothermal conditions, the rate equation

$$-\frac{dC_A}{d\theta} = k_1 C_A \qquad (16)$$

Since

$$C_A = n_A/V$$

$$\left[-\frac{dn_A}{d\theta} = k_1 n_A \right] \qquad (17)$$

Integrating between limits

$$\left[k_1 = \frac{2.303}{\theta} \log \frac{n_{A0}}{n_A} \right] \qquad (18)$$

Equation 18 can be rewritten in terms of initial and final pressure after a time lapse of θ

$$\left[k_1 = \frac{2.303}{\theta} \log \frac{p_0}{p_r} \right] \qquad (19)$$

Evaluating β_r by the method outlined in the beginning, k_1 can be determined from eq. 19 conveniently, by introducing the flexible membrane at different intervals in the line.

The author is indebted to Dr. T. Baron of Shell Development Co., California, for the suggestion of the problem.

STRESS RELAXATION, BIREFRINGENCE AND THE STRUCTURE OF GELATIN AND OTHER POLYMERIC GELS

By ARTHUR V. TOBOLSKY

Frick Chemical Laboratory, Princeton University, Princeton, N. J.

Whenever concentrated or dilute solutions of polycrystalline polymers form gels, there is a strong likelihood that such gels are held together by crystallites acting as cross-links. This has been shown to be true for polyvinyl chloride,[1] polyacrylonitrile[2] and for gelatin.[3,4]

Studies of relaxation of stress at constant extension coupled with simultaneous measurements of birefringence provides some interesting insights into polycrystalline polymers and their gels. Very frequently the relaxation of stress at constant extension for such systems (*e.g.*, plasticized polyvinyl chloride) is very slow and the change in birefringence is also very slight.[1] The crystallites appear to be acting as cross-links which are quite stable with respect to time, *i.e.*, they do not break and remake. As the temperature is increased the modulus of the sample decreases, indicating fewer crystallites (hence fewer cross-links). The relative rate of decay of stress is unaffected, however, by the increase in temperature.

Very often the decay in stress in polycrystalline polymers or their gels is accompanied by an increase in birefringence, as noted by Stein and Tobolsky,[1] indicating that the stress decay was caused by a growth and/or orientation of crystallites. In extreme cases, such as natural rubber held at constant length at $-25°$ the growth of oriental crystalline material might cause a relatively rapid decay of stress to zero stress followed by an actual lengthening of the sample beyond its stretched length. This phenomenon is called spontaneous elongation.[5] The birefringence in these cases obviously increases enormously.

The behavior of polycrystalline polymers with respect to simultaneous measurements of stress decay and birefringence is to be sharply contrasted with the behavior of linear amorphous polymers. For linear amorphous polymers in the temperature interval of "rubbery flow," or in the temperature interval of chemical stress relaxation the decay of stress to zero stress is paralleled by the decay of birefringence, so that the ratio of stress to birefringence remains constant during the relaxation.[1,6]

Studies have been made of the stress decay of gelatin gels maintained at constant extension.[7] It was postulated that this decay was due to a breaking and remaking of bonds between collagen chains acting as temporary cross-links.[7] If such were the case, however, it would be expected that the stress decay and birefringence decay would be strictly parallel. However, it has been noted that even when stress decay in a strained gelatin gel was complete, some double refraction persisted.[8]

It appears to me that the mechanism postulated for relaxation of gelatin gels, *i.e.*, the breaking and remaking of temporary cross-linkages, may not be entirely correct. If crystallites are acting as cross-linkages, they would not make and remake very readily. Part of the stress decay in the gelatin gels may well be due to the further growth of oriented crystalline material, perhaps around already existing nuclei, which would account for the persistence of birefringence after stress decay was complete.

(1) R. S. Stein and A. V. Tobolsky, *Textile Research J.*, **18**, 302 (1948); *ibid.*, **19**, 8 (1949).

(2) J. Bisschops, *J. Polymer Sci.*, **12**, 583 (1954).

(3) K. Hermann and O. Gerngross, *Kautschuk*, **8**, 181 (1932).

(4) H. Boedtker and P. Doty, THIS JOURNAL, **58**, 968 (1954).

(5) C. Park, *Rubber Chem. Tech.*, **12**, 278 (1939); G. M. Brown, Ph.D. Thesis, Princeton University, 1948.

(6) R. S. Stein, F. H. Holmes and A. V. Tobolsky, *J. Polymer Sci.*, **14**, 443 (1954).

(7) M. Miller, J. D. Ferry, F. W. Schremp and J. E. Eldridge, THIS JOURNAL, **55**, 387 (1951).

(8) J. D. Ferry, "Advances in Protein Chemistry," Vol. IV, Academic Press, Inc., New York, N. Y., 1948, p. 45.

CHARGE EFFECTS IN LIGHT-SCATTERING BY COLLOID SOLUTIONS

By W. Prins and J. J. Hermans

Laboratory for Inorganic and Physical Chemistry, The University, Leiden

The effect of particle charge on the light scattering by colloids has been extensively discussed by Mysels.[1] Since some of his statements may add to the confusion that appears to exist in this field, it may be worthwhile to reconsider the problem briefly.

Mysels considers colloidal cations of molecular weight M, charge p and concentration c, g./l., in the presence of univalent anions (y, equiv./l.) and univalent cations (x, equiv./l.). It is clear that $y = x + pc/M$. Three possibilities are discussed: in the first, the concentration of the colloidal electrolyte as a whole fluctuates independently of the simple electrolyte; in the other two, the concentration of the colloid cation fluctuates while maintaining a Donnan type of equilibrium with the electrolyte solution. Three different answers are obtained for the turbidity, one of which is believed to be the most probable. In all three cases the author correctly ignores fluctuations which create space charges since these play a negligible role in all but the most extreme dilution.[2]

However, according to the general theory of fluctuations in multicomponent systems[3,4] there is only one answer, which can be derived unambiguously when the thermodynamics of the system are known. In the notation used by Brinkman and Hermans[4] the turbidity is given by

$$\tau = -AVD/\Delta \qquad (1)$$

where D and Δ are determinants defined in the paper quoted, while V is the volume of the solution and A a constant. Now, Mysels assumes in his derivations that the solution is ideal. If we take as solute components: (1) the low molecular weight electrolyte of concentration x, and (2) the colloid ion with its counter ions, we can at once write down the partial Gibbs free energies of these components

$$\mu_1 = \mu_1{}^\circ + RT(\ln \xi + \ln \eta)$$

$$\mu_2 = \mu_2{}^\circ + RT(\ln \gamma + p \ln \eta)$$

Here ξ, η and γ are the *mole* fractions corresponding with x, y and c; μ_1° and μ_2° are independent of the composition. If n_0, n_1 and n_2 are the numbers of moles of the solvent and of the solute components, respectively, then the total number of moles in the solution is

$$n = n_0 + 2n_1 + (p + 1)n_2$$

and hence

$$\xi = n_1/n; \quad \eta = (n_1 + pn_2)/n; \quad \gamma = n_2/n$$

Following the recipe described in ref. 4 one can find the determinants in eq. 1. For all but very high concentrations of electrolytes

$$-D/RT = \nu_1{}^2\left(\frac{p^2}{n_1 + pn_2} + \frac{1}{n_2}\right) - 2\nu_1\nu_2 \frac{p}{n_1 + pn_2} + \nu_2{}^2\left(\frac{1}{n_1 + pn_2} + \frac{1}{n_1}\right) \quad (2)$$

$$\Delta/(RT)^2 = \frac{p^2}{n_1(n_1 + pn_2)} + \frac{1}{n_2(n_1 + pn_2)} + \frac{1}{n_1 n_2} \quad (3)$$

Here $\nu_1 = \partial\nu/\partial n_1$ and $\nu_2 = \partial\nu/\partial n_2$, where ν is the refractive index. The final equation for τ is simplified considerably if we use Mysels' additional assumption that the only significant contribution to the scattering is that due to the colloid component. This amounts to saying that the only significant term in eq. 2 is that which contains ν_2^2. Whether this is permissible depends on the system studied. It was shown by Edsall, *et al.*,[5] that it holds good for the protein solutions studied by them, and their subsequent treatment (which is essentially the same as ours) is based on it.

The equation for the turbidity becomes

$$AV\nu{}^2{}_2/\tau RT = \frac{1}{n_2} \times \frac{2n_1 + pn_2 + p^2n_2}{2n_1 + pn_2}$$

Remembering that $n_1 = Vx$, $n_2 = Vc/M$, $\nu_2 = \nu_c M/V$ (where $\nu_c = \partial\nu/\partial c$), and writing $H = A\nu_c{}^2/RT$, we get

$$\frac{Hc}{\tau} = \frac{1}{M}\left(1 + \frac{p^2(c/M)}{2x + pc/M}\right) \qquad (4)$$

This answer is identical with the third of the equations derived by Mysels and is considered by him to be the most probable. In our opinion it is the *only* answer to the problem. Mysels argues that the relaxation time for a fluctuation in the concentration of a colloid is much larger than that for the simple electrolyte and expects therefore that the concentration of the simple electrolyte "adjusts itself" to that of the colloid. Accordingly it is said by him that "the statistical treatment assumes implicitly an equilibrium distribution of all species whatever the relaxation time of a fluctuation." We believe that this fails to appreciate the nature of statistical mechanics. Equation 1 can be derived by the method of the grand ensemble and has nothing to do with the relaxation time of a fluctuation. Another method, which avoids the concept of grand ensemble, calculates the probability of fluctuations δ_i in the numbers n_i and, to that end, expands the change in the free energy in powers of the δ's. The extent to which the concentration of one component tends to "adjust itself" to the fluctuation of another is determined completely by the change in the free energy as a result of the fluctuations δ, and statistical mechanics leave no room for special assumptions regarding this adjustment.

(1) K. J. Mysels, This Journal, **58**, 303 (1954).

(2) J. J. Hermans, *Rec. trav. chim.*, **68**, 859 (1948).

(3) F. Zernike, *Arch. Neerland. Sci.*, [3A] **4**, 74 (1918); J. G. Kirkwood and R. J. Goldberg, *J. Chem. Phys.*, **18**, 54 (1950); W. H. Stockmayer, *ibid.*, **18**, 58 (1950).

(4) H. C. Brinkman and J. J. Hermans, *ibid.*, **17**, 574 (1949).

(5) J. T. Edsall, H. Edelhoch, R. Lontie and P. R. Morrison, *J. Am. Chem. Soc.*, **72**, 4641 (1950).